

On-line NIR analysis in a high density polyethene plant, evaluation of sampling system and optimal calibration strategy

M.Sc. (eng.) Thesis

Rune Mathisen

<mathrune@online.no> 

1999-06-11



Telemark College
Department of Technology
M.Sc. Programme



Telemark College
Department of Technology
M.Sc. Programme

Student: Rune Mathisen

Thesis title: On-line NIR analysis in a high density polyethene plant, evaluation of sampling system and optimal calibration strategy

Signature:

Number of pages: 167

Keywords: Multivariate data analysis, multivariate calibration, polyethene, density, melt flow rate, near infra-red spectroscopy, sampling

Supervisor: Kim H. Esbensen

Other supervisor: Kristian Helland

Sensor: Lars Nørgaard

External Partner: Borealis as

Availability: Confidential

Archive approval:

Abstract:

This thesis deals with the calibration of an on-line near infra-red (NIR) instrument measuring on high density polyethene (HDPE) powder. The goal was to recommend an “optimal” calibration strategy for the dynamic prediction system. Important aspects in relation to the calibration were thorough understanding of the NIR spectrum and of the sampling system. The physical polymer properties of interest in this application were density and melt flow rate (MFR).

Because of the collinearity and lack of selectivity in the NIR region, it is necessary to use many absorption frequencies and multivariate regression techniques like principal component regression (PCR) or partial least squares regression (PLSR).

The relation between polymer density and the NIR spectrum looks simple and direct using PLSR; a higher co-monomer content in the polymer lowers the density and give origin for an increased methyl content. Methyl (and methylene) is known to have overtone absorption bands in the NIR spectral region. The relation between the MFR property and the NIR spectra, is not as clear as for density. MFR predictions were found infeasible in this application.

It was found that particle properties (size a.o.) constitute the major variations in the NIR spectra, in addition to the problems with varying polymer concentration and a polymer film on the sampling system window. These variations should be reduced to a minimum prior to calibration.

The recommended calibration strategy for density predictions, is:

- Careful selection of the calibration data.
- Abandon the upper part of the acquired NIR spectrum.
- Pre-processing to reduce *all* baseline effects.
- A rigid outlier detection system.
- Continuous calibration model updating.

The sampling system under study suffers from many weaknesses, resulting in very unstable and noisy spectra. Variations in polymer concentration in the sampling system and a polymer film on the sampling system (sapphire) window are probably the two major problems.

Another problem with the system under study is the introduction of several measurement biases of unknown magnitude. These make it impossible to give reliable estimates of the prediction accuracy.

A rebuild of the sampling system is probably necessary to overcome the bias problem, and also for improving the spectrum quality.

Preface

This report is the result of a Master of Science (Eng.) thesis at Telemark College, Porsgrunn, Norway. The M.Sc. thesis is a individual research project, and marks the end of five years of studies in chemical engineering. The work is limited to 75 working-days.

The project proposal (given in Appendix A) gave wide suggestions for topics to include in the thesis. Unfortunately, there was not time to cover everything.

During this thesis work it became evident that the quality of the acquired near infra-red (NIR) spectra was a key issue. Therefore much weight was put on analyzing the sampling system, and a little less weight was put on the calibration work. Studies in calibration transfer were completely dropped, and Locally Weighted Regression was only briefly tested.

This thesis requires that the reader has some knowledge in multivariate data analysis and molecular spectroscopy, but good references are given for both topics. The reader should also have some knowledge in polymer chemistry.

All data analysis in this thesis work was done using *Matlab* (The Mathworks Inc.) and the *PLS_Toolbox* (Eigenvector Research Inc.). These tools proved to be excellent for the type of work done here.

Some of the data provided in the appendices may seem redundant, but this thesis leaves many open ends that give possibilities for further studies and the data may give some starting points.

Acknowledgements

First of all I want to thank my girlfriend Grace Beate Engstad for her patience and encouragement during the past five years.

My two supervisors, Kristian Helland and Kim H. Esbensen, are both very knowledgeable chemometricians, and were always supportive. It has been a joy working with them. Thanks!

I've had lots of useful discussions with several Borealis employees, and two of them deserves a particular thanks: Per Anker Hassel and Marit Seim. Also thanks to Vidar Almquist, Arild Follestad, Rune Nygaard, Richard Garner and Stein Helleborg.

Without the scholarship I've received from Borealis for the past two years, this thesis would not have been possible. Equally important is the scholarship i received from the Norwegian Confederation of Trade Unions (LO) during my three years of chemical engineering study. The involvement of the trade union leader Hallgeir Kjeldal at Nopef dept. 14 has been particularly important in both these scholarships.

I also want to thank Telemark College for providing the students with excellent computer equipment. The computers and software made available to me by Borealis was insufficient for many of the tasks in this thesis work. The powerful Unix workstations at Telemark College saved me a lot of working-hours! Thanks also to the people at the IT&S department at Telemark College for doing a very good job!

Barry M. Wise (Eigenvector Research Inc.) was very helpful with my OSC problems, and also gave kind permission to distribute a subset of the PLS_Toolbox with this report (for reproduction purposes).

Vidar B. Gundersen helped me getting started with Matlab, and typesetting this report. We've also had some very useful discussions on static models in a dynamic environment.

Contents

1	Introduction	1
1.1	Background	1
1.2	Scope of this thesis	2
1.3	Definitions	3
1.3.1	Notation	3
1.3.2	Data, information and knowledge	3
1.3.3	Multivariate instruments	4
1.3.4	Multivariate calibration	4
1.3.5	Model robustness	5
1.3.6	Optimal calibration strategy	6
1.4	The Rønningen HDPE plant	6
1.4.1	The process	6
1.4.2	The products	7
1.5	The Rønningen on-line installation	9
2	Near infra-red spectroscopy in HDPE applications	13
2.1	Basics of infra-red spectroscopy	13
2.2	Introduction to near infra-red spectroscopy	15
2.3	Assignment of NIR bands in HDPE	17
2.4	Relation between HDPE polymer structure, density and NIR spectra	17
2.5	Relation between HDPE polymer structure, MFR and NIR spectra	18
2.6	Baseline features	19
2.7	Summary and conclusion	20
3	System analysis	21
3.1	System definition	21
3.2	Polymer contribution in the NIR spectrum	21
3.2.1	Structural contributions	22
3.2.2	Particle size and porosity	22
3.2.3	Specular reflectance	24
3.3	Composition in process pipe	24
3.4	Temperature effects	25
3.5	Humidity	27
3.6	In-sample variations	27
3.7	The sapphire window	28
3.8	Polymer film on sapphire window	28
3.9	Sample concentration	31
3.10	Other sources of contribution to the NIR spectrum	32
3.11	Sampling and measurement errors	32
3.12	Summary and conclusion	33
4	Multivariate calibration: a review of methods	37
4.1	A generic calibration scheme: identification of the steps involved	37

4.2	Data pre-treatment and storage	39
4.2.1	Averaging data	39
4.2.2	Filtering data by spectral rejection	40
4.2.3	Fourier filtering	41
4.2.4	Other methods	43
4.3	Assembling calibration and validation data sets	43
4.4	Initial study	43
4.5	Pre-processing	44
4.5.1	Reflectance/Absorbance/Kubelka-Munk	44
4.5.2	Two-point baseline correction	44
4.5.3	Orthogonal signal correction	44
4.5.4	Smoothing and derivation (Savitzky-Golay algorithm)	45
4.5.5	Multiplicative Scatter Correction (MSC)	47
4.5.6	Standard Normal Variate (SNV)	48
4.5.7	Normalization	48
4.5.8	Variable selection	49
4.5.9	Linearization	49
4.5.10	Mean centering and autoscaling	50
4.6	Detecting outliers	51
4.6.1	Spectral residuals	51
4.6.2	Mahalanobis distance test on PLSR scores	52
4.6.3	Other methods	52
4.7	Selecting a regression algorithm	53
4.7.1	Principal Component Regression (PCR)	53
4.7.2	Partial Least Squares Regression (PLSR)	54
4.7.3	Locally Weighted Regression (LWR)	54
4.7.4	Other methods	54
4.8	Validating the model	55
4.8.1	Cross-validation	55
4.8.2	Test-set validation	55
4.9	Evaluating the model, quantification of quality	56
4.9.1	RMSEP and RMSECV	56
4.9.2	Bias	56
4.9.3	SEP	56
4.9.4	Correlation	57
4.10	Model durability	57
4.10.1	Robust modeling	57
4.10.2	Model updating	58
4.11	Summary and conclusion	58
5	Data-sets: description and pre-study	61
5.1	General overview	61
5.2	Density data	61
5.2.1	Data-set 1	63
5.2.2	Data-set 2	64
5.2.3	Data-set 3	66
5.2.4	Data-set 4	66
5.2.5	Data-set 5	69
5.2.6	Final remarks, density data	69
5.3	MFR data	72
5.3.1	Data-set 1	74
5.3.2	Data-set 2	76
5.4	Summary and conclusion	78
6	Calibration strategy applications and discussion	79
6.1	Outliers in the calibration and test-set data	79

6.2	Density models	81
6.2.1	Selection of calibration data	81
6.2.2	Selection of regression method	82
6.2.3	Calibration on raw data	82
6.2.4	Selection and optimization of the pre-processing step . . .	83
6.2.5	Final pre-processing schemes	84
6.2.6	Test-set validation of models	85
6.2.7	Application test with outlier detection system	86
6.2.8	Expanding the calibration data set	87
6.2.9	Excluding ME6930 in models	87
6.2.10	Model updating applications	88
6.3	MFR models	89
6.4	Summary and conclusion	92
7	Conclusion	93
A	F4291 Master of Science Thesis: Project Proposal	95
B	Rønningen HDPE products	97
C	Density analysis reference method	99
D	MFR analysis reference method	101
E	Particle size distribution data	103
F	Temperature study predicted measured plots	105
G	Suggestion for improvement of the existing sampling system	107
H	Suggestion for a new sampling system	109
I	Density data distribution	111
J	Assessing PCA loading vectors from spectral data	115
K	Matlab code	119
K.1	Mahalanobis distance on scores	119
K.2	SNV	120
K.3	Model statistics	120
L	Pre-processing optimalization	123
M	Graphical summaries, cross-validated density models	133
N	Density models validation plots	137
N.1	Scheme A	137
N.2	Scheme B	142
N.3	Scheme C	147
N.4	Scheme A*	147
O	Calibration model updating test results	157
O.1	Moving window PLSR	158
O.2	Growing PLSR	161
	Bibliography	165

List of Figures

1.1	Suggestion for a data processing model	4
1.2	Flow-sheet of the Rønningen HDPE process	7
1.3	HDPE polymer structure	7
1.4	HDPE polymer structure with chain-branch	8
1.5	Two possible polymer terminations, methyl and ethenyl	8
1.6	Polymer with chain-branch	8
1.7	Principle drawing of the AOTF crystal	9
1.8	Principle drawing of the NIR spectrometer	10
1.9	Location of NIR spectrometer (scales are not as built)	11
1.10	Location of sapphire window (scales are not as built)	11
2.1	The electromagnetic spectrum	13
2.2	Possible vibrational and deformation modes in CH_2	14
2.3	Mid-IR transmittance spectra acquired from HDPE produced with three different types of catalysts	15
2.4	Difference in mid-IR spectrum due to catalyst	16
2.5	Typical NIR spectrum acquired from HDPE powder (on-line analyzer, Rønningen). Asterisks mark expected overtone bands.	18
2.6	Density and co-monomer content	19
2.7	Baseline features	20
3.1	Characterization of particle size by PCA. Product names are used as plot symbols, type of catalyst is given outside the ellipses.	22
3.2	Loading plot, particle size analysis.	23
3.3	Loading weights, temperature-model A	26
3.4	“Old” spectrum with no oscillation, and “new” spectrum with oscillation	28
3.5	Sketch of sapphire window with thin polymer film.	29
3.6	Detail of “new” spectrum, expected interference fringes marked with an asterisk.	30
3.7	Single spectra (reflectance)	31
3.8	Major sources of variation in the NIR spectrum	34
4.1	A generic calibration scheme. For each step: yes/no. If yes: multiple options.	38
4.2	Effect of averaging data by using the mean or median of each variable.	40
4.3	Integral of each sample.	41
4.4	Detail of Fourier domain spectra	42
4.5	Fourier filtered (ffilt) and “new” spectra	42
4.6	Effect of two-point baseline-correction	45
4.7	Spectrum and derivatives (scaled)	46
4.8	Optimal window size, 2nd derivative of 2nd order polynomial	47
4.9	One spectrum plotted against average spectrum	48
4.10	Peak normalization	49

4.11	Mean and standard deviation of spectra	50
4.12	Typical and outlier spectrum	51
4.13	Mahalanobian (ellipse) and Euclidean (circle) distance	53
4.14	The PLSR NIPALS algorithm illustrated visually	54
5.1	Some NIR spectra acquired from the on-line installation	62
5.2	Reference density data, collected between 1998-07-30 and 1999-01-11	62
5.3	Histogram of all available density data	63
5.4	Score plot, data-set 1	64
5.5	Loadings PC1-6, data-set 1	65
5.6	Score plot, data-set 2	65
5.7	Loadings PC1-6, data-set 2	66
5.8	Score plot, data-set 3	67
5.9	Loadings PC1-6, data-set 3	67
5.10	Score plot, data-set 4	68
5.11	Loadings PC1-6, data-set 4	68
5.12	Score plot, data-set 5	69
5.13	Loadings PC1-6, data-set 5	70
5.14	Monitoring of shifts in spectra	71
5.15	Histogram of all available MFR 190/2,16 data	72
5.16	Distribution of available MFR 190/2,16 data with time	73
5.17	Objects scores and MFR 190/2,16 values	74
5.18	Loadings PC 1-6, MFR data-set 1	75
5.19	Objects scores and MFR 190/2,16 values	76
5.20	Loadings PC 1-6, MFR data-set 2	77
6.1	t vs. u, outlier example	80
6.2	Cross-validated density model, raw data	82
6.3	Global MFR model, test-set validation, 3 factors used	90
6.4	Local MFR model, 0-0.6, test-set validation, 4 factors used	91
6.5	Local MFR model, 4-7, test-set validation, 8 factors used	91
F.1	Predicted/measured, temperature-model A	105
F.2	Predicted/measured, temperature-model B	106
G.1	Suggested improvement of the sampling system	108
H.1	Suggested new sampling system	109
I.1	Histogram of density data in data-set 1	111
I.2	Histogram of density data in data-set 2	112
I.3	Histogram of density data in data-set 3	112
I.4	Histogram of density data in data-set 4	113
I.5	Histogram of density data in data-set 5	113
J.1	Design center (solid line) and two of the 243 simulated spectra	116
J.2	Loading vectors from designed experiment	117
L.1	1300-1800 nm, SNV + 2nd derivative, mean centered	124
L.2	1300-1800 nm, 2nd derivative, mean centered	124
L.3	1300-1800 nm, 2nd derivative + SNV, mean centered	125
L.4	1300-2110 nm, SNV + 2nd derivative, mean centered	125
L.5	1300-2110 nm, 2nd derivative, mean centered	126
L.6	1300-2110 nm, 2nd derivative + SNV, mean centered	126
L.7	1300-2110 nm, SNV + 2nd derivative, autoscaled	127
L.8	1300-2110 nm, 2nd derivative, autoscaled	127

L.9	1300-2110 nm, 2nd derivative + SNV, autoscaled	128
L.10	1300-2400 nm, SNV + 2nd derivative, mean centered	128
L.11	1300-2400 nm, 2nd derivative, mean centered	129
L.12	1300-2400 nm, 2nd derivative + SNV, mean centered	129
L.13	1300-2400 nm, SNV + 2nd derivative, autoscaled	130
L.14	1300-2400 nm, 2nd derivative, autoscaled	130
L.15	1300-2400 nm, 2nd derivative + SNV, autoscaled	131
M.1	Cross-validated density model A	133
M.2	Cross-validated density model B	134
M.3	Cross-validated density model C	134
M.4	Cross-validated density model A* (without ME6930)	135
N.1	Outlier detection, scheme A, test-set 2	137
N.2	Results, scheme A, test-set 2	138
N.3	Outlier detection, scheme A, test-set 3	138
N.4	Results, scheme A, test-set 3	139
N.5	Outlier detection, scheme A, test-set 4	139
N.6	Results, scheme A, test-set 4	140
N.7	Outlier detection, scheme A, test-set 5	140
N.8	Results, scheme A, test-set 5	141
N.9	Outlier detection, scheme B, test-set 2	142
N.10	Results, scheme B, test-set 2	143
N.11	Outlier detection, scheme B, test-set 3	143
N.12	Results, scheme B, test-set 3	144
N.13	Outlier detection, scheme B, test-set 4	144
N.14	Results, scheme B, test-set 4	145
N.15	Outlier detection, scheme B, test-set 5	145
N.16	Results, scheme B, test-set 5	146
N.17	Outlier detection, scheme C, test-set 2	147
N.18	Results, scheme C, test-set 2	148
N.19	Outlier detection, scheme C, test-set 3	148
N.20	Results, scheme C, test-set 3	149
N.21	Outlier detection, scheme C, test-set 4	149
N.22	Results, scheme C, test-set 4	150
N.23	Outlier detection, scheme C, test-set 5	150
N.24	Results, scheme C, test-set 5	151
N.25	Outlier detection, scheme A*, test-set 2	151
N.26	Results, scheme A*, test-set 2	152
N.27	Outlier detection, scheme A*, test-set 3	152
N.28	Results, scheme A*, test-set 3	153
N.29	Outlier detection, scheme A*, test-set 4	153
N.30	Results, scheme A*, test-set 4	154
N.31	Outlier detection, scheme A*, test-set 5	154
N.32	Results, scheme A*, test-set 5	155
O.1	Pre-processing scheme A, 4 factors, moving, predicted/measured	158
O.2	Pre-processing scheme A, 4 factors, moving, time/prediction error	158
O.3	Pre-processing scheme B, 4 factors, moving, predicted/measured	159
O.4	Pre-processing scheme B, 4 factors, moving, time/prediction error	159
O.5	Pre-processing scheme C, 4 factors, moving, predicted/measured	160
O.6	Pre-processing scheme C, 4 factors, moving, time/prediction error	160
O.7	Pre-processing scheme A, 4 factors, growing, predicted/measured	161
O.8	Pre-processing scheme A, 4 factors, growing, time/prediction error	161
O.9	Pre-processing scheme B, 4 factors, growing, predicted/measured	162
O.10	Pre-processing scheme B, 4 factors, growing, time/prediction error	162

O.11 Pre-processing scheme C, 4 factors, growing, predicted/measured	163
O.12 Pre-processing scheme C, 4 factors, growing, time/prediction error	163

List of Tables

2.1	Assignments of NIR bands in LLDPE [Shimoyama et al. (1998)]	17
3.1	Validation results, temperature model	26
3.2	Approximate film thickness	29
6.1	Cross- and test-set validated results, outlier example, density pre- dictions	80
6.2	Cross-validated density model, raw data	82
6.3	Test-set validated density model, raw data, known outliers removed	83
6.4	Cross-validated density model results	85
6.5	Test-set validation of density model A, known outliers removed .	85
6.6	Test-set validation of density model B, known outliers removed .	85
6.7	Test-set validation of density model C, known outliers removed .	86
6.8	Test-set validation of density model A, automatic outlier removal	86
6.9	Test-set validation of density model B, automatic outlier removal	86
6.10	Test-set validation of density model C, automatic outlier removal	87
6.11	Test-set validated density models, expanded calibration data-set	87
6.12	Cross-validated density model A* results	88
6.13	Test-set validation of density model A*, automatic outlier removal	88
6.14	Moving window PLSR results	89
6.15	Growing PLSR results	89
B.1	All products: type of catalyst, density and MFR specifications .	97
E.1	Particle size distribution data	103

Chapter 1

Introduction

This chapter gives the relevant background information and the scope of this thesis. Some fundamental definitions are also given, together with a short description of the high density polyethylene (HDPE) process, the sampling system and the instrument.

1.1 Background

The quality control laboratory is on the move. An increasing amount of analysis in the process industry, previously carried out off-line in a centralized laboratory, are now done on-line. More robust instruments, developments in fiber optic technology and multivariate data analysis (“chemometrics”) have made this possible. Process Analytical Chemistry (PAC) is the application of analytical science to the monitoring and control of industrial chemical processes [McLennan and Kowalski (ed) (1995)].

Off-line laboratory analysis data is used to characterize product properties and process performance in a retrospective manner. New on-line analysis techniques provides real-time or near real-time measurements, supplying process operators, chemical and process control engineers with data previously unavailable to them. Rapid feed-back on process- and product properties to operators and the process control system founds a good basis for a decrease in produced off-spec material. It may also be used for narrowing the product specification limits.

The on-line instruments provide new possibilities for describing the process state. Traditionally, properties like temperature, pressure and flow rate have been used to characterize and control chemical process systems. Analyzers like gas chromatographs, infra-red and mass spectrometers have also been used for some time, particularly in the petroleum, petrochemical and pharmaceutical industry. Improvements in these analytical methods, and the addition of “new” methods like near infra-red (NIR) spectroscopy and nuclear magnetic resonance (NMR), give new possibilities of using real-time measurements of product and process characteristics in the process control system.

There has been great progress in PAC technology during the past decade, with the most significant development within on-line spectroscopy. This R&D work has primarily been carried out by major chemical companies, but also by academic institutions like Center for Process Analytical Chemistry (CPAC), Seattle, USA. There are not too many application reports in recent literature, though. This is at least partly due to industrial secrecy, but maybe also due to unsuccessful implementations.

Borealis is implementing on-line NIR analysis at several production sites, and is at the moment in the phase of validating the installations. One of the plants for installation is the high density polyethylene (HDPE) plant at Rønningen, Norway, where one instrument is analyzing produced polymer powder after the reactor and another is analyzing polymer melt at the process extruder.

1.2 Scope of this thesis

This thesis will primarily deal with the calibration of an on-line near infra-red (NIR) instrument measuring on HDPE powder. The goal is to recommend an “optimal calibration strategy”. This term is further defined in Section 1.3.6. The project proposal is given in Appendix A.

The physical polymer properties of interest in this application are density and melt flow rate (MFR). The recommended calibration scheme should lead to regression models with reasonable prediction accuracy, compared to the reference methods. In relation to this it is important to find good estimates for the expected long-range prediction accuracy, i.e. different validation methods should also be evaluated.

Another important aspect is to make the model robust, i.e. to make a model that gives reliable predictions over time. At least two approaches are possible here; to do the modeling in such a way that it is less sensitive to the dynamics of the system (robust modeling), or to do some sort of model maintenance while it is in operation. If neither of these approaches are applicable, a calibration transfer strategy must be considered. In this thesis, work will be focused on robust modeling, but some suggestions for model maintenance will also be given.

In order to evaluate different calibration schemes, all parts of a “typical” multivariate calibration will be identified and a generic scheme outlined. For each step in the generic calibration scheme (e.g. pre-processing, regression, etc.), several options are considered. A theoretical brief basis for all data processing steps will be given. Based on both literature studies and prior knowledge in multivariate regression and analytical chemistry, a set of calibration schemes will be assembled and tested on “real life” data.

Except from locally weighted regression (LWR), non-linear regression methods will not be considered. Non-linear regression methods are complex and hard to interpret, and a study of such methods could easily fill a master thesis work in itself. Instead, non-linearities will be approached by the LWR method mentioned above, or by linearization in the pre-processing step. Linear regression methods like Partial Least Squares Regression (PLSR), may also handle non-linearities, if they are not too severe.

To fully exploit the power of process analytical chemistry and multivariate calibration, causal understanding of instrument response and production effects is crucial. Therefore, effort will also be put into understanding how chemical and physical properties of HDPE is reflected in the NIR spectra. The sampling system will also be investigated.

Although many methods will be reviewed in this thesis, emphasis will be put on the application; to find a calibration strategy that gives an accurate and stable prediction of MFR and density using an on-line NIR spectrometer in a polyethylene plant.

1.3 Definitions

Some fundamental concepts are defined in this section.

1.3.1 Notation

Text enclosed by square brackets [] are bibliography references.

Most chemical substances are named using the IUPAC conventions, or with their modern common names (e.g. “ethene” and not “ethylene”).

Except for temperature (given in °C, SI units are used throughout this thesis.

The math notation is as follows: boldface capital letters are matrices, boldface lower case letters are vectors, other letters are usually scalars. An over-bar ($\bar{}$) denotes a mean value, a hat ($\hat{}$) denotes an estimated value, a tilde (\sim) denotes a measured value. A letter without any accents is a “true” value.

All plots given in this thesis have a unique identifier at the bottom left corner. It usually consists of two or three parts, separated by a dash (-). The first part always gives the name of the script used to generate the plot. If the identifier consists of three parts, the second part usually gives some additional information of the plot (e.g. the name of the data-set used for the plot). The third part of the identifier (or second, if there are only two parts), is an index number, separating different plots generated by the same script. A CD-ROM with all data, Matlab functions and scripts used in this thesis is available on request to the author.

The bottom right of the plots gives the date on which the plot was generated, and the author initials. The purpose of this is that if other authors use the data Matlab functions and scripts in derivative work, these fields should be updated in order to separate them from the plots given here.

1.3.2 Data, information and knowledge

The terms *data*, *information*, *knowledge* and *understanding* are often confused. It is therefore appropriate to explain these important terms.

Data are recordings of reality. They are often stored as numbers, letters or images. Data has no meaning on its own. It must be interpreted by some kind of *data processing system* in order to give meaningful information.

When data is interpreted by e.g. a computer or the human brain, the goal is to extract structure (or patterns) and reject noise. This structural part is *information*. When processing large amounts of data, extracting the structural part may be a complicated task. It is therefore essential to have tools for extracting information from data.

Information is potential *knowledge*. When information is used in a specific context, new knowledge may be gained. Combined with previously acquired knowledge, we may get *understanding* or “wisdom”.

A suggestion for a *data processing model* is given in Figure 1.1. When reading a newspaper, the eye act as the input device, and the brain must do all the data processing. In this thesis, a NIR spectrometer is the main input device. This instrument delivers a vast amount of data, and computer tools are essential for extracting the relevant information.

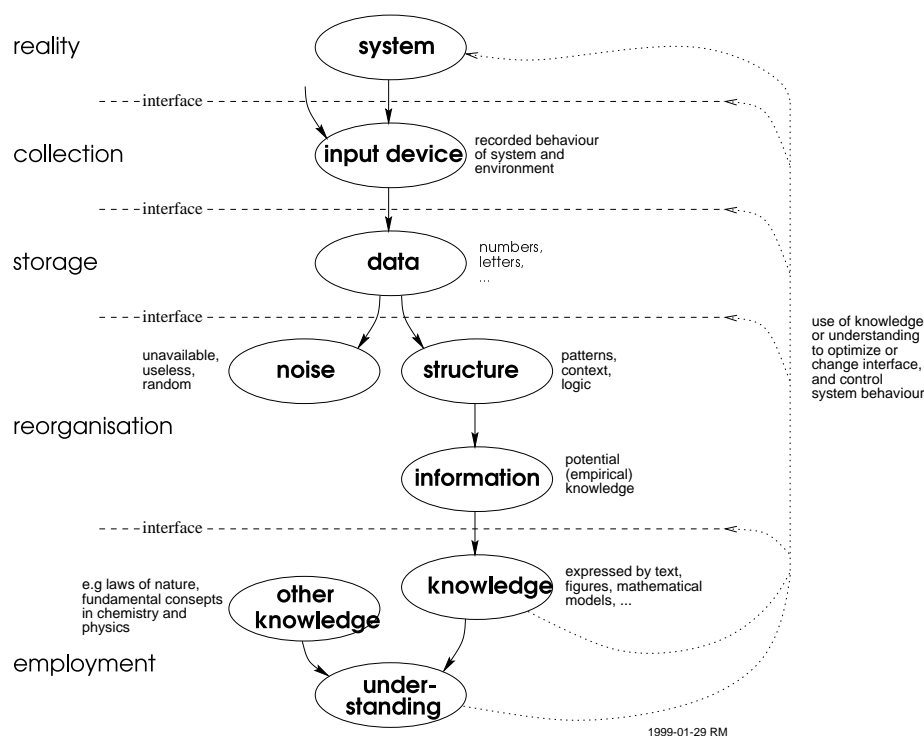


Figure 1.1: Suggestion for a data processing model

The following gives a data processing model example:

From the NIR spectra (data), we find (using multivariate analysis methods) that sample 4 to 19 and 51 to 72 are almost similar. This is information. We may then conclude that catalyst A and B gave the same response. This is knowledge. Combining this with knowledge in heterogenous catalysis and polymer chemistry, we may get new understanding.

1.3.3 Multivariate instruments

Many instruments, e.g. thermometers, pressure cells or pH-meters, deliver only one output signal containing information of one system property. A multivariate (or multichannel) instrument delivers an array of data for one single measurement. This data array indirectly contain information on several system or chemical properties.

A common type of multivariate instruments, are spectrometers. Although many IR applications only use one (or a few) wavelength(s), it is often necessary to use the covariation of many variables. This is especially true in NIR spectroscopy, where absorption bands may be highly overlapping.

1.3.4 Multivariate calibration

The goal of a multivariate calibration is to establish a connection between a multivariate signal $\tilde{\mathbf{x}}$ and one or more physical or chemical properties $\hat{\mathbf{y}}$. In order to do this, a mathematical function is found, enabling us to predict new $\hat{\mathbf{y}}$ values from measured $\tilde{\mathbf{x}}$ data:

$$\hat{\mathbf{y}} = f(\tilde{\mathbf{x}}) \quad (1.1)$$

This mapping function is called the *multivariate calibration model*. It is established by regression, using a calibration data-set. This data-set contains \mathbf{X} -data and their corresponding \mathbf{y} values, obtained from a reference method.

As discussed in Section 1.3.2, data contains a structural part and a noise part. Consequently a mathematical calibration model has a structure part representing systematic variations in the data, and a residual part representing the difference between data and structure. For a linear regression model with one response variable, we have:

$$\mathbf{y} = \mathbf{X}\mathbf{b} + \mathbf{e} \quad (1.2)$$

where $\mathbf{X}\mathbf{b}$ represents the structural part, and \mathbf{e} represents the residual. A multivariate calibration model must then be based on some chemical/physical, mathematical and statistical assumptions.

For a thorough introduction to multivariate calibration, see e.g. [Esbensen et al. (1994)] or [Martens and Næs (1991)].

1.3.5 Model robustness

Multivariate models are built upon statistical assumptions like normal distribution or covariance. Abnormal variations (outliers) may therefore have severe influence on the model (and in later predictions). It is therefore necessary to either detect and remove the outliers, or build the model in such a way that it is (to some extent) insensitive to outliers. On this basis, the following definition of robustness is suggested:

Model robustness is the model's ability to reduce the effect of outliers (or detect and remove them), and in addition be insensitive to small variations in the data.

An on-line analytical instrument resides in an environment that is by magnitude more complex than a laboratory installation. Since nature is dynamic, a static multivariate model will have a limited operating time. This fact gives a foundation for a slightly different definition of model robustness:

Model robustness is the calibration model's ability to give stable and precise prediction with time.

The prediction stability may be influenced by three main types of "disturbances":

- *system drift* - pressure/temperature/concentration or other system properties drift outside the calibration model range
- *instrument drift* - caused by drift in electronic circuits, temperature effects, fluctuations in power-supply etc.
- *discontinuity* - change of sensor, new product, mechanical changes etc. that cause a sudden abrupt change of the system/instrument

1.3.6 Optimal calibration strategy

The term *optimal calibration strategy* is very ambiguous, and needs to be defined for the purpose of the conclusions in this thesis. It should be evident that a true “optimal” calibration strategy cannot be found.

A multivariate calibration consists of a range of data processing steps (see Section 4.1), and evaluation of results. From literature studies and previous knowledge, some processing methods will be selected, and calibration schemes assembled. These schemes will be tested on NIR data acquired from the Rønningen HDPE plant. The model that performs best in respect to prediction accuracy and stability with time will be considered to be “optimal”. An outlier detection system will also be an important part of the finished application. The optimal strategy is then the basis that led to the “optimal” application.

The overall complexity of the calibration strategy is also important. A highly complex model is hard to interpret, and subsequently more difficult to evaluate. It will also be harder to implement a very complicated calibration scheme.

1.4 The Rønningen HDPE plant

This section gives a brief description of the process and products from the HDPE plant in Rønningen, Norway. An in depth analysis of the system under study is given in Chapter 3.

1.4.1 The process

The Rønningen HDPE process was originally licensed from Phillips Petroleum Company (the Phillips Particle Form polyethene process). It uses ethene as monomer, 1-hexene as co-monomer, and a chromium oxide on silica-alumina catalyst. In recent years, a proprietary Borealis catalyst (a metallocene) has been introduced.

A simple flow-sheet of the Rønningen HDPE process is given in Figure 1.2. The main processing steps are: feed preparation, reaction, polymer concentration, hydrocarbon recovery and purification, polymer de-volatilization, extrusion and storage.

The polymerisation is carried out in a 50 m³ loop reactor, using liquid iso-butane as a diluent/carrier. A large propel pump keeps the mixture (slurry) of iso-butane, ethene, 1-hexene and polymer in constant movement to prevent clogging and to keep the reactor content homogeneous. Hydrogen may also be added to control polymer termination.

The reactor pressure is held at 42 bar, while temperature is controlled within 95-110 °C (accuracy of control within $\pm 0,1^{\circ}\text{C}$). Reactor temperature is utilized to control polymer termination. The reaction is exothermic, and approximately 3324 kJ of heat need to be removed for each kilogram of polymer formed.

Polymer is constantly removed from the reactor using five “settling legs”. In these “settling legs” polymer concentration is higher than in the rest of the reactor, ensuring that as little iso-butane and monomers as possible are removed from the reactor.

After the reactor, pressure is reduced to about 0,5-1 bar. This causes the iso-butane to flash off, and the polymer (solid phase) and hydrocarbon gases are separated in a large cyclone-like vessel (the “flash tank”).

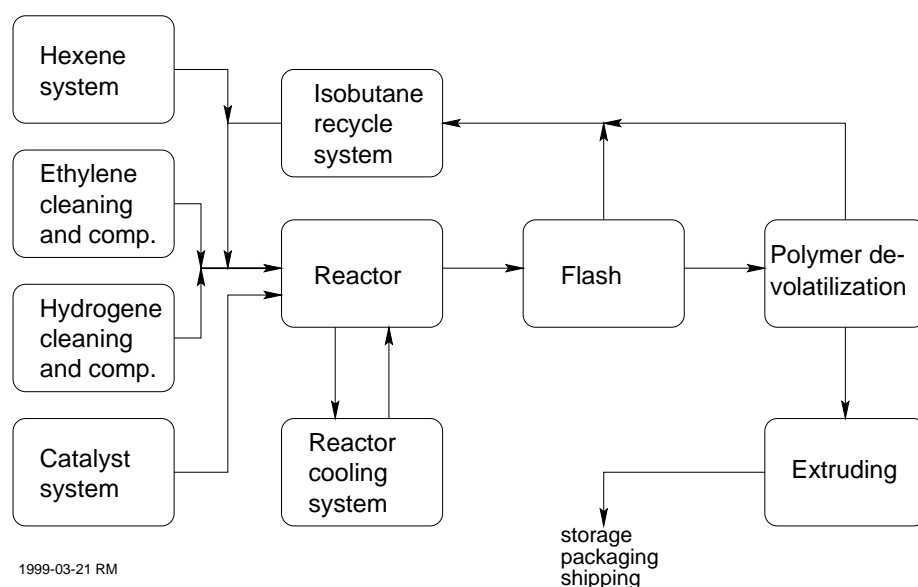


Figure 1.2: Flow-sheet of the Rønningen HDPE process

After the “flash tank”, remains of hydrocarbons in the polymer are removed. It is first led through the “powder drier”, a large horizontal cylinder with a center shaft on which a series of blades are mounted. These blades lifts and shuffles the polymer towards the end of the drier. Here the polymer falls by force of gravity into the “purge tank”, where the polymer is purged with heated nitrogen. The “purge tank” and “powder drier” are separated by two valves that are opening and closing sequentially (the “sequence valves”).

When the polymer is free from hydrocarbons, it is extruded (with additives added). The resulting pellets are then stored, packaged and shipped to customers.

1.4.2 The products

The polyethene produced at the Rønningen HDPE plant is essentially linear in structure, as shown in Figure 1.3. This section gives some rather simplified models of relation between polymer structure and physical properties, but they should be appropriate for the problems discussed in this thesis.

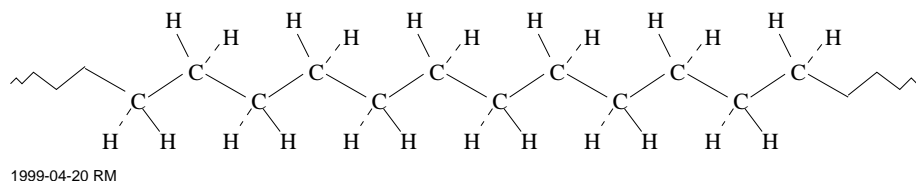
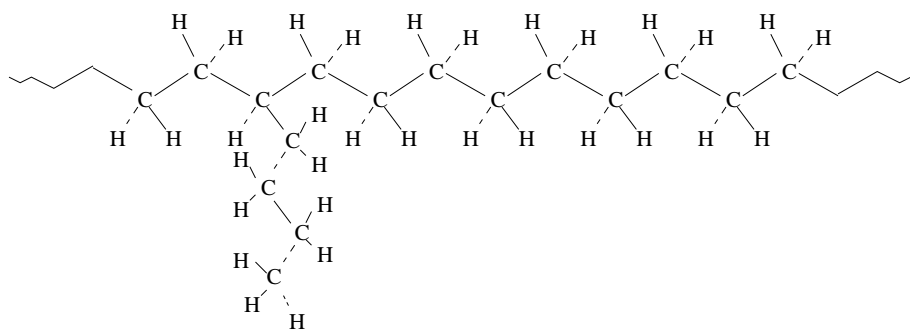


Figure 1.3: HDPE polymer structure

The two main physical properties of the polymer used for reactor control and product classification, are density and Melt Flow Rate (MFR) (see Appendix D). Density ranges from 934 kg/m³ to 961 kg/m³, with MFR values from 0.2 to 6 (190°C/2.16 kg), and from 2 to 96 (190°C/21.6 kg).

The addition of 1-hexene as a co-monomer lead to an increasing amount of chain-branches. This gives products with lower density. The inclusion of 1-hexene is shown in Figure 1.4.



1999-04-20 RM

Figure 1.4: HDPE polymer structure with chain-branch

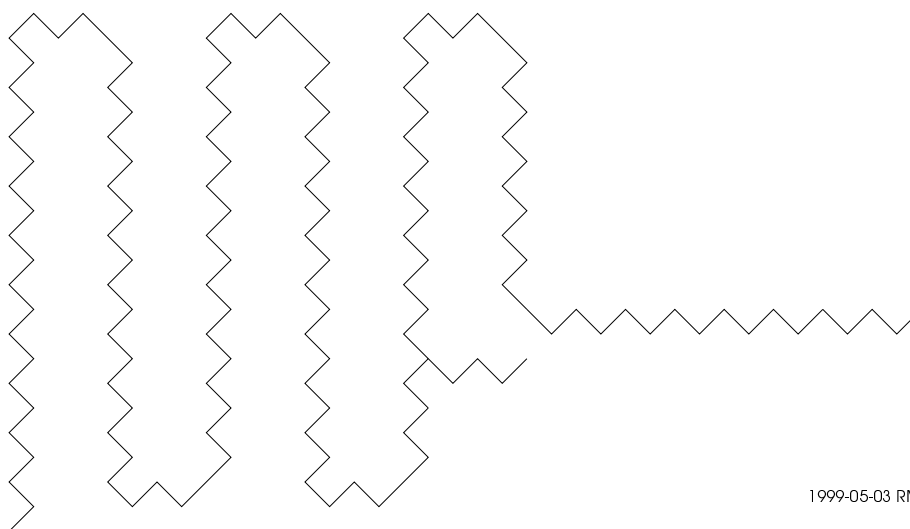
The polymerisation is ended with a termination. Two possible polymer terminations (methyl and ethenyl) are shown in Figure 1.5.



1999-04-20 RM

Figure 1.5: Two possible polymer terminations, methyl and ethenyl

A rather simple and straightforward model is sufficient to explain the relationship between density and polymer structure; the polyethene molecule is partly crystalline, folded back and forth in sharp angles [Boenig (1966)]. The co-monomer chain-branches disrupts these folded crystalline parts.¹ This is shown in Figure 1.6. More chain-branches lowers the polymer density.



1999-05-03 RM

Figure 1.6: Polymer with chain-branch

The MFR property may be viewed as a point on a viscosity curve. It is measured when a constant temperature and pressure is applied on the polymer. MFR is

¹Other parameters like crystallization temperature and time also influence the degree of crystallinity.

largely dependent on the weight-average molecular weight and molecular weight distribution ²[Boenig (1966)], and to a lesser extent of number of chain-branches. It is important to note, though, that products with different molecular weight distributions may have the same MFR value (but different viscosity curves).

The product specifications for all products analyzed in this thesis are given in Appendix B, together with the type of catalyst used.

1.5 The Rønningen on-line installation

The two NIR spectrometers at the Rønningen HDPE plant were first started up on June 26, 1998. This section gives a brief description of the spectrometer measuring on HDPE powder.³

The spectrometer is a *Luminar 3030* from Brimrose Corp. of America. The wavelength selector on the *Luminar* spectrometers is a so-called *Acousto-Optic Tunable Filter* (AOTF). This is essentially a TeO_2 crystal, with a variable Radio Frequency (RF) applied. The crystal acts as a filter, selecting wavelengths that correspond to the applied RF. A principle drawing of the AOTF is shown in Figure 1.7. The advantages of using an AOTF is that it is extremely fast (the wavelength access time is less than $250\mu\text{s}$), and that it is a solid-state device with no moving parts [Brimrose (1999)].

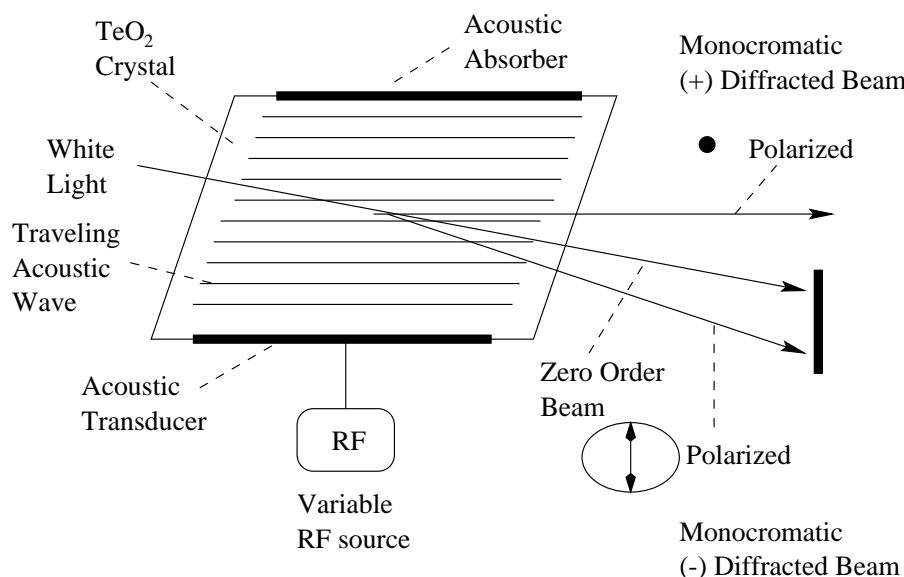


Figure 1.7: Principle drawing of the AOTF crystal

A 35W Tungsten/halogen lamp is the source of radiation, and the AOTF filters the outgoing beam. There are two *InGaAs* detectors in the spectrometer, one for internal reference and one for sample measurements. In normal operation, the internal reference is subtracted from the sample measurements, thus compensating for short term fluctuations in the radiant output. A polystyrene reference may also be inserted into the reference beam. It may be used for internal diagnostics of the spectrometer, and for calibrating the AOTF. A principle drawing of the spectrometer is shown in Figure 1.8. The spectral resolution

²This is a simplified model which may not be true for e.g. bimodal products (not produced at the Rønningen HDPE plant).

³In the remains of this thesis, the spectrometer measuring on HDPE powder is referred to as "the spectrometer".

is 5-10 nm in the spectral range from 1200 nm to 2200 nm, but it is interpolated in software to give a resolution of 1 nm.

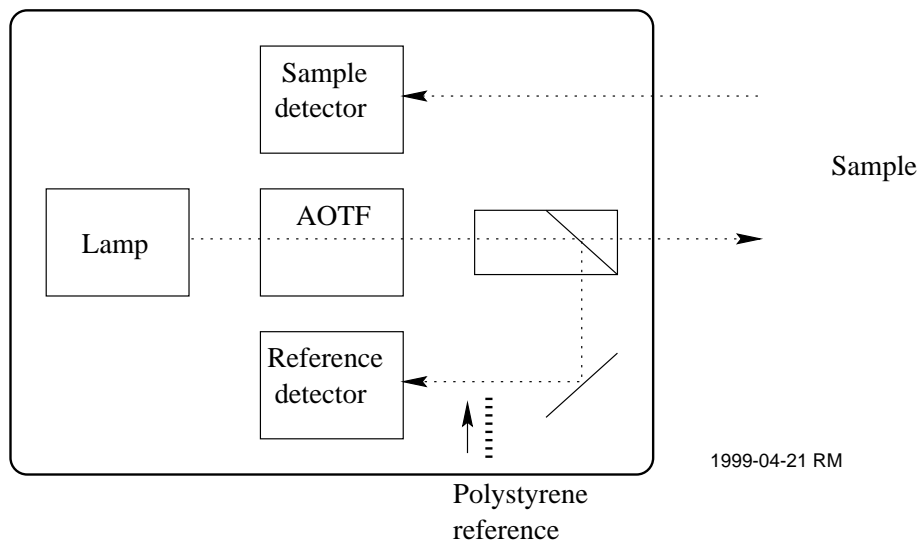


Figure 1.8: Principle drawing of the NIR spectrometer

The spectrometer is located between the “powder drier” and the “purge tank” (see Section 1.4.1). A sketch showing the approximate location is given in Figure 1.9.

The spectrometer beams into the pipe through a small sapphire window, measuring the diffuse reflectance from the process stream. This is shown in Figure 1.10. The HDPE powder flows past the window, in a gaseous hydrocarbon atmosphere. The spectrometer optics (the optical head) is located near to the window, while a control PC is located in a separate box. Its role is to control the RF source, process the data acquired and provide for remote access through a modem or ethernet connection.

There is a free space between the spectrometer and the process pipe of approximately 7,5 cm. The free space is shielded (but not completely sealed) by a “bellow” made from a synthetic material.

The intersection of the monochromatic light axis and the optical detector axis is on the surface of the sapphire window (facing the center of the pipe), with a working distance of ± 5 mm.

The spectrometer control PC is connected to a computer in the HDPE computer room, allowing for remote control and simple maintenance tasks. It is also connected to the Distributed Control System (DCS) in the HDPE plant via a Modbus communication protocol.

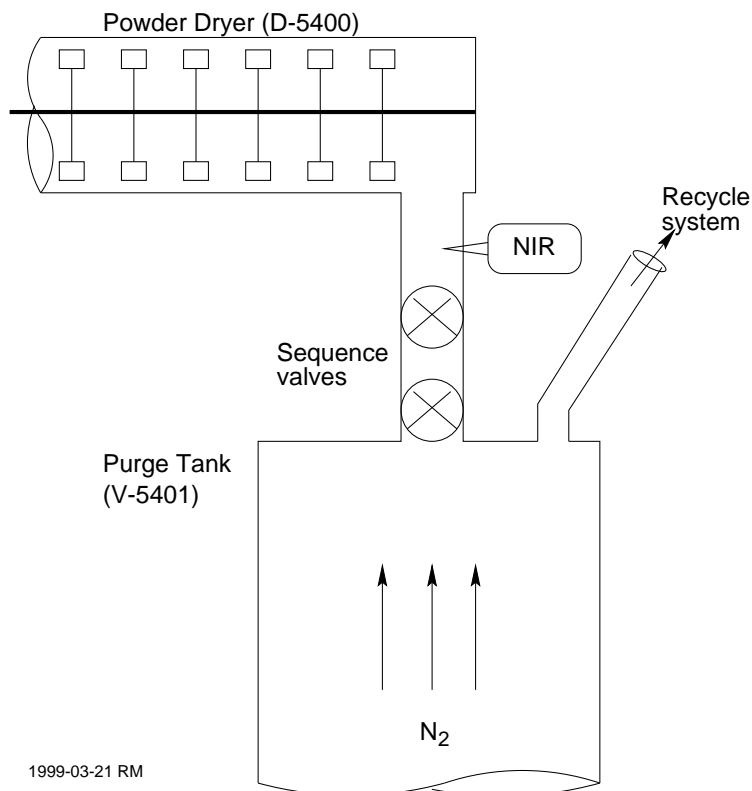


Figure 1.9: Location of NIR spectrometer (scales are not as built)

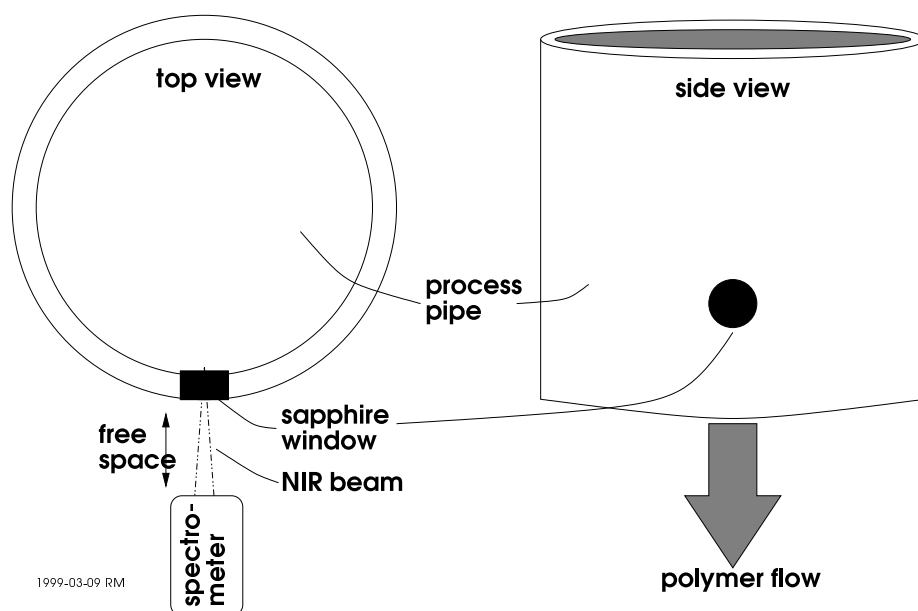


Figure 1.10: Location of sapphire window (scales are not as built)

Chapter 2

Near infra-red spectroscopy in HDPE applications

In this chapter an introduction to near infra-red spectroscopy is given, with special focus on HDPE applications.

2.1 Basics of infra-red spectroscopy

The infra-red region of the electromagnetic spectrum encompasses radiation with wavelengths from 780 nm to 1000 μm . Figure 2.1 shows the electromagnetic spectrum, with the location of the different spectral regions.

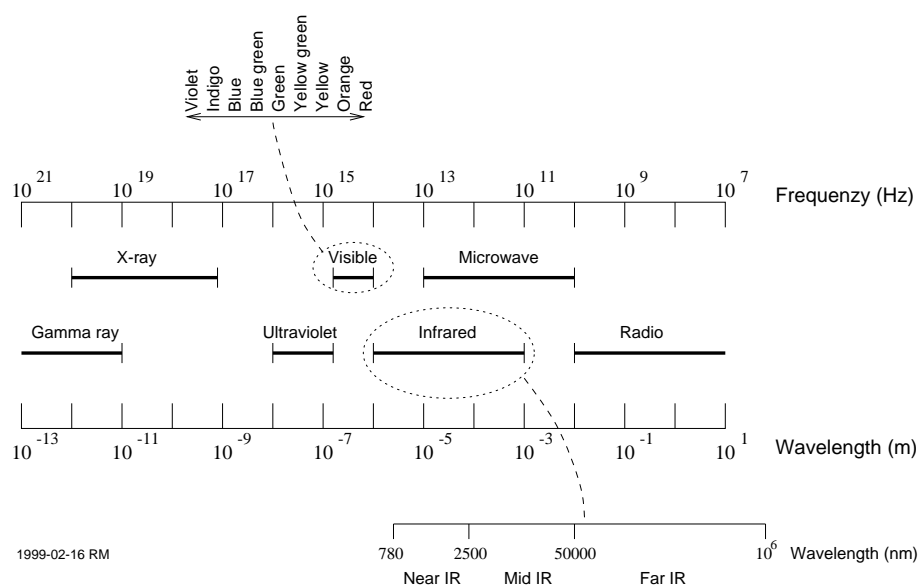


Figure 2.1: The electromagnetic spectrum

Molecular infra-red spectra arise from interaction with molecular species and the infra-red radiation. These interactions may be absorptions, emmissions or reflections, and can be rationalized by assuming that all arise from various changes in energy brought about by transitions of molecules from one vibrational or rotational state to another [Skoog et al. (1998)].

Molecular absorption spectroscopy is based on the measurement of the transmittance T or the absorption A , and may be represented by the equation:

$$A = -\log T = \log \frac{P_0}{P} = \epsilon bc \quad (2.1)$$

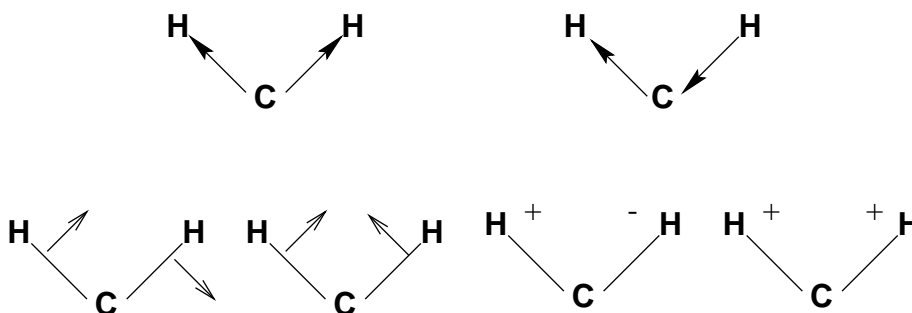
where P_0 and P refer to the power of radiation before and after passing through the analyte, ϵ is the molecular absorptivity, b is the path length and c is the absorbing analyte concentration. This is commonly known as *Beer's law*.

In order to absorb energy, a molecule must undergo a net change in dipole moment as a consequence of its vibrational or rotational motion. Only under these circumstances can the alternating electrical field of the radiation interact with the molecule, and change the amplitude on one of its motions.

Consider for example the charge distribution around a $C-H$ bond. It will not be symmetric, due to the difference in electron density around the atoms. Thus the $C-H$ bond has a dipole moment. As the $C-H$ bond vibrates, a fluctuation in the dipole moment occurs, and a field is established that can interact with the electrical field associated with radiation. If the frequency of the radiation exactly matches a natural vibrational frequency of the bond, a net change of energy takes place. The result is a change in the amplitude of the bond vibration.

For small molecules it is easy to identify the different rotational or vibrational modes that are associated with specific energy absorptions. For larger molecules, identification of these modes are more complex. This is both due to the large number of vibrational centers, and to the fact that interaction may occur among several centers.

In solids, such as HDPE, rotation of the molecule is highly restricted. Thus only vibrational and deformation modes will occur. The possible vibrational and deformation modes for CH_2 (methylene) are shown in Figure 2.2.



1999-04-30 RM

Figure 2.2: Possible vibrational and deformation modes in CH_2

Homonucleous species such as N_2 or O_2 do not have any change in their dipole moment during rotation or vibration, and therefore will not absorb infra-red radiation.

Three mid-IR transmission spectra are shown in Figure 2.3. These are acquired on HDPE produced on three different catalysts; Chromium oxide, Metallocene and Ziegler-Natta (the latter type is not produced at Rønningen). The strong band around 2900 cm^{-1} is due to various $C-H$ stretching modes. The band around 730 cm^{-1} have origins in the crystallinity of the polymer.

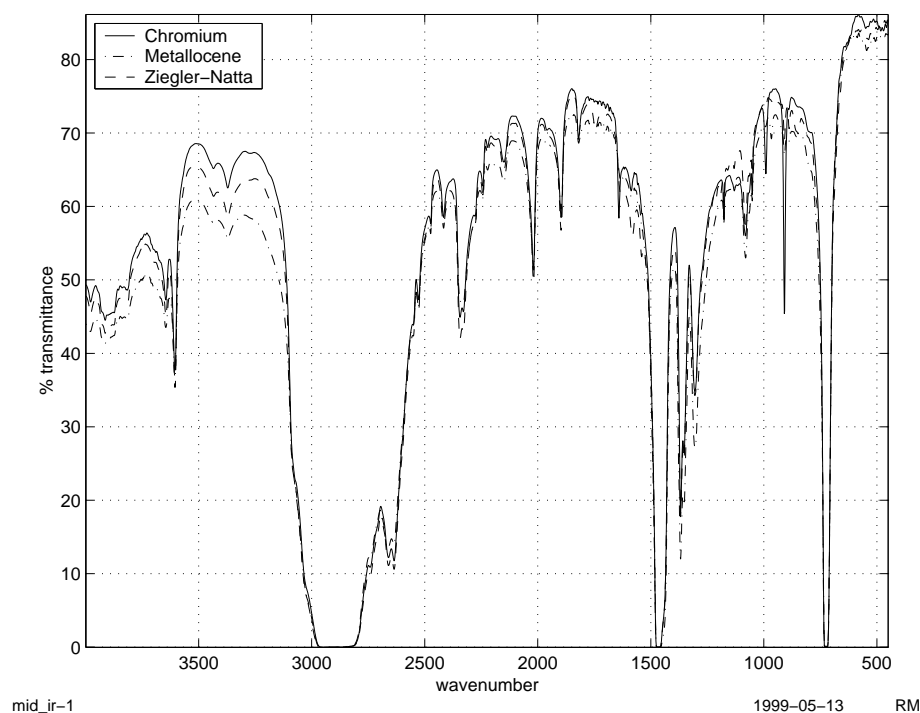


Figure 2.3: Mid-IR transmittance spectra acquired from HDPE produced with three different types of catalysts

These three types of HDPE can easily be identified by looking at the region from 1000cm^{-1} to 900cm^{-1} , a detail is shown in Figure 2.4. The difference here is due to the $C=C$ bonds and configurations (ethenyl {909 and 991}, vinylidene {890}, trans-vinylidene {965}) present in HDPE.

For good introductions to infra-red spectroscopy, see [Skoog et al. (1998)] or [Kemp (1991)].

2.2 Introduction to near infra-red spectroscopy

The near infra-red spectral region is commonly defined to be the part of the electromagnetic spectrum range from 780 nm to 2500 nm [Skoog et al. (1998)]. Absorption bands in this region are overtones or combinations of fundamental stretching vibrational bands that occur in the mid-IR region. Because of this, the molecular absorptivities are low.

In mid-IR spectroscopy the absorption peaks are relatively narrow and well defined. This makes it suitable for qualitative analysis, and also for quantitative analysis using only one or a few absorption frequencies and simple relations like Beer's law. Multivariate methods are (of course) also widely used.

In the NIR region, the overtone and combinational bands are broad and overlapping, making it hard to use for both qualitative and quantitative analysis. Because of the collinearity and lack of selectivity in the NIR region, it is necessary to use many absorption frequencies and multivariate regression techniques like PCR or PLSR. Techniques like Multiple Linear Regression (MLR) will fail on NIR spectra due to the collinearity in the data (redundant variables must be eliminated prior to regression).

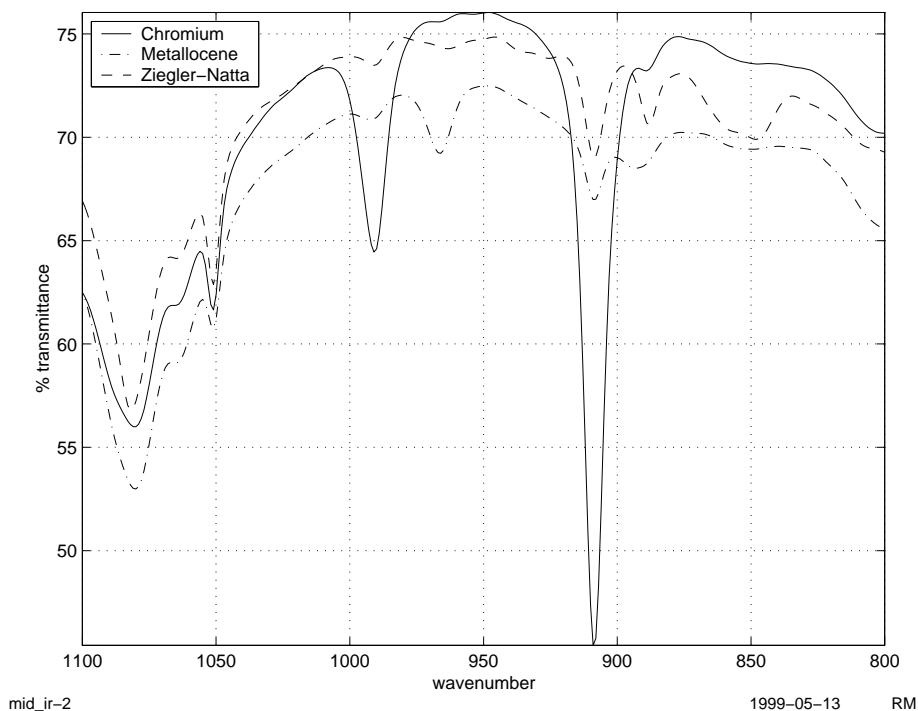


Figure 2.4: Difference in mid-IR spectrum due to catalyst

Despite these drawbacks, NIR spectroscopy is gaining more and more attention, particularly for on-line installations. Some of the benefits of using NIR spectroscopy, are [McLennan and Kowalski (ed) (1995)]:

- Low sensitivity allows direct measurements, even on concentrated process streams (no dilution of the sample is necessary)
- The shorter NIR wavelengths reflect more efficiently than mid-IR radiation, suitable for reflectance applications
- NIR radiation can be transmitted efficiently on relatively low-cost fiber-optics

Diffuse reflectance is often used to obtain near infra-red spectra directly on powder samples, with a minimum of sample preparation. Diffuse reflectance is a complex process that occurs when the radiation penetrates the surface layer of the particle and excites vibrational modes. The radiation is then scattered in all directions. Diffuse reflectance is accompanied with specular reflectance, where the radiation is reflected directly on the surface of the sample. The angle of reflection from specular reflectance will be identical to the incident angle of the radiation [Skoog et al. (1998)].

Diffuse reflectance serves as the basis in reflectance spectroscopy. Spectrometers (like the one installed at Rønningen) will then be designed in such a way that as little as possible of the specular component is detected [Brimrose (1999)].

Reflectance data is often expressed in terms of percent reflectance, analogous to transmittance in absorption spectroscopy [Skoog et al. (1998)]:

$$\%R = \frac{I_s}{I_r} \times 100\% \quad (2.2)$$

where I_s is the intensity of the beam reflected from the sample and I_r intensity from a reference standard.

2.3 Assignment of NIR bands in HDPE

The overtone bands in the NIR region may easily be calculated as integer multiples of the wavenumber where a fundamental vibrational mode absorbs energy. Thus for a peak at 2890 cm^{-1} , the first overtone might be expected at 1730 nm and the second overtone at 1153 nm . However, several bands may be present simultaneously because structural differences within the HDPE macromolecules will give small shifts in the wavelengths. Assignments of some NIR absorption bands are given in Table 2.1. The assignments were found studying linear low density polyethene (LLDPE), but it is assumed that they apply to HDPE also.

Table 2.1: Assignments of NIR bands in LLDPE [Shimoyama et al. (1998)]

Bands (nm)	Assignments
1374	2 x C-H stretch + C-H deformation (CH3)
1392	2 x C-H stretch + C-H deformation (CH2)
1416	2 x C-H stretch + C-H deformation (CH2)
1542	(CH2)
1634	(CH3)
1698	C-H stretch first overtone
1710	(CH2)
1728	C-H stretch first overtone (CH2)
1764	C-H stretch first overtone (CH2)

In addition to the assignments given in Table 2.1, the peak at 2314 nm is probably a first overtone $C-H$ deformation (at 1460 cm^{-1}). The range from 2200 to 2440 also contain various methyl and methylene combination bands.

It is also possible (in theory) that the different ethenyl bands (shown in Figure 2.4) and the band related to crystallinity (around 730 cm^{-1}) have detectable overtone bands in the NIR region, thus making it possible to discriminate between products produced with different catalysts. In [Miller (1993)] a band at 2318 nm is reported to be related to crystallinity in HDPE.

In [Lambert et al. (1995)] it is suggested that crystallinity bands should be avoided when calibrating the NIR instrument for density predictions on HDPE powder. The arguments for this is that although density and crystallinity are strongly correlated, the relationship can be modified by operating conditions in the plant (temperature, catalyst etc.).

In Figure 2.5 a typical NIR spectrum acquired from the powder spectrometer at Rønningen is shown. The bands given in Table 2.1 are marked with an asterisk in the plot.

2.4 Relation between HDPE polymer structure, density and NIR spectra

An introduction to the Rønningen HDPE products was given in Section 1.4.2. The models given there found the basis for the following.

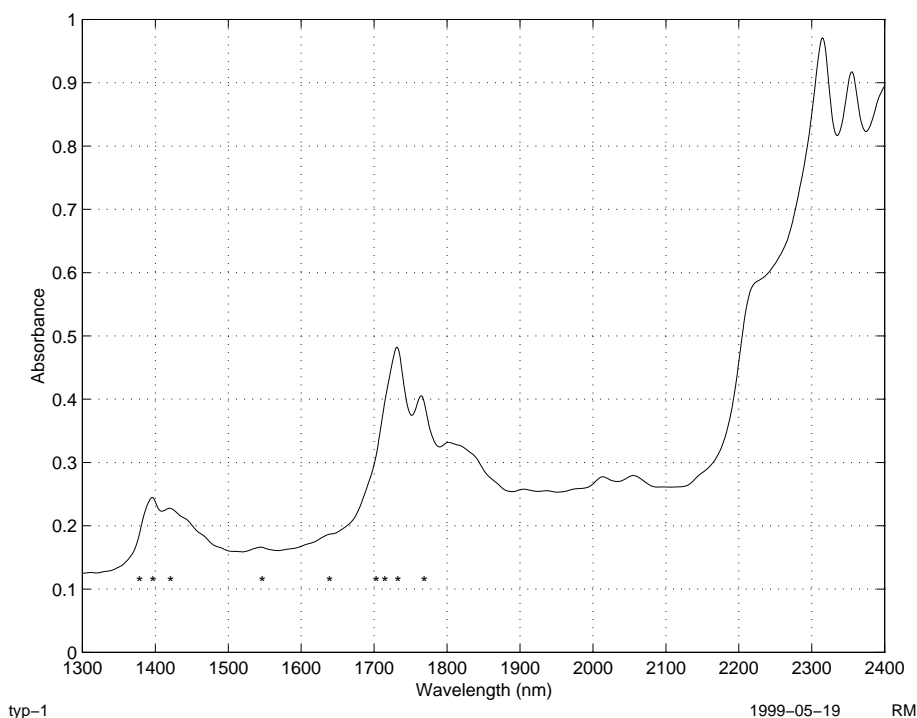


Figure 2.5: Typical NIR spectrum acquired from HDPE powder (on-line analyzer, Rønningen). Asterisks mark expected overtone bands.

More chain-branches will give an increased concentration of methyl groups. Since the NIR spectrum carry various C-H overtones and combination bands, one might deduce that density can be found from the spectra as the CH_3 concentration. Main-chain methyl will have absorption bands slightly different than chain-branch methyl. More chain-branches will also increase the concentration of CH-groups. See [Tosi and Pinto (1972)] for a good discussion on how molecular structural properties affects the functional group absorptivities.

Absorption bands (and possibly also band shifts) related to crystallinity may also play a role in the determination of the polymer density.

The relationship between co-monomer contents and density is non-linear, with density reaching a limit as more co-monomer is added. This suggest that one might experience non-linearities when regressing the NIR spectra onto density. The non-linear relation is illustrated in Figure 2.6, where density is plotted against hexene content in the “flash gas”. The data is collected from HDPE plant control logs, and include only chromium catalyst based products. The function $937 + \frac{20}{e^x}$ (found by trial-and-error) is fitted through the data.

2.5 Relation between HDPE polymer structure, MFR and NIR spectra

As explained in Section 1.4.2, the melt flow rate (MFR) is a point on a viscosity curve, where pressure and temperature are held constant. MFR is largely dependent on polymer chain-length distribution.

Shorter chain-lengths will increase the methyl (or ethenyl) concentration (see Figure 1.5), due to a higher number of terminal groups. It is possible that the

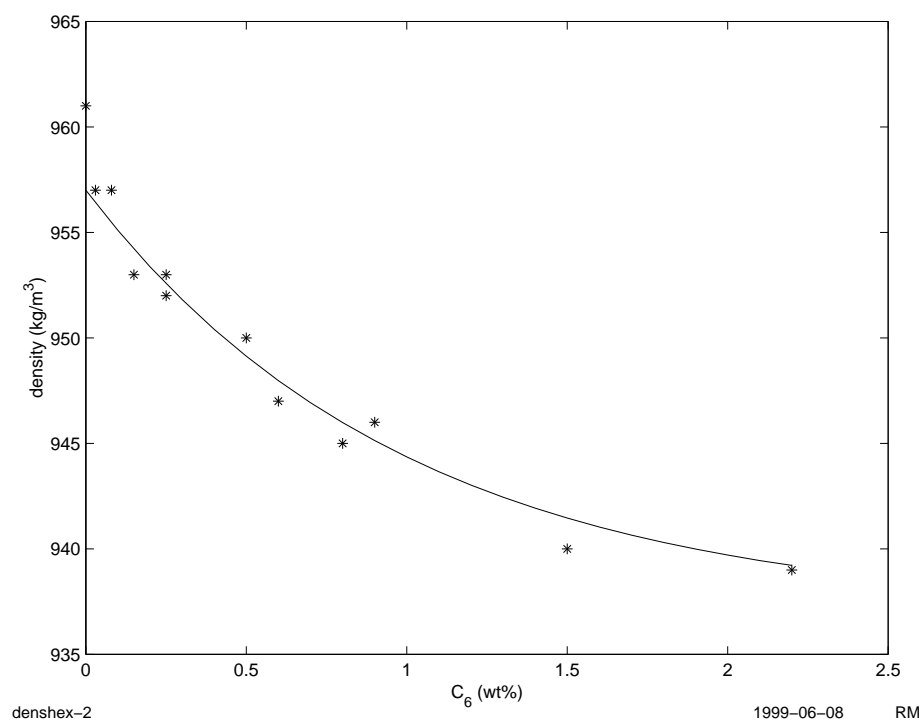


Figure 2.6: Density and co-monomer content

main-chain methyl have slightly different absorption bands than the methyl on the chain-branches, due to the different configuration. This suggests that information on molecular weight may be found in the NIR spectra. The concentration of main-chain methyl is much lower than chain-branch methyl, though. An ethenyl termination may give absorption bands in the NIR spectrum, and this will be unique to main-chain termination (chain-branches always end with a methyl group).

There may be some sort of relation between MFR and particle size. Since there is a well known relation between particle size and scattering effects (scattered radiation increases with particle size [Skoog et al. (1998)]), this may be exploited for calibration purposes. This is further discussed in Section 3.2.2.

[Hansen and Vedula (1998)] reports successful NIR spectroscopy calibrations for MFR on poly(ethene vinyl acetate), but measurements are done when stressing the polymer (with pressure and temperature). A successful MFR calibration was also reported in [Henriksen (1993)], but the objective in that report was to test an instrument, not to develop a method for doing MFR predictions using NIR spectroscopy. The tests carried out in [Henriksen (1993)] were done using diffuse reflectance spectroscopy on specially treated powder samples in a laboratory, with MFR $190^\circ\text{C}/2.16\text{ kg}$ values in the range 0.44-1.8. No reports have been found confirming that MFR predictions may be done under the conditions given by the sampling system under study.

2.6 Baseline features

Samples that are measured using diffuse reflectance often exhibit significant differences in the spectra due to the non-homogeneous distribution of particles

[PLSplus/IQ users guide]. Other factors like the effective sample size and specular reflectance also give response in the NIR spectrum that is not due to absorptivity by the polymer. These responses are often called *baseline features* [Beebe et al. (1998)].

In Figure 2.7 three possible types of baseline features are shown. Some suggestions for the origins of these features, are:

- Multiplicative effects might arise from differences in the effective sample size (variation in concentration).
- An offset may be due to specular reflectance.
- Particle size effects may give a baseline slope.

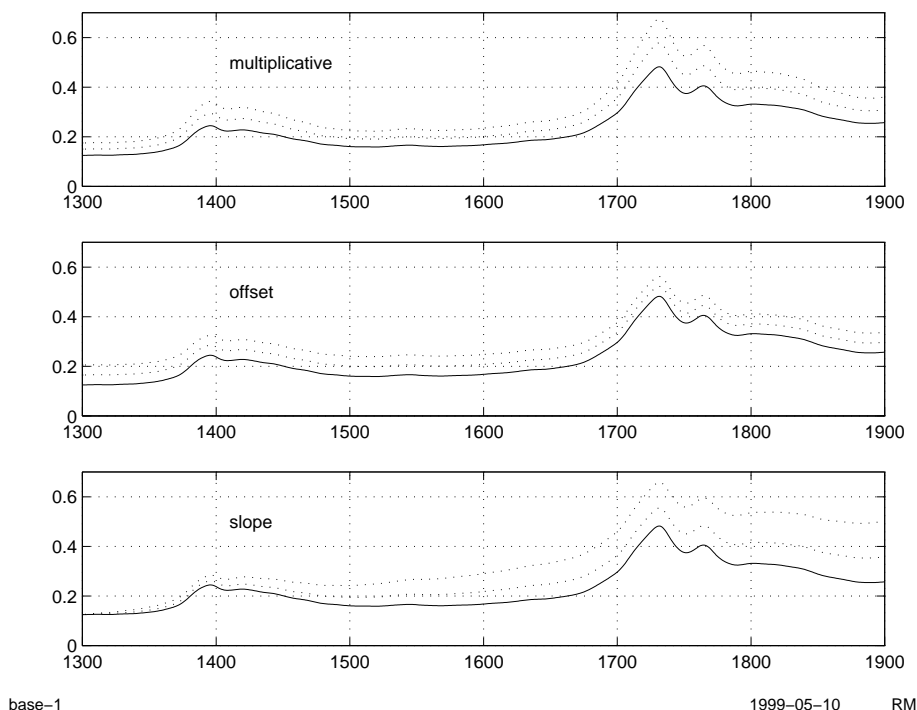


Figure 2.7: Baseline features

2.7 Summary and conclusion

Near infra-red spectroscopy applications appears to be ideal for on-line analysis; it is a fast and non-destructive technique with a good signal-to-noise ratio. Low sensitivity makes it possible to do measurements directly in concentrated process streams.

The relation between polymer density and the NIR spectrum looks simple and direct; a higher co-monomer content in the polymer lowers the density and give origin for an increased methyl content. Methyl (and methylene) is known to have overtone absorption bands in the NIR spectral region.

The relation between the MFR property and the NIR spectra, is not as clear as for density. It might be possible to calibrate the NIR instrument for MFR predictions through detection of main chain methyl and ethenyl terminations, possibly also exploiting very indirect relations like particle size.

Chapter 3

System analysis

This chapter gives an in depth analysis of the system under study, focusing on what gives response in the NIR spectra. A general description of the system was given in Section 1.5.

3.1 System definition

For the purpose of this analysis, *the system* is considered to be:

The system is the process pipe (and its contents) from the outlet of the “powder drier” (D-5400) to the top of the first sequence valve (HV-54004). Also included in the system definition is the sapphire window and the free space between the process pipe and the spectrometer optical head.

Observe that the spectrometer itself is not included in this system definition, and no analysis of the noise-level in the instrument has been done. Refer to Section 1.5 for some details of the spectrometer. Good diagnostics for the instrument are provided through the polystyrene reference, but there is no way to enter a standard into the sampling system. Thus it is important to understand what parameters in the system give response in the NIR spectrum.

It is also necessary to define what is considered to be the sample:

The sample is the polymer powder that passes the sample window during the acquisition of one stored spectrum. This, in turn, may be the mean spectrum of several hundred spectra. The sampling time is then the time it takes to acquire the spectra used for one average.

These definitions are the basis for the following discussion.

3.2 Polymer contribution in the NIR spectrum

The HDPE polymer pass the system in the form of powder particles (made up from many polyethene molecules). For an explanation of how the powder enters and leaves the system, see Section 1.4.1. This section discusses how the polymer gives contributions to the NIR spectra.

3.2.1 Structural contributions

In Section 2.2 and Section 2.4 it was explained how the HDPE polymer structure contributes to the NIR spectra, and band assignments were given in Section 2.3. For the purpose of calibrating the spectrometer for density predictions, this is probably the only signal of interest. All other contributions to the NIR spectra may then be considered to be noise¹. When calibrating for MFR, other responses may also be interesting (discussed in Section 3.2.2).

3.2.2 Particle size and porosity

It is known that scattered radiation increases with particle size [Skoog et al. (1998)]. Light scattering variations in diffuse reflectance can give multiplicative interferences [Martens and Næs (1991)].

Particle size distribution data, originally acquired for a settling efficiency study at the Rønningen HDPE plant, has been analyzed to find correlations between size distribution and type of catalyst used [Bjåland and Helleborg (1997)]. Observe that this analysis does not include all products produced at the Rønningen HDPE plant.

In this analysis, the parameters D10, D50, D90 and bulk density (loose) was used for characterization of the particles. The data is given in Appendix E. When using bulk density, some information on porosity is also included. The score plot from a Principal Component Analysis (PCA) [Wold et al. (1987)] is shown in Figure 3.1, and the corresponding loading plot is given in Figure 3.2. The D-values constitutes the major variations in the data (PC1).

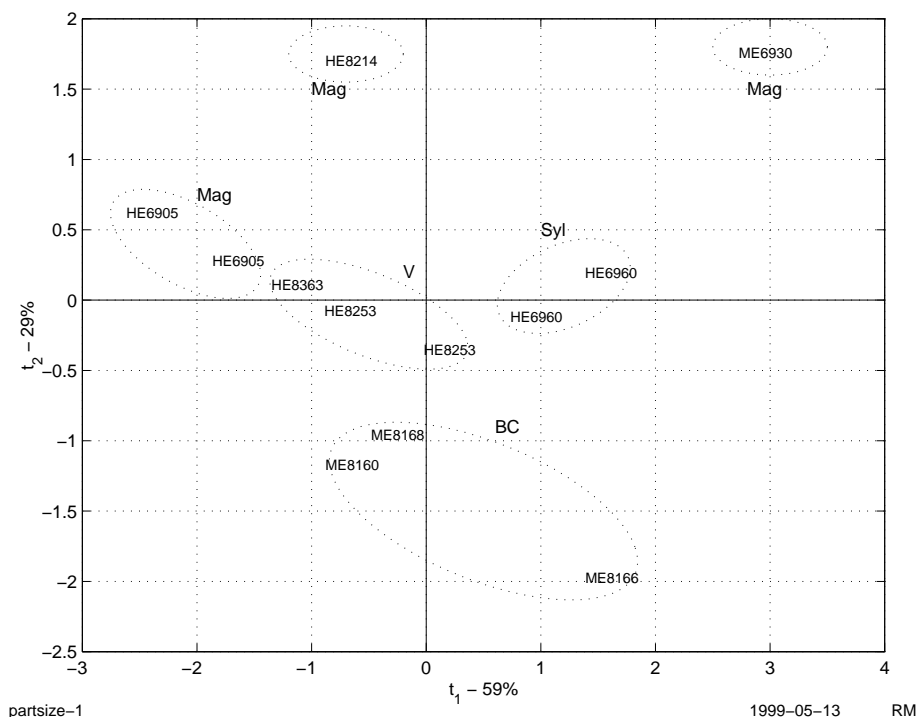


Figure 3.1: Characterization of particle size by PCA. Product names are used as plot symbols, type of catalyst is given outside the ellipses.

¹Observe that the term noise does not mean “white noise” in this context

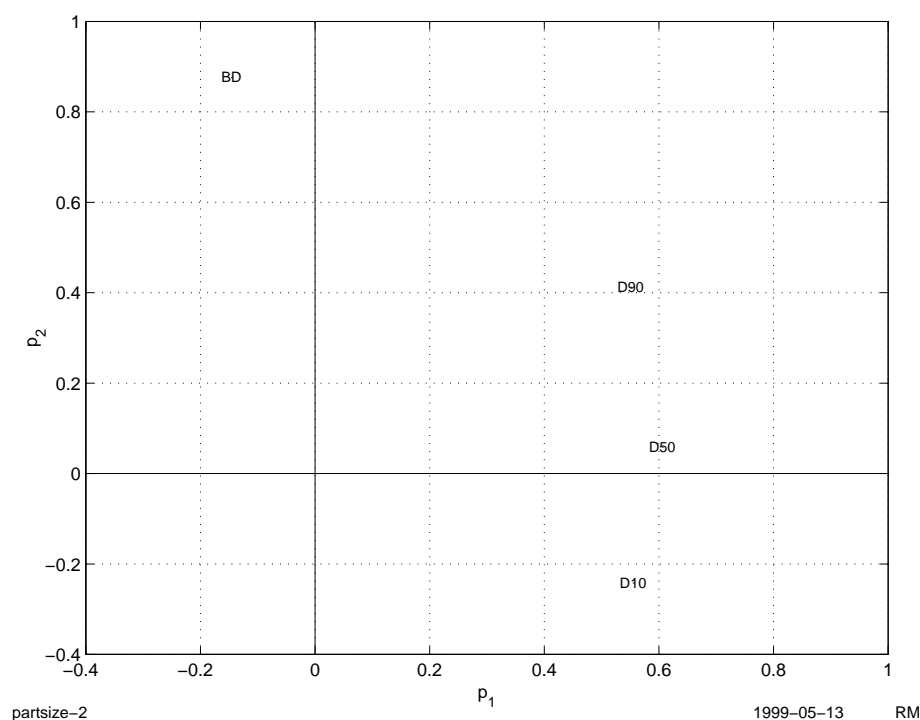


Figure 3.2: Loading plot, particle size analysis.

From Figure 3.1 it looks like two Magnapore products, HE8214 and ME6930, stand out. A closer study of the conditions under which ME6930 was produced shows that this product is produced with an extremely low reactor temperature. It is also known that the ME6930 particles are very heterogenous [Almquist and Follestad (1986)].

The HE8214 sample is also located a little bit away from the two HE6905 samples, although they are all produced with a Magnapore catalyst, and at about the same reactor temperature. One explanation might be that the Magnapore catalysts used are not exactly the same, but other process parameters might also influence the particle characteristics. It has also been reported that the polymer particles will inherit the geometry of the catalyst particles [Almquist and Follestad (1986)].

It is known that the powder particles experience some pulverization inside the HDPE reactor (due to shearing stress). The pulverization probably also occur when the “sequence valves” are emptied. It is also known that products with high MFR (low molecular weight (MW)) are more easily pulverized, and thus give smaller powder particles.

In [Almquist and Follestad (1986)], weight average particle diameter is reported to be a function of:

- Catalyst activation temperature
- Catalyst type
- Reactor temperature
- MFR/MW

The results in [Almquist and Follestad (1986)] are based on a study of chromium catalyst based products only.

As a consequence of this, particle related scattering effects in the NIR spectrum is probably a function of catalyst type, catalyst activation temperature, reactor temperature and other process parameters.

Catalyst type and reactor temperature are also the most important variables for controlling MFR (in addition to H₂ feed), so one might hope that it is possible to exploit the NIR scattering effects for MFR calibration purposes (in addition to methyl and ethenyl absorption bands). By studying the MFR specs (given in Appendix B) and the location of the different products in Figure 3.1, this relation is not very obvious, though. The relation between MFR and particle size is not well founded, but it may be interesting to test its effects on MFR calibrations.

3.2.3 Specular reflectance

If the polymer passing through the system is to contribute to the absorption spectra, the NIR radiation must penetrate the powder particles and interact with the molecular vibrations (Section 2.2). However, some of the radiation will always reflect directly on the surface of the powder particles. When this reflected radiation hits the detector, it will contain little information of the polymer structure. If no other absorptions occur either (see Section 3.3), the result is an additive contribution to the spectrum.

It was shown in Section 3.2.2 that particle size (and surface) might be a function of catalyst and reactor temperature. It might be suggested that if a particle has a large surface, the probability for specular reflectance is bigger than for a particle with a small surface. If this holds, specular reflectance effects will also be a function of catalyst and reactor temperature.

3.3 Composition in process pipe

Under normal plant operation, the pipe will probably contain mostly iso-butane in addition to polymer. There will also be some N₂, and probably small amounts of ethene, 1-hexene and hydrogen. Neither N₂ nor H₂ absorb infra-red radiation (see Section 2.1), but iso-butane will probably give a contribution to the absorption bands in the NIR spectrum (CH and CH₃ absorptions).

The radiation will have to pass through the gaseous iso-butane phase twice before reaching the detector, both before and after hitting the sample.

The pressure inside the process pipe systematically varies between 0.5-1.0 bar (approximate values). This is because the “settling legs” are emptied sequentially (see Section 1.4.1). The sequence time (from one pressure peak to another) is about 10-40 seconds, depending on the production rate a.o. The relation between pressure and concentration should be well known (the ideal gas law may be used as a simple model).

In the current setup (spring 1999) the spectrometer scans the sample 900 times, and the mean of these scans are used for analysis. The scanning process takes about 40-50 seconds.

From this it is clear that one scanning sequence will contain one or more pressure peaks. Since the iso-butane concentration is not constant, the system pressure may be an important noise factor.

There are no pressure measurements in or close to the system. Readings from a manual pressure gauge on the top of the “flash tank” was used for this analysis.

The pressure fluctuation is probably somewhat dampened through the process, so the pressure variation from 0.5-1 bar may probably be considered a “worst case”.

3.4 Temperature effects

Temperature changes in the sample might be a cause for response in the NIR spectrum. To investigate this, a large data-set (626 samples) consisting of NIR spectra and system temperature was assembled. It is here assumed that the polymer particle temperature is correlated to the system temperature. The temperature readings are acquired from a PT100 thermo element positioned about 20 cm above the sapphire window.

The temperature interval in the data-set ranged from 70°C to 83°C . This is about what one might expect under normal plant operation, although some products give a system temperature as low as 63°C (based on a study of the sample temperature over more than one year).

The origins of the temperature fluctuations in the system has not been studied thoroughly, but it shows a weak correlation with the reactor temperature and no correlation with the outdoor temperature. It is thinkable that the amount of iso-butane transported with (on and in) the polymer particles is important for the polymer temperature, due to the energy needed for the evaporation process. Energy is also added through steam-tracing in the “flash-tank” and the “powder dryer”.

A calibration model was built using Partial Least Squares Regression (PLSR). A brief introduction to this regression method is given in Section 4.7.2. See also [Martens and Næs (1991)] and [Esbensen et al. (1994)]. The baseline slope and offset was removed prior to the calibration (see Section 4.5.2).

Various strategies for assembling a representative test-set were tested. The validation result varied a lot, depending on how this was done. This made it hard to give reliable conclusions to this analysis.

Using every third object for testing gave exceptionally good validation results, and it was therefore suspected that autocorrelation between the objects gave false results (RMSEC and RMSEP was about the same). The data-set was then split into blocks of five and five samples, using every second block in the calibration set and the remaining blocks in the test-set. The motivation for this was to reduce the autocorrelation between the calibration and test-set objects. The validation results from this strategy was about the same as when using every third object for testing.

To make the calibration and test-set time independent, test-sets of about 200 samples were picked from the beginning and end of the data-set (the objects were sorted on time of acquisition). The results are given in Table 3.1. The goal here was not to build an optimized model for prediction of temperature, but to find structure in the NIR spectra related to temperature.

The validation results are rather different, particularly in that it was possible to use 10 factors in model A without over-fitting it, but only four factors in model B. Predicted/measured plots for the two test-set validated models are given in Appendix F.

Loading-weights for the factors 1 to 6 for model A are shown in Figure 3.3. Little $\tilde{\mathbf{y}}$ variance is captured in the first two factors, and these are probably needed to account for various baseline features. The remaining factors captures

Table 3.1: Validation results, temperature model

Model name	Validation objects	Factors	RMSEC	RMSEP	bias	corr.	X explained (%)	y explained (%)
A	first 200	10	1.16	1.30	0.07	0.76	99.98	77.45
B	last 200	4	0.81	2.06	-0.83	0.61	99.94	85.24

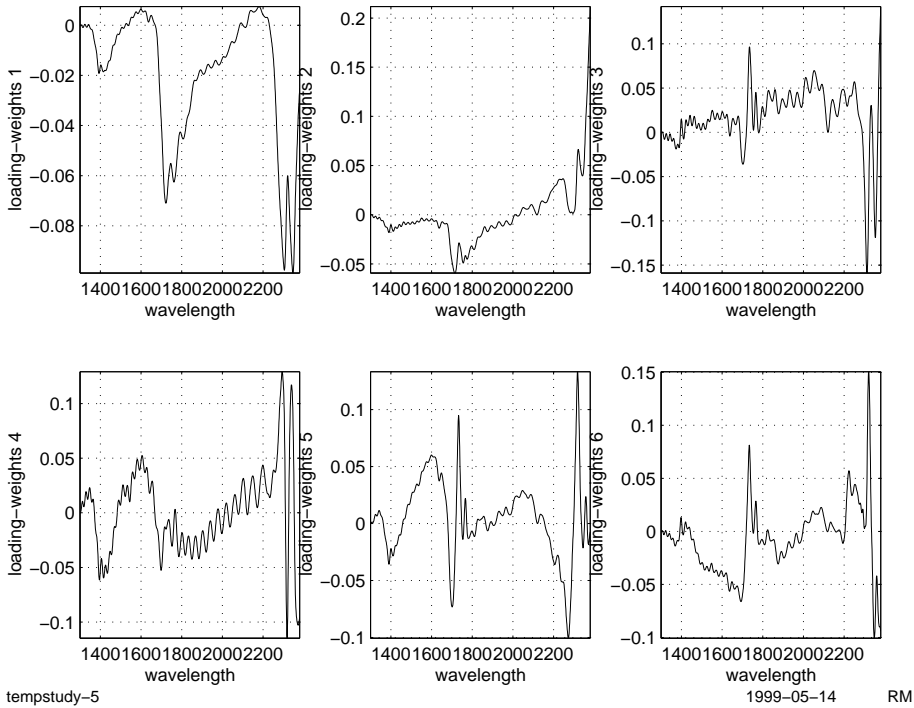


Figure 3.3: Loading weights, temperature-model A

more $\tilde{\mathbf{y}}$ variance, but given the relatively poor correlation and varying validation results for the models, it is hard to interpret these loading weight vectors.

From this analysis it appears that the temperature have some influence on the NIR spectrum, but the relation is weak and unclear. It is likely that temperature changes in the system will have a greater influence on the gaseous phase (isobutane) than the solid phase (polymer).

3.5 Humidity

NIR spectroscopy is known to be sensitive to water, with peaks expected at 1445 nm and 1940 nm.

The Phillips Particle Form polyethene process is extremely sensitive to water (or other species with —OH groups). Thus it may be concluded that no water exists in the sample.

As described in Section 1.5, the free space between the spectrometer optical head and the process pipe is not completely sealed by the bellow. Therefore one might expect that the molal humidity² in the light path is about the same as in the surroundings (the outdoor humidity).

Despite this, no water peaks have been observed (visually) in the NIR spectra (see e.g. Figure 2.5).

3.6 In-sample variations

Studies of variations in physical polymer properties may be done at several different levels:

- The five “settling legs” (Section 1.4) may contain products with slightly different properties, due to the different locations of the “settling legs” on the reactor. The emptying of the “settling legs” is done in a sequence that takes about 1-2 minutes.
- There are particle-to-particle variations in the physical properties, and it may be correlated to particle size or shape.
- There are variations in the physical properties within one single polymer particle.

As shown in Appendix E, a sample may be characterized by a particle size distribution. The discussion in Section 3.2.2 regarding relationship between MFR and particle size may not only be true between product, but also within one sample. For the chromium-oxide catalyst products, there may also be in-sample variations in density that is correlated to particle size.

The intersection of the monochromatic light axis and the optical detector axis is on the surface of the sapphire window (see Section 1.5). Thus only a small fraction of the powder is screened by the NIR spectrometer. If some sort of segregation of the powder occurs during the free fall in the process pipe, the measurements may be biased. This is further discussed in Section 3.11.

²Molal humidity is moles of vapor divided by moles of dry gas

3.7 The sapphire window

The sapphire window is made from a single crystal aluminium oxide. The transmittance characteristics is very flat (and constant) throughout the near infra-red region. Thus, the sapphire window itself should not introduce any problems when calibrating the spectrometer.

3.8 Polymer film on sapphire window

A oscillation signal was first observed in the NIR spectrum in September 1998. Two spectra are studied in this analysis; an “old” spectrum acquired in beginning of August 1998, and a “new” spectrum acquired in mid-December 1998. In both cases the product is ME8168. A detail of two parts of the spectra is shown in Figure 3.4. In this analysis these spectra are referred to as “old” and “new”.

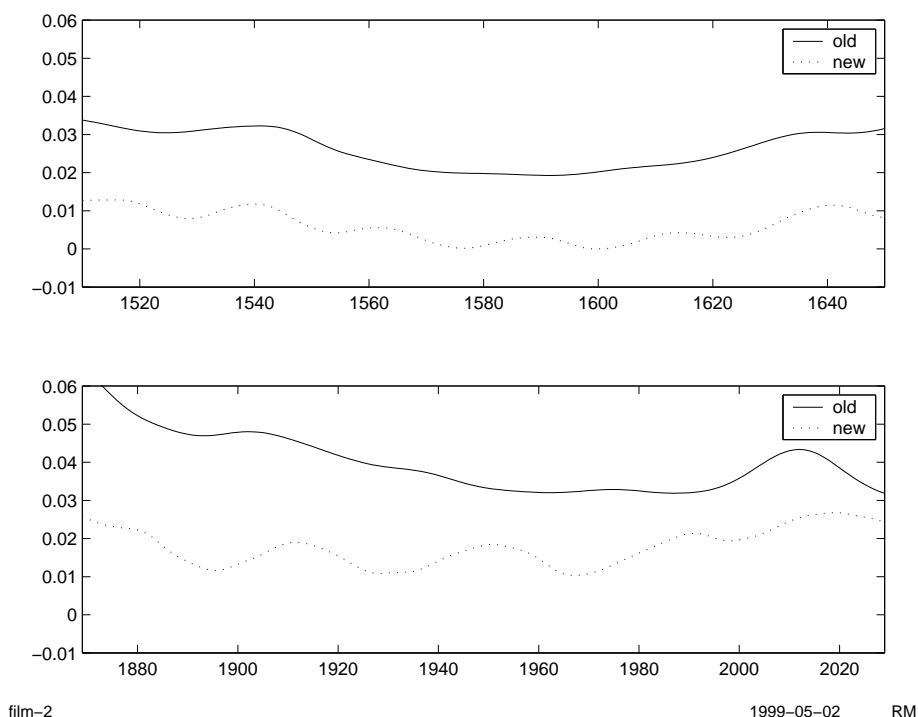


Figure 3.4: “Old” spectrum with no oscillation, and “new” spectrum with oscillation

The oscillating signal in the spectra may be caused by a thin polymer film/layer on the sapphire window. It is known that a thin sample with parallel sides will cause interference fringes (also known as channel spectra) in the spectrum [Griffiths and Haseth (1986)]. In this context, a polymer film on the sapphire window may act as an interference filter (see Figure 3.5).

Interference fringes arise from constructive and destructive interference of internally reflected waves inside the film. The wavelengths of radiation transmitted by the filter, are given by [Skoog et al. (1998)]:

$$\lambda = \frac{2t\eta}{N \cos \alpha} \quad (3.1)$$

$$\Downarrow$$

$$\nu = \frac{N \cos \alpha}{2t\eta} \quad (3.2)$$

where η is the refractive index, t is the film thickness, N is the interference order, α is the angle of the incoming radiation and λ and ν are wavelength and wavenumber respectively. If the angle of the incoming radiation is near perpendicular, then $\cos(\alpha) \approx 1$. For two different wavenumbers, we then have:

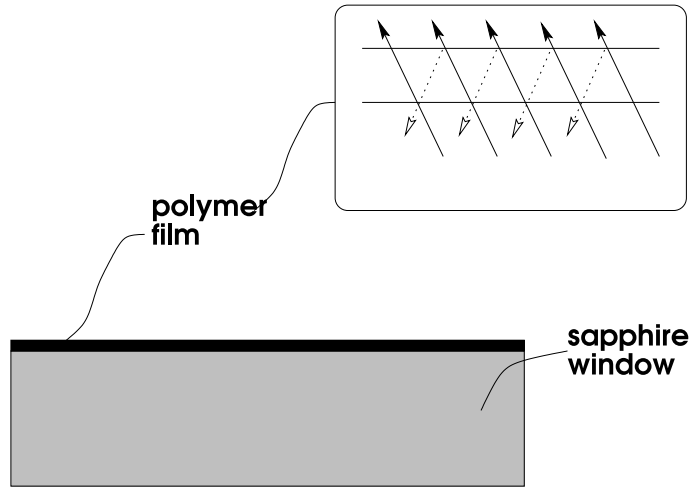
$$\nu_1 = \frac{N_1}{2t\eta} \quad , \quad \nu_2 = \frac{N_2}{2t\eta} \quad (3.3)$$

$$\Downarrow$$

$$\nu_1 - \nu_2 = \frac{N_1 - N_2}{2t\eta} \quad (3.4)$$

$$\Downarrow$$

$$t = \frac{N_1 - N_2}{2\eta(\nu_1 - \nu_2)} \quad (3.5)$$



1999-03-09 RM

Figure 3.5: Sketch of sapphire window with thin polymer film.

The refraction index of polyethylene with density 940 kg/m^3 is 1,52 [Branderup and Immergut (1989)]. By counting the number of peaks within given ranges of the spectra and use this number as $(N_1 - N_2)$, it is possible to calculate the thickness of the polymer film on the sapphire window. From Figure 3.4 the following was found:

Table 3.2: Approximate film thickness

wavelength range (nm)	number of peaks	film thickness (μm)
1530-1650	5	34,6
1900-2000	3	37,5
1870-2030	5	39,0

This procedure of finding the film thickness is not too accurate, but may be used as a rough estimate. The difference in calculated film thickness between 1530-

1650 nm and 1870-2030 nm may be interpreted as an estimate of the uncertainty of this calculation.

In the following, a film thickness of $37\text{ }\mu\text{m}$ is assumed. It is now possible to calculate the wavelengths where the interference fringes are expected to occur.

A comparison of the calculated wavelengths for interference orders 55 to 75 with the “new” spectrum shown in Figure 3.4 gives a fairly good match. In Figure 3.6 expected interference fringes are marked with an asterisk, together with the “new” spectrum.

Laboratory tests³ have strengthened the theory that a thin polymer film might be the cause for the observed oscillations. By applying a $60\text{ }\mu\text{m}$ film on a sample probe, oscillations were clearly visible in the NIR spectrum.

The film thickness on the sapphire window was measured in June 1999, and was found to be $42\pm 5\text{ }\mu\text{m}$.

From this one might conclude that the theory of interference fringes as the cause for the observed oscillating signal is viable. The oscillating signal will have a decreasing frequency throughout the NIR spectrum, as the distance between the interference orders increase.

As a counter-argument, it has been claimed that a possible reflection in the polymer will have an intensity below the detector sensitivity [Brimrose (1999)], and thus cannot be detected. So far, no other theories that might explain the oscillating signal have been put forward.

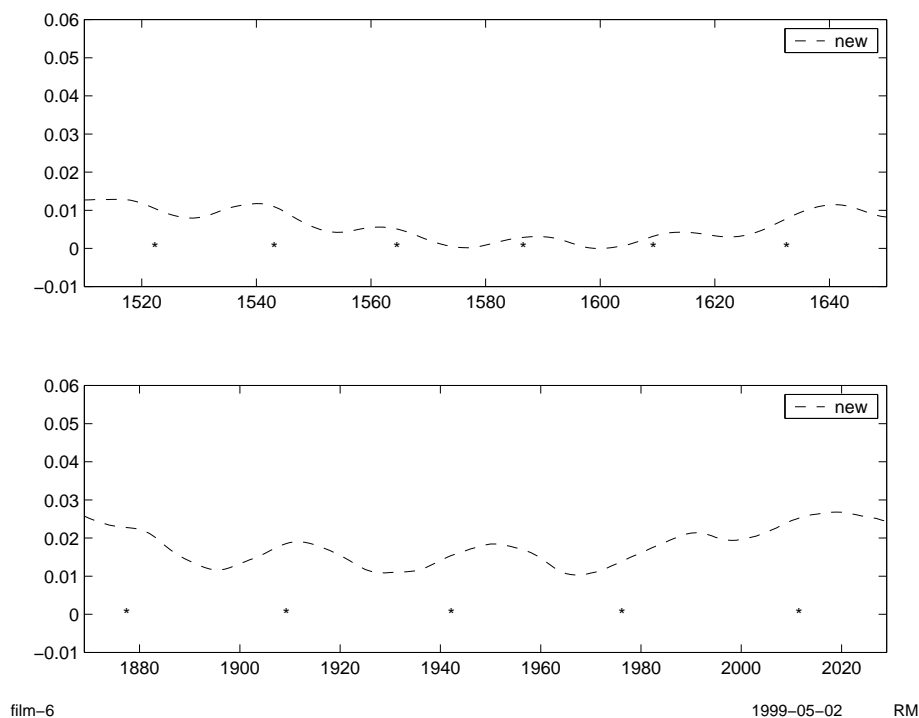


Figure 3.6: Detail of “new” spectrum, expected interference fringes marked with an asterisk.

It has been reported that low density products (ME6930/ME8168) are more prone to have this oscillating signal in their NIR spectra [Seim (1999)].

The current sampling system can not be isolated from the process for the purpose of cleaning the sapphire window without shutting down the production.

³Done in Porvoo, Finland, by Markku Vahteri, Borealis

3.9 Sample concentration

The sample concentration, as presented to the NIR beam, is not constant. Rapid pulsations of polymer powder are probably produced by the “powder dryer” (see Section 1.4). Concentration variations may also be induced as the “settling legs” are emptied sequentially (about every 10-40 seconds). Other parameters may also contribute to a complex polymer flow pattern past the sapphire window.

100 single⁴ reflectance spectra, acquired in rapid succession, are shown in Figure 3.7. As can be seen, the spectrum-to-spectrum variation is huge with some spectra carrying almost no information. It is also interesting to note that the oscillation described in Section 3.8 is very noticeable in the spectra that carry little polymer information.

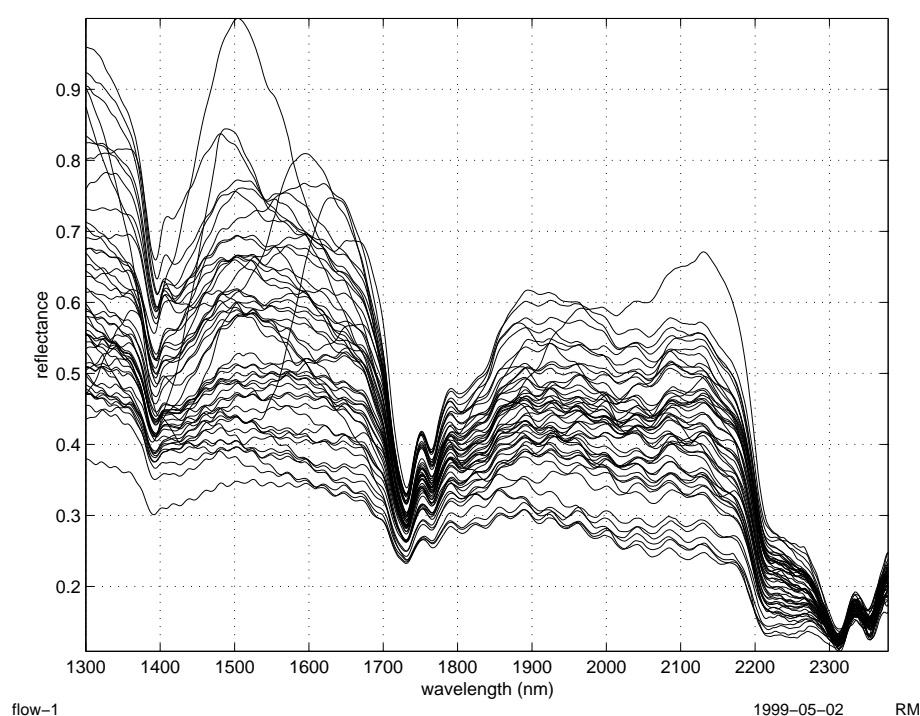


Figure 3.7: Single spectra (reflectance)

Another interesting feature seen in Figure 3.7 is that the single spectra do not only differ in their overall spectral intensity, but also carry different (apparent) absorption bands. The cause for this has not been investigated.

The reason for this spectrum-to-spectrum variation is not completely known, but fluctuating concentration of polymer in front of the sample window is one probable reason. Varying concentration may lead to multiplicative effects in the NIR spectra (see Section 2.6).

⁴These spectra have their origin in one single scan, i.e. they are not made up from an average of many.

3.10 Other sources of contribution to the NIR spectrum

Tests have shown that removing “the bellow” from the free space gives detectable but very small variations to the spectrum.

Since the spectrometer only screens a very small portion of the process stream, the flow pattern inside the pipe is critical for the acquired spectra. It has been tested how the spectral response is when stopping both “sequence valves” (see Section 1.4.1) in open position. This will change both the flow pattern and the composition in the system (more N₂). The result was a radical change in the spectrum above 2300 nm.

3.11 Sampling and measurement errors

Sampling errors arise from the existence of heterogeneity, in one form or another. In [Gy (1998)] it is stated that:

- Heterogeneity is the only state in which a set of material units or groups of units can be observed in practice.
- Heterogeneity is seen as the sole source of all sampling errors.
- A sample is representative when it is taken by a selection method that is both accurate and reproducible.

The last statement implies that sample representativeness is characterized by the absence of bias and an acceptable variance.

According to [Gy (1998)] the only correct method for sampling flowing streams is to take *the whole of the stream for a fraction of the time*.

Reference samples analyzed at the QC laboratory are taken out at the bottom of the “purge tank”. There is a time-lag between this sample location and the NIR sampling system of about 40 minutes (varying with production rate). The estimated time-lag was used when connecting reference measurements to the NIR spectra, but a bias is introduced to the measurements due to the distance between the sampling points and the very roughly estimated time-lag. Mixing of the process stream will also occur when it passes through the “flash tank”, so it is by no means possible to take out the sample that was actually screened by the NIR sampling system. A new sample point has recently been built, enabling the operators to take out QC laboratory samples at about the same location as the NIR sampling system. Still, the sample that is sent to the QC lab is *not* the sample that was screened by the NIR sampling system.

The QC laboratory sample is not taken out in a way that ensures the sample to be representative of the process stream (true for both the “old” and “new” sample point). This will also introduce an uncontrolled bias that will be present in all calibrations carried out on the NIR instrument. When the sample arrives at the QC laboratory, only parts of the sample is used for the analysis. Nothing is done to ensure that the polymer used in the analysis are representative for the sample. This introduce yet another bias.

It is emphasized in [Gy (1998)] that this situation is amplified by the fact that the present sampling situation does not give possibilities for monitoring the size of the biases introduced, or to check if the biases are constant.

In the NIR sampling system only a very small fraction of the process stream close to the pipe wall is screened. It is thus not representative for a cross-cut of the process stream, and a bias may be introduced here also.

In Appendix G a suggestion for modification of the current sampling system is given, and a new sampling system is proposed in Appendix H. Unfortunately neither of these proposals solves all the problems discussed here.

All these biases are present in the data-sets used for calibration in this thesis work. There is no reason to consider them to be constant, neither to assume that these errors have some symmetrical distribution.

Some thoughts of the heterogeneity to expect in a cross-section of the process stream were given in Section 3.6, but it appears that little work has been done by Borealis on this topic. An analysis of the expected heterogeneity is outside the scope of this thesis.

In addition to these sampling biases, there will also be measurement errors. The “true” linear regression model is:

$$\mathbf{y} = \mathbf{X}\mathbf{b} + \mathbf{e} \quad (3.6)$$

Measurement errors in the reference method and NIR spectrum gives:

$$\tilde{\mathbf{y}} = \mathbf{y} + \Delta\mathbf{y} \quad (3.7)$$

$$\tilde{\mathbf{X}} = \mathbf{X} + \Delta\mathbf{X} \quad (3.8)$$

The linear regression model is then:

$$\tilde{\mathbf{y}} = \tilde{\mathbf{X}}\hat{\mathbf{b}} + \Delta\mathbf{X}\mathbf{b} + \Delta\mathbf{y} + \mathbf{e} \quad (3.9)$$

In addition to this, measurement biases due to the time-lag (1), primary sampling (2), secondary sampling in QC lab (3) and NIR sampling system (4) are introduced. We now have:

$$\tilde{\mathbf{y}} = \tilde{\mathbf{X}}\hat{\mathbf{b}} + \Delta\mathbf{X}\mathbf{b} + \Delta\mathbf{y} + bias_1 + bias_2 + bias_3 + bias_4 + \mathbf{e} \quad (3.10)$$

These non-symmetrical distributed errors in the sampling makes it impossible to give estimates regarding the prediction accuracy of the multivariate regression models used in the Rønningen HDPE plant.

3.12 Summary and conclusion

The sampling system is extremely simple, with the simplicity in itself as the major advantage. The current implementation have several weaknesses, though.

A summary of the major sources of variation in the NIR spectrum is given in Figure 3.8.

The polymer is responsible for the major variations in the NIR spectra. The origin of the variation comes from both chemical structure and the powder particles. Structural variations (methyl/methylene) may be exploited for density calibration purposes, and maybe also for MFR calibrations. Variations in

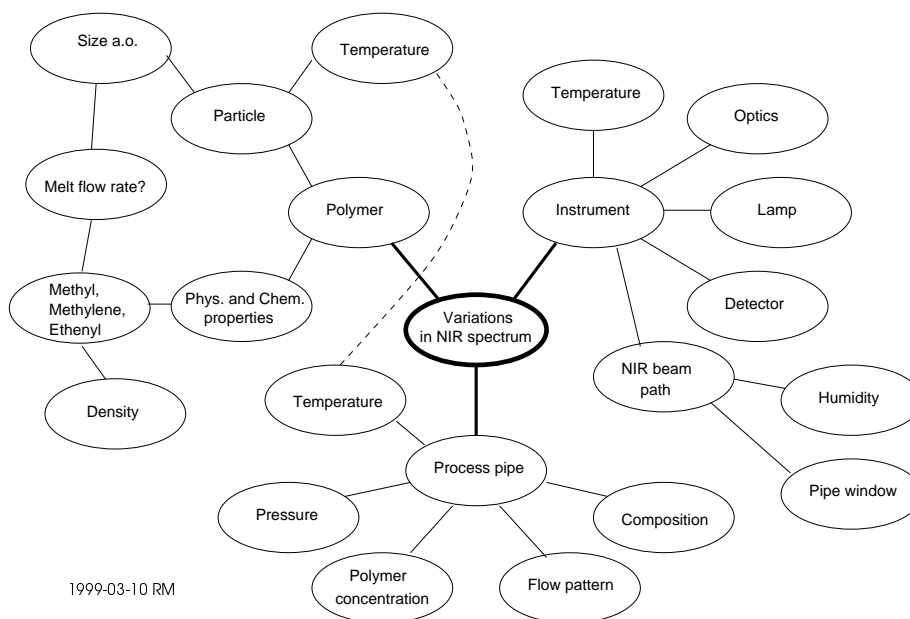


Figure 3.8: Major sources of variation in the NIR spectrum

ethenyl concentration may also play a role in MFR calibrations, and possibly also scattering due to particle size variations.

Pressure fluctuations in the system will vary the iso-butane concentration. The iso-butane may in turn give contribution to the NIR spectrum.

There may be some correlation between system temperature and the NIR spectrum, but the relation and the extent of the problem is unclear. More work should probably be put into the understanding on how temperature affects the NIR spectrum. When calibrating the instrument, temperature effects should be accounted for. Two approaches are possible: either explicitly include the temperature in \mathbf{X} , or implicitly include it in the spectra (the first approach also imply the latter). In both cases it is important to know that the expected temperature variation is completely spanned.

The sample concentration vary a lot. The quality of the acquired spectra may probably be improved a lot by changing the sampling system so that the polymer concentration is high and constant in front of the sapphire window. Another approach may be to detect and remove spectra with low polymer information before taking the sample mean spectrum. This is further discussed in Section 4.2.2.

A polymer film on the sapphire window is probably causing an oscillation in the NIR spectra. This must be incorporated into the multivariate models until a way is found to prevent it from forming.

The current sampling system and reference sampling system introduces several biases. There is no reason to consider these biases neither constant nor symmetrically distributed. Thus, expected errors for the calibration models cannot be estimated.

An ideal sample system (from a spectroscopists viewpoint) would be a compartment containing a representative sample under constant temperature in an inert atmosphere. This kind of system may be hard and costly to implement, and much more complex than the current system. A suggestion for improvement of

the current system is given in Appendix G, and a suggestion for a new sample system is given in Appendix H.

Chapter 4

Multivariate calibration: a review of methods

This chapter gives brief theoretical introductions to data processing methods used throughout the multivariate calibration process. An evaluation of the methods related to the application under study is also given. But first, a “generic” calibration scheme is outlined.

Some pre-selection of methods has already been done at this stage. Numerous data processing methods are left out because they are considered unfruitful in this application. Some methods that might have been useful but are not investigated, are mentioned in the “Other methods” sections. These are left out mainly due to time limitations.

4.1 A generic calibration scheme: identification of the steps involved

The process of calibrating a multivariate instrument, i.e a multivariate calibration (defined in Section 1.3.4), may be subdivided into several discrete steps. A suggestion of how a calibration might elapse, is shown in Figure 4.1. The goal here is to identify all the steps involved in the calibration process, not to give a complete description on how a calibration should be done. Figure 4.1 is based on the authors experience, many other approaches are possible.

For each step given in Figure 4.1 a choice must be made: should the step be performed on the data or not? If the answer is yes, several options are possible. Suggestions are given in the following sections, and the effect of some of these methods on the application under study are fully explored later in this thesis.

Multivariate calibration is a highly iterative process. Each step in the process will have implications on all the following steps. Searching for an optimal calibration strategy will then be a very time-consuming process.

It is important to remember that the goal for the calibration is not the multivariate model in itself, but rather a model that gives stable and accurate predictions from future measurements. A discussion of criteria for a “good” model is given in Section 4.9.

Another important fact is that although a “finished model” is the end step in Figure 4.1, the model performance must be continuously evaluated. In a controlled laboratory environment this may not be necessary to do frequently, but

in a highly dynamic on-line environment it should be done for every prediction carried out by the model. There is a contradiction here: in the laboratory the model may easily be tested with standards, but in an on-line environment this may be impossible.

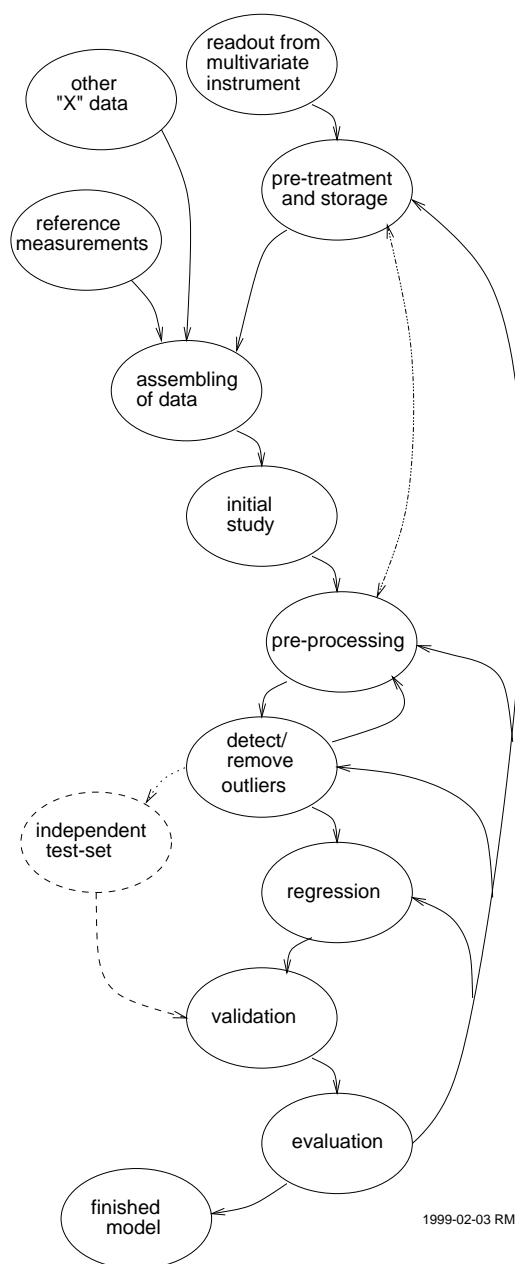


Figure 4.1: A generic calibration scheme. For each step: yes/no. If yes: multiple options.

4.2 Data pre-treatment and storage

Although many multivariate regression methods efficiently extracts relevant information from a “noisy” input signal, an increased signal-to-noise (S/N) ratio will always improve the model.

The signal-to-noise ratio is defined as [Skoog et al. (1998)]:

$$\frac{S}{N} = \frac{\bar{x}}{std} \quad (4.1)$$

where \bar{x} is the variable mean, and std is the variable standard deviation.

The term noise is often applied to describe random fluctuations whenever replicate measurements are made on signals that are monitored continuously [Skoog et al. (1998)]. In this context, everything that is not correlated to the property we want to predict is considered to be noise. Therefore, two types of noise are defined for this thesis work: random (white) noise and deterministic (systematic) noise.

The deterministic noise is related to the dynamics of the system under study, e.g. variations in temperature, pressure or concentration. Sources of random noise might be [Skoog et al. (1998)]:

- Thermal noise - agitation of electrons or other charge carriers in resistive elements in an instrument.
- Shot noise - encountered whenever electrons or other charged particles cross a junction.
- Flicker noise - dependent of frequency of signal under study, causes are not well understood.
- Environmental noise - different forms of noise that arise from the surroundings, e.g. power lines, electrical motors etc.

In this chapter only methods for noise-reduction that can be implemented in software are studied. Improvements in instrument electronics are not investigated. Some suggestions for improvement of the sampling-system where given in Section 3.12.

4.2.1 Averaging data

Under the assumption that the “random” noise is truly random and normal distributed, averaging of input data will increase the S/N ratio. This might be done by scanning the sample several times, and then use the mean of each **X**-variable (wavelength).

One problem with averaging is that one (or a few) severe outlier(s) might destroy several other “good” data. This is shown in Figure 4.2. In the first sub-plot, the raw data is displayed. Three data arrays are almost similar (the “good” data), while the fourth is very different from the others. In the second sub-plot, the mean of the three “good” data arrays are plotted, together with the mean and median values of all raw data. As one can see, the outlier has a big effect on the variable mean. The median value handles the outlier well, and is almost similar to the mean of the “good” data.

It can be shown that the signal-to-noise ratio (S/N) is given by [Skoog et al. (1998)]:

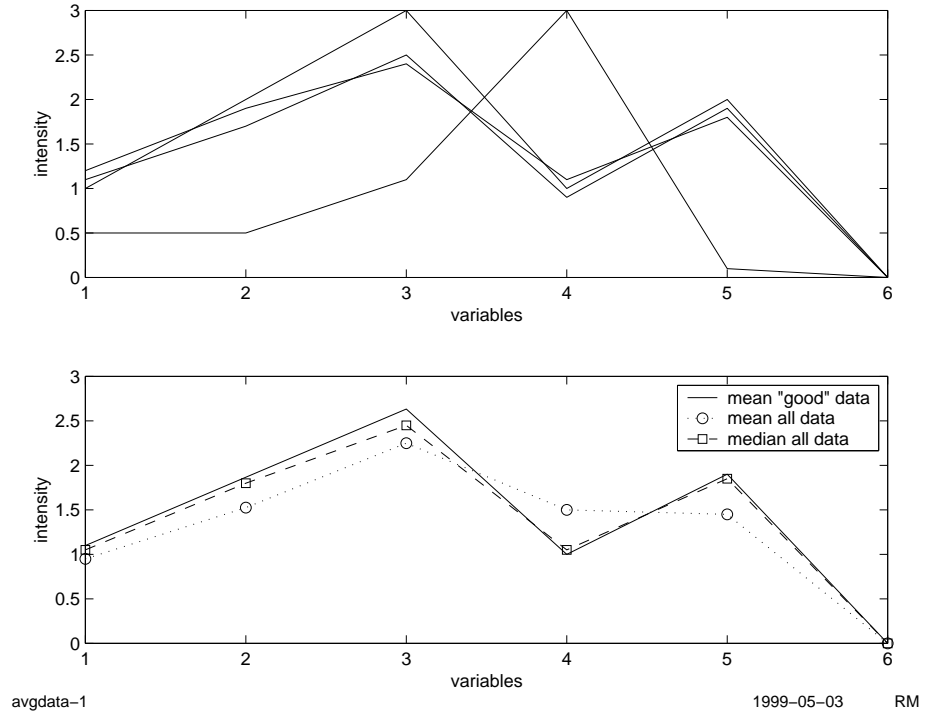


Figure 4.2: Effect of averaging data by using the mean or median of each variable.

$$\frac{S}{N} = \sqrt{n} \frac{S_x}{\sqrt{\sum_{i=1}^n (S_x - S_i)^2}} \quad (4.2)$$

where n is the number of measurements. Thus, increasing n will give a better S/N ratio. All spectra analyzed in this thesis work, are averages of 900 single spectra.

4.2.2 Filtering data by spectral rejection

Another approach to averaging is to filter the data before doing the variable mean. Spectral rejection was first suggested in [Hassel (1998)]. The essence of this method is to reject single spectra that fall outside some (arbitrary) criteria, and then take the mean of the remaining spectra. Spectral rejection is a sort of weighted mean, where some samples are given the weight 0 while the others get weight 1.

One simple application of spectral rejection is to require that the area under the curves meets some specified max/min criteria. In Figure 4.3 the integral of each sample (see Figure 4.2) are plotted as bars. Given suitable control limits, sample 4 would be rejected before averaging.

Another more rigorous rejection criteria would be to test each acquired spectrum against a known “good” spectrum, require every single variable to be within specified min/max limits. This approach has not been tested.

In [Hassel (1999)] spectral rejection is discussed, and it is suggested to do the rejection by using min/max intensity criteria for selected wavelengths. In that memo it is assumed that only polymer concentration in front of the sapphire window is responsible for the spectral variation between single spectra, and

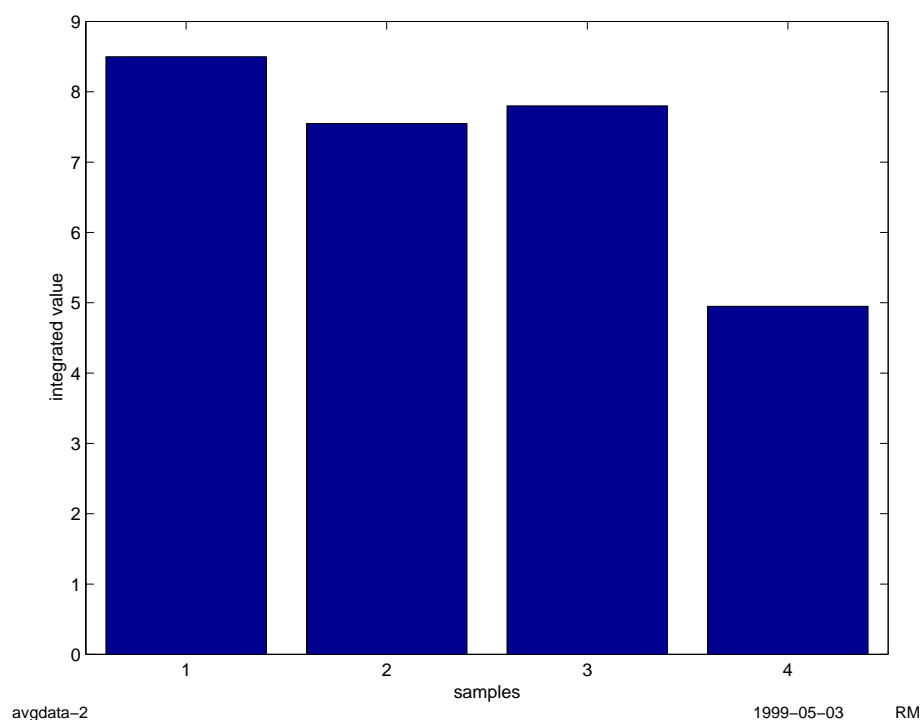


Figure 4.3: Integral of each sample.

that all other sources of spectral responses are constant. This is probably a too simplified model (see Chapter 3).

Spectral rejection is not investigated further in this thesis, but the method looks interesting for S/N improvement. Work should probably be put into the interpretation of each single spectra (shown in Figure 3.7) before a new spectral rejection scheme is suggested.

4.2.3 Fourier filtering

Fourier filtering may be used to remove periodic features in a data array. If the oscillating signal described in Section 3.8 had a constant frequency throughout the NIR spectrum, it would stand out as a spike in the Fourier domain spectrum. By zeroing out the Fourier coefficients containing the spike and then do an inverse Fourier transform, the periodic feature would be removed.

For the particular problem described in Section 3.8, the frequency of the oscillation is not constant, but decreasing throughout the spectrum. This means that a broad band in the Fourier domain spectrum must be removed.

The Fourier domain spectra from from the “old” and “new” spectra defined in Section 3.8 are shown in Figure 4.4. The oscillation in the “new” spectrum is weak (in amplitude) and probably span a broad region in the Fourier domain spectrum. It cannot be identified in the plot given here.

The expected Fourier domain frequencies for the oscillation was calculated to be around 34-46. Fourier coefficients 34 ± 3 and 46 ± 3 were zeroed out, and the resulting coefficient array was inverse Fourier transformed. The Fourier filtered (ffilt) and “new” spectra are shown in Figure 4.5. It is evident that the effect of the oscillation have been reduced.

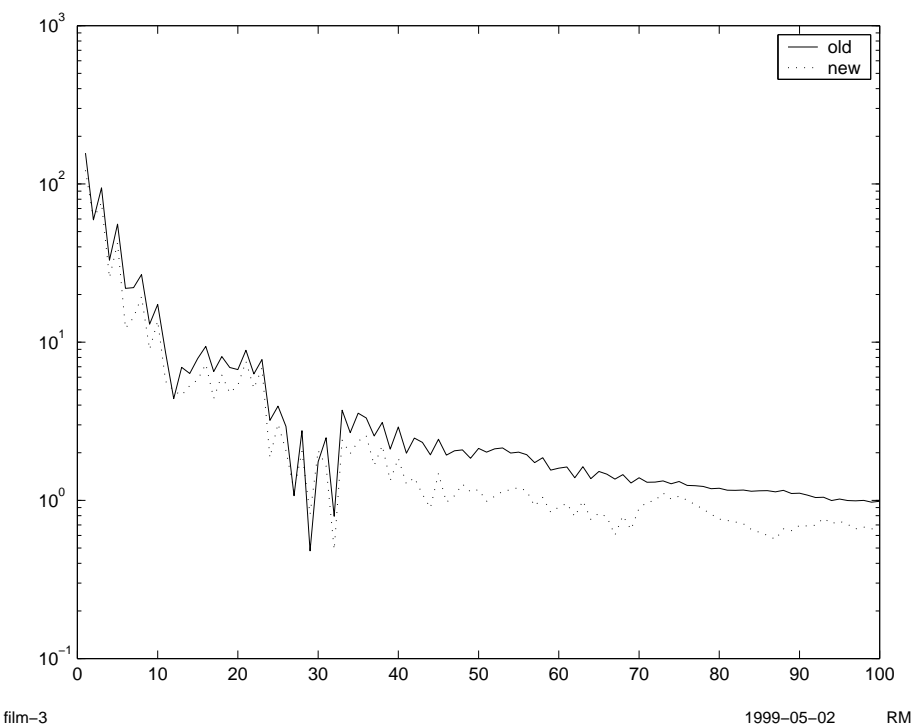


Figure 4.4: Detail of Fourier domain spectra

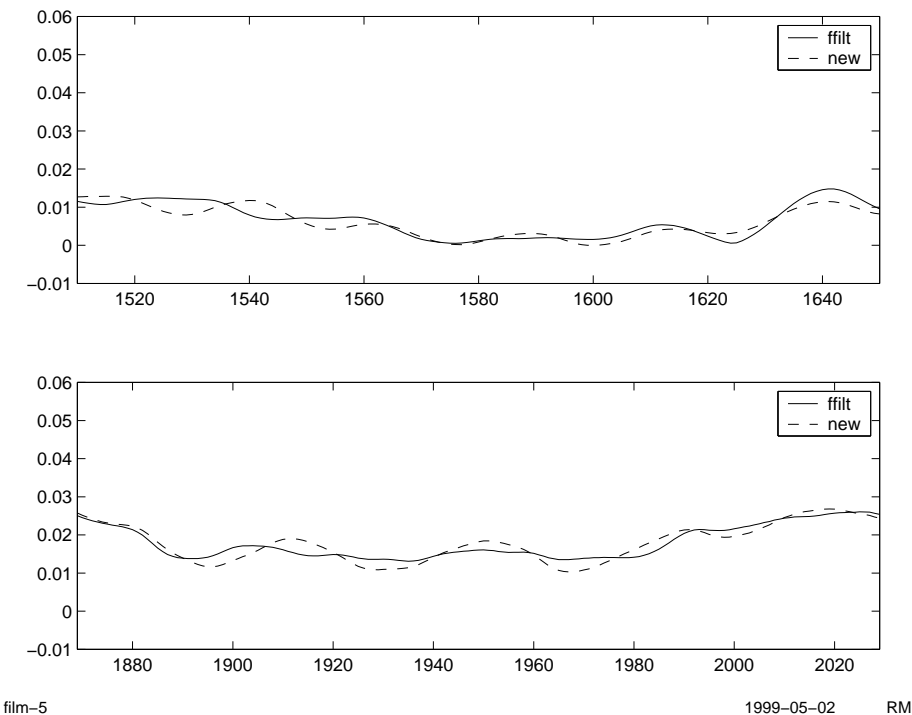


Figure 4.5: Fourier filtered (ffilt) and "new" spectra

The effect of this Fourier filtering on density predictions have also been evaluated. Tests showed that an additional latent variable was needed in order to obtain the same RMSECV as for a non-filtered model. The reason for this is probably that the Fourier filtering removes important variations in the spectra as a bi-effect, thus decreasing the signal-to-noise ratio.

4.2.4 Other methods

A number of different digital filtering schemes (including averaging and FFT) are well known in literature. Most of these methods perform some sort of data smoothing.

A “new” and interesting tool for data filtering (and for many other purposes), is the use of wavelets.

4.3 Assembling calibration and validation data sets

Ideally, all possible variations should be included in the calibration set, i.e. the \mathbf{X} -space should be completely spanned. In the complex and dynamic chemical process in which the sampling system under study resides, this is clearly not possible.

One way to ensure that *as much as possible* of the \mathbf{X} -space is spanned, is to include all available products in the calibration set. Unfortunately, every time a product is produced, it is done under slightly different process conditions. In Chapter 6 it will be investigated if the calibration models are improved when including samples from products produced in two different product campaigns.

When trying to span the \mathbf{X} -space it is important to also include variations other than those directly related to the y-variable(s). This might for example be temperature (see Section 3.4). At the very least it is important to be aware of such effects, and to have some understanding of their response in \mathbf{X} . One should also assure that other unwanted effects are not correlated to the effects that are studied.

The measurement inaccuracy should also be incorporated into the model. This may be done by including replicate measurements.

4.4 Initial study

Multivariate calibration may easily be used as a “black box” method for fitting massive amounts of data onto some property of interest. This is a pitfall, one should always be familiar with the data and understand the fundamental concepts of responses. Up to this point in the thesis, this has been the aim. Fundamental understanding will always be helpful when selecting pre-processing methods, regression methods and when evaluating the regression models.

When understanding the fundamental concepts of response, a thorough study of the raw data is often helpful. One way of doing this, is by a Principal Component Analysis (PCA). This is done in Chapter 5.

4.5 Pre-processing

One of the major problems when making multivariate calibration models is that the input \mathbf{X} -data is dependent on many different and often uncontrollable factors not related to the (chemical) response of interest. The system analysis in Chapter 3 has already revealed that this is truly the case for the application under study. Severe baseline effects due to light scattering and variations in effective sample size are responsible for a major part of the spectral variation (explored further in Chapter 5).

It is sometimes possible to correct for unwanted effects by using additional factors in the multivariate calibration model, but the models will generally perform better if the response of these effects are reduced or removed prior to the calibration (and prediction).

In the following sub-sections, various pre-processing methods are considered. The selection of the “right” pre-processing method is a combination of knowledge of the system and the analytical method, and a “trial-and-error” process.

4.5.1 Reflectance/Absorbance/Kubelka-Munk

Beer’s law (see Section 2.1) states that for monochromatic radiation, absorbance A is directly proportional to the path-length b and the concentration c . Due to the proportionality between absorbance units and concentration, this measurement unit is commonly used.

Only absorbance-units were used in this study. Other instrument response units like reflectance or Kubelka-Munk were not tested due to time limitations.

4.5.2 Two-point baseline correction

A simple and effective way of removing a sloping baseline is to select two points in a spectrum, draw a line between the points and then subtract it from the spectral response. The two points should be located in areas of the spectrum where there is no absorption bands, and preferably in each end of the spectrum. The effect of two-point baseline correction is shown in Figure 4.6. The selected points were at 1300 nm and 2120 nm. The offset was also removed by setting the ground level to zero.

The two-point baseline correction method may be made more robust by specifying two regions to use for the correction, and locate and use the minima in each of these regions for each spectra to be corrected. Multiplicative effects will not be removed by this method.

4.5.3 Orthogonal signal correction

Orthogonal signal correction (OSC) is a recently proposed pre-processing method [Wold et al. (1998)] [PLS-Toolbox: Wise and Gallagher]. The idea is to remove bilinear components from $\tilde{\mathbf{X}}$ that are orthogonal to $\tilde{\mathbf{y}}$, i.e. a signal correction that does not remove $\tilde{\mathbf{y}}$ information from $\tilde{\mathbf{X}}$.

An OSC NIPALS algorithm will be identical to an PLSR NIPALS algorithm, except for the crucial step of calculating the $\tilde{\mathbf{X}}$ weights, $\hat{\mathbf{w}}$. These are calculated as to maximize the covariance between $\tilde{\mathbf{X}}$ and $\tilde{\mathbf{y}}$ in the PLSR algorithm, but in OSC they are calculated as to minimize the covariance.

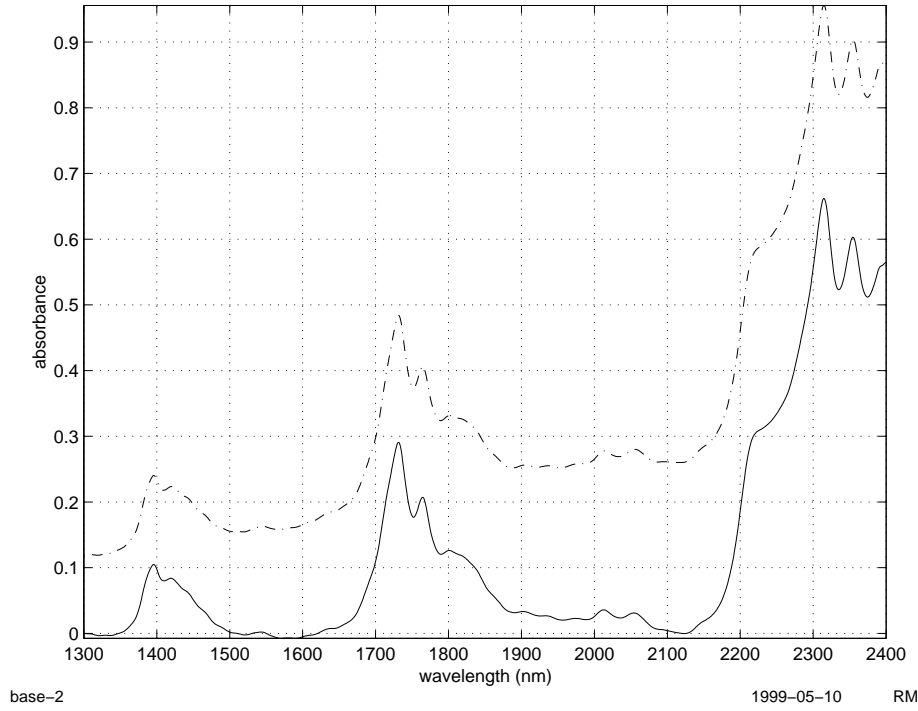


Figure 4.6: Effect of two-point baseline-correction

When the OSC loads and weights have been found, new “OSC corrected” data may be calculated using¹:

$$\mathbf{x}_{new,osc} = \tilde{\mathbf{x}}_{new} - \tilde{\mathbf{x}}_{new} \hat{\mathbf{w}}_{osc} (\hat{\mathbf{p}}_{osc}^T \hat{\mathbf{w}}_{osc})^{-1} \hat{\mathbf{p}}_{osc}^T \quad (4.3)$$

OSC is only applicable when a lot of $\tilde{\mathbf{X}}$ variance that is not correlated to $\tilde{\mathbf{y}}$ is captured in the first few PLSR factors. This is due to the fact that OSC is a fitting (or rather anti-fitting) process of $\tilde{\mathbf{y}}$ -data onto $\tilde{\mathbf{X}}$. Thus OSC-correcting the $\tilde{\mathbf{X}}$ -data significantly reduces its degrees of freedom. The result of using PLSR on OSC-corrected where a lot of $\tilde{\mathbf{y}}$ variance is modeled in the first factors is an instant over-fit of the model.

OSC seems to be an intuitively “right” way to remove variations in $\tilde{\mathbf{X}}$ that is not correlated to $\tilde{\mathbf{y}}$. Despite this, OSC did not work well in preliminary tests in the application under study. More work should be put down into learning how to use this method optimally.

4.5.4 Smoothing and derivation (Savintzky-Golay algorithm)

An effective way of removing baseline-effects is to use derivatives of the original spectra for calibration. The first derivative will remove an offset, and the second derivative will remove both a slope and an offset. This is shown in Figure 4.7. The derivatives are scaled for clarity.

Using the difference between each variable in the spectrum is a very simple way of obtaining the derivatives. This between-point difference estimation of the derivative will in most cases only enhance the noise in the data, though.

¹This is *not* as given in [Wold et al. (1998)], but as implemented in [PLS_Toolbox: Wise and Gallagher].

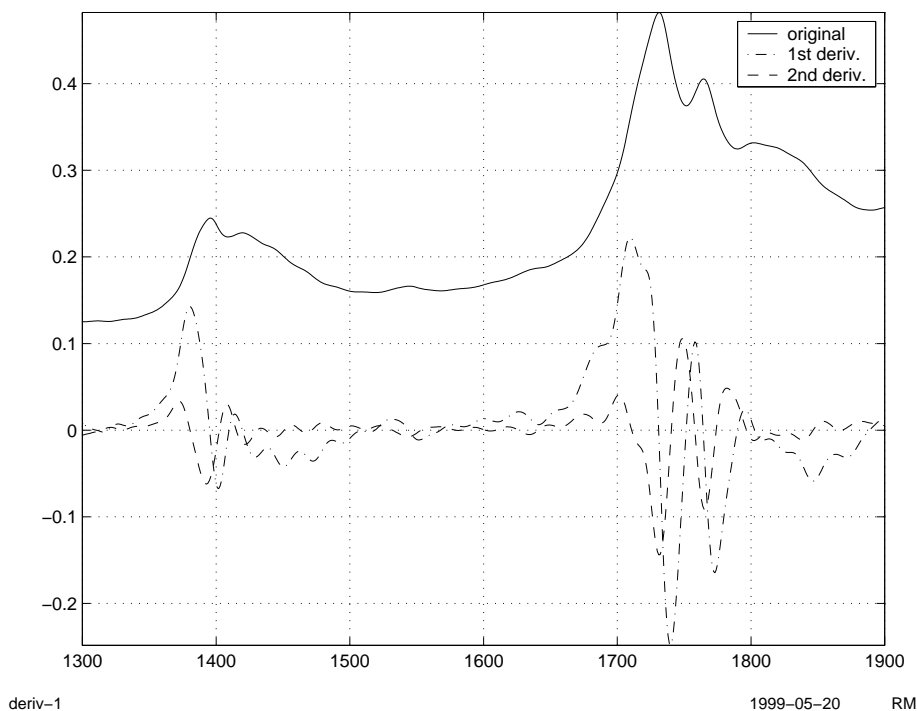


Figure 4.7: Spectrum and derivatives (scaled)

A far more sophisticated method of obtaining the derivatives is based on the Savintzky-Golay algorithm (modified to include end-points in [Gorry (1990)]). This method fits a polynomial to a running local region of the spectrum, and thus give a smoothing effect. Because polynomials are fitted to the spectrum, they may easily be replaced by their derivatives.

The spectra acquired in the application under study do not really need any smoothing (they were already smoothed at the time of acquisition), but it is still beneficial to use the Savintzky-Golay algorithm for obtaining the spectrum derivatives. The method must be optimized for the window size and polynomial order.

Results from one optimization run with different window sizes and a second order polynomial is shown in Figure 4.8. The calibration was done using PLSR, and the calibration model was test-set validated. A window size of 37 points was optimal here, using four factors (best test-set validation result). The wavelength range was from 1300 nm to 2110 nm.

The 37 point window size is very large, and does not really give a good fit to the spectra when using a second order polynomial. Window sizes from 5-11 points generally fitted the spectra most optimal, i.e. these window sizes gave the smallest residual between the original and the smoothed data (but not necessarily the best regression models).

Additional tests revealed that other window sizes were optimal when using different spectral ranges or other pre-processing methods in combination with a derivative. The tests also showed that a 2nd order polynomial generally worked better than a 3rd order polynomial.

A problem with using derivatives is that the resulting spectrum is hard to interpret. It will also decrease the signal-to-noise ratio. Despite this, preliminary

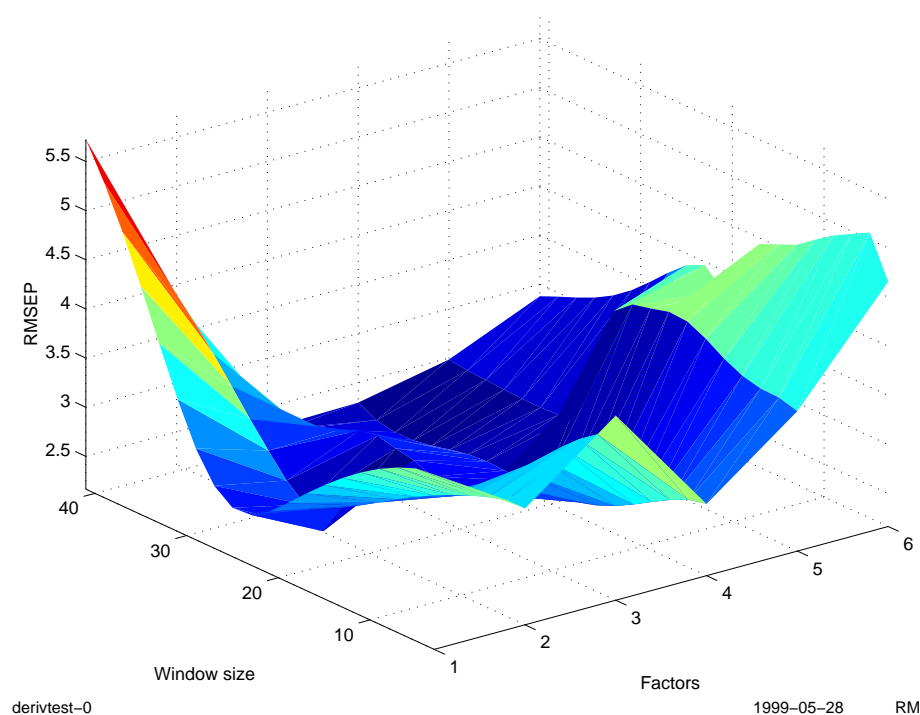


Figure 4.8: Optimal window size, 2nd derivative of 2nd order polynomial

tests showed that using the second derivative spectra greatly improved the density models in the application under study, compared to using raw spectra.

4.5.5 Multiplicative Scatter Correction (MSC)

Multiplicative Scatter Correction (MSC) is a pre-processing tool developed to correct for the significant light-scattering problems in reflectance spectroscopy [Martens and Næs (1991)].

The idea behind MSC is to remove multiplicative (amplification) and additive (offset) effects in the spectra. This is done by a least squares regression of a range of a spectrum onto a reference (e.g. an average spectrum). The intercept α and slope β are then removed from the spectrum:

$$\mathbf{x}_{i,new} = \frac{\mathbf{x}_i - \alpha}{\beta} \quad (4.4)$$

The spectral range used for calculation of α and β should be free from chemical information.

In Figure 4.9 one spectrum is plotted against an average spectrum. It indicates that the MSC base should be calculated on the region between 2100 nm and 2230 nm. This is also a region of the spectrum where no absorption bands are expected (see Section 2.3). The whirls in Figure 4.9 are representations of the peaks in the NIR spectrum.

Preliminary tests showed no significant improvements in models based on MSC-processed data, compared to using raw data. Many regions other than the one indicated above were also tested when calculating the MSC base. The problem with MSC is that it is built on the assumption that additive and multiplicative

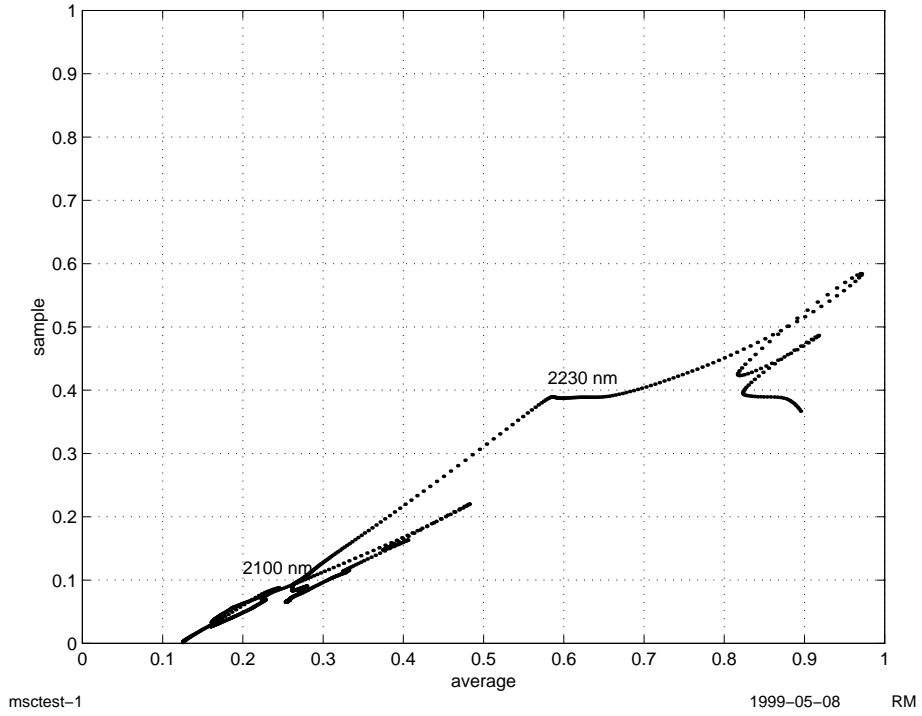


Figure 4.9: One spectrum plotted against average spectrum

effects are independent of wavelength. These assumptions are probably violated in the application under study.

4.5.6 Standard Normal Variate (SNV)

Standard Normal Variate (SNV) uses a different approach than MSC to correct for scattering effects. No reference spectrum is required for the correction. Instead, the scattering is removed by normalizing each spectrum by the standard deviation across the entire spectral range [PLSplus/IQ users guide]. The mean response is calculated as:

$$\bar{x}_i = \sum_{j=1}^p \tilde{\mathbf{X}}_{i,j} \quad (4.5)$$

The corrected spectrum is then calculated as:

$$\mathbf{X}_{i,SNV} = \frac{(\tilde{\mathbf{X}}_i - \bar{x}_i)}{\sqrt{\frac{\sum_{j=1}^p (\tilde{\mathbf{X}}_{i,j} - \bar{x}_i)^2}{p-1}}} \quad (4.6)$$

where $\tilde{\mathbf{X}}$ is the n by p matrix of spectral responses for all wavelengths. A Matlab implementation is given in Appendix K.2. Preliminary tests using SNV on density calibration models gave good results.

4.5.7 Normalization

Beer's law (given in Section 4.5.1) may be used as a simple model of why the absorbance changes when the effective sample size changes. To compensate for

variations in the sample size, normalization to a given level may be applicable.

In Figure 4.10 the absorbance peak around 1720 nm is shown. The raw spectra are shown in the left plot. In the middle plot, a sloping baseline has been removed. The peaks are then normalized to unit length, shown in the right plot.

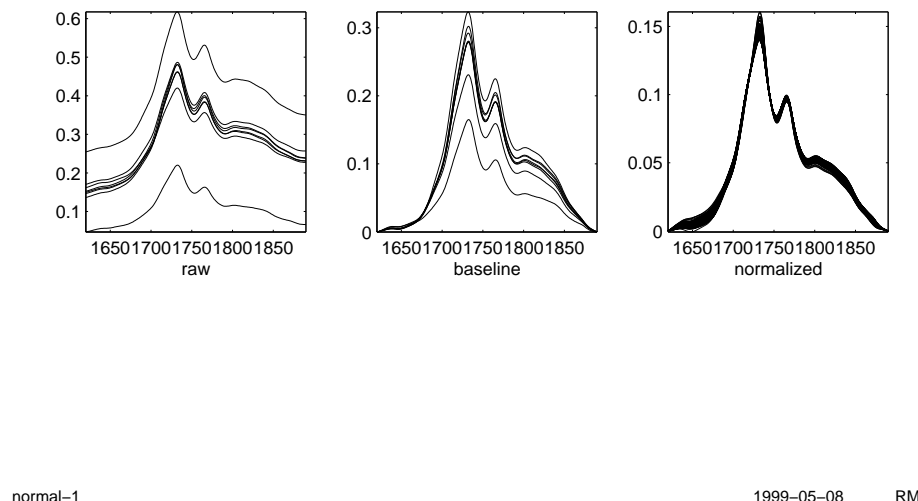


Figure 4.10: Peak normalization

Preliminary tests showed that normalization improved the density calibration models, compared to models built on raw spectra.

4.5.8 Variable selection

While the PLSR algorithm should extract relevant structure from the X -data, there are many reports on improvements of the calibration models when using subsets of the available variables. In [Spiegelman et al. (1998)] a theoretical justification for variable selection is given.

In some cases it may be possible to identify regions in the spectra that are tied up with response from specific unwanted effects in the sampling system. Removal of such spectral regions may improve the robustness of the calibration model (see e.g. [de Noord (1994)]).

To search for the optimal set of wavelengths, the numerical optimization technique Genetic Algorithms (GA) have been employed. A brief introduction and suggestions for further reading is given in [Davies and Fearn (1997)].

Preliminary tests showed that removing the upper part of the acquired NIR spectra gave somewhat more robust models. Wavelength selection using GA gave very promising results.

4.5.9 Linearization

Although PLSR and PCR are linear regression methods, they may be able to handle non-linear relations between \mathbf{X} and \mathbf{y} [Martens and Næs (1991)]. A higher number of bilinear factors are needed to account for the non-linearities, though.

In many cases, it is sufficient to linearize the $\mathbf{X} \rightarrow \mathbf{y}$ relation by simply transforming the input data (X and/or y) by simply using e.g. the squared or logarithm values.

4.5.10 Mean centering and autoscaling

Mean centering of variables is done by subtracting the mean of a variable vector from all its elements. Data-sets are often mean centered to account for an intercept term in regression models. In this thesis work, all models have been mean centered.

Variable weighting by dividing each element by the standard deviation of the variable vector (variance scaling) is an often used pre-processing method in multivariate calibration. The effect of this transformation is that every variable get the same variance.

Consider the plots shown in Figure 4.11 (mean and standard deviation spectrum). Although the variance is highest at 2400 nm, this may not be the most important absorption band for the calibration. This is the motivation for scaling all variables to the same variance level prior to the calibration.

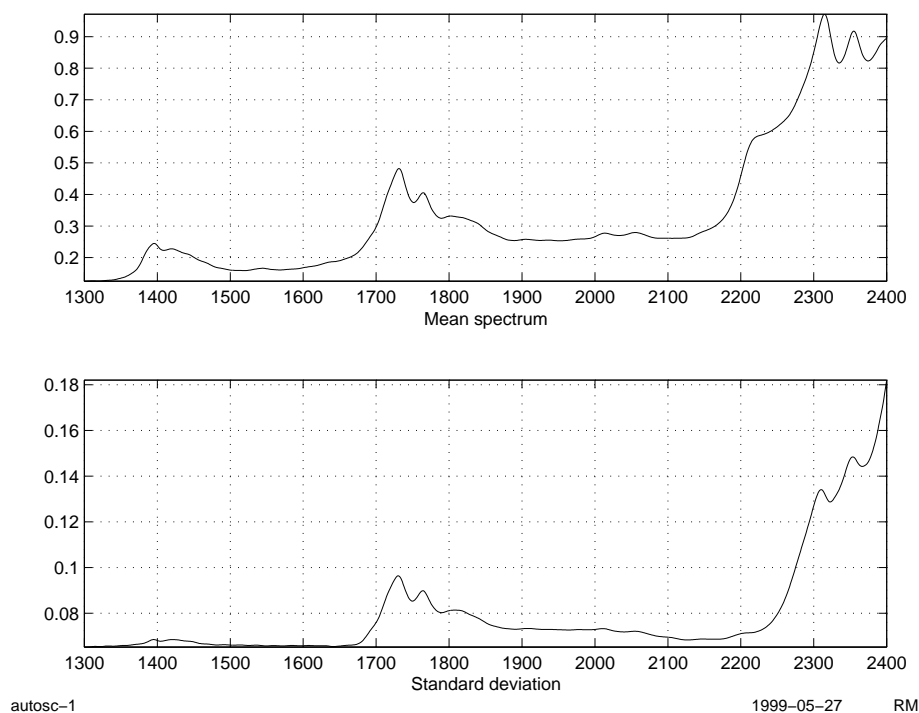


Figure 4.11: Mean and standard deviation of spectra

For variables with little chemical information, the result of this scaling is a significant amplification of the noise. This should also be taken into consideration prior to the scaling.

When the \mathbf{X} -variables are both mean centered and variance scaled, it is commonly called *autoscaling* of the variables.

4.6 Detecting outliers

As discussed in Section 4.3, spanning the \mathbf{X} -space as much as possible is very important. This brings up a dilemma: is an extreme object an outlier or an important extrema? In this thesis work, outliers in calibration data-sets were detected “manually” by studying score or t vs. u plots (or score-plots from a PCA), leverages and object residuals. When a suspicious object was found, the spectrum was studied. In most cases it was easy to reject outlier objects from the calibration data-set this way. One of these outliers is shown in Figure 4.12, together with a “typical” spectrum.

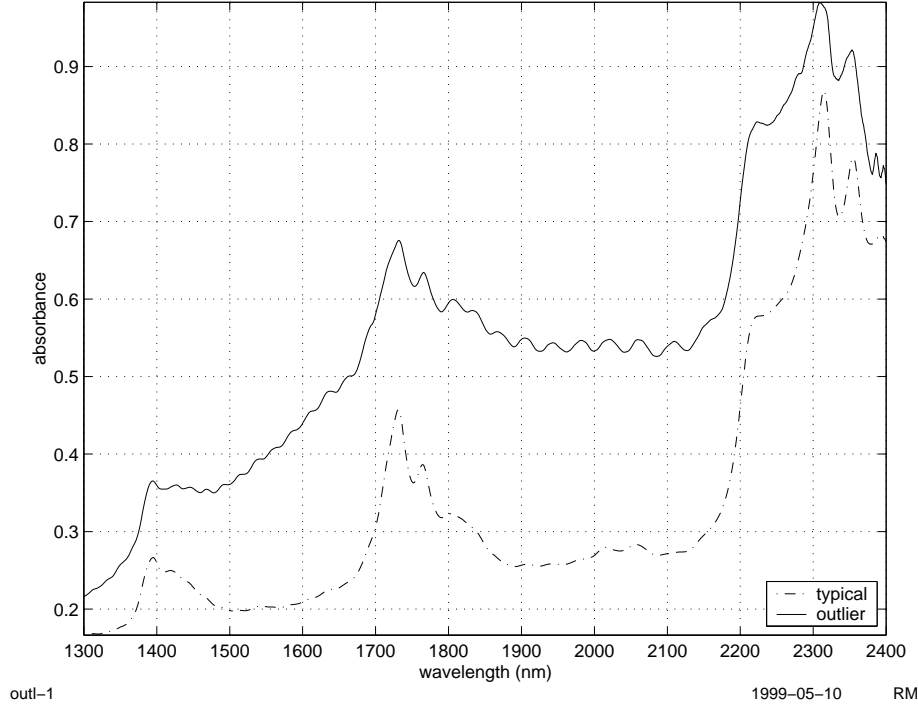


Figure 4.12: Typical and outlier spectrum

When the calibration model is doing on-line predictions, it is important to detect outliers to prevent erroneous results from being reported to the process control system and the operators. Some methods for automatically detecting outliers are discussed in the following sub-sections.

4.6.1 Spectral residuals

After subtracting the model mean (center of the calibration objects), scores for new objects may be calculated as:

$$\hat{t}_{i,a} = \mathbf{x}_{i,a-1}^T \hat{\mathbf{w}}_a \quad (4.7)$$

where $\hat{\mathbf{w}}_a$ is the model loading weights vector for factor a . The object residual is then:

$$\mathbf{x}_{i,a} = \mathbf{x}_{i,a-1} - \hat{t}_{i,a} \hat{\mathbf{p}}_a^T \quad (4.8)$$

This is repeated for factors $a = 1 \dots A$, where A is the number of bilinear factors to use in the model. The sum of squares spectral residual may now be calculated as:

$$r_i = \sum_{j=1}^n \mathbf{x}_{i,A} \quad (4.9)$$

A large spectral residual means the object does not fit well into the calibration model, and thus might be an outlier.

4.6.2 Mahalanobis distance test on PLSR scores

One possible approach for detecting an outlier object is to measure its distance from the model center in the A -dimensional score space, where A is the number of bilinear factors used in the calibration model. A simple way of determine each objects distance from the model center is to calculate their Euclidean distance. The problem with this method is that it does not take into account the variability of the values in all dimensions.

A distance measurement that do take the sample variability into account, is the Mahalanobis distance. The Mahalanobis distance (as implemented in this thesis work) is found as:

$$D^2 = \mathbf{t}_{un} \left(\frac{\mathbf{T}^T \mathbf{T}}{n-1} \right)^{-1} \mathbf{t}_{un}^T \quad (4.10)$$

where \mathbf{T} are the calibration model object \mathbf{X} scores, \mathbf{t}_{un} are the scores of the unknown sample and D^2 is the squared Mahalanobis distance. The difference between Mahalanobis and Euclidean distance is demonstrated in Figure 4.13.

In Section 6.1 it is tested if Mahalanobis distance in the \mathbf{X} score space is a feasible method for outlier detection. An additional approach, where the spectral residual is appended to the scores before calculating the Mahalanobis distance, is also tested. A Matlab function for calculating Mahalanobis distance on scores is given in Appendix K.1.

4.6.3 Other methods

In [Høy et al. (1998)] methods suggested by De Vries/Ter Braak and Faber/Kowalski for estimating the prediction error are discussed. The results in [Høy et al. (1998)] indicated that the uncertainty estimation suggested by De Vries/Ter Braak worked for low levels of normally distributed noise in the data. The methods have not been tested in this thesis work, but as indicated in Section 3.11 the noise in the data is complex, and it cannot be assumed to have a symmetrical distribution.

Another method for detecting outliers is to require that the predicted result falls within the values of the calibration objects, i.e. that extrapolation is not allowed.

Refer to [Martens and Næs (1991)] for an extensive discussion on outlier-detection.

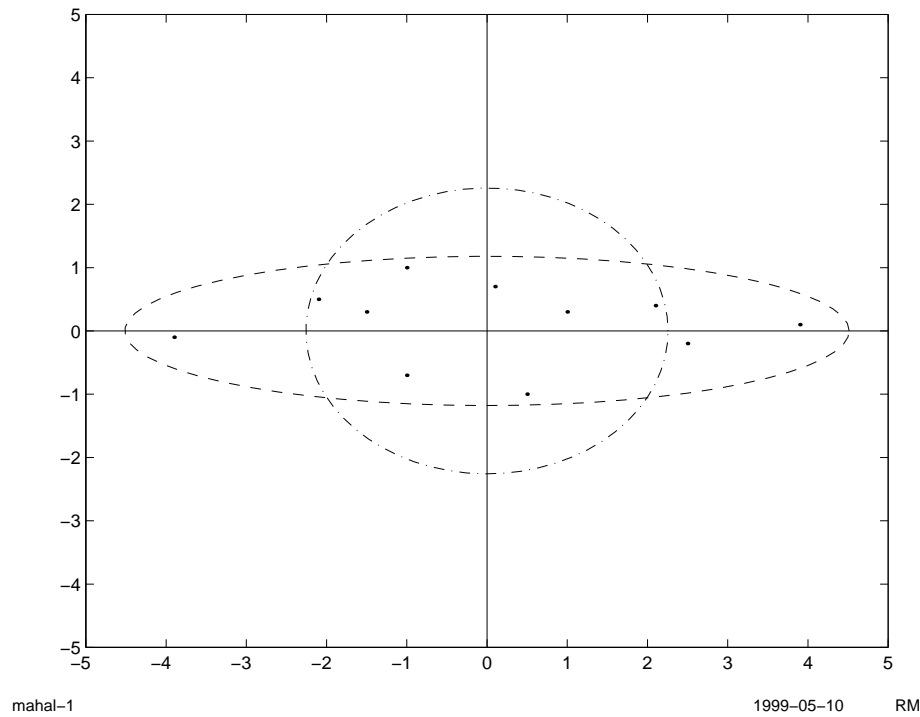


Figure 4.13: Mahalanobian (ellipse) and Euclidean (circle) distance

4.7 Selecting a regression algorithm

Some regression methods are briefly introduced in the following sub-sections. See [Martens and Næs (1991)] for thorough explanations to these linear regression methods.

4.7.1 Principal Component Regression (PCR)

Principal Component Analysis (PCA) provides an approximation of a data matrix \mathbf{X} , in terms of the product of scores \mathbf{T} and loadings \mathbf{P} . The purpose is to express the main information in the variables by a lower number of variables, called the principal components (PC) of \mathbf{X} . This is possible because in many cases the \mathbf{X} -variables are expected to be collinear. This collinearity means that the data matrix \mathbf{X} will have some dominating types of variability that carry most of the available information. The PCA algorithm performs a projection down on a subspace in such a way that each of these “hidden” directions becomes a new variable. For a mean centered data matrix, we have:

$$\tilde{\mathbf{X}} = \hat{\mathbf{T}}\hat{\mathbf{P}}^T + \mathbf{E} \quad (4.11)$$

In PCR the scores $\hat{\mathbf{T}}$ from a PCA decomposition are used as regressors in the regression equation with y : PCR is MLR done on scores found with PCA. This means that the effective structure part is used in the $\mathbf{X} \rightarrow y$ regression, and the noise is removed. The structure part may not be correlated to the response variable, though.

4.7.2 Partial Least Squares Regression (PLSR)

PLSR regression is a guided decomposition, where the \mathbf{y} data structure is allowed to intervene directly in the \mathbf{X} decomposition. PLSR is therefore well suited for analysis of \mathbf{X} and \mathbf{y} relationships, as well as for building regression models.

The advantages of PLSR over PCR is that when \mathbf{y} information is used directly when regressing, the model will very often turn out to be better for prediction purposes. It also handles noisy \mathbf{X} -data better than PCR. The method reduces the impact of large but irrelevant variations in \mathbf{X} . It must be noted that these advantages may be subject to discussion.

The NIPALS algorithm used to calculate PLSR is presented visually in Figure 4.14. The most important aspect of the algorithm is that the score vectors for \mathbf{X} and \mathbf{y} are calculated interdependently, with the score vector for the “opposite space” used as starting point for each iteration. This way the y data will affect the decomposition of \mathbf{X} , and the other way around.

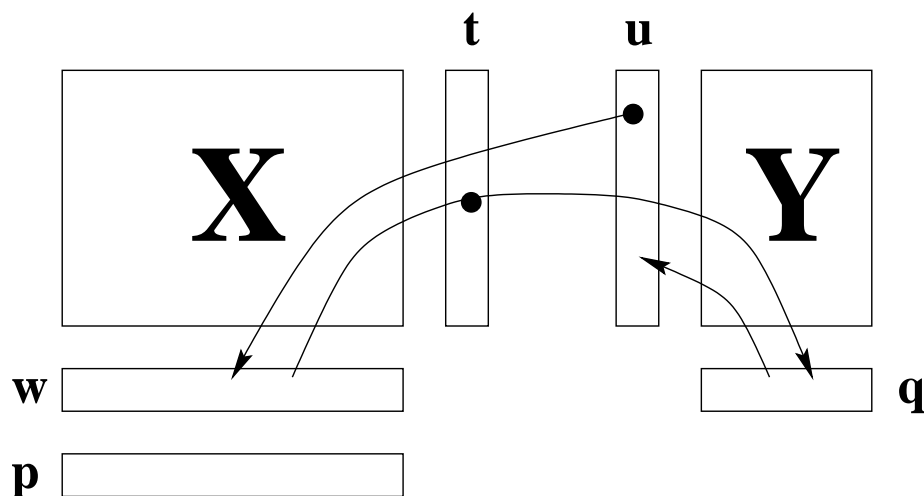


Figure 4.14: The PLSR NIPALS algorithm illustrated visually

4.7.3 Locally Weighted Regression (LWR)

The idea behind Locally Weighted Regression (LWR) is to use regression models that are made from objects that are near the sample to be predicted in the independent variable space. In addition to this, the calibration objects are weighted according to how close they are to the sample to be predicted [PLS_Toolbox: Wise and Gallagher].

4.7.4 Other methods

The Genetic Algorithm (GA) for variable selection discussed in Section 4.5.8 could have been used to search for possible Multiple Linear Regression (MLR) solutions. This was not tested.

Some possible candidates if non-linear modeling were to be tested, are:

- Neural Network PLSR (NN-PLSR)

- PLSR with polynomial inner relations (poly-pls)
- PLSR with spline inner relations (spline-pls)

4.8 Validating the model

The importance of validation was briefly discussed in Section 4.3. The purpose of validation is to:

- make sure that the model will work in the future for new, similar data
- to avoid either over-fitting or under-fitting of the model

See [Esbensen et al. (1994)] for a good discussion on model validation. In the following sub-sections some validation schemes are discussed.

4.8.1 Cross-validation

In cross-validation one or more of the calibration objects are taken out of the data-set, and a model is built on the remaining objects. The objects that were taken out, are then used for testing the model. This is repeated until all calibration objects have been taken out once. The final calibration model is then built on all objects. Model statistics are accumulated from each of the sub-models.

Taking out only one object at a time (full cross-validation) is a much used validation method on small data-sets. For larger data-sets, this method is not realistic. When taking out only one sample at a time, the risk is high that an almost similar (effectively a replicate) sample is still in the data-set. Thus, full cross-validation cannot give any information on the model's prediction ability in this context.

A problem-dependent cross-validation scheme was developed specifically for this thesis work. The *cross-validation by class* scheme is done by assigning every object in the calibration data-set to a class, according to some sort of problem-related similarity. This might be e.g. the y data value, PCA scores etc. Each of the classes are then used as a test-set in a cross-validation scheme. The purpose is to test how the model performs when new variability in the X-space is introduced.

In this thesis work, product names were used for class assignment. The product name is a sort of product pre-classification, where the catalyst and other process parameters are about the same. This is probably the most relevant criterion to use for the application under study.

4.8.2 Test-set validation

Test-set validation of the multivariate model requires two separate data-sets with known $\tilde{\mathbf{y}}$ values. One data-set is used for the calibration, and one for testing the model. The prediction error found from the test-set may then be used as realistic estimates for prediction error on future data. Using an independent test-set is also the most reliable way of determining how many bilinear factors to use in the calibration model.

If the objects in the data-sets are sorted on time of acquisition, there may be some auto-correlation between them. Therefore, using every second or third element in the data-set as a test-set may not reveal possible problems. This fact was very prominent when making the temperature models (see Section 3.4). The test-set should be time independent of the calibration data, it must be representative for *future* measurements!

4.9 Evaluating the model, quantification of quality

In order to compare different calibration models, a range of different statistic measures may be calculated. These statistics may also be used as estimates for the prediction uncertainty when doing predictions on future data. The measures used in this thesis work is presented in the following sub-sections. Matlab code is given in Appendix K.3.

4.9.1 RMSEP and RMSECV

Root Mean Squared Error of Prediction (RMSEP) is defined as the squared root of the average of the squared differences between predicted and measured y-values of the validation objects [Esbensen et al. (1994)]:

$$RMSEP = \sqrt{\frac{\sum_{i=1}^n (\hat{y}_i - \tilde{y}_i)^2}{n}} \quad (4.12)$$

In this thesis work, %RMSEP is also used to express the prediction error. It is defined as:

$$\%RMSEP = \frac{RMSEP \times 100\%}{\frac{\tilde{y}_{max} - \tilde{y}_{min}}{2}} \quad (4.13)$$

In order to indicate whether the RMSEP value was found from test-set or cross-validation, the abbreviation RMSECV is used for cross-validated results in this report.

4.9.2 Bias

Bias is the averaged difference between predicted and measured **y**-values for all samples in the validation set [Esbensen et al. (1994)]:

$$Bias = \frac{\sum_{i=1}^n (\hat{y}_i - \tilde{y}_i)}{n} \quad (4.14)$$

4.9.3 SEP

Standard error of performance (SEP) expresses the precision of the predicted results, corrected for the bias [Esbensen et al. (1994)]:

$$SEP = \sqrt{\frac{\sum_{i=1}^n (\hat{y}_i - \tilde{y}_i - Bias)^2}{n - 1}} \quad (4.15)$$

4.9.4 Correlation

The covariance between two variables x and y is a measure of their linear association:

$$\text{cov}(x, y) = \frac{\sum_{i=1}^p (x_i - \bar{x})(y_i - \bar{y})}{p - 1} \quad (4.16)$$

The correlation between two variables is found by dividing the correlation by with the product of the standard deviations:

$$r = \frac{\text{cov}(x, y)}{S_x S_y} \quad (4.17)$$

The square of the correlation coefficient (r^2) is often used as a measure of the fraction of the total variance that can be modeled by this linear association measure [Esbensen et al. (1994)].

4.10 Model durability

An important goal for the calibration process is to make your model so that it is valid for as long as possible (i.e. the model give reliable predictions). Two approaches are briefly discussed here; to do the modeling in such a way that it is less sensitive to the dynamics of the system (robust modeling), or to do some sort of model maintenance while it is in operation. If neither of these approaches are applicable, a calibration transfer strategy must be considered. The latter is not treated here, interested readers should refer to e.g. [Wang and Kowalski (1992)].

4.10.1 Robust modeling

One strategy for reducing the need of re-calibration, is to develop multivariate calibration models which are robust against variations in the instrument, sampling system or environment. Some approaches for doing this, are [de Noord (1994)]:

- Incorporate all relevant sources of variation in the calibration design, in order to develop a more or less “universal” calibration model. For the highly dynamic environment in which the Rønningen on-line system resides, this is not applicable.
- Eliminate by means of data pre-processing the sources of variation that are not intrinsically related to the property to be predicted.
- Selection of parts of the spectrum which are robust against variations.

In this thesis work, the two latter strategies are tested.

4.10.2 Model updating

To overcome the problems with using a static calibration model in a dynamic on-line applications, the model can be made “quasi-dynamic” by continuously update it with new calibration objects.

If new objects are added to the calibration data-set without removing any old objects, it is obvious that the data-set would grow rather big with time. If one assumes that all possible measurement errors have a symmetrical distribution, many calibration objects would lead to more precise predictions. The problem with using many calibration objects is that the computing time for making the model will be longer and longer. One might also question if very old objects are relevant for the current state of the sampling system. In addition, a model made from many samples will have a “heavy” center.

An interesting suggestion for calibration model maintenance is given in [Helland (1993)], the *recursive PLS* (RPLS). In this scheme, new data are included in the model by recursive updating of the loading vectors. This is done by representing old data by modifications of their loading matrices, while new data are represented by their \mathbf{x} and \mathbf{y} vectors. The algorithm keeps the calibration matrices at constant size.

4.11 Summary and conclusion

The multivariate calibration process consists of many discrete data processing and evaluation steps. The whole process is highly iterative, the processing performed in one step may have severe effects on other steps.

In order to increase the signal-to-noise ratio, variable averaging of several measurements is a common procedure. This may be further refined by weighting each single spectrum before the averaging is done. Some suggestions for *spectral rejection* criteria was given in Section 4.2.2, but its effect has not been tested.

Fourier filtering may be used to remove periodic features in a data array, but it was not found suitable as a tool for removal of the oscillating signal observed in the NIR spectra from the Rønningen HDPE plant.

The $\tilde{\mathbf{X}}$ data is often pre-processed prior to calibration (and prediction) to reduce or remove variations that are not related to \mathbf{y} . This may improve the model robustness, and increase its prediction accuracy. From initial tests, two-point baseline correction, derivation, SNV and normalization (and combination of these) were found interesting.

Variable selections using genetic algorithms (GA) gave very promising results in preliminary tests.

Outliers in the calibration data are often found “manually”, by interpreting various plots. In an on-line application it is also important to automatically determine whether a prediction is valid or not. Three measures were outlined: Mahalanobis distance, spectral residual and extrapolation limits.

Three regression methods were briefly outlined: PCR, PLSR and LWR. The latter is a local linearization approach that may be applicable if PCR or PLSR does not give reliable results (e.g. when the $\mathbf{X} \rightarrow \mathbf{y}$ relation is strongly non-linear).

Validation of the multivariate models is important for determination of number of factors to use in the model, and for estimation of prediction accuracy. The

model may then be described by the means of different statistical measures like bias, RMSEP, SEP and correlation.

The models should be valid for as long as possible, in order to avoid time-consuming re-calibrations. Two methods were outlined: to do robust modeling, and to continuously update the models.

Chapter 5

Data-sets: description and pre-study

In this chapter, a description and a pre-study of the NIR data used for modeling and testing in this thesis work is given. For information on the calibration reference methods, see Appendix C and Appendix D.

5.1 General overview

The data-sets used in this thesis were acquired between 1998-07-30 and 1999-01-11. There were 440 density and 383 MFR 2.16 kg/190°C reference measurements available for this period. All NIR spectra were collected in the range from 1300 nm to 2500 nm, but the wavelengths 2401-2500 nm were removed from all spectra due to a very high noise level in that range.

The available data was studied using PCA [Wold et al. (1987)]. Except for mean centering, no pre-processing was done prior to the analysis.

Outliers were found by studying object leverages and residuals. Spectra with high values in both these measures were then studied visually. This proved to be a very effective way of identifying outlier objects.

A small selection of some “typical” spectra acquired from the on-line NIR installation is given in Figure 5.1.

5.2 Density data

The available density data were divided into five blocks. The first block contained one “production cycle”, the next four contained about two cycles¹. A density/time plot for all available data is given in Figure 5.2. The location of five data blocks are given at the top of the plot.

It is important to note that only a subset of all products (see Appendix B) are produced within one production cycle. The cycles, as defined here, are based on density range and not on the actual products produced.

It is believed that sub-dividing the data into these production cycle related groups is the most relevant for the application under study. No matter what

¹One strives to produce the products in a specific sequence, in order to reduce the amount of off-spec material

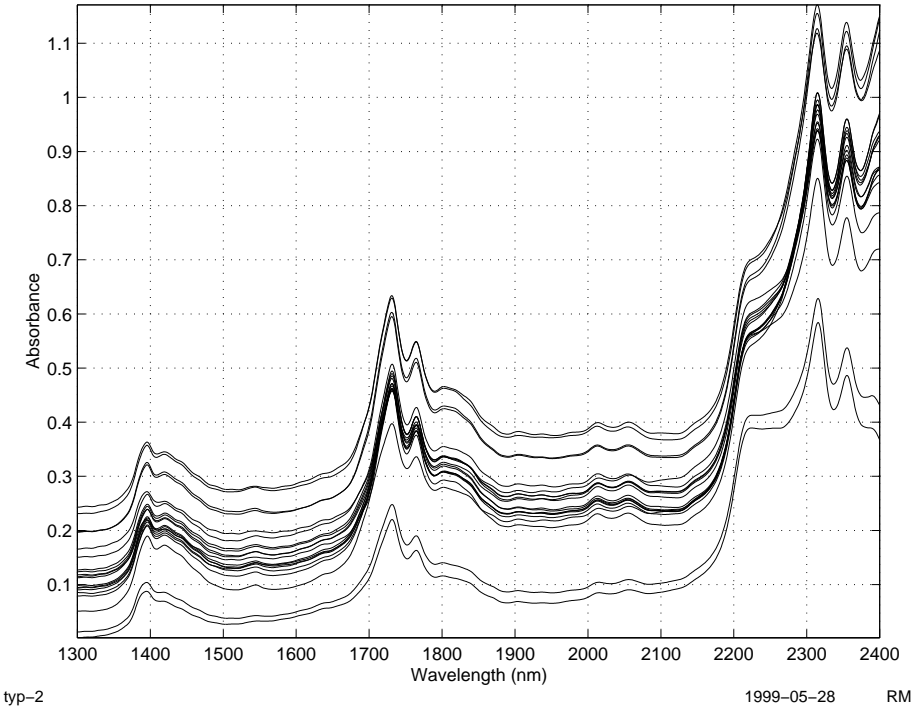


Figure 5.1: Some NIR spectra acquired from the on-line installation

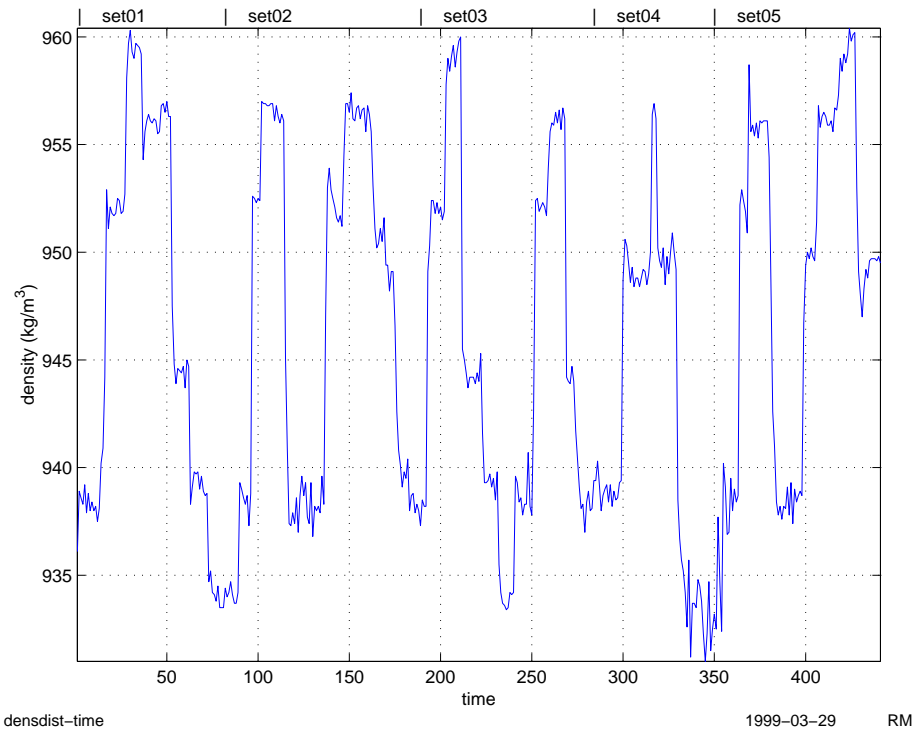


Figure 5.2: Reference density data, collected between 1998-07-30 and 1999-01-11

one includes in a single data-set, new variations (new products/new process parameter settings) will always be ahead in time.

The density reference data were collected approximately every eight hours, but during product transitions the sampling frequency is increased. In November and December the HDPE plant was down several times, and thus there are gaps of several days without samples. Spectrometer down-time has also caused some gaps. These gaps do not appear in Figure 5.2.

A histogram of the available density data is shown in Figure 5.3. Histograms and statistics for each of the data sub-sets are given in Appendix I

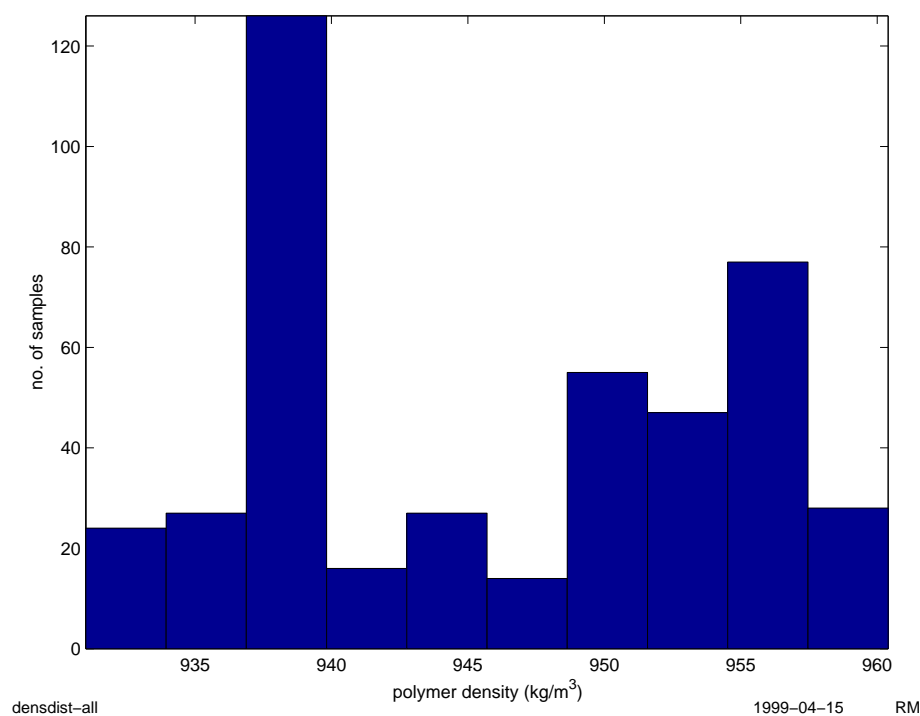


Figure 5.3: Histogram of all available density data

5.2.1 Data-set 1

The NIR spectra in data-set 1 was not collected in the same way as the other data sets. The bellow between the process pipe and spectrometer (see Section 1.5) was not installed when data-set 1 was acquired.

In Figure 5.4 a score-plot (PC1 vs. PC2) is shown. The catalyst names are used as plot markers. It is interesting to compare this score-plot to the particle characterization score plot given in Figure 3.1, as it shows some interesting similarities.

In Figure 5.4 the right-most Magnapore product is ME6930. The Magnapore products with scores about zero on PC1 are HE6905 and HE2615 (there are no HE8214 samples in this data-set). The BC products are more or less clustered to the left of the plot (the BC product with score 0 on PC1 is a transition sample). The spread along PC1 in Figure 5.4 corresponds well with the spread along PC2 in Figure 3.1, and suggests that the major direction in the NIR spectra are connected to particle properties.

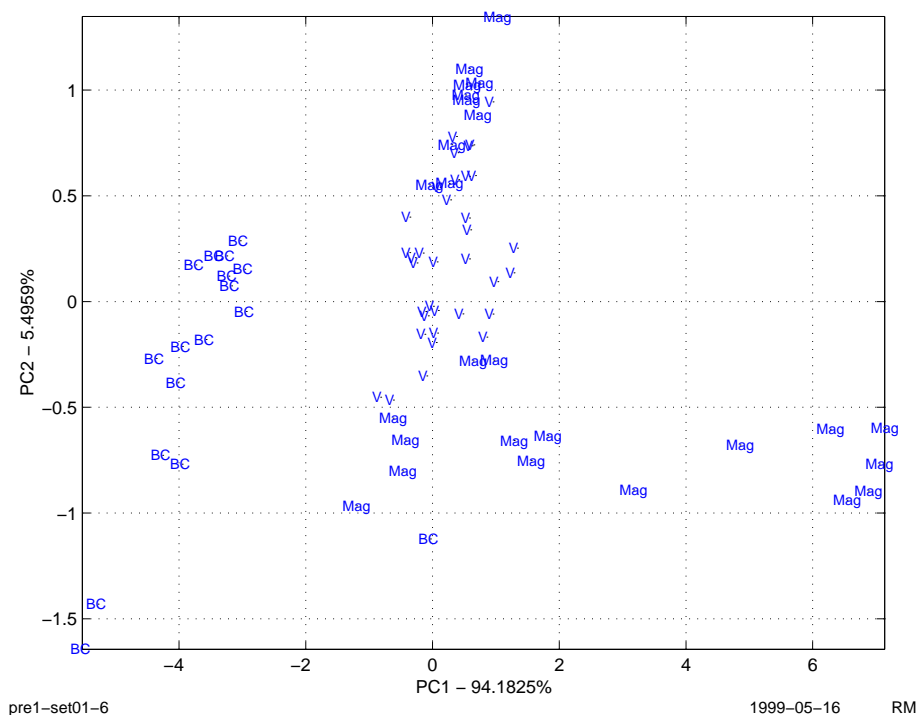


Figure 5.4: Score plot, data-set 1

The loadings for the first six principal components in data-set 1 are given in Figure 5.5. The first two loading-vectors are very similar to the NIR spectra, and are probably modeling baseline features (see Appendix J). PC1 may be modeling particle scattering effects (as discussed above), while PC2 may be modeling variations in concentration of polymer in front of the sapphire window.

An interesting feature in this data-set is that the scores on PC1 correlates with time. The reason for this is not known.

It was found that PC3 was the only component with some correlation to polymer density, with a squared correlation coefficient $r^2=0,49$. Loading-vector three (in Figure 5.5) does not correspond too well with the band assignments given in Section 2.3, except for the bands above 2200 nm.

The methylene first overtone bands are clearly visible in the loading-vector for PC4 (around 1760 nm).

5.2.2 Data-set 2

A score plot for data-set 2 (PC1 vs. PC2) is shown in Figure 5.6. The patterns here do not resemble the score-plot for data-set 1 (shown in Figure 5.4). Here, Magnapore and BC products have about the same score on PC1 and PC2.

Loading vectors 1 to 6 for the PCA on data-set 2 is shown in Figure 5.7. The first four loading vectors are quite similar to those found for data-set 1. Loadings for PC5 and PC6 are quite dissimilar, maybe due to a growing polymer film on the sapphire window? Another surprising feature is that scores on PC1 correlates somewhat with density ($r^2=0,46$), the other PC's do not correlate at all. The look of loading vector 1 suggests that it is modeling baseline features, and not chemical information. None of the calculated PC's correlates with time in this data set.

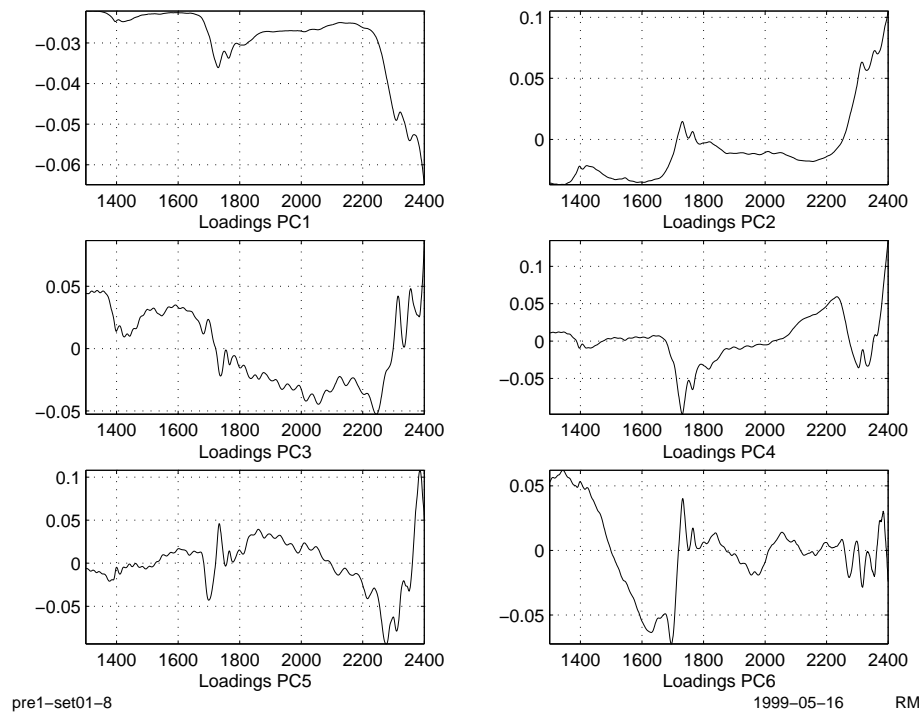


Figure 5.5: Loadings PC1-6, data-set 1

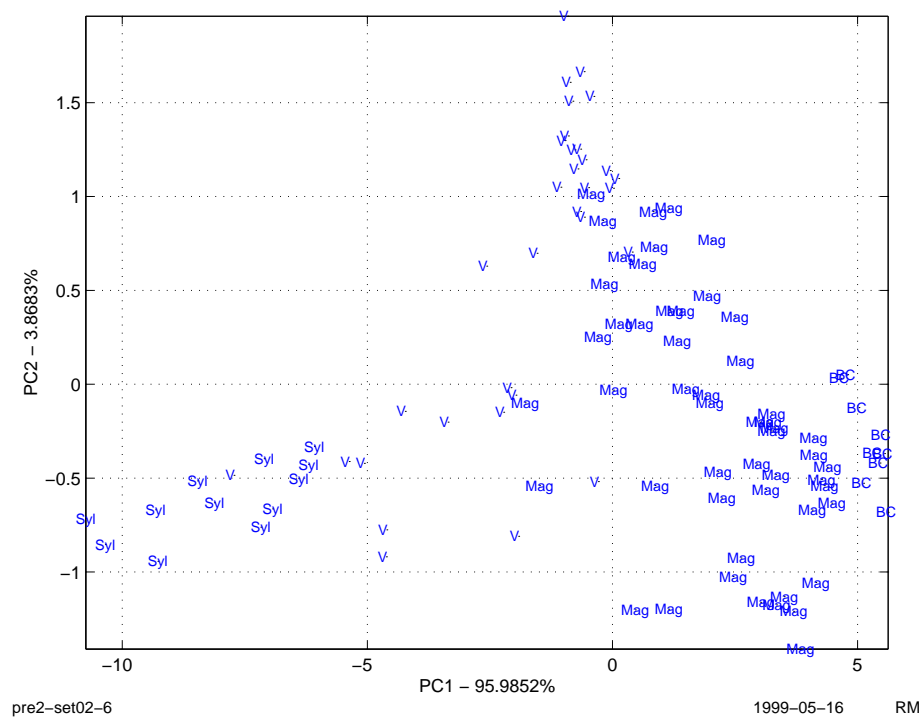


Figure 5.6: Score plot, data-set 2

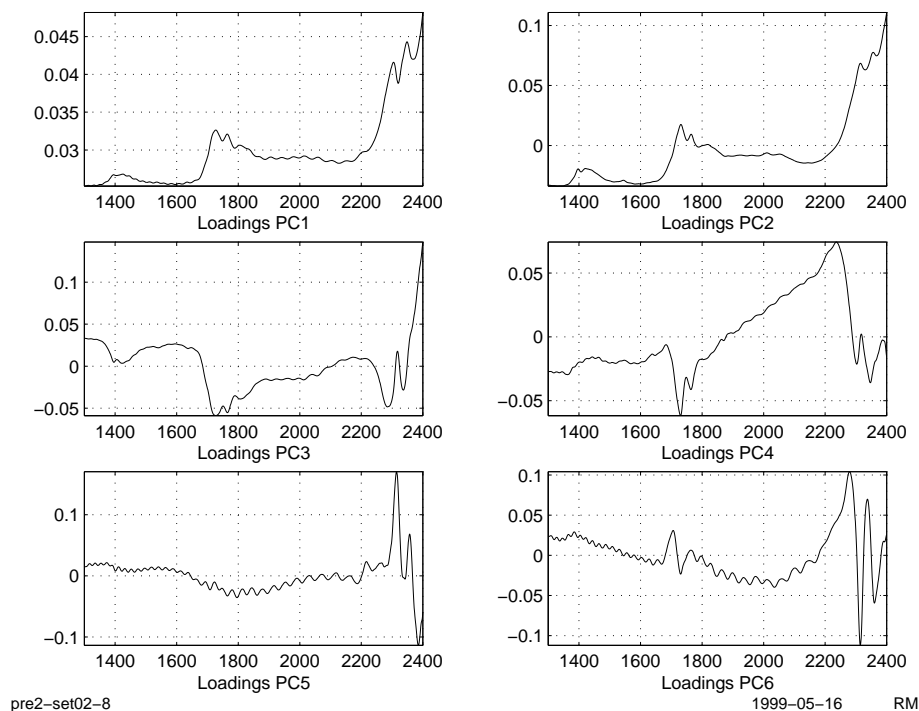


Figure 5.7: Loadings PC1-6, data-set 2

5.2.3 Data-set 3

A score plot for data-set 3 (PC1 vs. PC2) is shown in Figure 5.8. The Magnapore product at the top middle of the plot is HE6905. The Magnapore product in the bottom half of the plot, spread all over PC1, is ME6930. As stated in Section 3.2.2, the particles of this product are known to be very heterogenous. This might explain why it is not clustered as well as the other products.

Loading vectors 1 to 6 for the PCA on data-set 3 is shown in Figure 5.9. Again, the first four loading vectors are quite similar to those found for data-set 1 and 2. Loadings for PC5 and PC6 have similarities with data-set 2. In this data-set, scores on PC4 correlates somewhat with density ($r^2=0,30$). The oscillating noise (described in Section 3.8) can now be seen in the loading vector for PC1.

None of the calculated PC's correlates with time in this data-set either.

5.2.4 Data-set 4

A score plot for data-set 4 (PC1 vs. PC2) is shown in Figure 5.10. This score-plot is quite similar to the score-plot for data-set 1 (Figure 5.4). ME6930 is the only Magnapore product in Figure 5.10.

An oscillation with decreasing frequency from 1300 nm to 2400 nm is clearly visible in loading vector 1, 4, 5 and 6 for data-set 4, shown in Figure 5.11. Loading vectors 3 to 6 have now changed, compared to the other data-sets. Scores on PC2 correlates somewhat with density ($r^2=0,42$). Again it looks like density correlates with a PC that apparently models baseline effects.

As for data-set 1, there is correlation between PC1 and time in this data-set also.

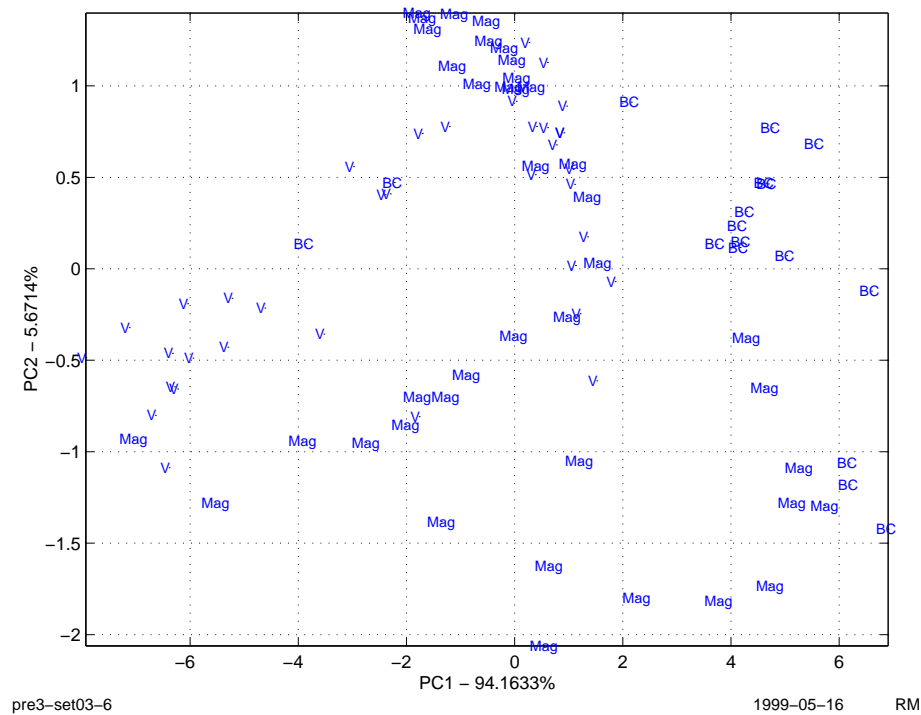


Figure 5.8: Score plot, data-set 3

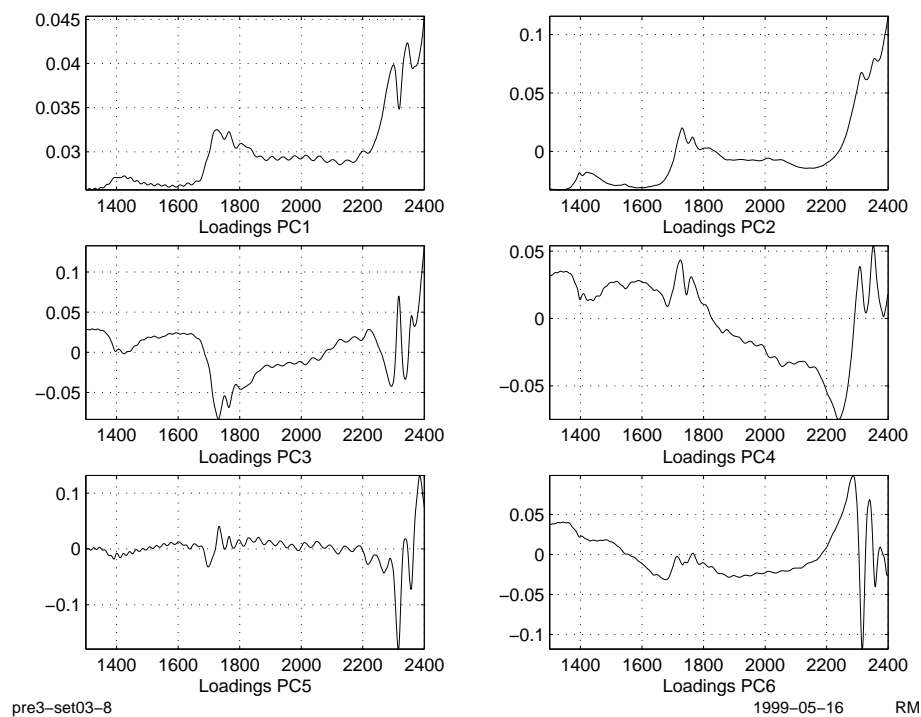


Figure 5.9: Loadings PC1-6, data-set 3

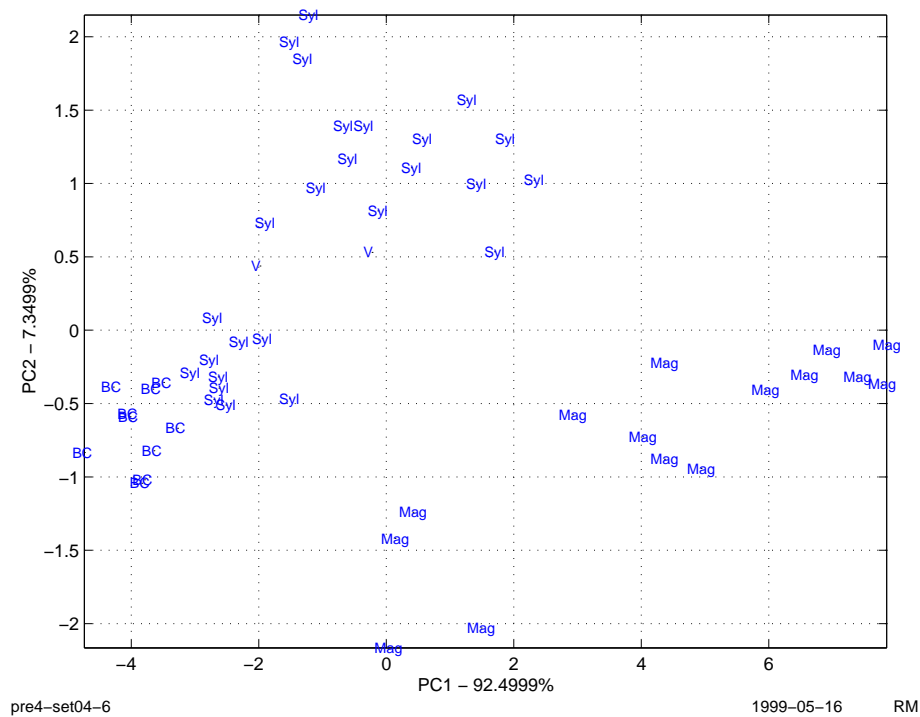


Figure 5.10: Score plot, data-set 4

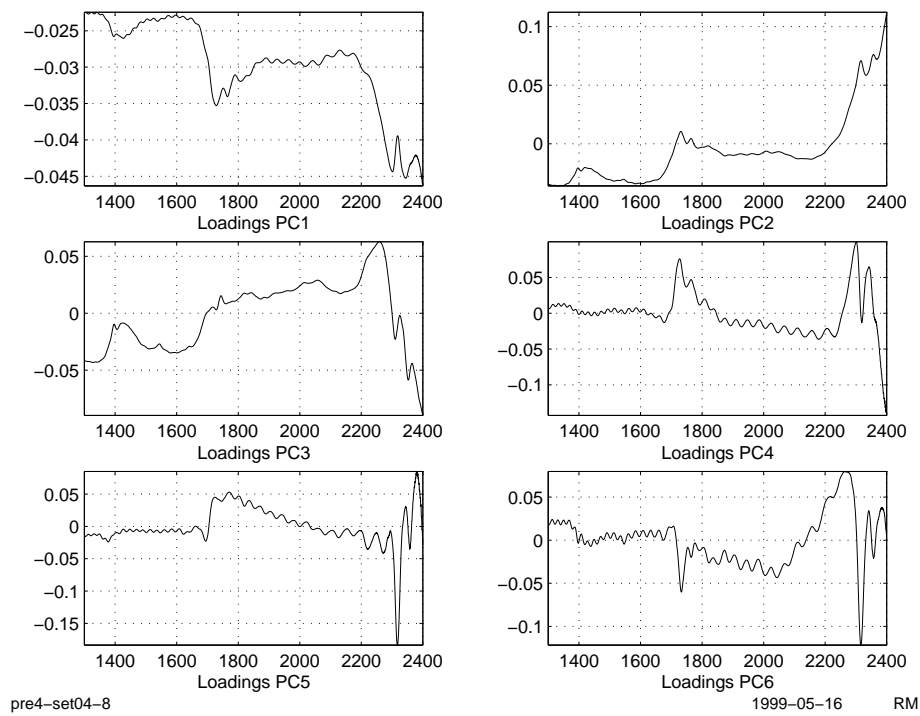


Figure 5.11: Loadings PC1-6, data-set 4

5.2.5 Data-set 5

A score plot for data-set 5 (PC1 vs. PC2) is shown in Figure 5.12. It is interesting to note that a smaller amount of variance is captured in PC1 (90%), compared to the previous data-sets (around 95%). The Magnapore cluster at the left is ME6930.

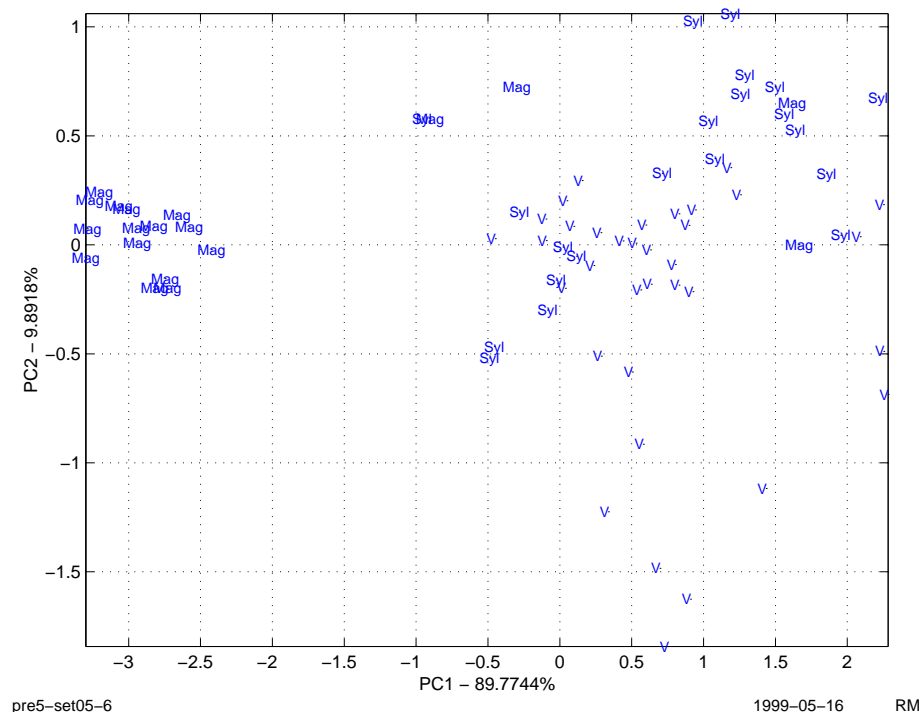


Figure 5.12: Score plot, data-set 5

The oscillation evident in data-set 4, is also easily spotted in data-set 5. Loadings for PC1-6 are shown in Figure 5.13. Loading vectors for PC 4-6 have changed, compared to the previous data-sets.

Scores on PC1 now correlates somewhat with density ($r^2=0.66$). Again it looks like this is related to baseline effects. None of the calculated PC's correlate with time.

5.2.6 Final remarks, density data

It appears like that the noise-level in the spectra has increased in time. One evidence of this is the number of outliers that had to be removed for this pre-study:

Data-set	outliers removed
1	2
2	1
3	2
4	13
5	18

Preliminary regression model tests also emphasized the problem with very noisy data. It was possible to make good internally (cross-) validated models using

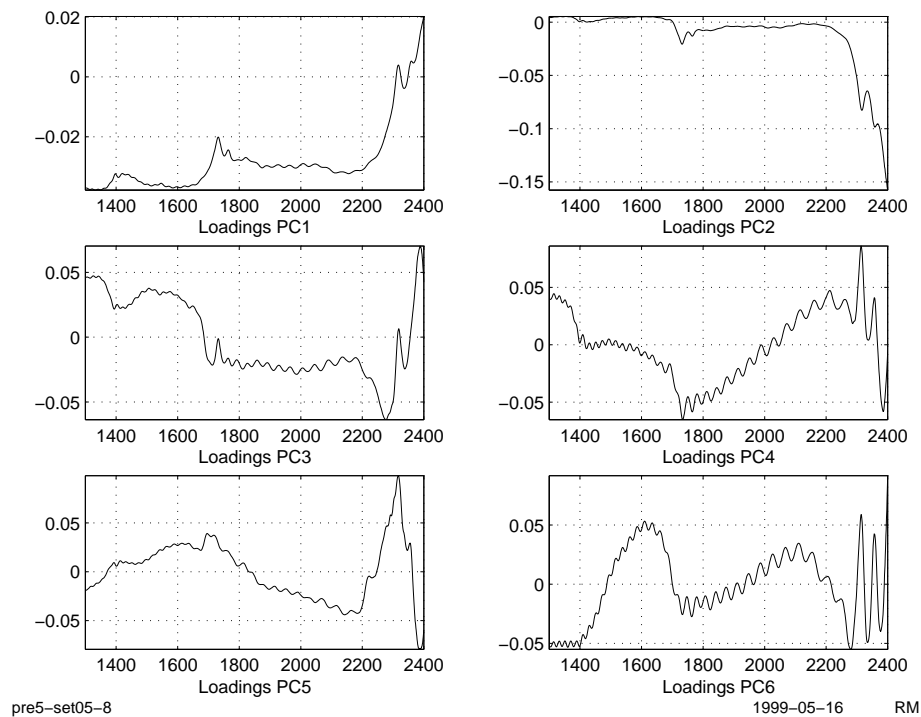


Figure 5.13: Loadings PC1-6, data-set 5

data-set 1 and 5. Data-set 2 and 3 were problematic, and it was not possible to make any reasonable internally validated model on data-set 4.

The position of three different peaks in the NIR-spectra has been monitored over time. It looks like the problem with shifts in the spectra was particularly prominent at time $t=350$ (data-set 4), see Figure 5.14. Comparing this to Figure 5.2 one notices that this contains the overall minima of density-values for all available data. The product produced at that time was ME8168.

The sapphire window was cleaned in week 44, 1998. This is between sample 321 and 322 in the density-data (both samples are in data-set 4). It is suggested that there might be a connection between the cleaning of the window and the shift around $t=350$, but this has not been investigated further.

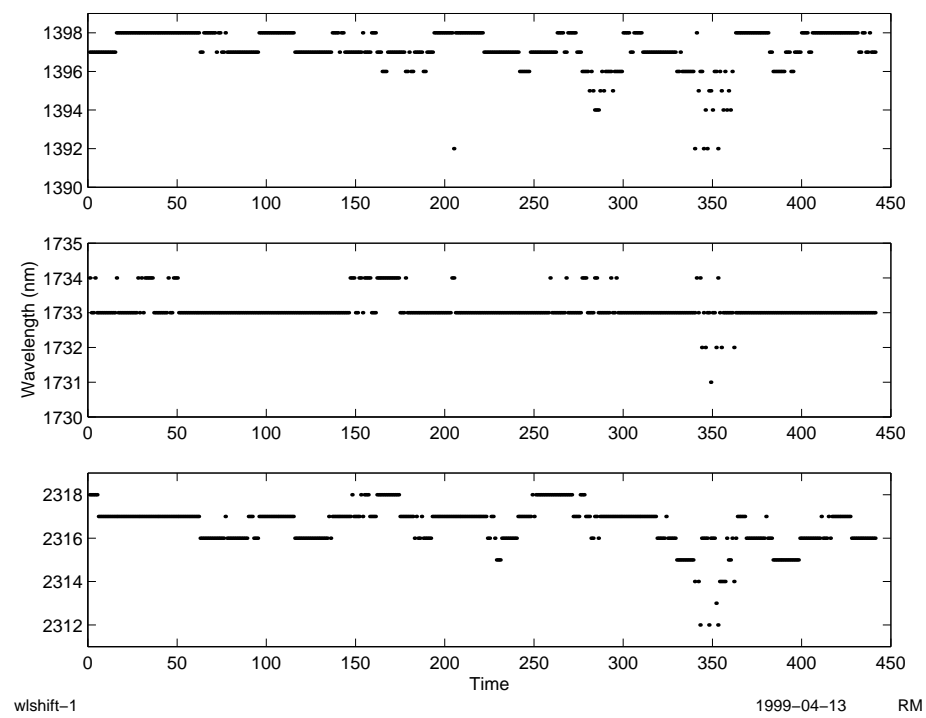


Figure 5.14: Monitoring of shifts in spectra

5.3 MFR data

The MFR 190°C/2,16 kg data was divided into two data-sets. The distribution of values is shown in Figure 5.15. There are three distinct levels: below 1, around 3 and around 6. MFR 190°C/2,16 kg are only measured for these products:

HE6905	HE8343	HE8363
ME8160	ME8164	ME8166
ME8168		

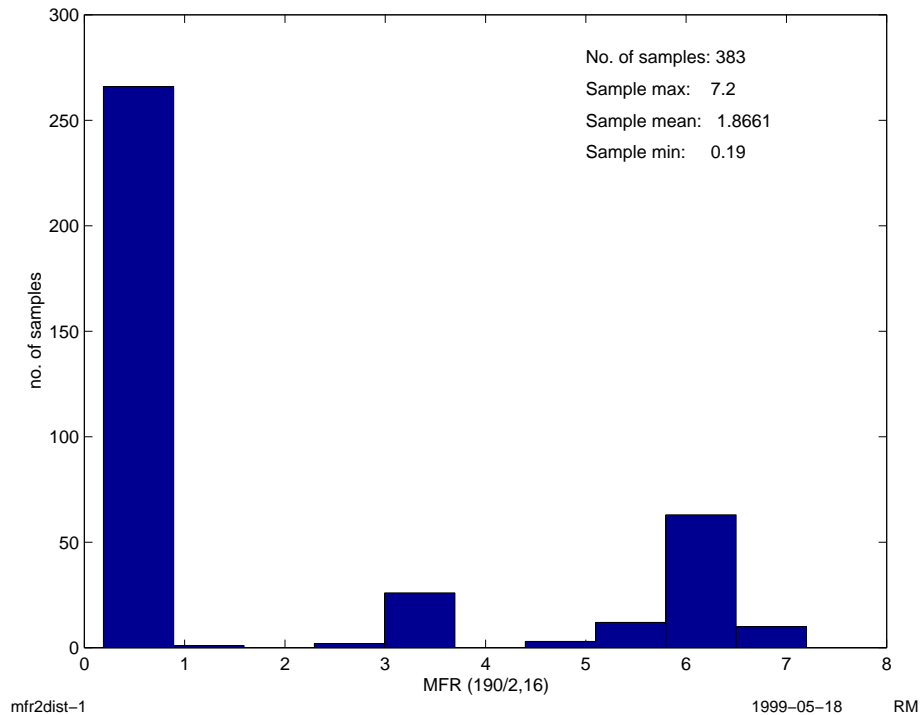


Figure 5.15: Histogram of all available MFR 190/2,16 data

The distribution of the MFR values with time is shown in Figure 5.16 (position of data-set one and two is marked with a vertical line). Because MFR 190°C/2,16 kg are not measured on all products, the samples are *not* evenly spaced in the time-domain.

The sapphire window was cleaned in week 44, 1998. This is between sample 285 and 286 in the MFR-data.

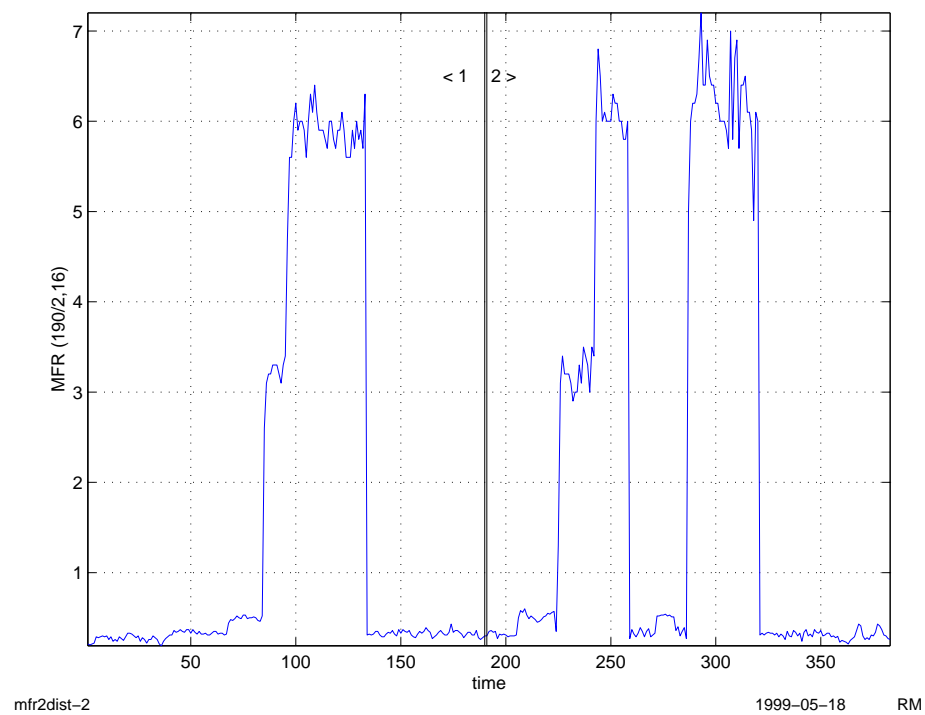
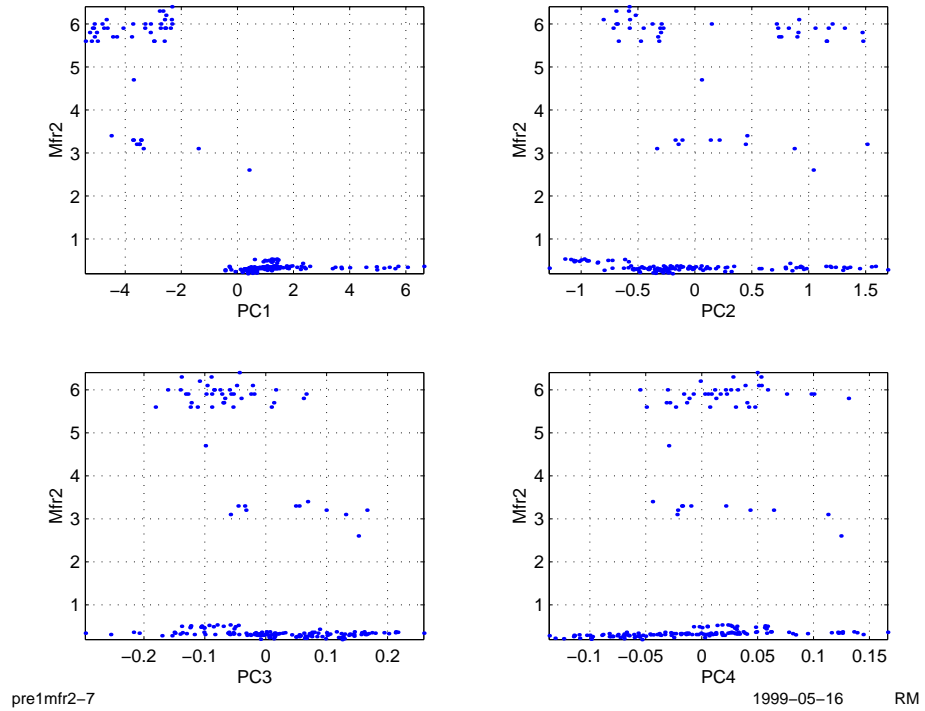


Figure 5.16: Distribution of available MFR 190/2,16 data with time

5.3.1 Data-set 1

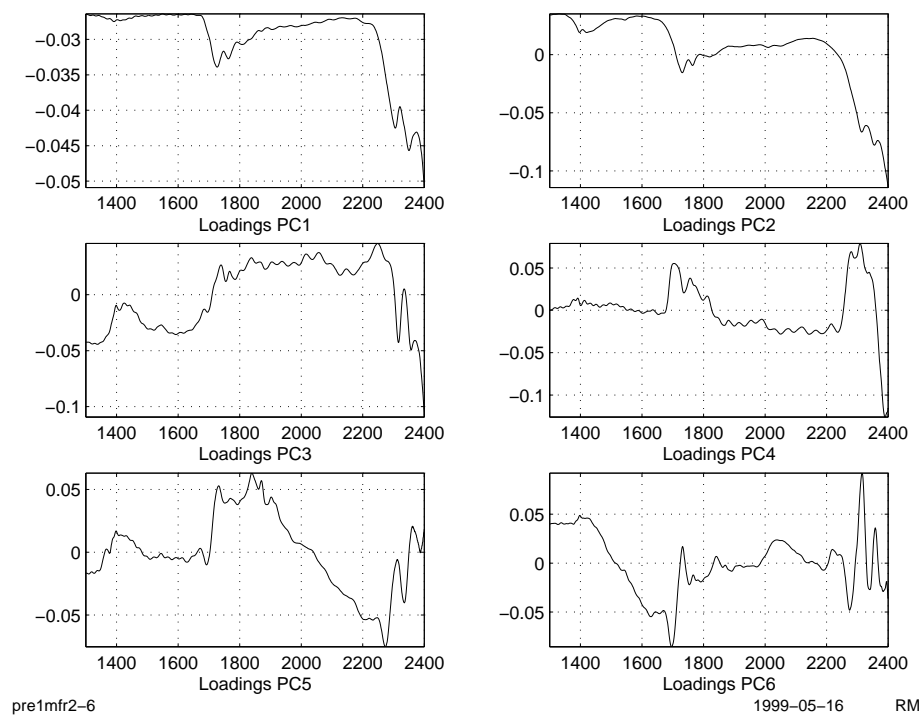
In Figure 5.17 object scores for PC 1-4 are plotted against MFR values. It is obvious from these plots that objects with low MFR have high scores on PC1. The squared correlation coefficient is $r^2=0.69$.

Figure 5.17: Objects scores and MFR 190/2,16 values



The loadings for the six first principal components are shown in Figure 5.18. As for the density data analysis, the two first components appears to be modeling baseline features.

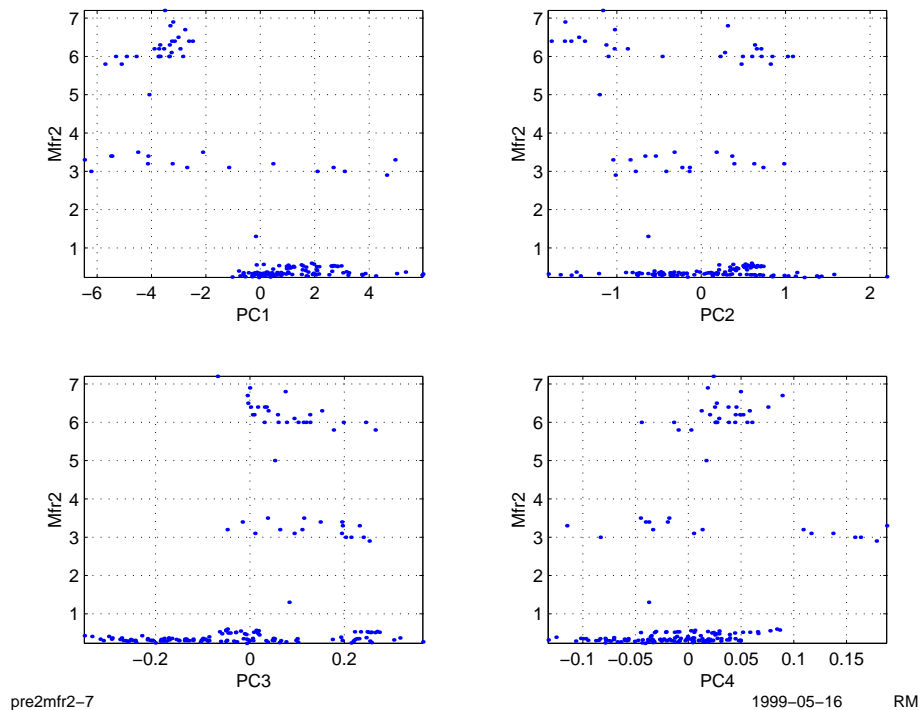
Figure 5.18: Loadings PC 1-6, MFR data-set 1



5.3.2 Data-set 2

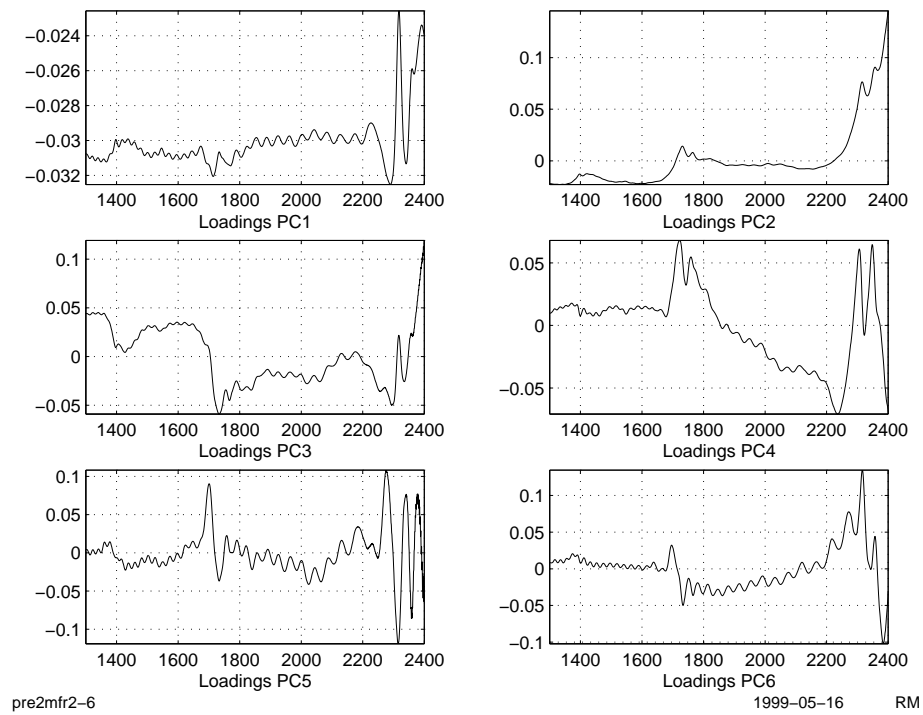
In Figure 5.19 object scores for PC 1-4 are plotted against MFR values. Again it can be seen that objects with low MFR have high scores on PC1, but the objects with MFR-values around 3 are spread all over PC1. The squared correlation coefficient is $r^2=0.52$.

Figure 5.19: Objects scores and MFR 190/2,16 values



The loadings for the six first principal components are shown in Figure 5.20. It is interesting to note here that the first component is *not* a typical baseline feature. The oscillating signal is clearly visible, and the loadings around 2300 nm looks like a shift.

Figure 5.20: Loadings PC 1-6, MFR data-set 2



5.4 Summary and conclusion

The major variations in the available NIR data seems to be related to particle properties (seen as baseline effects), and probably also to concentration of polymer in front of the window. These effects probably makes up about 95-99% of the variations in the NIR spectra.

The spectra seem to undergo constant changes with time. Most noticeable is the oscillating signal, responsible for more and more variation in the spectra with time (seen from the PCA loading vectors).

Chapter 6

Calibration strategy applications and discussion

In this chapter some strategies for calibration of the NIR instrument are presented. General considerations regarding outlier detection is given in the first section.

Many strategies for selecting calibration data, wavelengths and pre-processing techniques were tested. Only the most interesting strategies are presented here.

The two regression methods PLSR and PCR were considered for the density calibration application. In addition, LWR was considered for the MFR calibration application.

6.1 Outliers in the calibration and test-set data

Outliers in the calibration data-sets were identified by studying their PCA scores (see Section 5.1), $\tilde{\mathbf{X}}$ and $\tilde{\mathbf{y}}$ residual, leverages and position in t vs. u plots. Cross- and test-set validations were used to verify that the suspicious objects were in fact outliers, and not important extremes.

Using test-sets for identifying outliers in the calibration data proved to be very important. Removal of some objects gave far better cross-validation results, but poorer test-set validation results. They were in fact important extremes, and this could only be identified by test-set validation.

Consider as an example the t vs. u plots shown in Figure 6.1. Object 21 has a high leverage, and the t vs. u plots suggests that this object is an outlier (see e.g. t_5/u_5 and t_6/u_6). The model used here is a density calibration, using 6 bilinear factors. The spectra were pre-processed by using the Savitzky-Golay algorithm to obtain second derivative spectra.

Removal of object 21 gave better cross-validated results, but worse test-set validated results. Object 21 was in fact an important extrema! The cross- and test-set validated results are given in Table 6.1.

Outlier removal in the test-set data was done automatically, no objects were removed manually prior to the validation. This strategy was selected for two reasons:

1. As a basis for the application, large prediction errors must be considered to be due to either an insufficient model, or due to a spectral outlier in the test-set data.

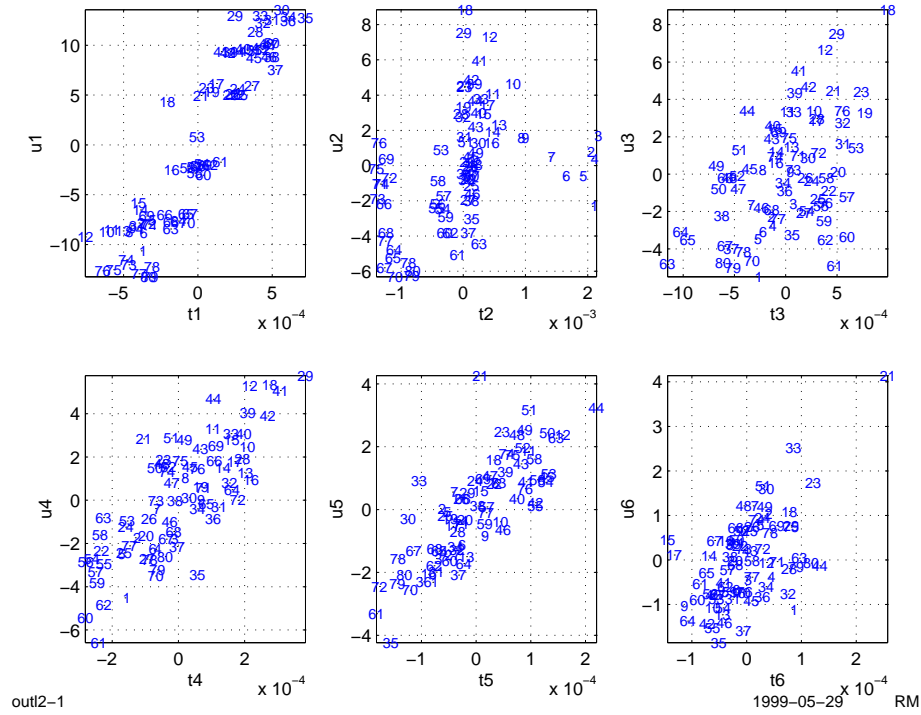
Figure 6.1: t vs. u , outlier example

Table 6.1: Cross- and test-set validated results, outlier example, density predictions

-	RMSECV	RMSEP
With object 21	2.98	2.90
Without object 21	2.76	3.36

2. The automatic outlier removal scheme must be an integral part of the on-line application.

For the models presented in the following sections, the number of removed outliers is an important measure of the model quality together with RMSEP. The optimization criteria is then to minimize number of outliers removed while simultaneously minimizing RMSEP.

The automatic outlier detection scheme is solely based on $\tilde{\mathbf{X}}$ information, the available $\tilde{\mathbf{y}}$ information was not used. Each test-set prediction had to pass three criterias:

1. A maximum Mahalanobis distance limit.
2. A maximum spectral residual limit.
3. An extrapolation limit.

The Mahalanobis distance and spectral residual are dependent on the model, and the limits must be optimized individually for each tested model. In the implementations tested in this thesis work, the limits were set so that all calibration samples of the final models passed the tests. The extrapolation limit was set to ± 0.1 of the max and min density value of the calibration objects, i.e. effectively no extrapolation was allowed.

The outlined outlier detection scheme is a simple implementation of [ASTM D 6122 (1997)]. The ASTM standard suggests a very rigid outlier detection scheme, but there was not time to implement the full standard. The implemented scheme fulfills the minimum requirements set by the standard¹.

6.2 Density models

Calibration strategies for density calibrations are given in the following subsections. The strategy for detecting (and removing) outlier objects in the test data was done as described in Section 6.1.

There appeared to be a slightly non-linear relation between $\tilde{\mathbf{X}}$ and $\tilde{\mathbf{y}}$ in some of the tested models (observed in t vs. u plots), but attempts to linearize (by simple transforms of $\tilde{\mathbf{X}}$ or $\tilde{\mathbf{y}}$, e.g. using the square root) did not improve the models. It was also found that only small changes in the pre-processing or wavelength selection “straightened” the non-linear t/u -relation.

6.2.1 Selection of calibration data

As noted in Section 5.2.6 some of the data-sets were excessively noisy, and more or less unusable for calibration purposes². Data-set 1 was therefore used for calibration, and the remaining data-sets were used for testing. No objects were identified as outliers in data-set 1.

¹The ASTM standard covers everything from initial tests of the spectrometer after installation, to continuous verification of instrument and calibration model performance. In this thesis work, only the outlier detection part of the standard was tested.

²If all outliers in these data-sets were removed, they would also (of course) be usable for calibration purposes.

6.2.2 Selection of regression method

Because the major variations in the NIR spectra are due to baseline features (see Chapter 5), it was found that PCR was not feasible as the regression method. It was found that it was necessary to use 2-3 more factors in models built using PCR to make them perform about as well as models built using PLSR. It was also found that if the data was autoscaled prior to calibration, the PCR-based models failed completely. PLSR is used in all density models presented here.

6.2.3 Calibration on raw data

This calibration scheme is presented for comparison reasons only. The calibration is done on raw data (no pre-processing) using all wavelength variables (1300-2400 nm).

A graphical presentation of the model is given in Figure 6.2, and a summary of statistics is given in Table 6.2. Accepting that the peaks in the RMSECV curve are due to the complex baseline features in the spectra, 7 factors were used in this model (optimal number of factors were found from later test-set validation).

Very little \hat{y} variance is captured in the first two factors (see Figure 6.2). If these factors are needed to model the baseline features, it is also clear that these features have effectively no correlation with density.

Figure 6.2: Cross-validated density model, raw data

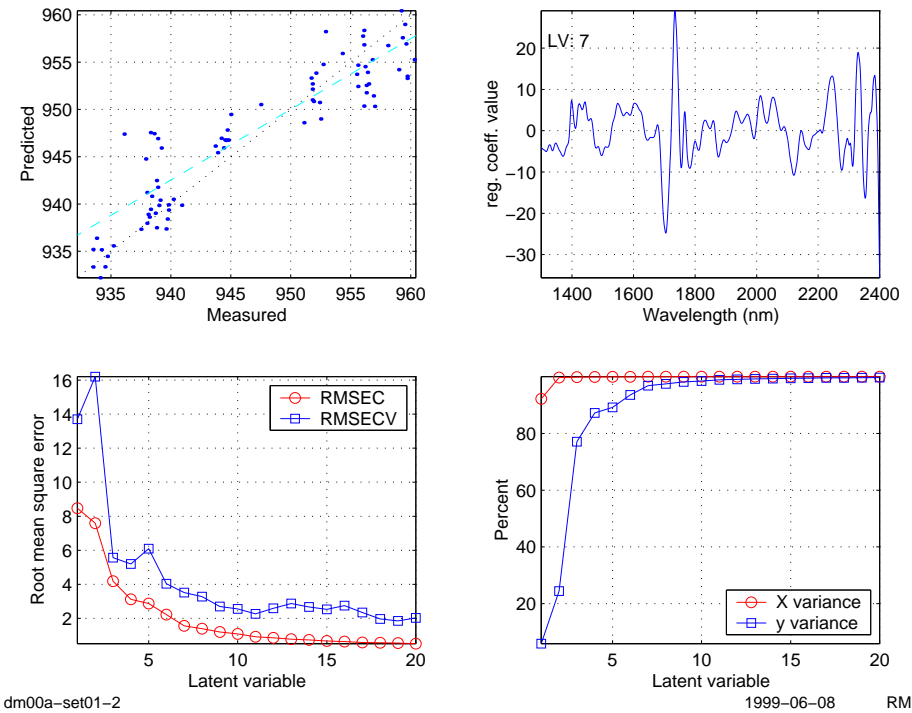


Table 6.2: Cross-validated density model, raw data

Bias	Correlation	SEC	RMSECV	Factors used
0.39	0.92	3.51	3.51	7

An interesting feature due to the *cross-validation by class* scheme is that ME6930 is not predicted well. This is seen as the little cluster with measured values just below 940 and predicted values between 940-950. This may be due to the fact that ME6930 particles are very heterogenous (see Section 3.2.2), or due to the problem with polymer film on the sapphire window when producing this product (see Section 3.8). One should maybe expect this last problem on ME8168 too, but it is not the case here.

It may be suggested that ME6930 represents an outlier group, and thus should be removed from the calibration data-set. This would imply that a separate calibration model must be built for prediction of density for this product. It will further result in a need for a system that detects that ME6930 is produced and automatically switches to the correct model, or the operators must change models manually.

It may also be argued that ME6930 represents important extremes in the \mathbf{X} space, and thus are important to include in the model. The effect of removing ME6930 is tested in Section 6.2.9.

A summary of the test-set validation results are given in Table 6.3. The outlier detection system was switched off in this test, only the known outliers found in the pre-study (see Chapter 5) were removed prior to the test (34 objects, or 9.4% of the total test-set data). No further plots are given for this model, but extensive graphical presentations for the density calibration schemes presented in Section 6.2.5 are given in Appendix N.

Table 6.3: Test-set validated density model, raw data, known outliers removed

Test-set name	Bias	Correlation	SEP	RMSEP	%RMSEP
set02	-3.82	0.81	4.94	6.23	52.1
set03	-4.55	0.85	4.26	6.22	46.8
set04	-2.96	0.79	5.40	6.11	47.6
set05	3.26	0.93	2.66	4.20	36.5

6.2.4 Selection and optimization of the pre-processing step

It is clear from the pre-study and the calibration model built on raw data that there are severe baseline effects that should be reduced as much as possible prior to the calibration (and prediction). Many different combinations of all the pre-processing methods presented in Section 4.5 were tested.

After the preliminary tests, it was decided to go for a combination of SNV and second derivative spectra. It is believed that this combination reduces all the baseline effects: offsets, multiplicative and additive. A combination of MSC and second derivative spectra also gave promising results. SNV was selected because it appeared to work as well as MSC, and because it is much easier to use than MSC (it requires no reference spectrum).

Further work focused on optimizing the number of points to include in the window used for the Savitzky-Golay algorithm, in conjunction with:

- mean centering or autoscaling
- applying SNV before or after derivation
- the wavelength range to use

- number of bilinear factors to include in the model

300 different models were built to find the optimal combination of these elements. A graphical presentation of all 300 models is given in Appendix L.

In summary it was found that using the optimal number of points in the Savintzky-Golay algorithm had great effect on the prediction accuracy. Depending on the other pre-processing performed on the data, the optimal window size varied from 3 to 37. Thus it is hard to predict the optimal number of points, it must be found from extensive testing.

Some of the tests were done without performing SNV (i.e. only using the second derivative spectra). These models always performed poorer than the models that also used SNV.

As stated in Section 4.5.8, wavelength selections found by using GA gave very promising cross-validated results. Unfortunately, the selections were not successful in later test-set validations. Better design of the data to use in the algorithm, and better understanding of setting the initial parameters for the algorithm is probably needed for later employment.

For the tests done at this stage, three wavelength regions were used: 1300-1800 nm, 1300-2110 nm and 1300-2400 nm. It was found that using the full spectra (1300-2400 nm) gave poorest prediction results, and that using the region 1300-2110 nm performed slightly better than 1300-1800 nm.

In most of the tested models, the optimal number of bilinear factors were found to be four (max number of calculated factors were six).

6.2.5 Final pre-processing schemes

Three pre-processing schemes were selected for the final tests.

Modeling scheme A This model uses the wavelength range 1300-2110 nm. The data is first treated with SNV. The Savintzky-Golay algorithm is then used to obtain the second derivative spectra, fitting a second order polynomial with a 31 point window (see the discussion in Section 4.5.4 on this). Finally, the $\tilde{\mathbf{X}}$ -data is mean centered.

Modeling scheme B This model uses the wavelength range 1300-2110 nm. The data is first treated with SNV. The Savintzky-Golay algorithm is then used to obtain the second derivative spectra, fitting a second order polynomial with a 5 point window. Finally the $\tilde{\mathbf{X}}$ -variables are autoscaled.

Modeling scheme C This model uses the wavelength range 1300-2110 nm. The second derivative spectra is obtained using the Savintzky-Golay algorithm, fitting a second order polynomial with a 23 point window. The second derivative spectra are then treated with SNV. Finally the $\tilde{\mathbf{X}}$ variables are autoscaled.

A summary of cross-validation results are given in Table 6.4. Graphical summaries are given in Appendix M. It may there be observed that much more of the $\tilde{\mathbf{y}}$ variance is modeled in the first two factors, compared to the model made from raw data. It appears that the pre-processing done on the data has in fact removed variations that are un-related to density.

It is apparent from the cross-validated results that model C performs much better than the other two models.

Table 6.4: Cross-validated density model results

Model	Bias	Correlation	SEP	RMSECV	Factors used
A	0.29	0.98	2.05	2.05	4
B	0.14	0.98	1.85	1.84	4
C	-0.20	0.99	1.44	1.44	4

It was found that the cross-validated results did not give a good basis for selecting the optimal number of factors to use in the models. Therefore the number of factors were chosen from evaluation of the test-set validation results.

The regression vectors for the models A, B and C are shown in Section M. It is easy to see from the regression vectors for model B and C that the raw data was autoscaled, the vector is very “messy” and hard to interpret. The regression vector for model A has high values at all expected absorption bands (see Table 2.1), some of them are slightly shifted. There are also some peaks in the regression vector that are unidentified, e.g. the peak at 1684nm. Both neighbor peaks were assigned in Table 2.1, the peak at 1634nm (coming exactly at that position in the regression vector) and at 1698nm (probably appearing at 1695nm in the regression vector).

The previously discussed problem with ME6930 may also be observed in model A, and to some extent in model B. It is not very noticeable in model C.

6.2.6 Test-set validation of models

In this test the models were test-set validated. Only the known outliers found in the pre-study (see Chapter 5) were removed prior to the test (34 objects, or 9.4% of the total test-set data). A summary of the results are given in Table 6.5, Table 6.6 and Table 6.7.

Table 6.5: Test-set validation of density model A, known outliers removed

Test-set name	Bias	Correlation	SEP	RMSEP	%RMSEP
set02	0.31	0.97	1.95	1.97	16.5
set03	-1.86	0.92	3.05	3.55	26.7
set04	-3.70	0.95	2.85	4.65	36.2
set05	0.01	0.97	2.78	2.76	24.0

Table 6.6: Test-set validation of density model B, known outliers removed

Test-set name	Bias	Correlation	SEP	RMSEP	%RMSEP
set02	0.11	0.98	1.87	1.86	15.6
set03	-0.47	0.96	2.38	2.41	15.5
set04	-3.16	0.92	3.65	4.80	37.4
set05	-0.46	0.97	3.15	3.16	27.5

The test-set validation results indicates that the estimated prediction errors found from the cross-validation (given in Table 6.4) are reliable “short term”

Table 6.7: Test-set validation of density model C, known outliers removed

Test-set name	Bias	Correlation	SEP	RMSEP	%RMSEP
set02	-0.18	0.97	2.06	2.06	17.2
set03	-1.36	0.95	2.66	2.98	22.4
set04	-2.54	0.91	3.84	4.58	35.6
set05	-0.65	0.96	3.47	3.50	30.5

estimates for model A and B (set02 is closest in the time-domain to the calibration data-set). Model C got very good cross-validated results, but do not perform better than the other models in the test-set validation. The reason for this is not known.

6.2.7 Application test with outlier detection system

In this test all available data were used as test-sets, and the automatic outlier detection system was activated. None of the known outliers were removed prior to the test.

The test-set validation results with automatic outlier removal for the three models, A, B and C, are given in Table 6.8, Table 6.9 and Table 6.10. Outlier detection limits (residual, Mahalanobis distance and extrapolation) were set according to the description given in Section 6.1. Extensive graphical presentations of the test-set validations are given in Appendix N.

Table 6.8: Test-set validation of density model A, automatic outlier removal

Test-set name	Outliers removed (%)	Bias	Correlation	SEP	RMSEP	%RMSEP
set02	38.7	0.71	0.98	1.50	1.65	13.8
set03	61.1	-0.15	0.99	1.10	1.09	8.2
set04	72.7	-1.67	0.58	2.05	2.60	61.1
set05	75.3	0.87	0.79	1.66	1.84	38.3

Table 6.9: Test-set validation of density model B, automatic outlier removal

Test-set name	Outliers removed (%)	Bias	Correlation	SEP	RMSEP	%RMSEP
set02	23.6	0.09	0.98	1.66	1.65	13.8
set03	38.9	0.62	0.97	1.93	2.01	15.1
set04	71.2	0.11	0.61	2.79	2.72	31.1
set05	79.6	1.53	0.98	0.85	1.74	28.5

The number of detected (and removed) outlier predictions are increasing with time for all models. This is an expected behavior; as the model gets older, it gets more and more “outdated”.

As seen from the plots in Appendix N, most of the severe outlier predictions are correctly identified for all three models, but too many “good” predictions are

Table 6.10: Test-set validation of density model C, automatic outlier removal

Test-set name	Outliers removed (%)	Bias	Correlation	SEP	RMSEP	%RMSEP
set02	17.9	0.06	0.97	2.07	2.06	17.2
set03	36.8	-0.28	0.97	1.94	1.95	14.6
set04	71.2	0.26	0.65	2.68	2.62	30.0
set05	86.0	0.95	0.95	1.31	1.58	35.1

also removed. The implemented outlier detection scheme appears to need some optimization/improvements.

It appears from the graphical presentations that the prediction error is greatest on high density products at the beginning of the time period (set02 and set03), and then shifts to have problems on low density products (set04 and set05). This observation is general for all three models. The reason for this has not been found.

6.2.8 Expanding the calibration data set

It was expected that including samples from more than one product campaign in the calibration data set would improve the calibration model. The reason for expecting this, was:

- more of the expected variation in the polymer and sample system would be incorporated into the model
- if the error in the reference method has a symmetrical distribution, more samples would improve the model

A new calibration data-set was assembled from data-set 1 and 2. Outlier objects were removed, and the pre-processing schemes A, B and C were tested.

The models made from scheme A, B and C gave less precise predictions when an expanded calibration set was used (compared to the previously presented models), which was not as expected. At the same time, more objects were let through the outlier detection system. This is probably due to the fact that more variation is included in the model. The test-set validation results are given in Table 6.11.

Table 6.11: Test-set validated density models, expanded calibration data-set

Pre-processing scheme	RMSECV	RMSEP set03	Outliers set03 (%)	RMSEP set04	Outliers set04 (%)	RMSEP set05	Outliers set05 (%)
A	2.31	3.38	6.3	3.16	55	1.59	32
B	2.59	2.16	9.5	3.09	56	1.79	39
C	2.54	2.82	7.4	2.78	65	2.75	51

6.2.9 Excluding ME6930 in models

The previous models suggest that it might be suitable to use two different models for density predictions: one with ME6930 included, and one without this

product. A graphical summary of a model built without ME6930 is shown in Appendix M. It was made as described for modeling scheme A (see Section 6.2.5), and is named A* here and in the appendix. A summary of the cross-validated results is given in Table 6.12. As for the previously presented models, the optimal number of factors were chosen from the test-set validation results.

Table 6.12: Cross-validated density model A* results

Bias	Correlation	SEP	RMSECV	Factors used
-0.05	0.96	2.32	2.30	3

The cross-validation predicted/measured plot (given in Appendix M) shows a really interesting feature. While a cluster of ME6930 samples previously showed up as a possible outlier group, a new group of samples shows the exact same feature here. All three HE2615 samples in the calibration data gets far to high predicted density values.

A possible explanation to this behavior is that ME6930 defines some subspace limits in $\tilde{\mathbf{X}}$ (e.g. variations due to particle scattering effects). When the ME6930 objects are removed from the calibration data-set, another product take this role. Unfortunately, HE2615 is not among the products analyzed in Section 3.2.2, but it is interesting to note that this is also a Magnapore product.

The test-set validation results is given in Table 6.13. All ME6930 samples in the test-sets were removed prior to the validation. The outlier detection system was active. Graphical summaries of this test-set validation is given in Appendix N.

Table 6.13: Test-set validation of density model A*, automatic outlier removal

Test-set name	Outliers removed (%)	Bias	Correlation	SEP	RMSEP	%RMSEP
set02	54.8	1.46	0.99	1.24	1.90	16.2
set03	58.6	-0.05	0.99	0.81	0.79	6.0
set04	63.3	-0.59	0.74	1.73	1.78	42.0
set05	84.6	1.00	0.96	0.86	1.30	36.0

The test-set validation results show that unacceptably many outlier predictions are removed already in the first data-set. This may again suggest that ME6930 is important for proper spanning of the \mathbf{X} space.

6.2.10 Model updating applications

Some strategies for calibration model updating were discussed in Section 4.10.2. Due to time-limitations, only two simple strategies were tested.

In the first test the calibration model was kept at a constant size of 100 calibration objects. Prediction was then done on five objects ahead in time of the last object included in the model. Under normal plant operation five reference measurements is acquired in about 40 hours. After prediction the objects were included in the model, the five oldest objects were removed, and a new model was built. This is denoted the *moving window PLSR* in the following.

In the second test the calibration model initially contained 100 calibration objects. Prediction was then done on five objects ahead in time of the last object

included in the model. After prediction the objects were included in the model, and a new model was built. This is denoted the *growing PLSR* in the following.

No outlier detection scheme was implemented for any of these test (again due to time-limitations), but prior to the tests all known outliers found in the pre-study (Chapter 5) were removed (a total of 34 objects, or 9.4% of the total test-set data).

The *moving window PLSR* worked very well for all the pre-processing schemes (A, B and C) described in the previous sub-sections. A summary of results from this test is given in Table 6.14. Taking into account that only 34 known outliers were removed prior to this test (with a total of 300 objects), the improvement in prediction ability is significant for all schemes. Graphical summaries are given in Appendix O.

Table 6.14: Moving window PLSR results

Pre-processing scheme	Bias	Correlation	SEP	RMSEP
A	0.01	0.95	2.48	2.48
B	0.25	0.93	2.88	2.89
C	0.23	0.94	2.63	2.63

The *growing PLSR* scheme also worked well for all the pre-processing schemes (A, B and C). A summary of results from this test is given in Table 6.15. Graphical summaries are given in Appendix O.

Table 6.15: Growing PLSR results

Pre-processing scheme	Bias	Correlation	SEP	RMSEP
A	-0.44	0.95	2.51	2.54
B	0.05	0.95	2.61	2.60
C	-0.10	0.94	2.79	2.79

The model updating scheme looks very promising. It is apparent that the system under study is highly dynamic, and a static calibration model is quickly decaying. Thus it is necessary to update the model often. The tested updating scheme handled the dynamics very well. If an outlier detection scheme was also applied, an improvement of these results should be expected.

It is interesting to note that the moving window PLSR performs as good as the growing PLSR, although it contains only 100 samples at any given time. As discussed in Section 4.10.2, this may be due to progressively more old and irrelevant calibration objects.

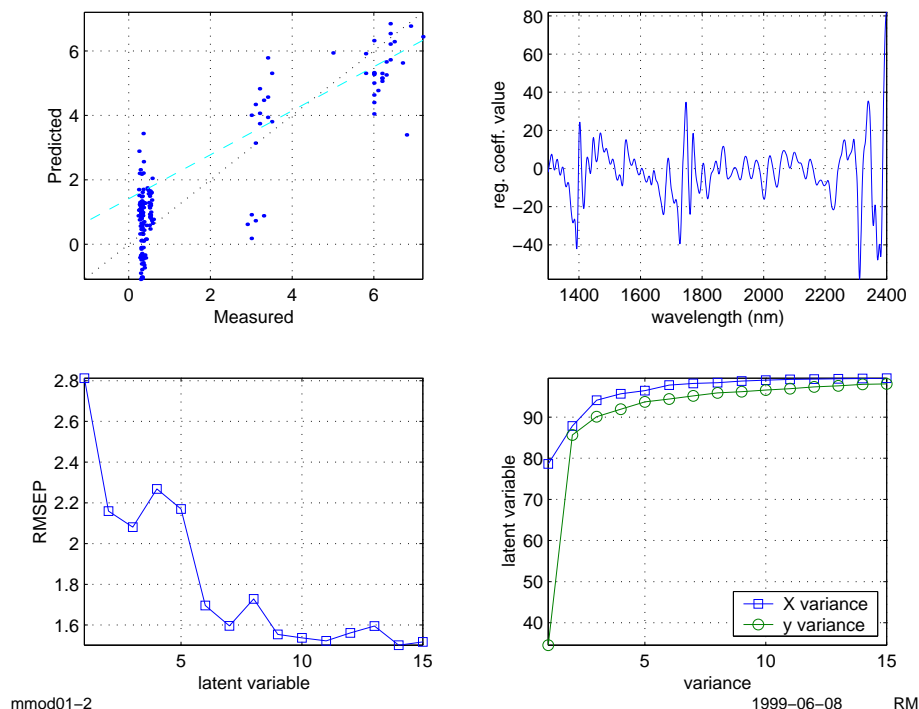
6.3 MFR models

As stated in Section 2.5, the relation between the NIR spectrum and the MFR property is unclear. It was suggested in Section 3.2.2 that there may be a relation between particle properties and MFR. In the following sub-section some MFR applications are tested and discussed.

The available data was split in two, as described in Section 5.3. One set was used for calibration, and the other was used for test-set validation.

A graphical summary of a global MFR model is showed in Figure 6.3 (test-set validation results). The number of bilinear factors selected was 3. As can be seen, the model does not work for MFR predictions. A number of pre-processing schemes were tried, and it was found that schemes that tries to remove all baseline effects have a negative impact on this model. Using either of the regression methods PCR or PLSR did not make much difference. In this particular case PLSR and the first derivative spectra are used.

Figure 6.3: Global MFR model, test-set validation, 3 factors used



Two different LWR implementations from [PLS-Toolbox: Wise and Gallagher] were tested, but showed no improvement compared to the global model.

To demonstrate that local modeling does not improve MFR predictions, the available $\tilde{\mathbf{y}}$ data (MFR values) were used to split the data into three groups: 0-0.6, 2-4 and 4-7. Local PLSR models were then made for each of these subsets. Graphical summaries for two of the models are given in Figure 6.4 and Figure 6.5. It should be evident that these models cannot be used for prediction. The first model (Figure 6.4) may have some structure, and 4 factors were used for the model. In the second model (Figure 6.4) 8 factors were selected, but this is really meaningless here.

The only pre-processing done prior to the calibration of both models, was to find the first derivative spectra using the Savitzky-Golay algorithm. This was done to remove baseline offsets.

It is interesting to compare the predicted/measured plot given in Figure 6.3 with the scores on PC1 plotted against MFR, given in Figure 5.17. It is apparent that there are similarities. In the pre-study, PC1 was assigned to baseline features. Thus it is suggested that the major variations in $\tilde{\mathbf{X}}$ that is correlated to MFR, is particle scattering effects.

Figure 6.4: Local MFR model, 0-0.6, test-set validation, 4 factors used

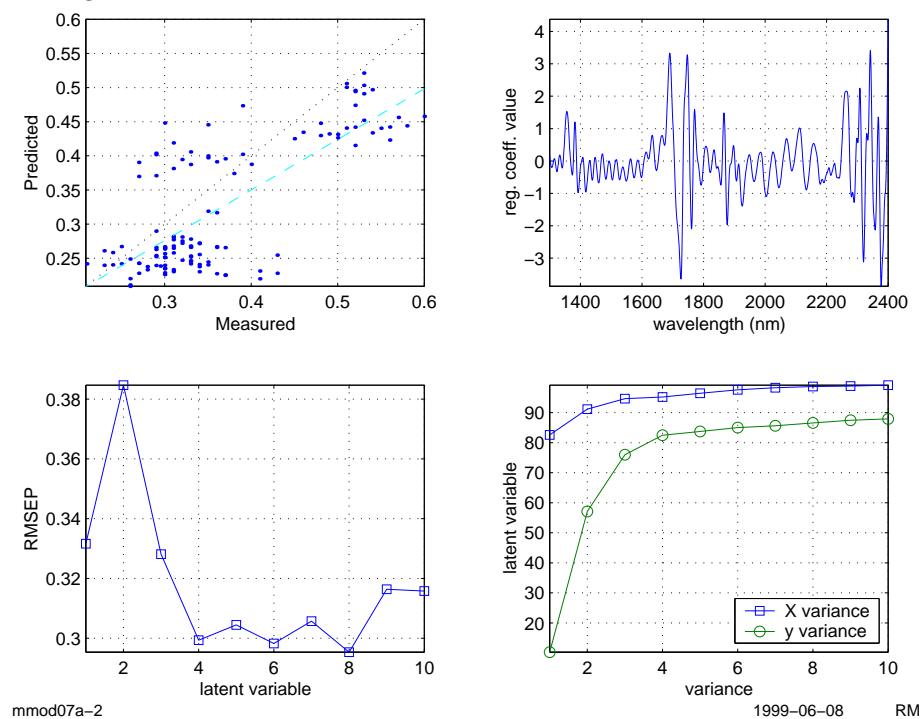
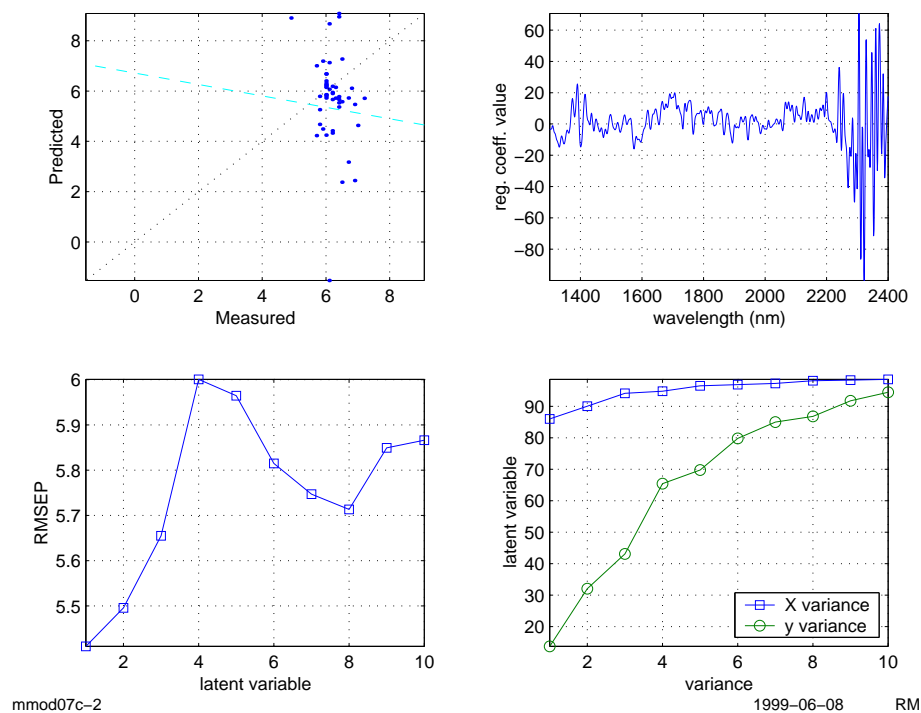


Figure 6.5: Local MFR model, 4-7, test-set validation, 8 factors used



It may be due to the above suggestion that the local models do not work very well. The particles screened by the NIR spectrometer are probably too similar, and there is little other variation in the spectrum that is related to MFR.

6.4 Summary and conclusion

Predicting density using NIR spectroscopy and linear regression works well. With appropriate pre-processing and outlier detection systems an RMSEP of 1.5-2.0 kg/m³ is probably possible, with the current sampling system as a limiting factor.

Using second derivative spectra is a very common pre-processing tool for NIR spectroscopic data, but it is not sufficient in this application. The severe baseline effects are not properly reduced.

The compound of pre-processing outlined in Section 6.2.7 manages the test-sets much better. Common for these schemes are that they do not use the upper part of the NIR spectrum, second derivatives are used to remove baseline offsets and slope, and SNV is used to reduce multiplicative scattering effects.

Three variants of pre-processing were subject to extensive testing:

1. SNV + 2nd derivative + mean centering
2. SNV + 2nd derivative + autoscaling
3. 2nd derivative + SNV + autoscaling

Scheme A and B generally worked best in most test, possibly in a little favour to scheme B.

The implemented *cross validation by class* scheme was insufficient when used as a guide for selecting the correct number of bilinear factors to use in the model, and also for identifying outliers. When the optimal number of factors were found (using test-set), this cross-validation scheme gave very realistic prediction error estimates however.

The *cross validation by class* scheme revealed that ME6930 was special in some way. It apparently spans the edges of some subspace in X . When all ME6930 objects are removed, another product appears to take its role. It is suggested that particle scattering effects are responsible for this behavior.

The density model must be made “quasi-dynamic” by continuously updating it with new samples. This makes the model much more robust, resulting in more precise predictions and probably fewer rejected outliers.

The sampling system is insufficient, and the NIR spectrum may be excessively noisy at times. Thus for further improvement in the RMSEP, the current sampling system needs to be modified or rebuilt. This would probably reduce the need for model updating.

Predicting MFR with NIR does not seem feasible in the application under study. The major variations in the NIR spectrum correlated to the MFR property seems to be due to particle scattering effects. These variations in the spectrum are not sufficient for doing MFR predictions.

MFR predictions on polymer melt is reported to be possible in [Hansen and Vedula (1998)]. Thus, further work on MFR calibration models should probably be focused on HDPE melt.

Chapter 7

Conclusion

The employment of near infra-red (NIR) spectroscopy for determination of density in high density polyethylene (HDPE) seems to be feasible. A higher content of co-monomer in HDPE lowers the density. As a consequence of higher co-monomer content, there is an increase in number of methyl-groups in the polymer. This is detectable NIR spectroscopy. As for the polymer property melt flow rate (MFR), there is no such clear relation between absorption bands in the NIR spectra and the property.

The current sampling system suffers from many weaknesses, resulting in very unstable and noisy spectra. Variations in polymer concentration in the sampling system and a polymer film on the sampling system (sapphire) window are probably the two major problems. The system should be modified or rebuilt to give higher quality spectra. This would increase the accuracy of the density predictions, and give more robust models. It would probably reduce the need for updating the calibration model, thus reducing QC laboratory man-hours.

Another problem with the current system is the introduction of several measurement biases of unknown magnitude. These make it impossible to give reliable estimates of the prediction accuracy. A rebuild of the sampling system is probably necessary to overcome this problem.

A large number of calibration schemes were tested, both for density and MFR predictions on HDPE powder. It was found that doing MFR predictions on HDPE powder was infeasible in the current application. Although particle properties (size etc.) are probably related to MFR and may be detected in the NIR spectra, this is apparently not sufficient for making reliable regression models.

Particle properties (size a.o.) constitute the major variations in the NIR spectra, in addition to problems with varying polymer concentration and a polymer film on the sampling system window. These effects should be reduced to a minimum prior to calibrating the instrument for density predictions.

The final recommended “optimal” calibration scheme is:

1. Careful selection of the calibration data.
 - (a) Noisy data makes unreliable models.
 - (b) Outlier objects can only be properly identified using test-set validation.
2. Abandon the upper part of the acquired NIR spectrum.

- (a) Spectrum above approximately 2120 nm appears to be very noisy. Removing it from the regression models gives more robust models.
- 3. Pre-processing to reduce *all* baseline effects.
 - (a) Pre-processing by taking the second derivative is insufficient.
 - (b) SNV, and probably also MSC, in conjunction with 2nd derivative, improves the prediction accuracy.
- 4. A rigid outlier detection system.
 - (a) Mahalanobis distance limit.
 - (b) Spectral residual limit.
 - (c) Extrapolation not allowed.
 - (d) Other methods.
- 5. Continuous calibration model updating.
 - (a) Making the model “quasi-dynamic” will give more precise predictions, and probably reduce the number of rejected outliers
 - (b) Old samples should be removed from the calibration data.

Both the wavelength selection, pre-processing and outlier detection system may be further optimized. Genetic algorithms may perhaps be used both for wavelength selection and selection of optimal pre-processing, but the tests done in this thesis work were not successful.

The implemented outlier detection system, fulfilling the minimum requirements in [ASTM D 6122 (1997)], properly detected most severe outlier predictions. Unfortunately it also removed a substantial amount of good predictions. The implemented system need more optimization.

Appendix A

F4291 Master of Science Thesis: Project Proposal

Title: On-Line NIR analysis in HDPE plant, evaluation of optimal calibration strategy

Proposer: Kristian Helland, Principal Engineer, Borealis as

Main Supervisor (at Telemark College): Prof. Kim H. Esbensen

Associate supervisor(s): Kristian Helland, Principal Engineer, Borealis as

Problem statement: An increasing amount of on-line NIR data and lab reference measurements are building up as two on-line NIR instrument installations have been running at Borealis, Rønningen, since June 1998, and will continue to build up during the working period for the thesis. These data, and the ability to run lab reference analysis as needed, represent a valuable opportunity to build and test methods and strategies for on-line implementations. Tools should be standard chemometric tools in use in Borealis, and method development tools like Matlab a.o.

The M.Sc. (eng) thesis may include:

- Instrument and installation robustness and shortcomings.
- Causal understanding/evaluation of instrument response and production effects studied.
- Effects of data pre-treatment and wavelength selection.
- Model stability and robustness with time and between different campaigns, and correction strategies. Evaluate the effect of calibration transfer.
- Effect of, and strategies for using Locally Weighted Regression.
- On-line outlier detection, and action strategies. Relate to ASTM Standards.

These and other aspects are to be evaluated at start-up, as well as during ongoing work with the thesis. The student should, as part of the project work, develop a project plan with tasks and time schedule, and work according to this plan, or if needed, revise the plan.

Background: Borealis is implementing on-line NIR analysis at several production sites, and is at the moment in the phase of validating the installations.

One of the plants for installation is the HDPE plant at Rønningen, Norway, where one instrument is analysing produced polymer powder after the reactor, another is analysing polymer melt at the process extruder.

Category of students (special conditions, required qualification, etc.):

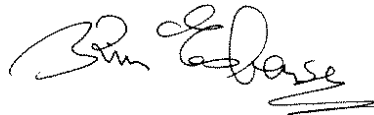
The thesis work is reserved for Rune Mathisen, 2PT, who is on leave from Borealis, and who has been closely involved in the initial work after the on-line NIR installation.

Practical conditions (localization, equipment, etc.): An agreement will be signed by Borealis, HiT, main supervisor and student regarding Confidentiality, Commercial utilisation and Patent rights regarding potential findings during the thesis work.

The student will have a working place at Borealis, Rønningen, and will be free to work where it is best suited (HiT vs. Borealis). The student may utilise lab and computer resources at Borealis, and will take part in Borealis' NIR analysis project team.

All reporting will be in English.

Date for preparation of project proposal: 1998-11-08

A handwritten signature in black ink, appearing to read 'Rune Mathisen', with a double underline at the end.

Appendix B

Rønningen HDPE products

The product specifications for the Rønningen HDPE products studied in this thesis are given in Table B.1. Also given are the type of catalyst used for the product. The different catalyst types are:

Syl Sylopole (chromium oxide)
Mag Magnapore (chromium oxide)
V V-catalyst (chromium oxide)
BC BC2000 (metallocene)

Table B.1: All products: type of catalyst, density and MFR specifications

Product name	Catalyst	MFR $190^{\circ}C$ 2.16 kg	MFR $190^{\circ}C$ 5.00 kg	MFR $190^{\circ}C$ 21.6 kg	Density (kg/m ³)
HE2615	Mag		0.72		940
HE2630	V		0.7		957
HE6905	Mag	0.4			945
HE6960	Syl		0.35	8	950
HE8214	Mag			2.8	952
HE8343	V	0.23			957
HE8253	V			11	953
HE8363	V	0.24			961
ME6930	Mag		0.7	13	939
ME8160	BC	6			940
ME8164	BC	6			934
ME8166	BC	3.2			940
ME8168	BC	6		96	934

Appendix C

Density analysis reference method

Borealis Test Method: BTM16010

Principle: The sample is melted and re-crystallized under controlled conditions. Pieces of the re-crystallized sample are put into a gradient column, and the sinking is measured. The gradient column contain a mixture of 2-propanol and water.

References: ISO1183-1987(E)

Notes: An analysis of the uncertainty in this method (BTM16010) was done by Per Anker Hassel in May 1998. See his memo “Density of HDPE standards Rønningen, - Historical Data” for more information. The mean values and standard deviation for the three standards used to calibrate the method are:

Standard 1

950.45±0.39 kg/m³

Standard 2

961.33±0.67 kg/m³

Standard 1

941.35±0.40 kg/m³

Appendix D

MFR analysis reference method

Borealis Test Method: BTM16003

Principle: The polymer is heated above its melting point, and a standard pressure is applied. It is then forced through a nozzle. The extruded material is weight, and calculated to units of g/10mins.

References: ISO 1133:1991(E)

Standard temperature: 190°C

Standard pressure(s): 2.16 kg, 5.00 kg and 21.6 kg

Appendix E

Particle size distribution data

In Table E.1 particle size distribution data for products produced at the Rønningen HDPE plant is given. Origin of data: [Bjåland and Helleborg (1997)].

The powder samples were mechanically sieved, with sieves from 0.045 mm to 4 mm. The samples were collected between 1997-06-19 and 1997-07-29. A total of 119 samples were analyzed.

The measures D10/D50/D90 means the diameter where 10%/50%/90% of the particles in the sample are smaller than the given value.

Table E.1: Particle size distribution data

Product name	D10 (μm)	D50 (μm)	D90 (μm)	Bulk density (loose)
HE6905	233.0	523.0	1013.0	469.0
HE6905	214.0	500.6	936.6	486.0
HE6960	338.2	670.8	1255.4	460.0
HE6960	320.6	642.2	1182.2	453.0
HE8214	245.2	577.2	1187.7	505.0
HE8253	247.4	554.9	1142.2	445.0
HE8253	277.8	566.9	1231.4	432.0
HE8363	234.0	529.0	1117.3	452.0
ME6930	289.0	850.7	1513.5	477.0
ME8160	241.3	625.8	1012.7	415.0
ME8166	332.5	709.0	1130.5	391.0
ME8168	258.7	617.0	1078.7	420.0

Appendix F

Temperature study predicted measured plots

Figure F.1: Predicted/measured, temperature-model A

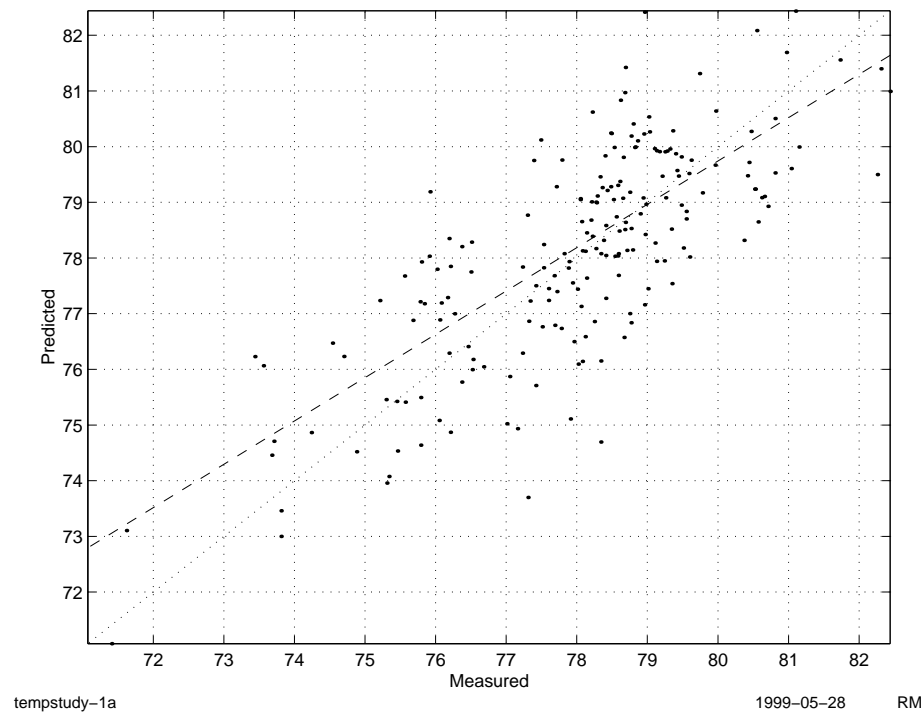
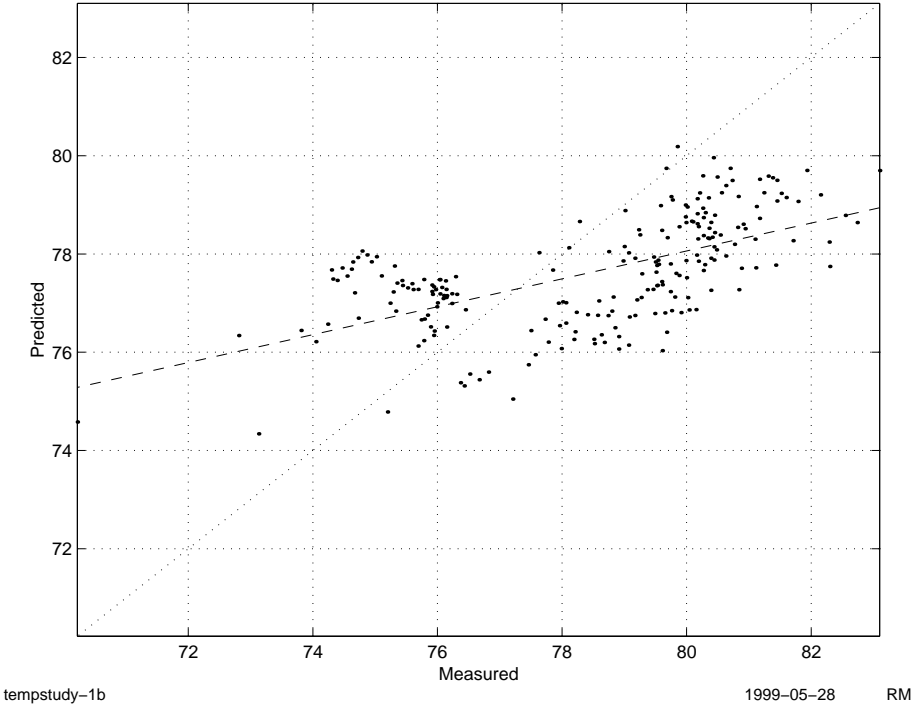


Figure F.2: Predicted/measured, temperature-model B



Appendix G

Suggestion for improvement of the existing sampling system

One of the major problems with the current sampling system is that the concentration of polymer in front of the sapphire window is fluctuating, and sometimes very low.

It is suggested to mount a tract inside the pipe with the purpose of guiding a part of the powder stream in front of the window. This would increase the amount of polymer screened by the spectrometer, and also make the concentration of polymer more constant. It must be noted that this type of sampling is not according to the sampling theories given by [Gy (1998)].

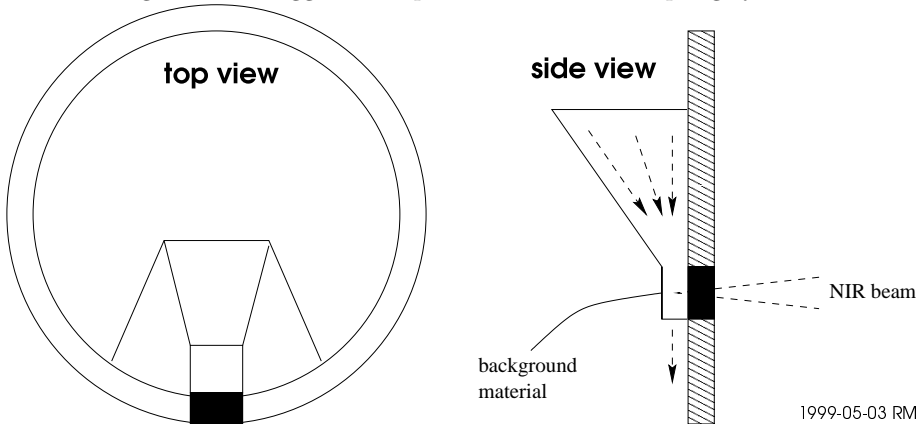
In addition to this, it is suggested to apply a spectroscopic reference material on the tract wall, in front of the sapphire window. This background material have (at least) two purposes:

- Estimation of effective sample size and particle size distribution. See [Berntsson et al. (1998)].
- Provide a means for monitoring the sampling system.

The known and constant background may also have other (not identified) advantages.

A simple sketch of the suggested system is shown in Figure G.1. To prevent lumps of polymer from clogging the tract, an inlet cover should also be implemented (not shown in sketch).

Figure G.1: Suggested improvement of the sampling system



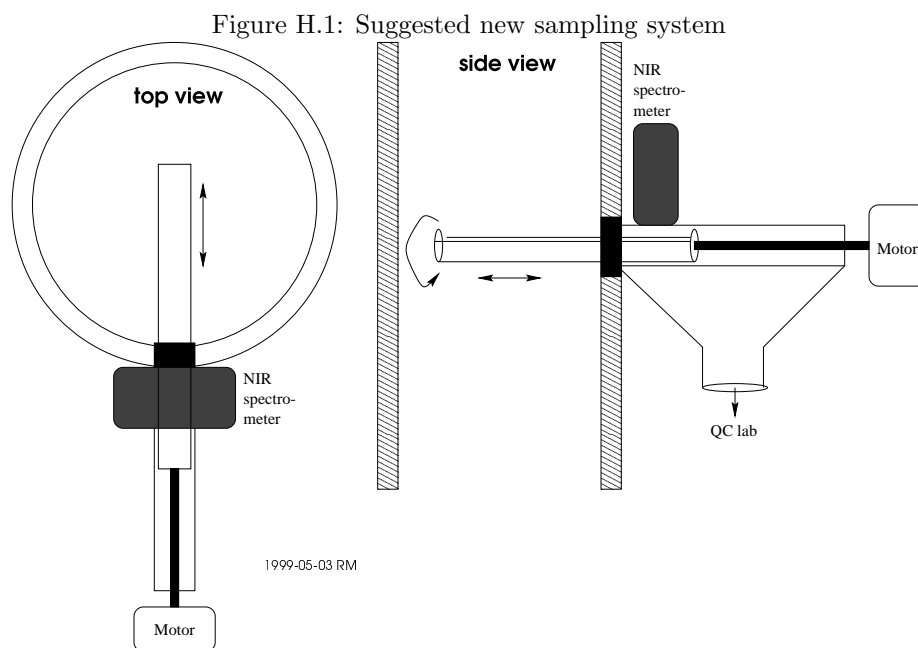
Appendix H

Suggestion for a new sampling system

The following suggestion was compiled in cooperation with Per Anker Hassel (Borealis).

A suggestion for a new (at-line) sampling system is given in Figure H.1. A cylinder with a slit is inserted into the pipe with the slit facing down. When the cylinder is fully inserted, it is rotated so that the slit is facing upward. The sample compartment is now filled with polymer. When the cylinder is pulled out of the pipe, it is continuously scanned by the NIR spectrometer. The top layer of polymer should be scraped off when the sample compartment is pulled in. An average of the scanned spectra is stored. After the sample has been scanned, it may be returned to the process or taken out for QC laboratory analysis. In this way one gets reference values for the sample that was actually scanned.

Although it is expected that this sampling system will lead to much more accurate predictions than the current sampling system, it must be noted that it is not according to the sampling theories given by [Gy (1998)].



Appendix I

Density data distribution

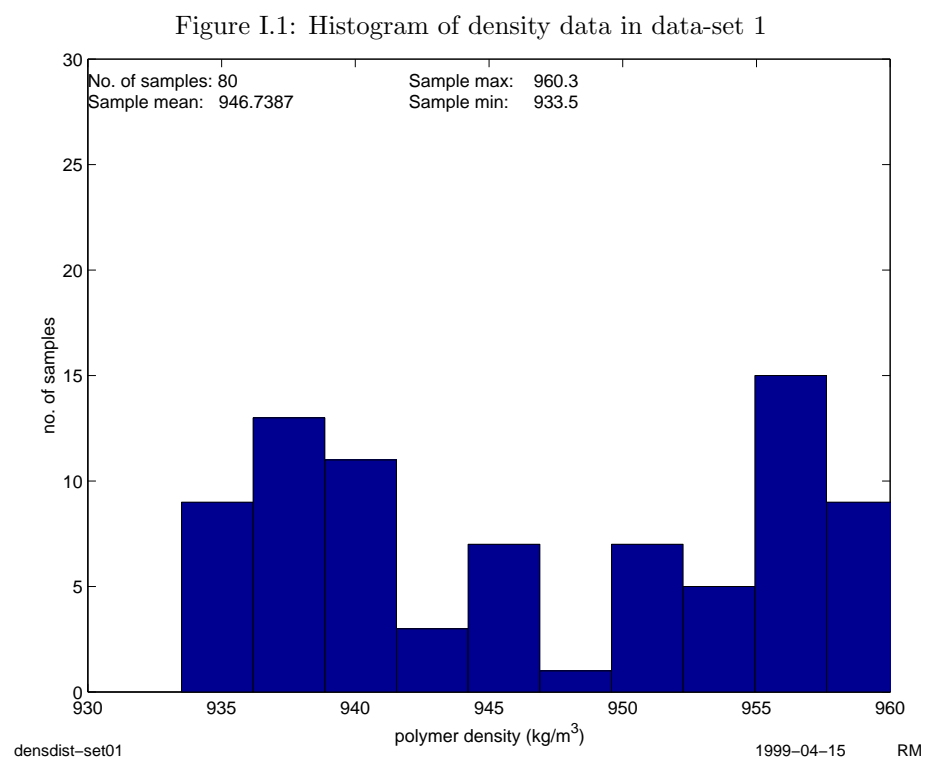


Figure I.2: Histogram of density data in data-set 2

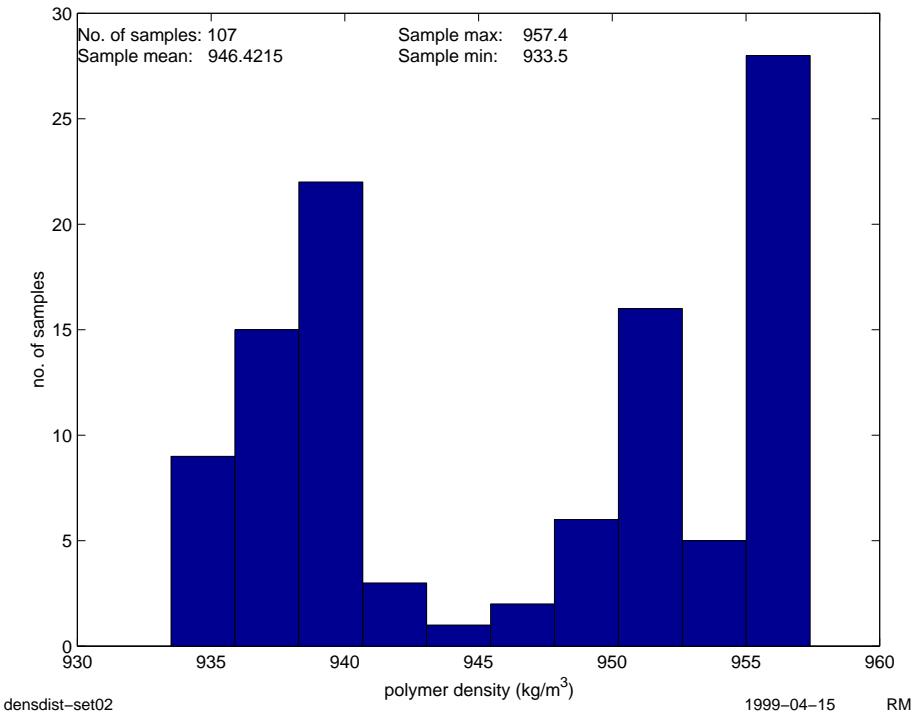


Figure I.3: Histogram of density data in data-set 3

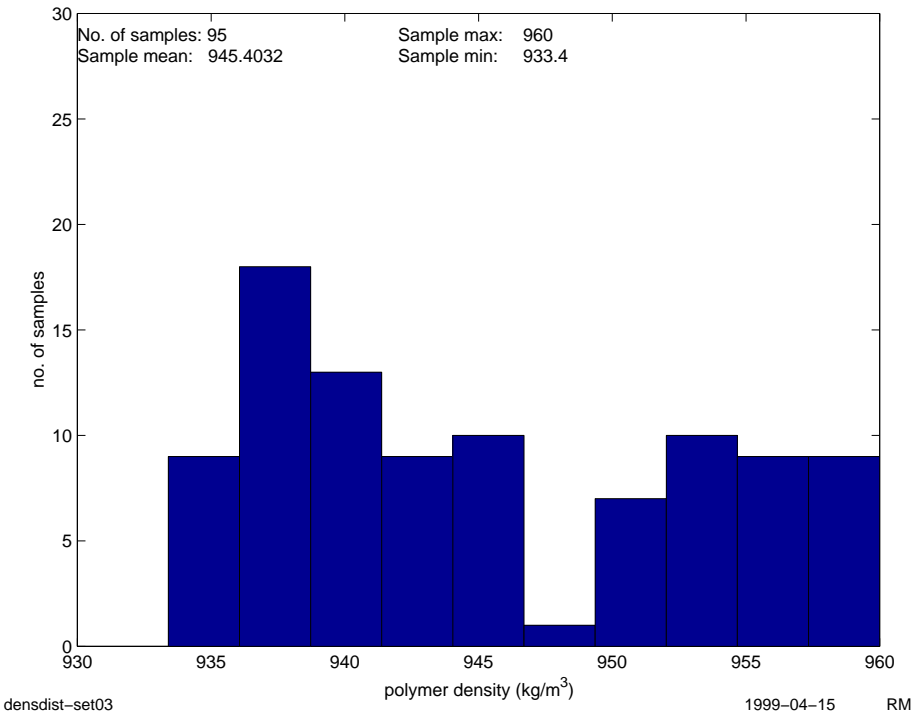


Figure I.4: Histogram of density data in data-set 4

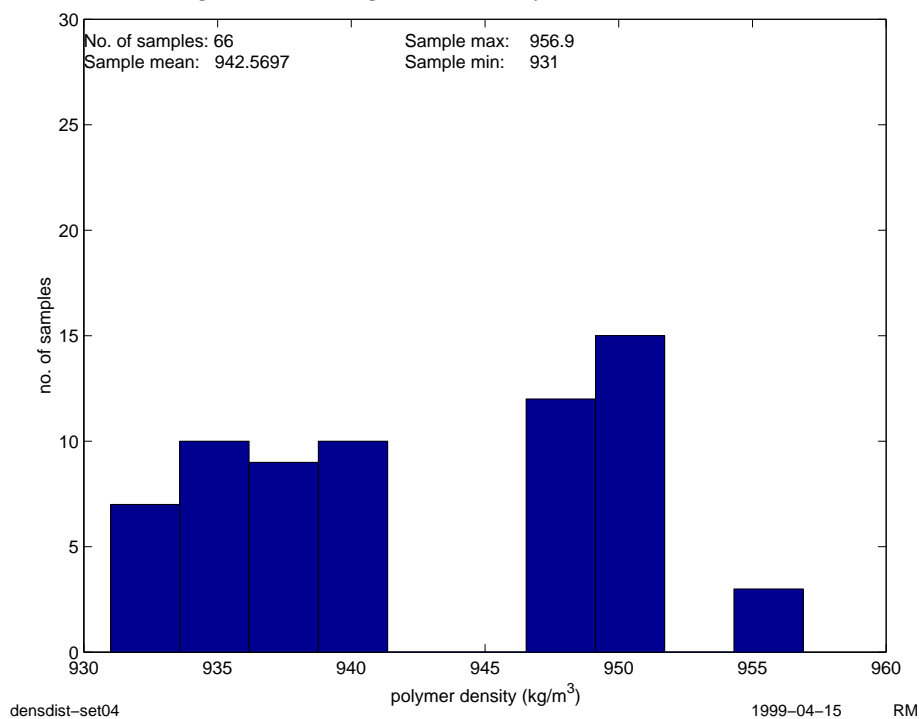
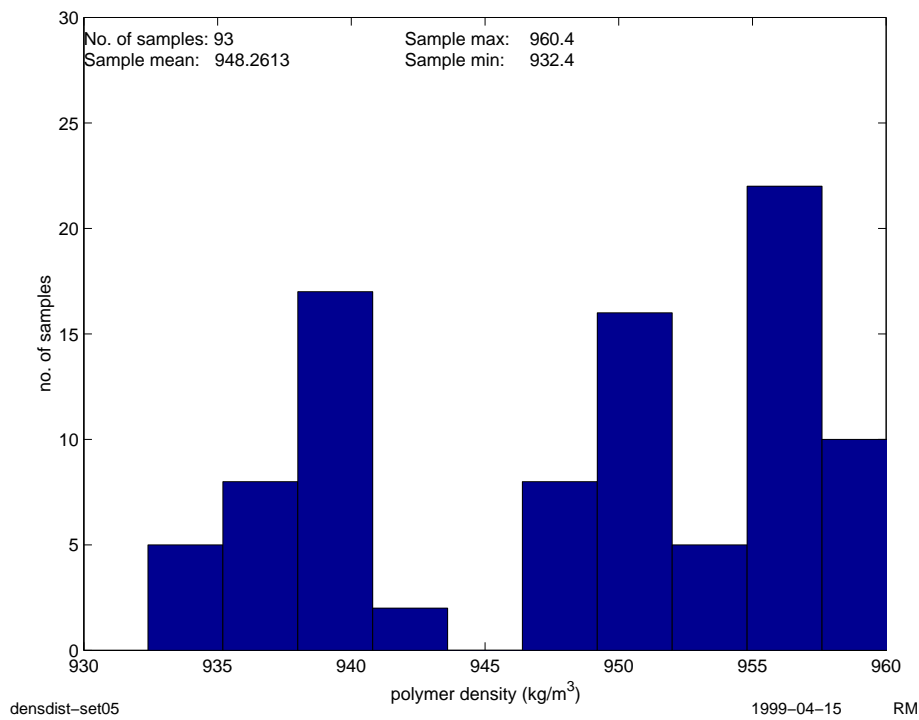


Figure I.5: Histogram of density data in data-set 5



Appendix J

Assessing PCA loading vectors from spectral data

An experiment was performed to get better understanding of the effects in spectral data and their response in PCA loading vectors. The experiment was set up using a three level full factorial experimental design, with the following design factors:

1. Wavelength shift (-2 / 0 / 2 nm)
2. Offset (-0.1 / 0 / 0.1 abs. units)
3. Multiplicative contribution (-0.2 / 0 / 0.2 \factors\)
4. Baseline slope (-6 / 0 / 6 degrees)
5. Sine (-1 / 0 / 1 \phase\ Freq:30Hz Ampl: 0.003)

Normally distributed random noise was also added to each variable in the spectra.

A “typical” NIR spectrum from the Rønningen HDPE plant was used as the design center. The design center spectrum is shown in Figure J.1, together with two examples of simulated spectra. A total of $3^5=243$ samples was then analyzed using PCA. The resulting loading vectors are given in Figure J.2.

The following relations were found between input in X and response in the loading vectors (correlation given in parenthesis):

PC 1

Models offset ($r^2=0.42$) and multiplicative effects ($r^2=0.44$), and to a lesser extent the baseline slope ($r^2=0.14$)

PC 2

Models offset ($r^2=0.56$) and multiplicative effects ($r^2=0.40$)

PC 3

Models the baseline slope ($r^2=0.83$), and to a lesser extent multiplicative effects ($r^2=0.16$)

PC 4

Models the wavelength shift ($r^2=0.94$)

PC 5

Models the sine ($r^2=0.98$)

PC 6

Noise

Figure J.1: Design center (solid line) and two of the 243 simulated spectra

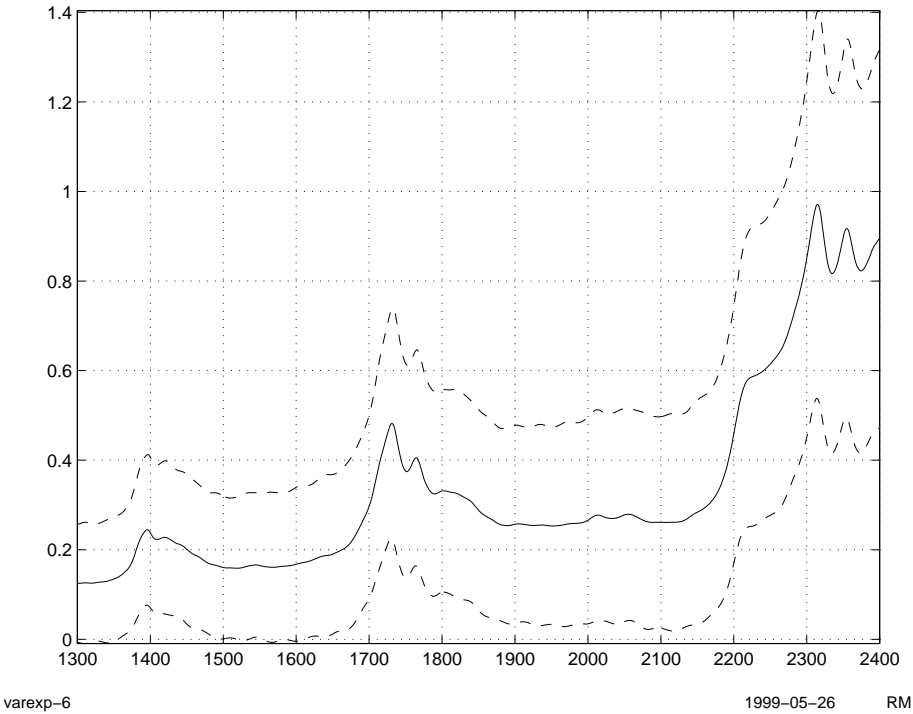
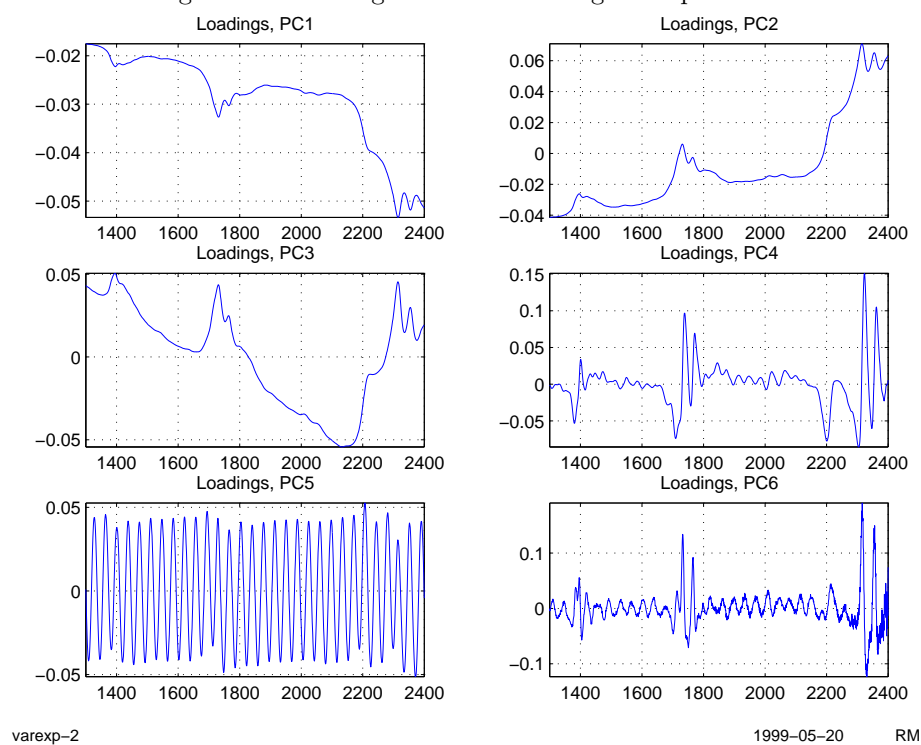


Figure J.2: Loading vectors from designed experiment



Appendix K

Matlab code

PLS_Toolbox for Matlab version 2.0.1c by Barry M. Wise and Neil B. Gallagher was used for all multivariate data analysis in this thesis study [PLS_Toolbox: Wise and Gallagher]. In addition, some data processing functions were developed using Matlab. The code for these functions are given in the following sub-sections. Plotting functions etc. are available by contacting the author.

K.1 Mahalanobis distance on scores

```
function [mdist] = mdistscores(X,Y)
%MDISTSCORES -- mahalanobis distance on PCA or PLS scores
%
% Usage:
%   [mdist] = mdistscores(X,Y)
%
% Inputs:
%   X      model scores
%   Y      unknown sample scores
%
% Outputs:
%   mdist  the mahalanobis distance
%
% Description:
%   Returns Mahalanobis' D-square distance between the scores of a
%   multivariate model X and the scores of an unknown sample Y.
%
% Author/revisions:
%   1999-04-13 Rune Mathisen: initial version
%
% Source:
%   "PLSplus/IQ users guide", Galactic Industries, 1996

if (nargin ~= 2)
    usage('mdist = mdistscores(X,Y)');
end

[xr,xc] = size(X);
[yr,yc] = size(Y);

if (xc ~= yc),
    error('mdistscores: X and Y must have the same number of columns!');
end

M = X'*X/(xr-1);

mdist = Y*inv(M)*Y';
```

K.2 SNV

```
function [Xsnv] = snv(X)
%SNV -- Standard Normal Variate
%
% Usage:
%   [Xsnv] = snv(X)
%
% Inputs:
%   X       the input data matrix
%
% Outputs:
%   Xsnv    the SNV-corrected data
%
% Description:
%   Reduces scattering effects in spectral data by normalizing each
%   spectrum by the standard deviation of the responses across the
%   entire spectral range.
%
% Author/revisions:
%   1999-05-22 Rune Mathisen: code cleanup
%   1999-05-08 Rune Mathisen: initial version
%
% Source:
%   "PLSplus/IQ users guide", Galactic Industries, 1996

% finding the size of X
[rx,cx] = size(X);

% mean response
mr = mean(X,2);

% remove the response mean
rdiff = X - repmat(mr,1,cx);

% SNV correction
Xsnv = rdiff./(repmat(sqrt(sum(rdiff.^2,2)/(cx-1)),1,cx));
```

K.3 Model statistics

```
function [press,sep,rmse,slope,bias,offset,r] = pmstats(pred,meas)
%PMSTATS -- predicted/measured statistics
%
% Usage:
%   [press,sep,rmse,slope,bias,offset,r] = pmstats(pred,meas)
%
% Inputs:
%   pred    predicted values (row oriented matrix)
%   meas    reference measurements (vector)
%
% Outputs:
%   press   predicted error sum of squares
%   sep     standard error of performance
%   rmse    root mean square error of (cross-validation | prediction)
%   slope   slope of the least squares line between predicted
%           and measured
%   bias    average error between predicted and measured
%   offset  point where the regression line crosses the y axis
%   r       correlation coefficient
%
% Description:
%   Calculates common statistics measures for a multivariate
%   calibration model.
%
% Author/revisions:
%   1999-05-07 Rune Mathisen: I/O change, and a bug-fix
%   1999-04-18 Rune Mathisen: use the Matlab corrcoef function
```

```
%    1999-03-25 Rune Mathisen: initial version

[m,n] = size(pred);
[p,q] = size(meas);

% predicted error sum of squares
press = (pred - meas).^2;

% root mean square error
rmse = sqrt(sum(press,1)/m);

% Bias
bias = sum(pred - meas)/m;

% standard error of performance
sep = sqrt(sum((pred - meas - bias).^2)/(m-1));

% slope and offset
[P,S] = polyfit(meas,pred,1);
slope = P(1);
offset = P(2);

% correlation coefficient
ccmat = corrcoef(pred,meas);
r = ccmat(1,2);
```


Appendix L

Pre-processing optimizationalization

In the following figures, 300 models that were built to optimize the pre-processing steps are presented. The test involved different window widths in the Savintzky-Golay algorithm (2nd derivative, 2nd order polynom), different wavelenght regions, performing SNV before or after derivation (or not at all), autoscaling or mean centering.

The window width was changed from 3 to 41 points with an increment of two points (the window must be odd-numbered). For each increment a model was built and validated with a test-set. One model is then seen as a horizontal line from an odd number on the window-axis.

It was selected to present the models in contour plots rather than 3D surfaces, because the contour plots are easier to visualize. A side-effect from the Matlab surface plots is that the contour lines are continus, and that one thus might read RMSEP values from fractions of bilinear factors. It is not understood how this should be interpreted, or if it should be interpreted at all.

The colors in the plots are visualizations of the RMSEP. Dark blue colors are low values, dark red colors are high values. The absolute minima in the surface is given at the top of each plot.

The wavelenght range used, and the pre-processing performed, are given in the figure texts. The order of the pre-processing steps are also important!

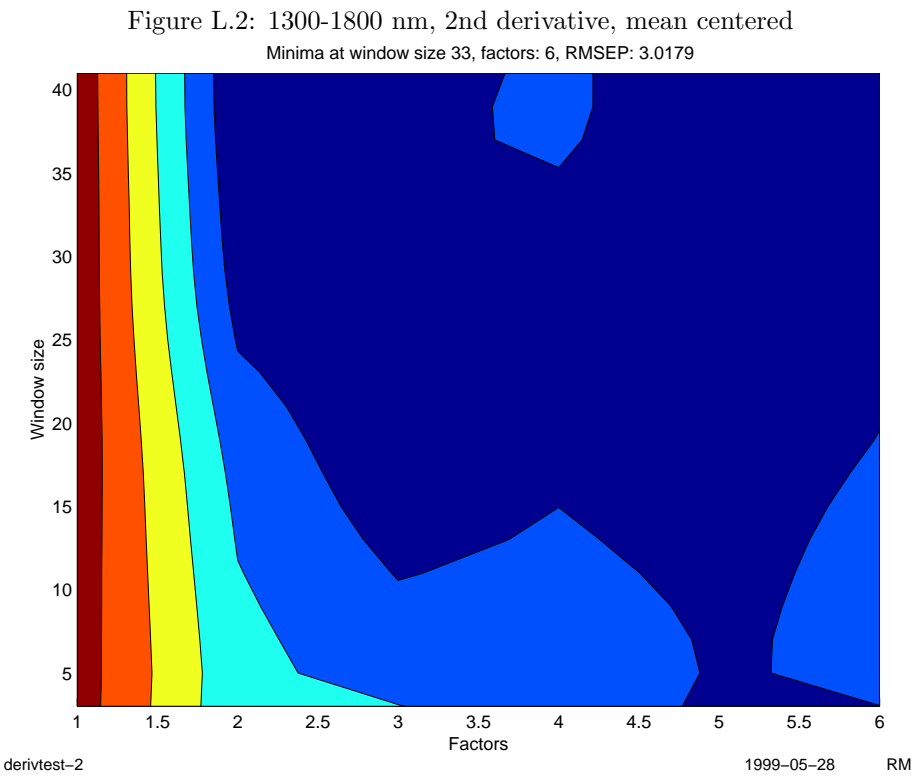
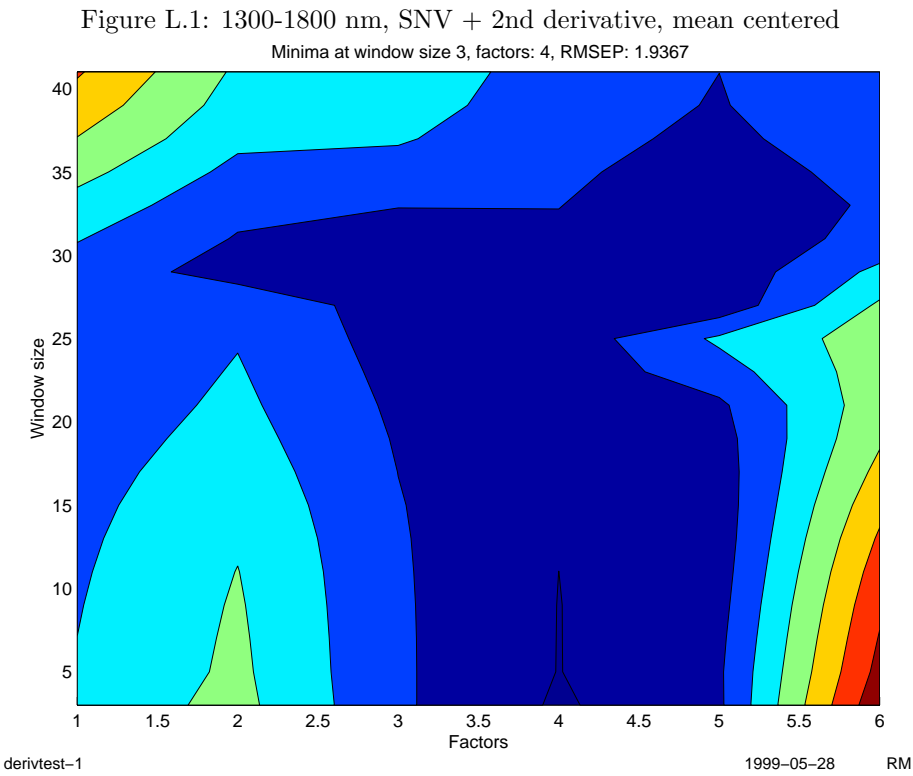


Figure L.3: 1300-1800 nm, 2nd derivative + SNV, mean centered

Minima at window size 31, factors: 4, RMSEP: 2.1958

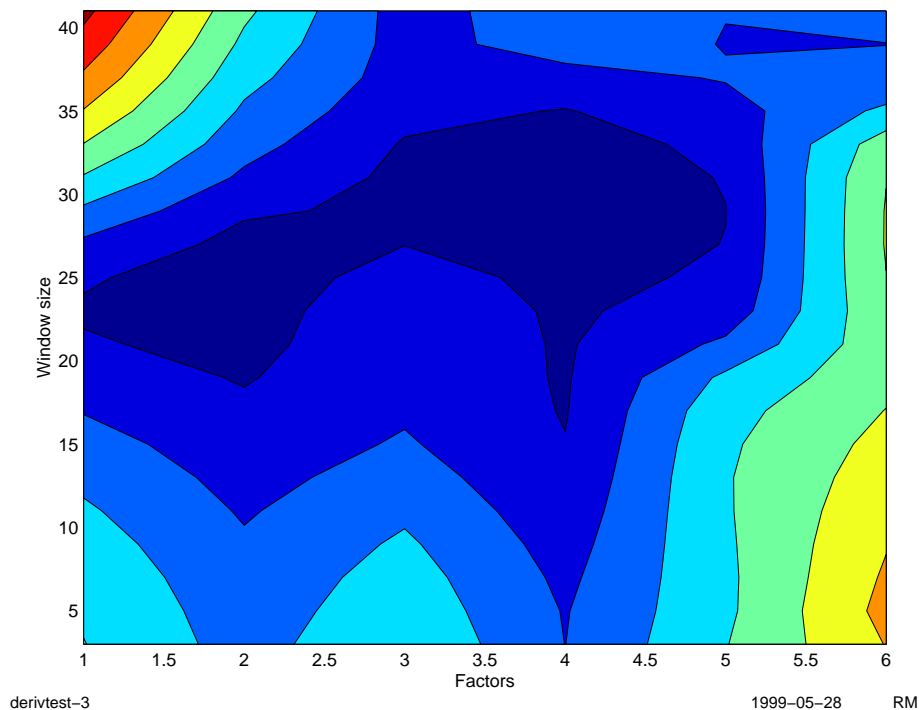


Figure L.4: 1300-2110 nm, SNV + 2nd derivative, mean centered

Minima at window size 5, factors: 4, RMSEP: 1.9305

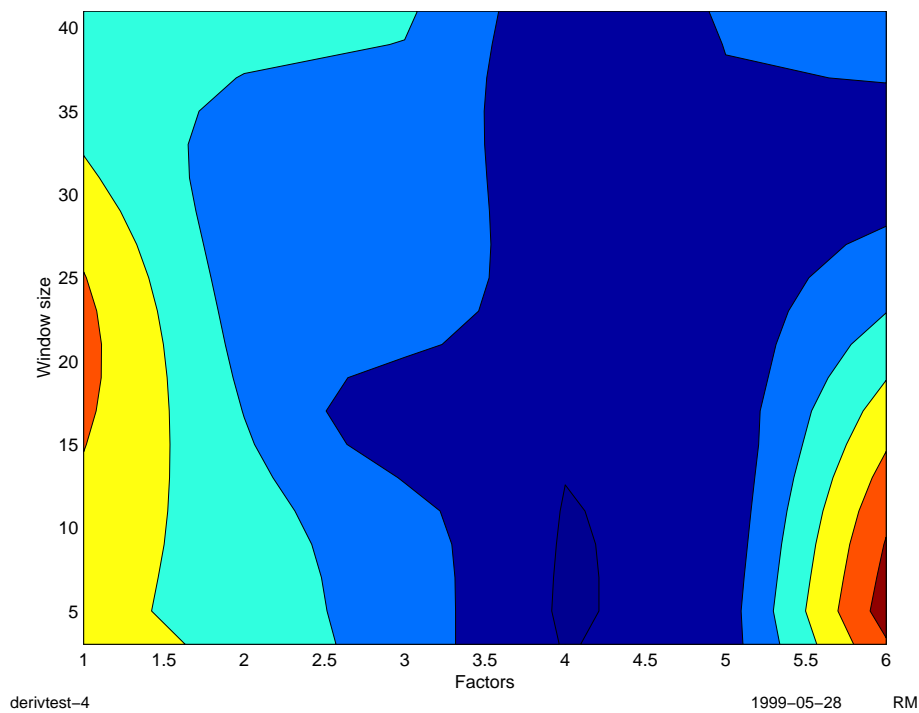


Figure L.5: 1300-2110 nm, 2nd derivative, mean centered

Minima at window size 27, factors: 3, RMSEP: 2.8943

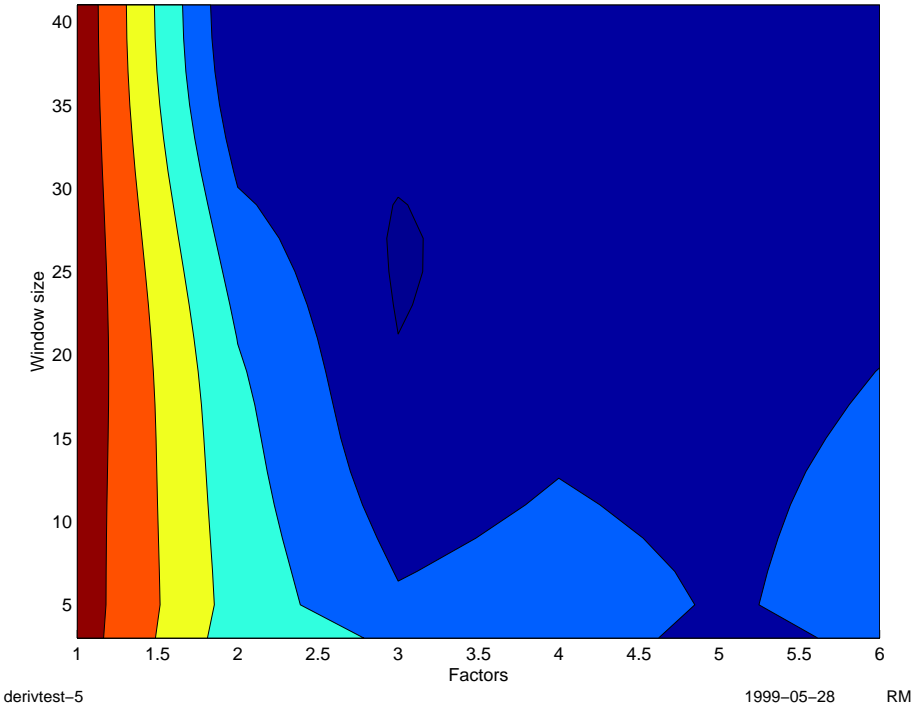


Figure L.6: 1300-2110 nm, 2nd derivative + SNV, mean centered

Minima at window size 37, factors: 4, RMSEP: 2.1659

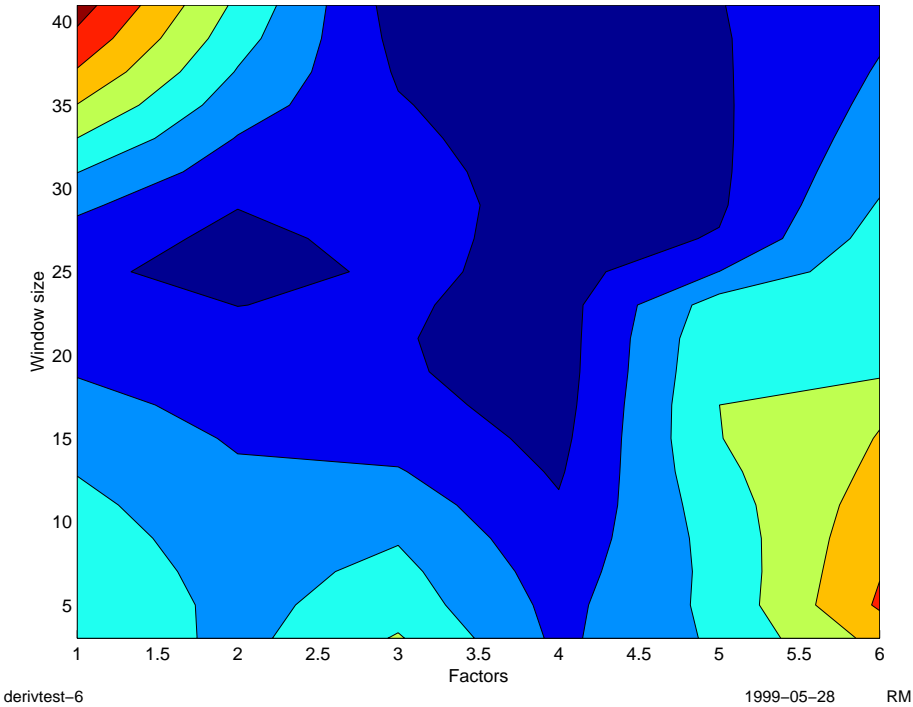


Figure L.7: 1300-2110 nm, SNV + 2nd derivative, autoscaled

Minima at window size 31, factors: 4, RMSEP: 1.798

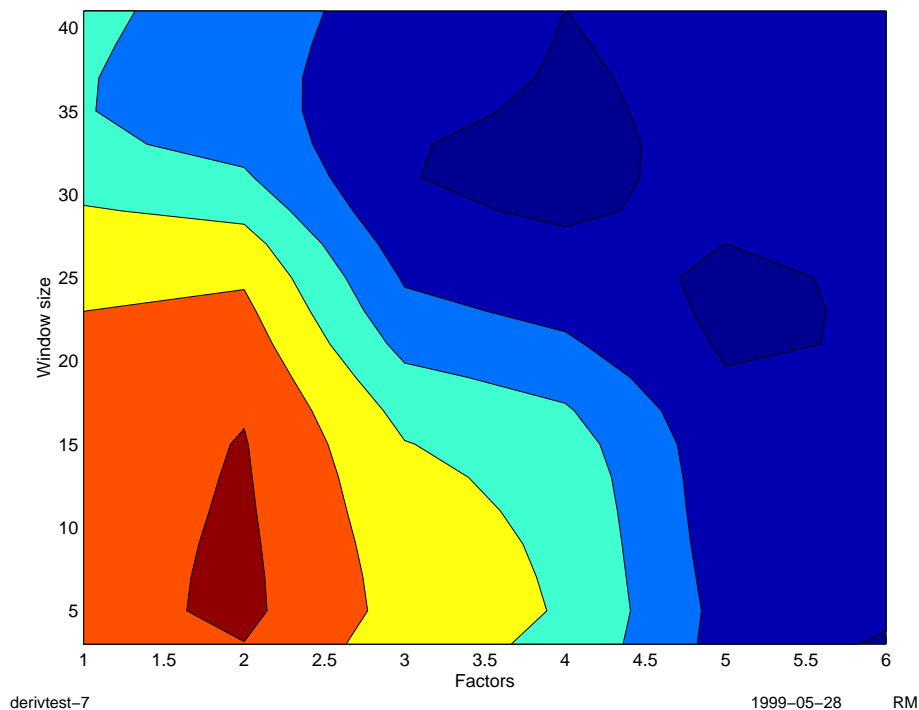


Figure L.8: 1300-2110 nm, 2nd derivative, autoscaled

Minima at window size 23, factors: 3, RMSEP: 2.7117

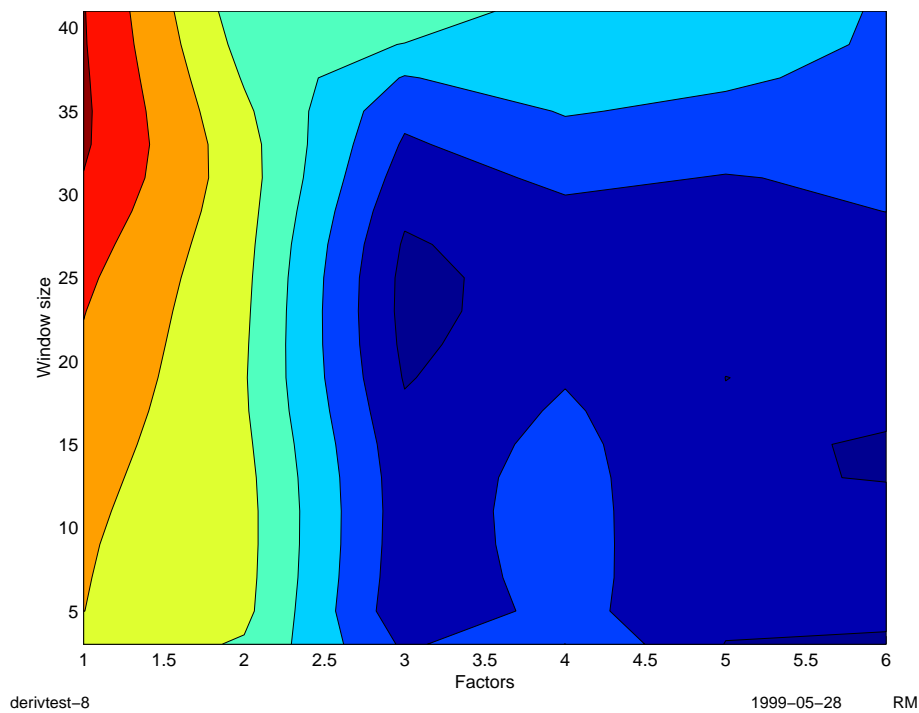


Figure L.9: 1300-2110 nm, 2nd derivative + SNV, autoscaled

Minima at window size 23, factors: 5, RMSEP: 1.8668

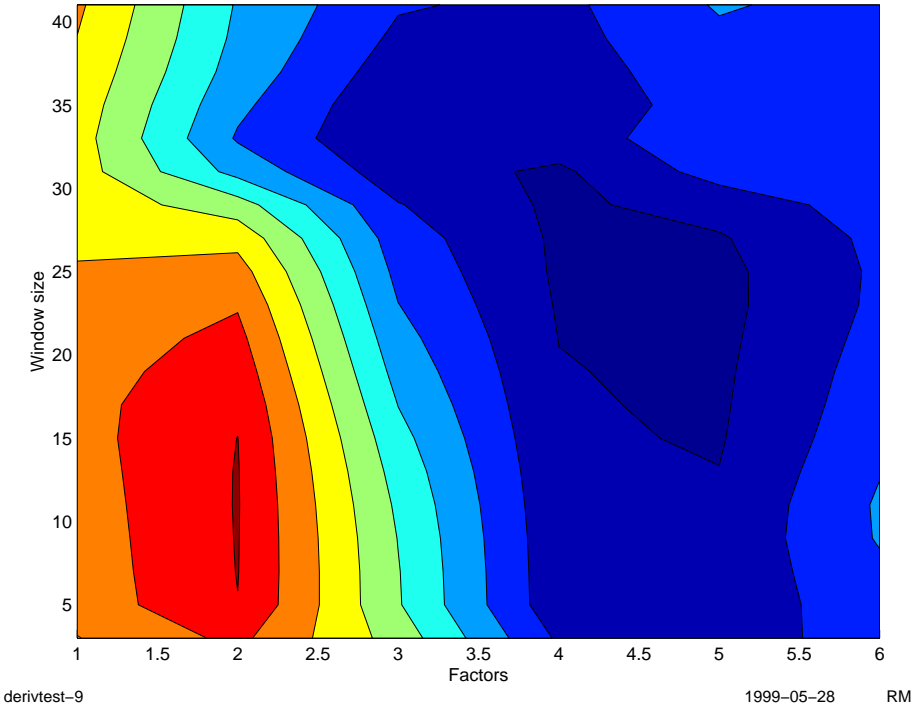


Figure L.10: 1300-2400 nm, SNV + 2nd derivative, mean centered

Minima at window size 11, factors: 6, RMSEP: 2.8111

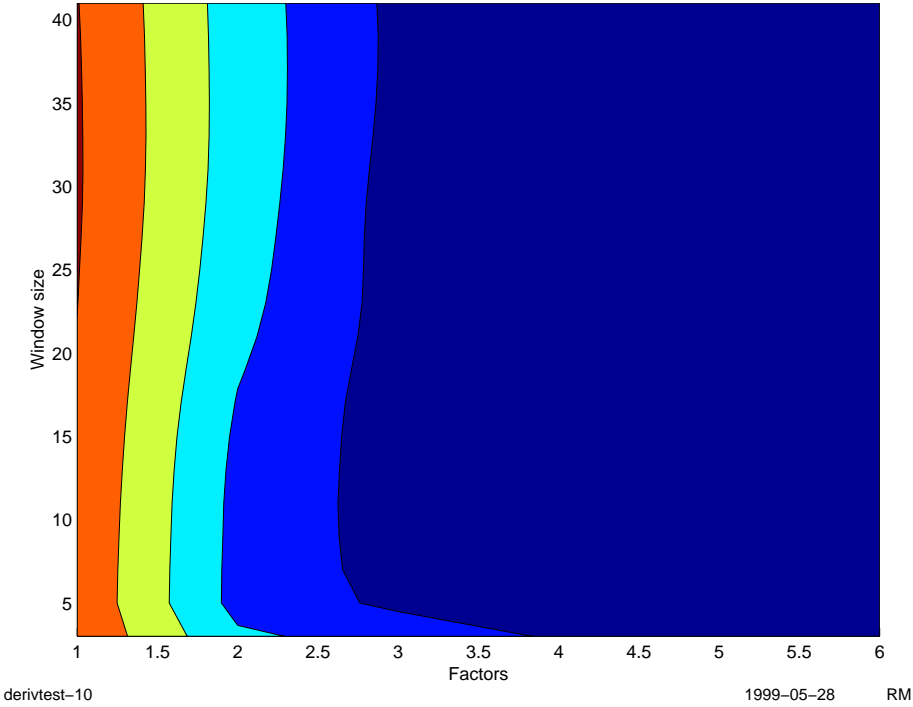


Figure L.11: 1300-2400 nm, 2nd derivative, mean centered

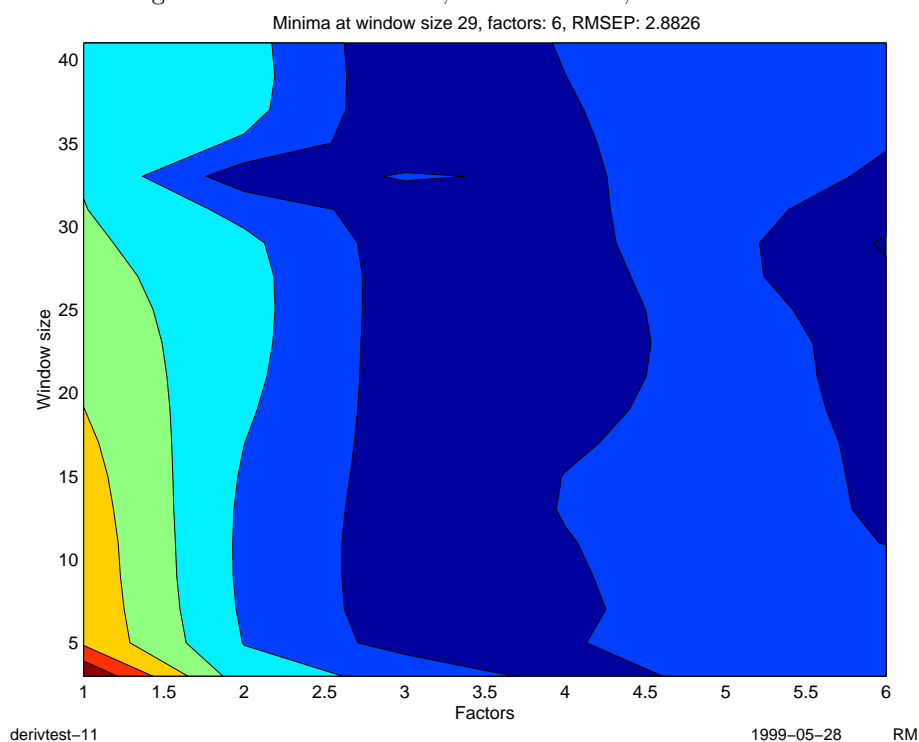


Figure L.12: 1300-2400 nm, 2nd derivative + SNV, mean centered

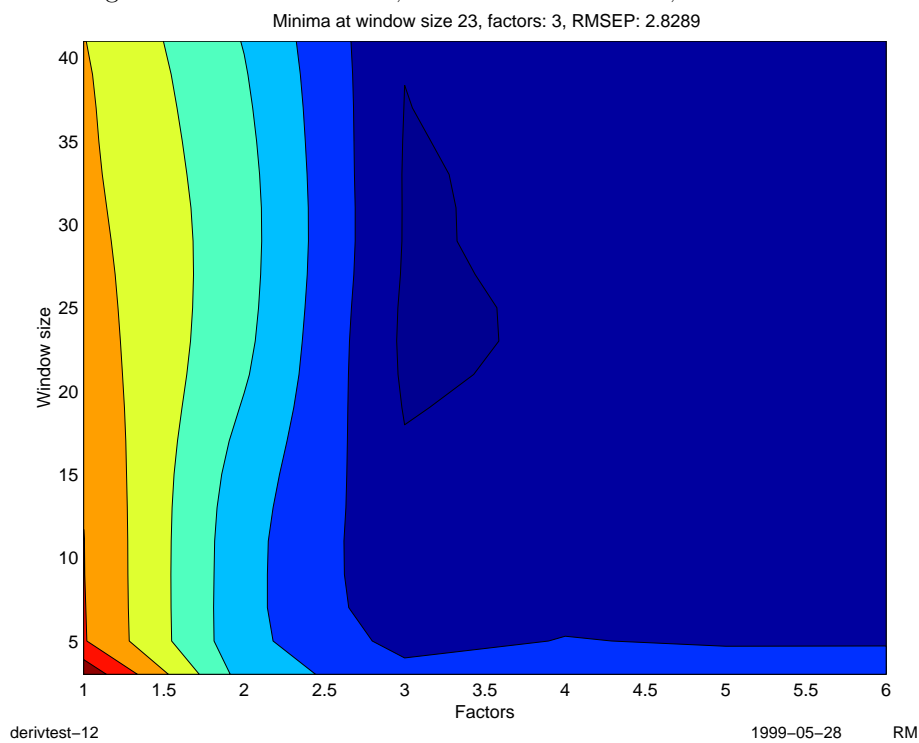


Figure L.13: 1300-2400 nm, SNV + 2nd derivative, autoscaled
Minima at window size 3, factors: 6, RMSEP: 2.8558

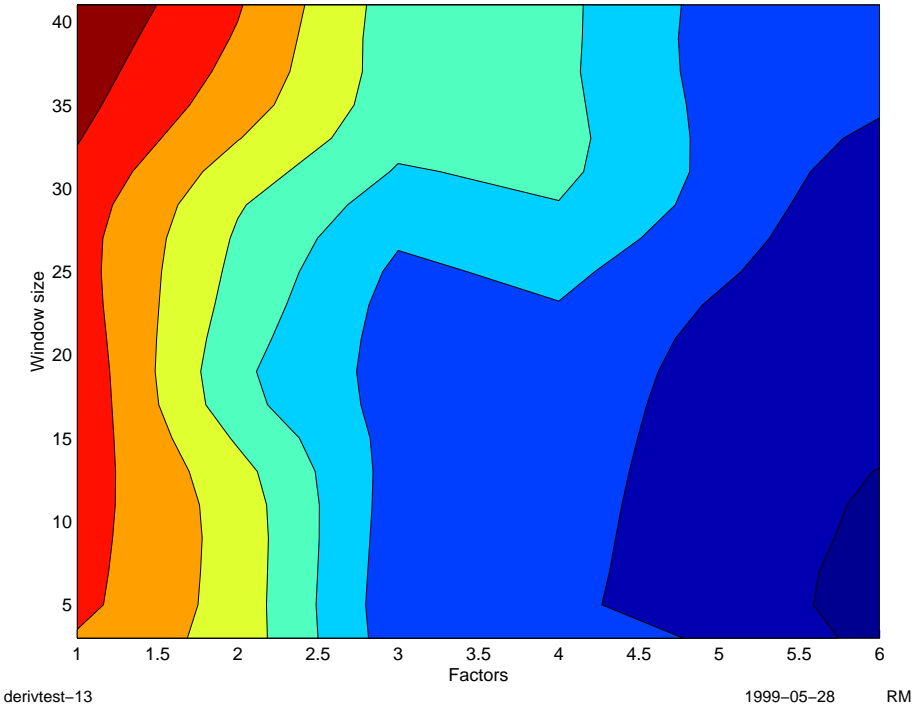


Figure L.14: 1300-2400 nm, 2nd derivative, autoscaled
Minima at window size 15, factors: 3, RMSEP: 2.7972

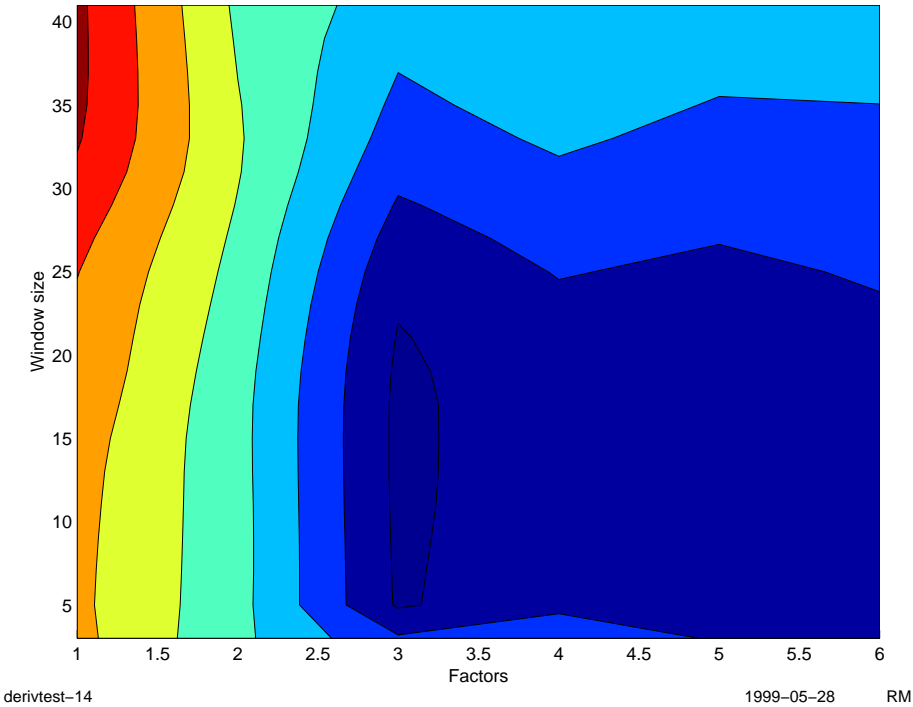
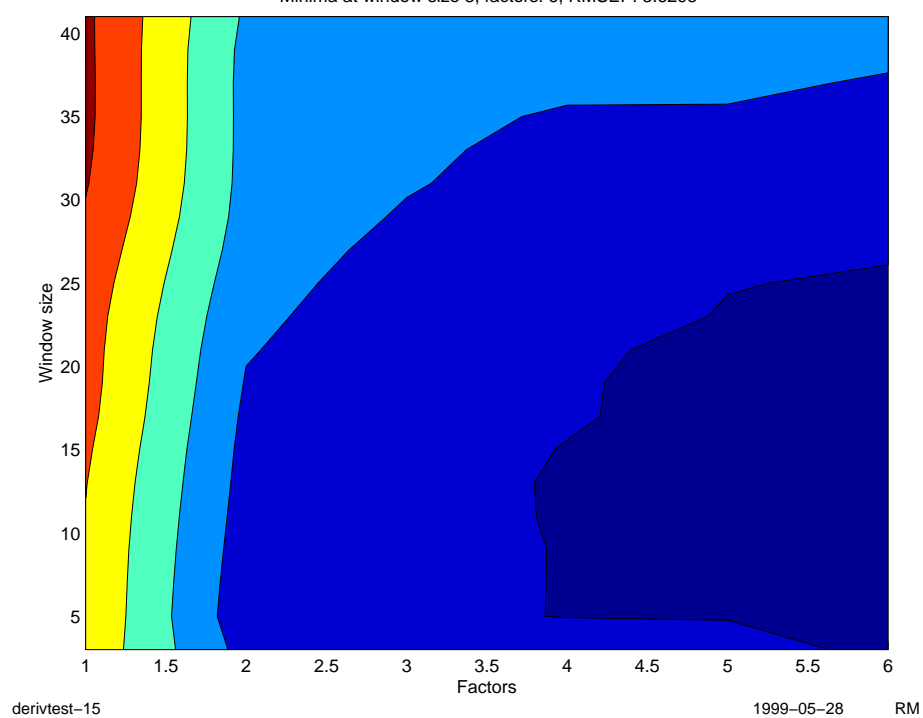


Figure L.15: 1300-2400 nm, 2nd derivative + SNV, autoscaled

Minima at window size 3, factors: 6, RMSEP: 3.6295



Appendix M

Graphical summaries, cross-validated density models

Presented here are graphical summaries of the cross-validated models described in Section 6.2.5 and Section 6.2.9.

Figure M.1: Cross-validated density model A

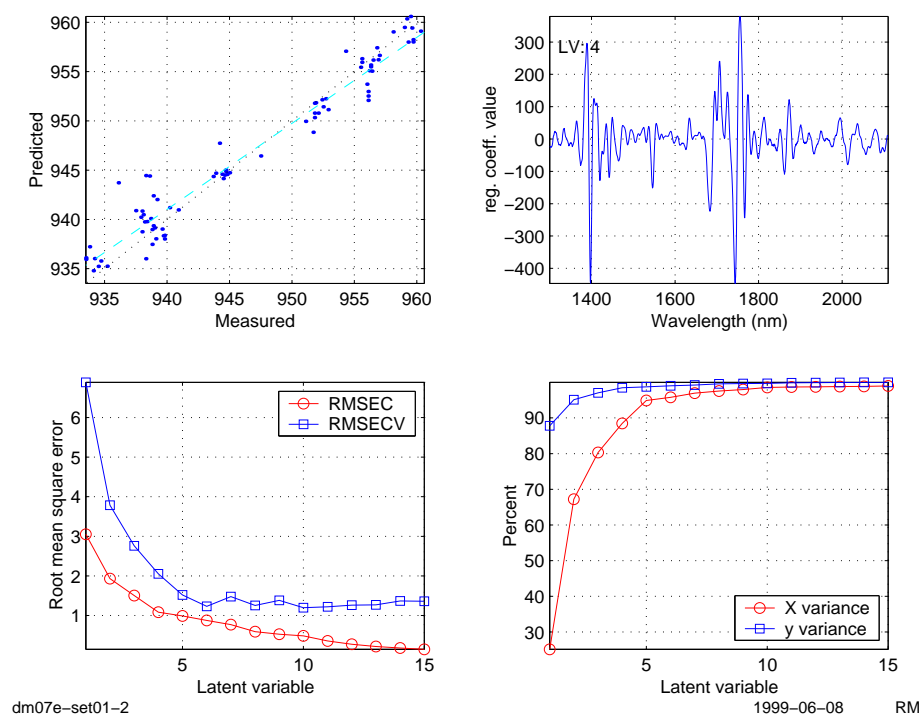


Figure M.2: Cross-validated density model B

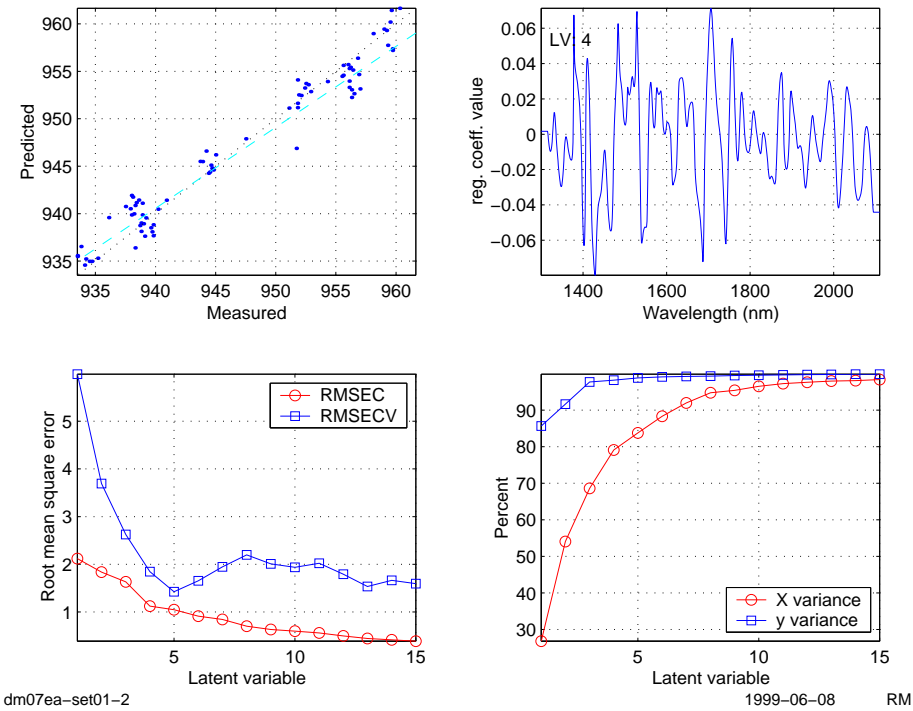


Figure M.3: Cross-validated density model C

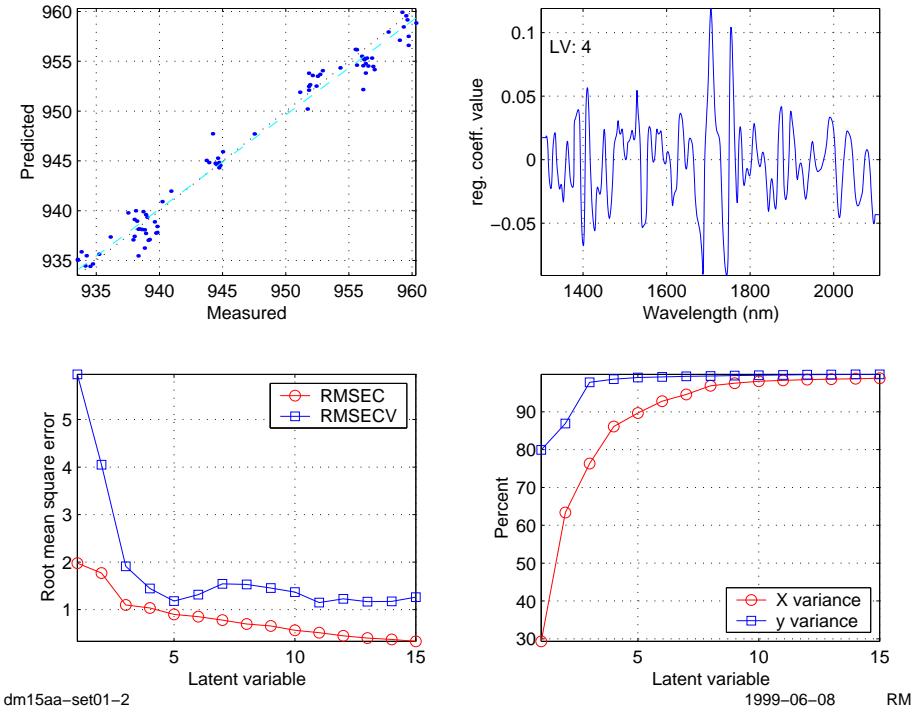
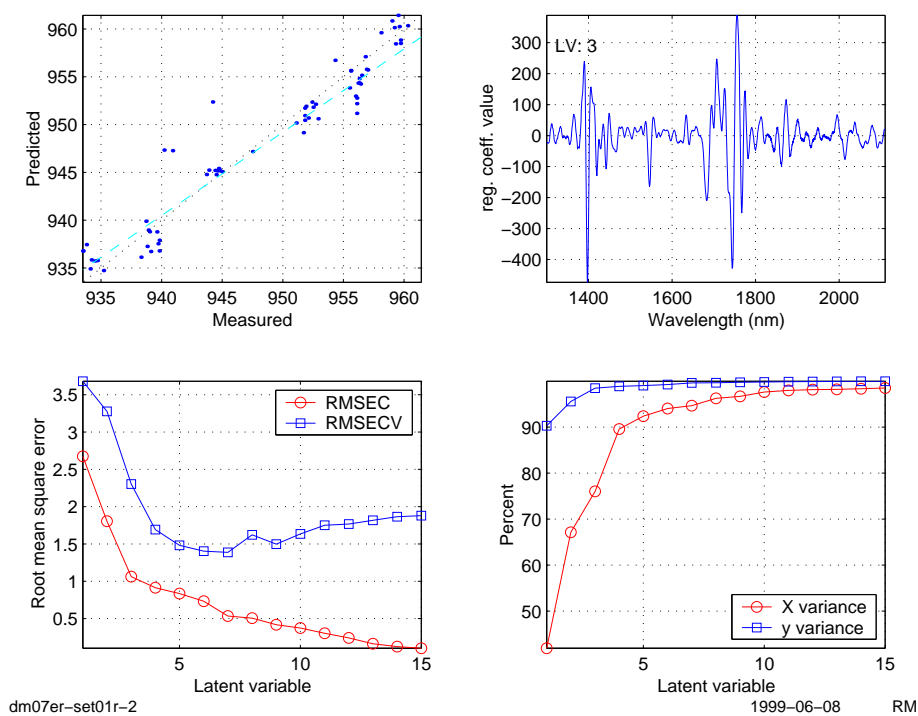


Figure M.4: Cross-validated density model A* (without ME6930)



Appendix N

Density models validation plots

Detected (and removed) outliers are marked with an asterisk. The horizontal lines in the m-dist and residual plots give the outlier limits. The pred/meas-plots, RMSEP-plots, error distribution plots and cumulated error plots are compiled after removal of outliers.

N.1 Scheme A

Figure N.1: Outlier detection, scheme A, test-set 2

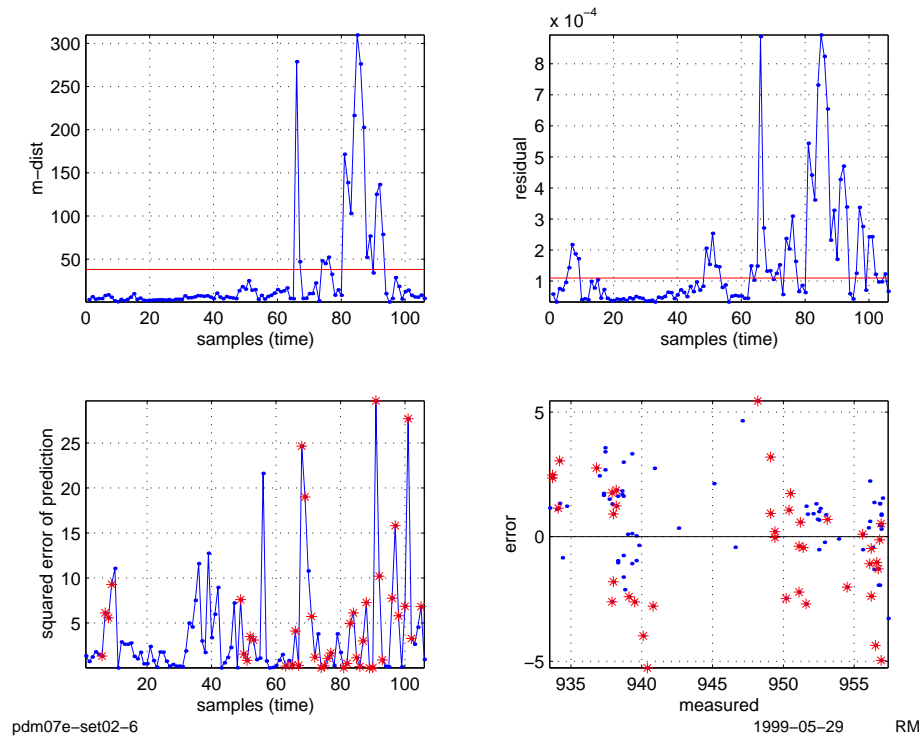


Figure N.2: Results, scheme A, test-set 2

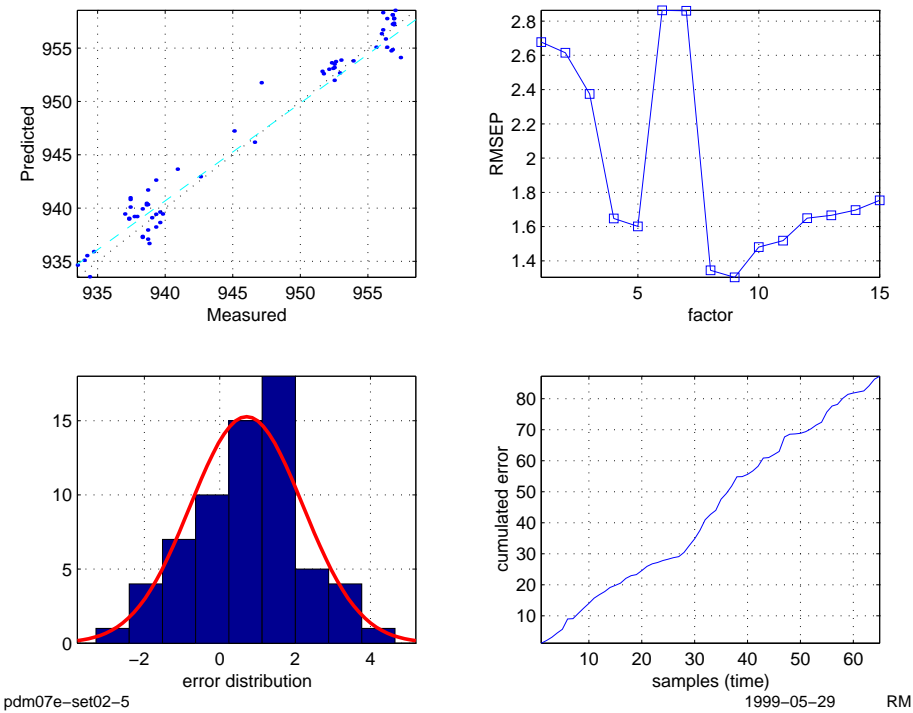


Figure N.3: Outlier detection, scheme A, test-set 3

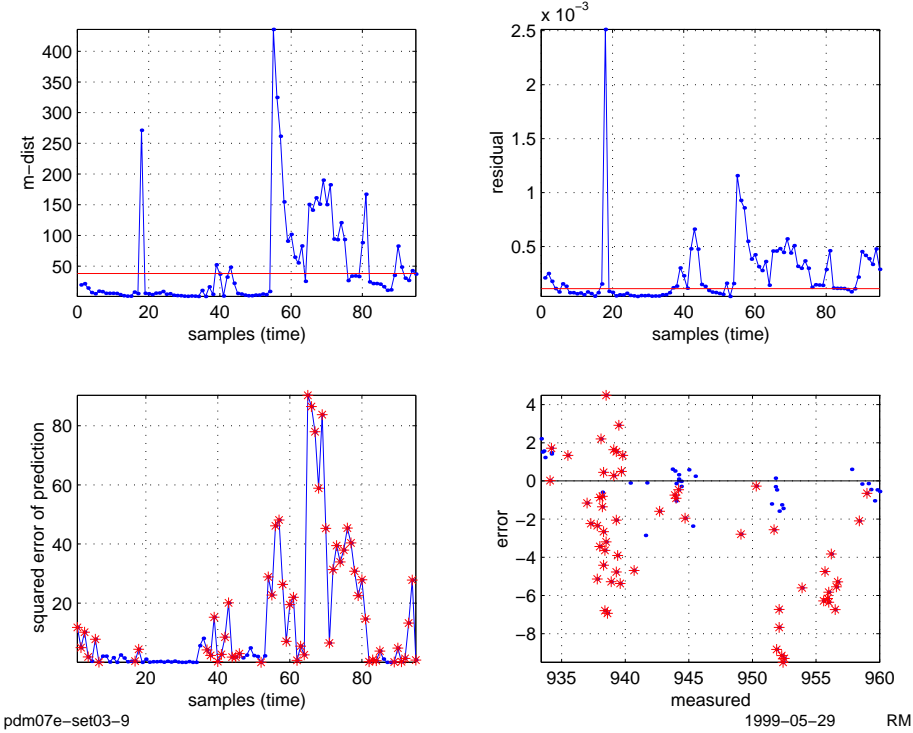


Figure N.4: Results, scheme A, test-set 3

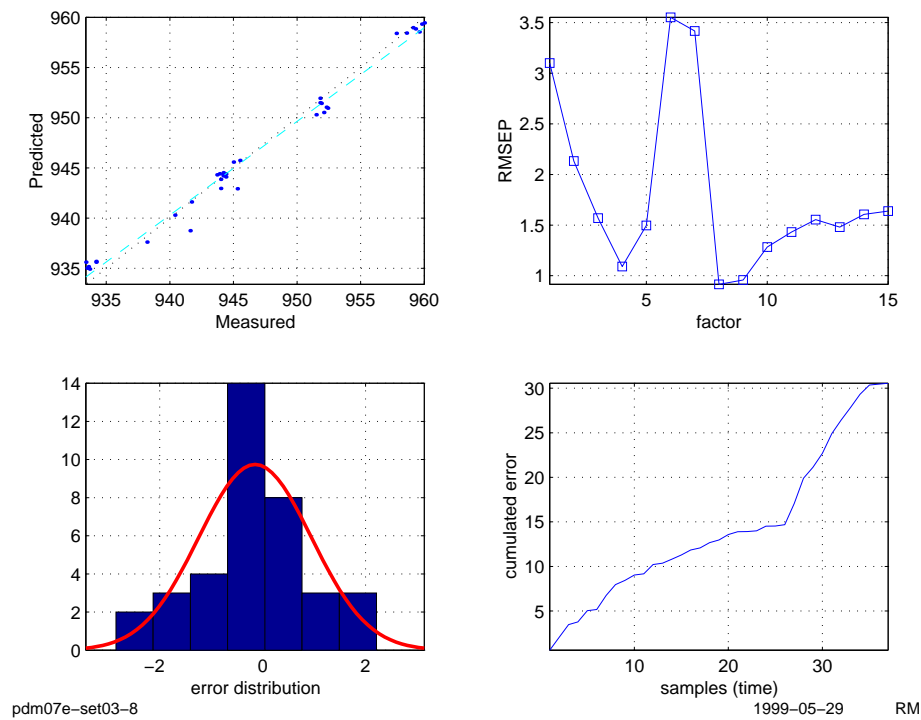


Figure N.5: Outlier detection, scheme A, test-set 4

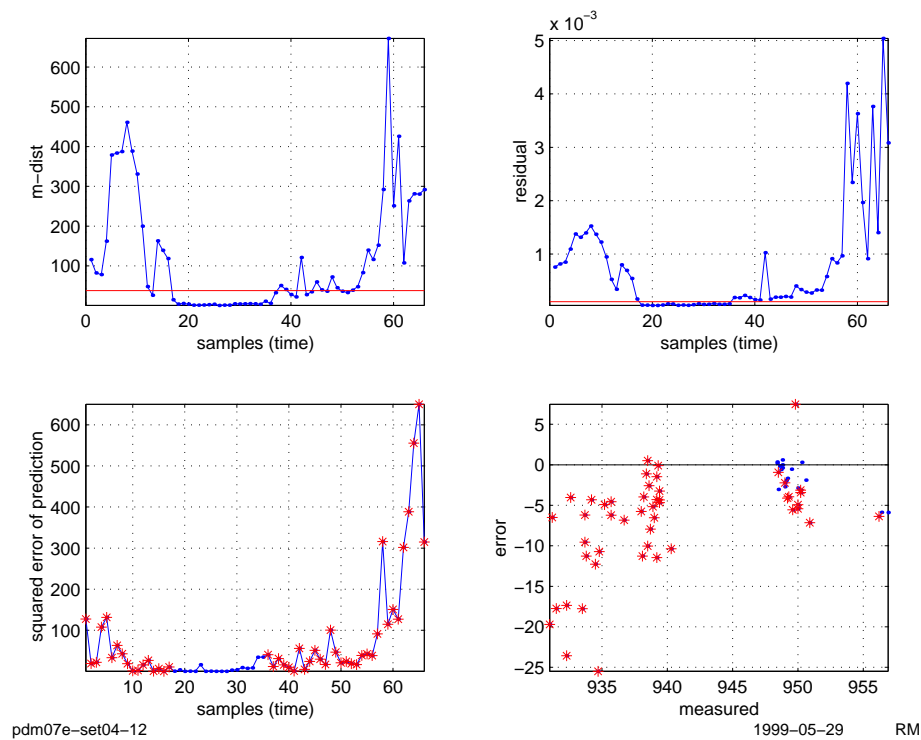


Figure N.6: Results, scheme A, test-set 4

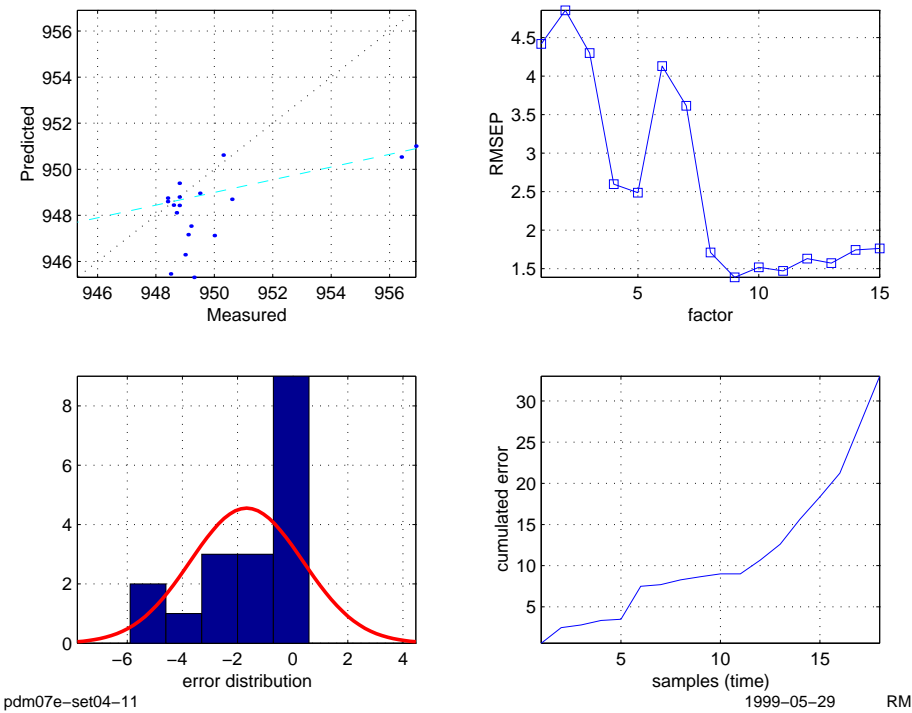


Figure N.7: Outlier detection, scheme A, test-set 5

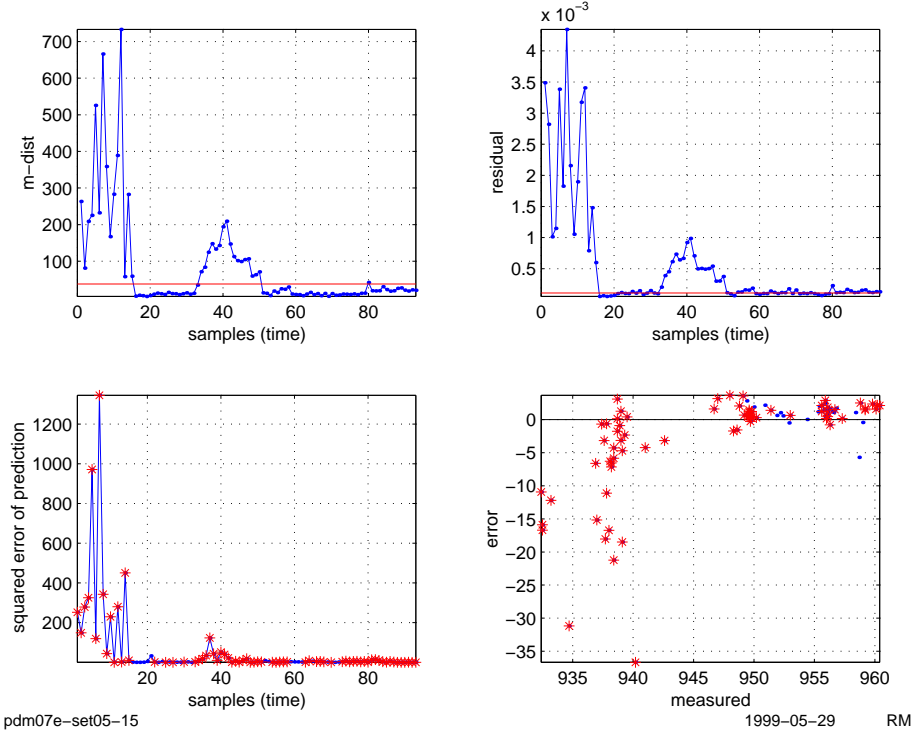
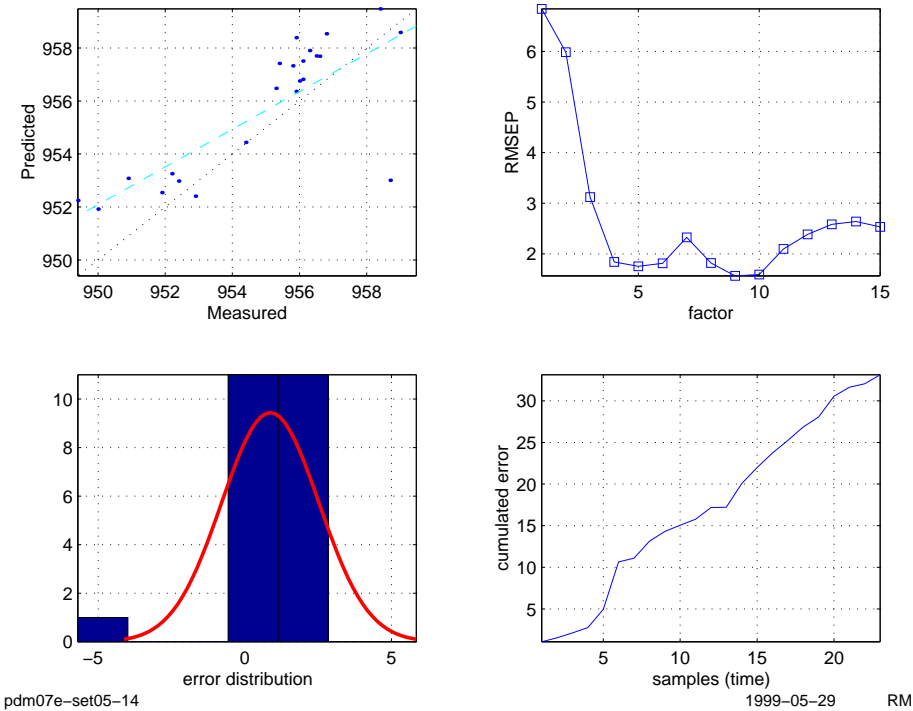


Figure N.8: Results, scheme A, test-set 5



N.2 Scheme B

Figure N.9: Outlier detection, scheme B, test-set 2

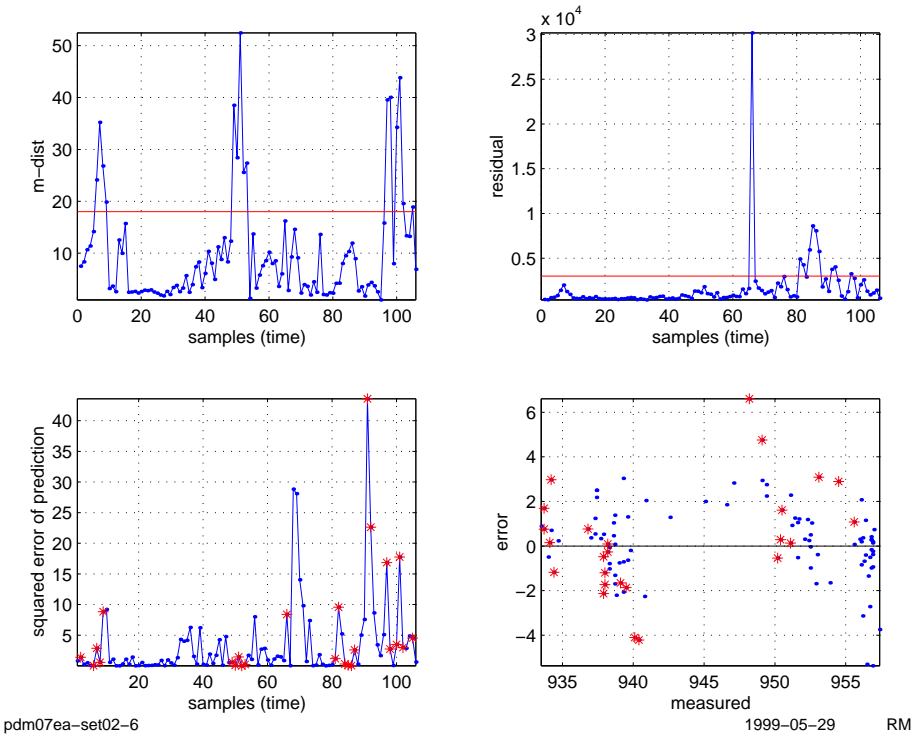


Figure N.10: Results, scheme B, test-set 2

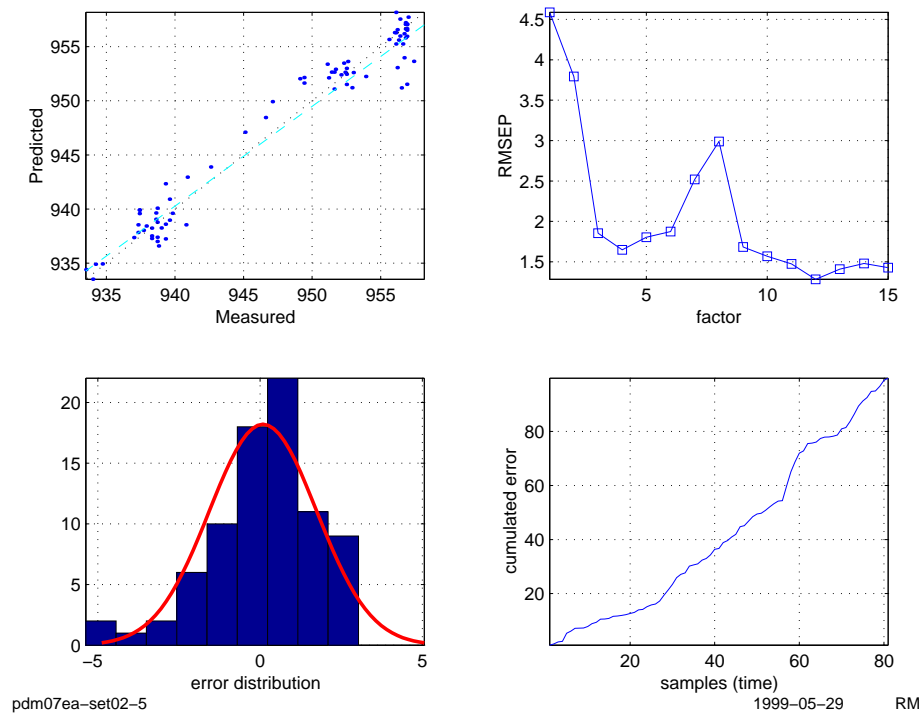


Figure N.11: Outlier detection, scheme B, test-set 3

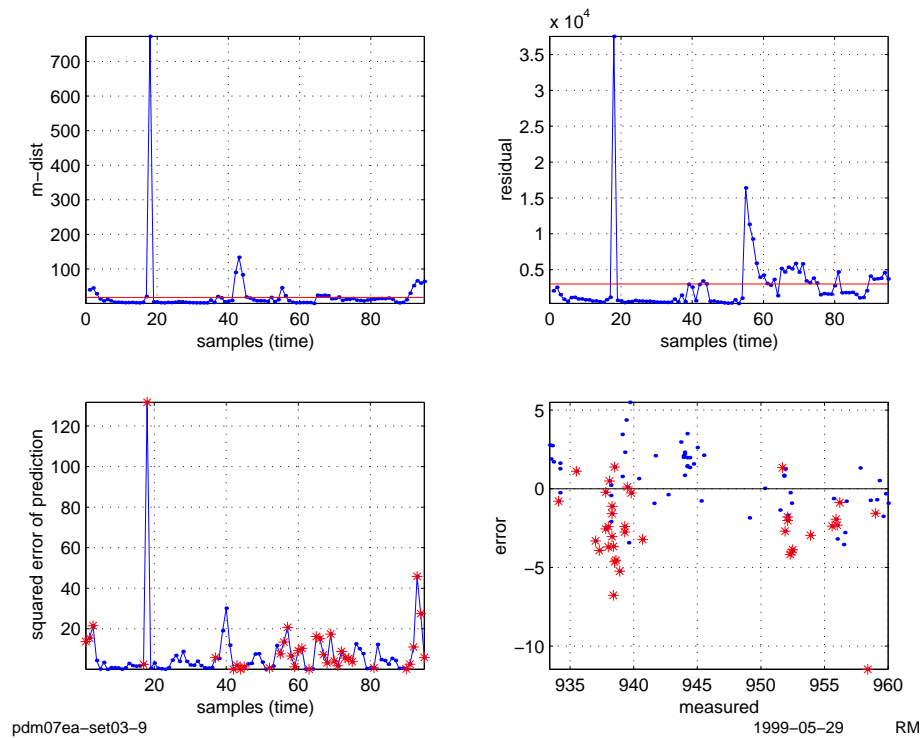


Figure N.12: Results, scheme B, test-set 3

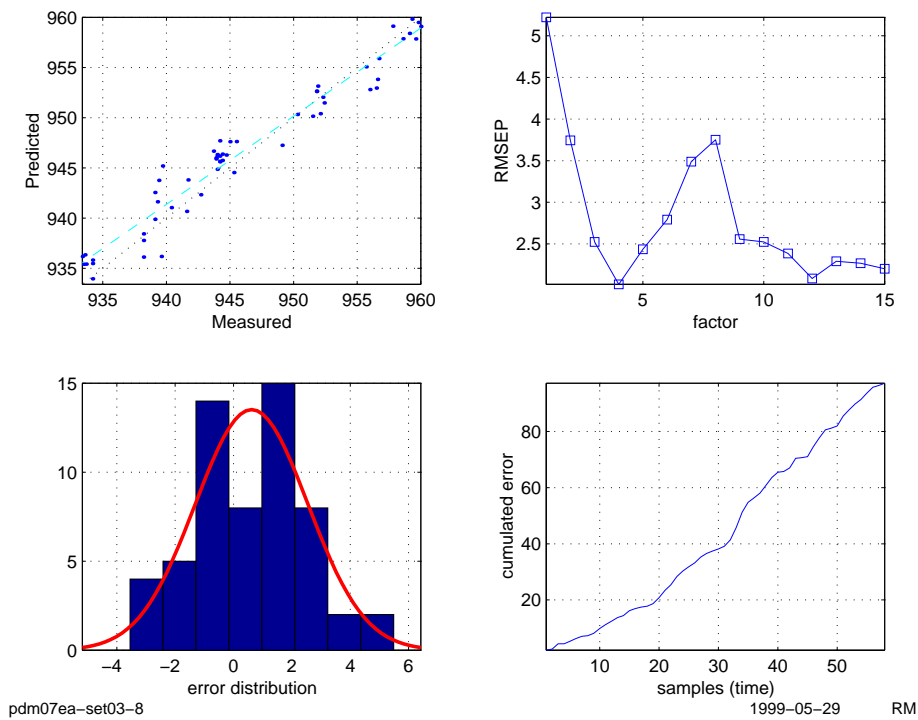


Figure N.13: Outlier detection, scheme B, test-set 4

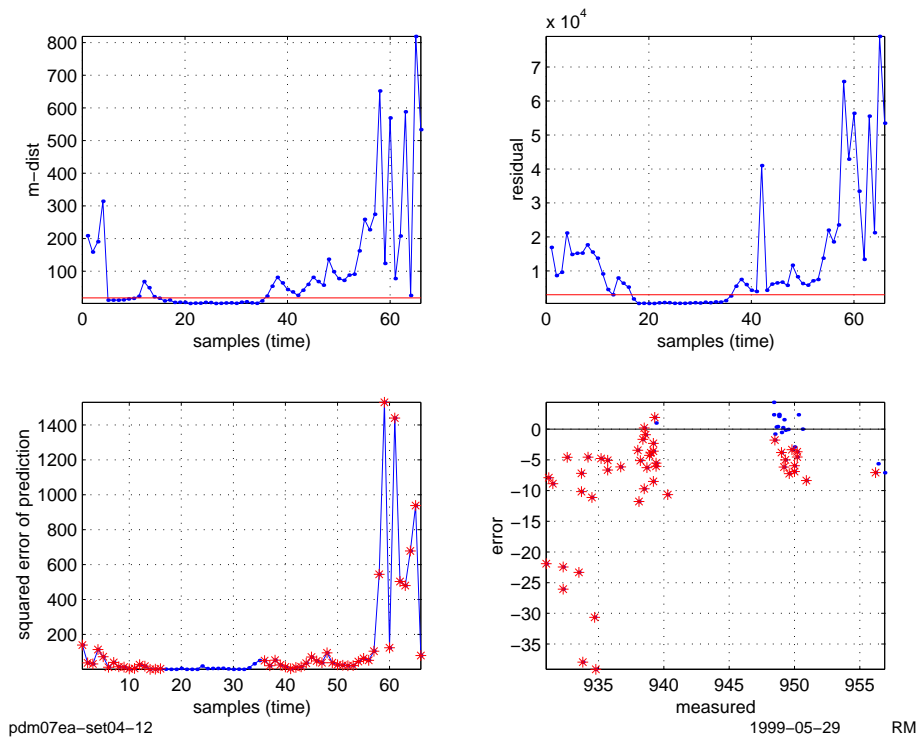


Figure N.14: Results, scheme B, test-set 4

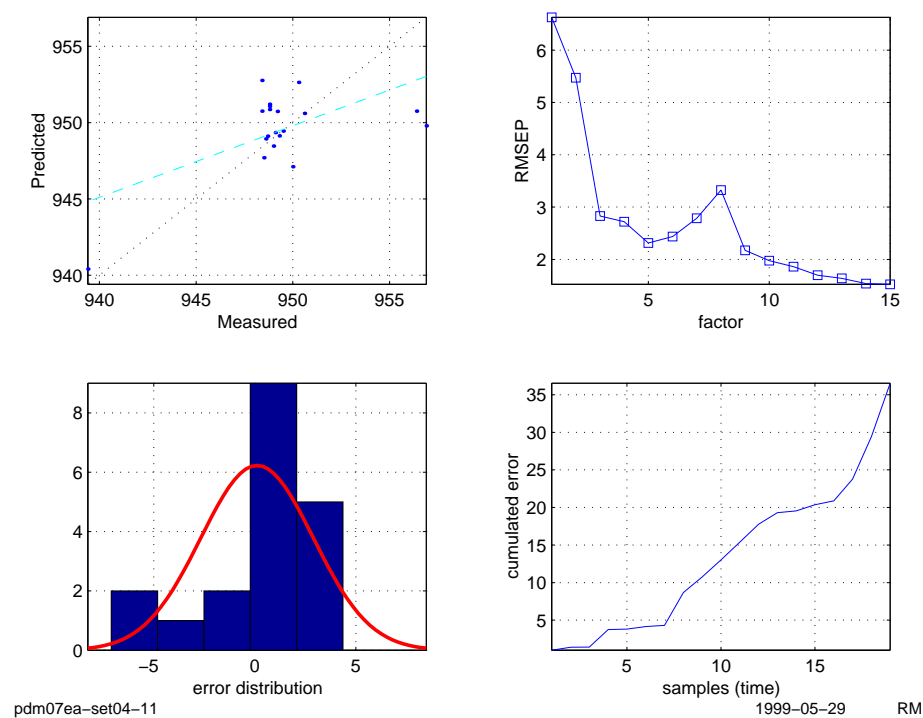


Figure N.15: Outlier detection, scheme B, test-set 5

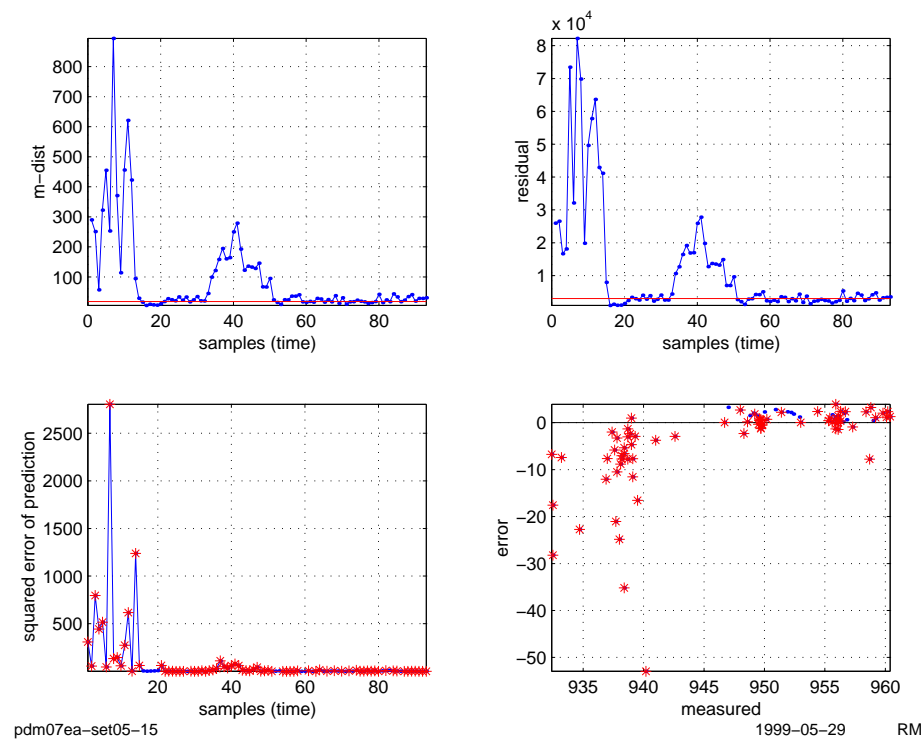
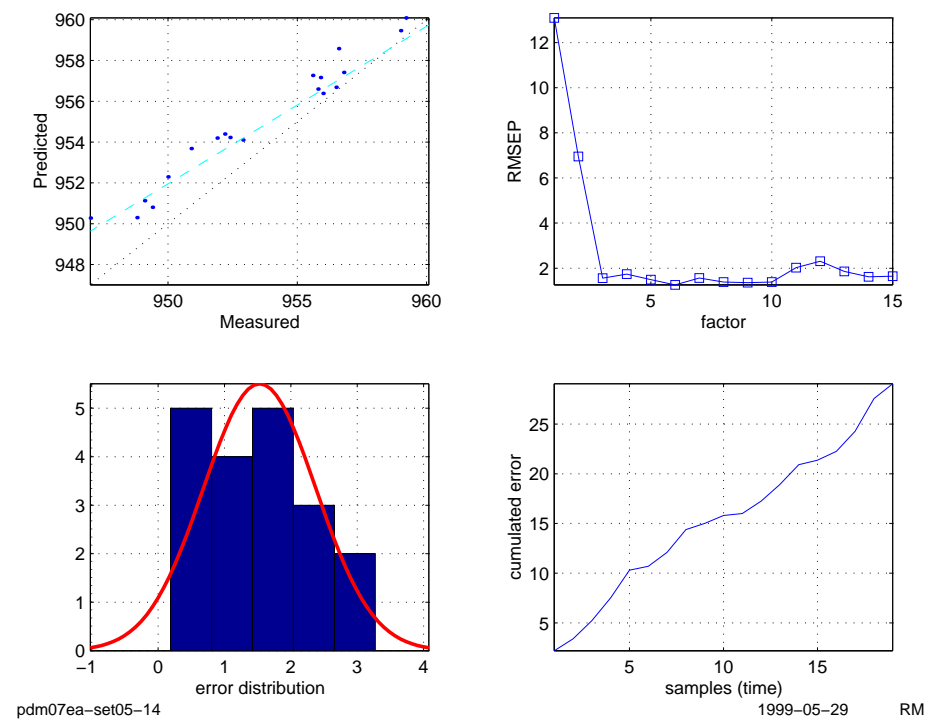
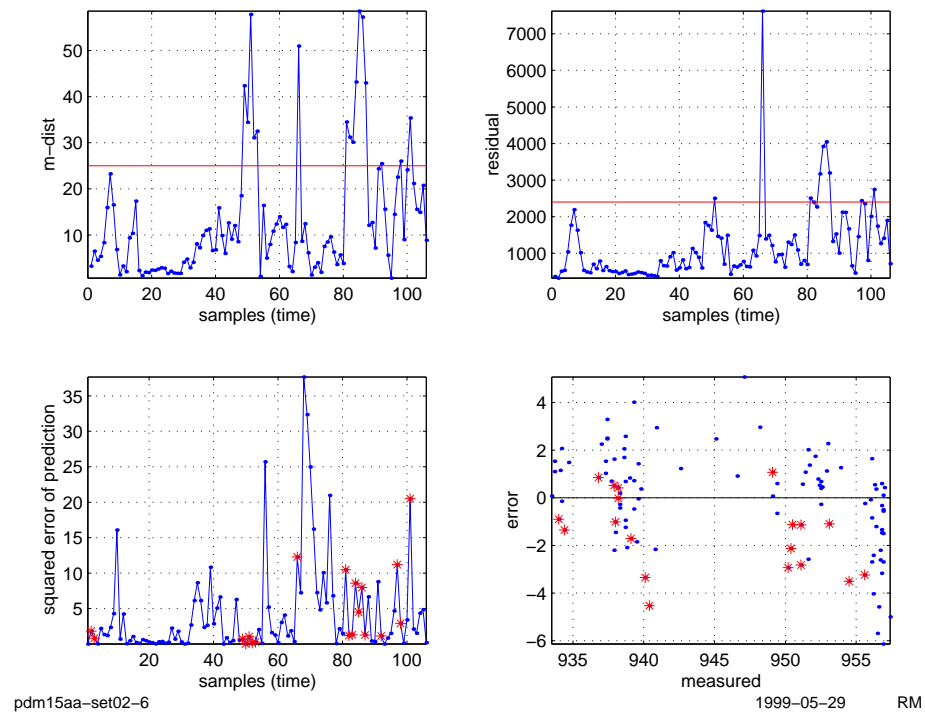


Figure N.16: Results, scheme B, test-set 5



N.3 Scheme C

Figure N.17: Outlier detection, scheme C, test-set 2



N.4 Scheme A*

Figure N.18: Results, scheme C, test-set 2

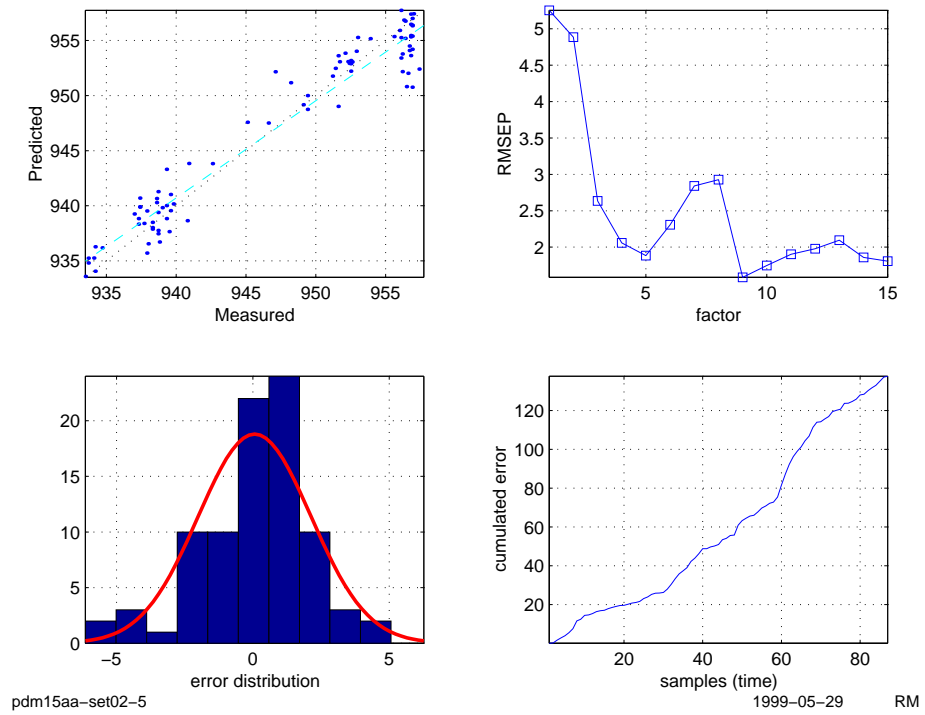


Figure N.19: Outlier detection, scheme C, test-set 3

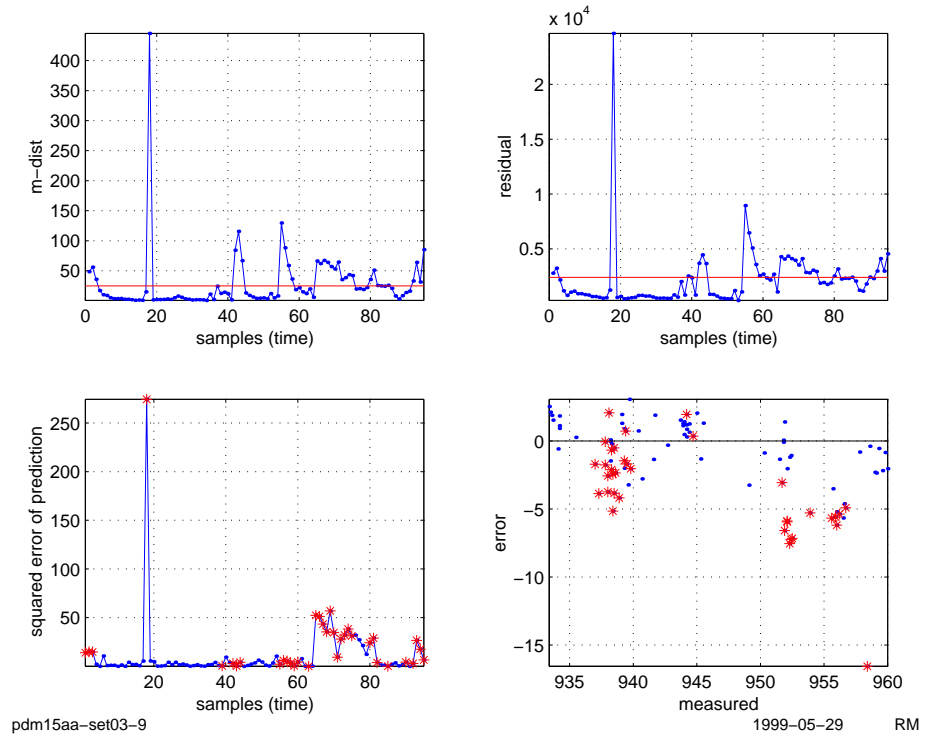


Figure N.20: Results, scheme C, test-set 3

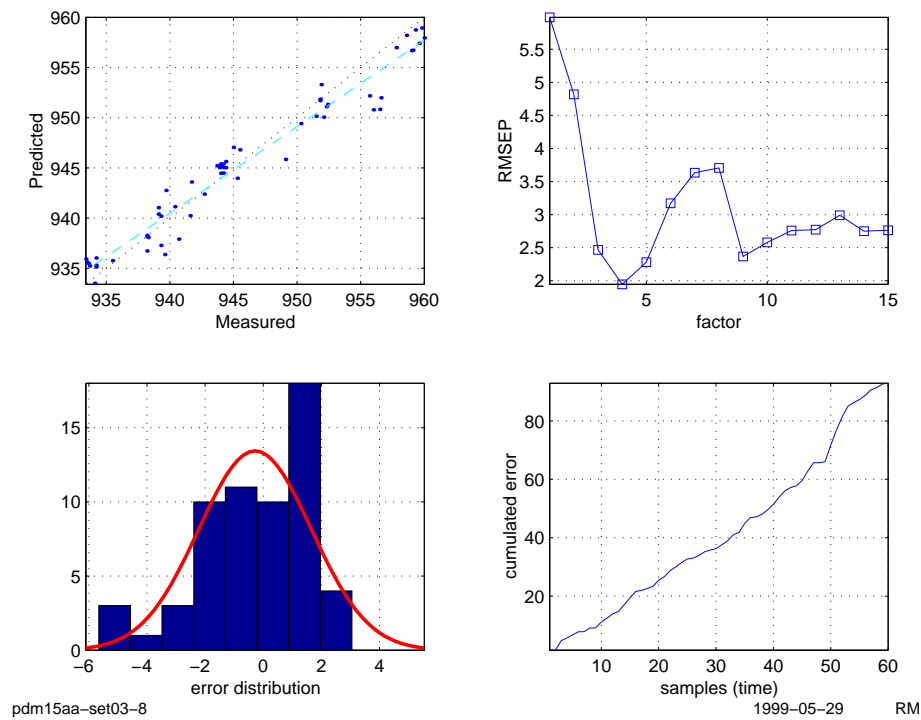


Figure N.21: Outlier detection, scheme C, test-set 4

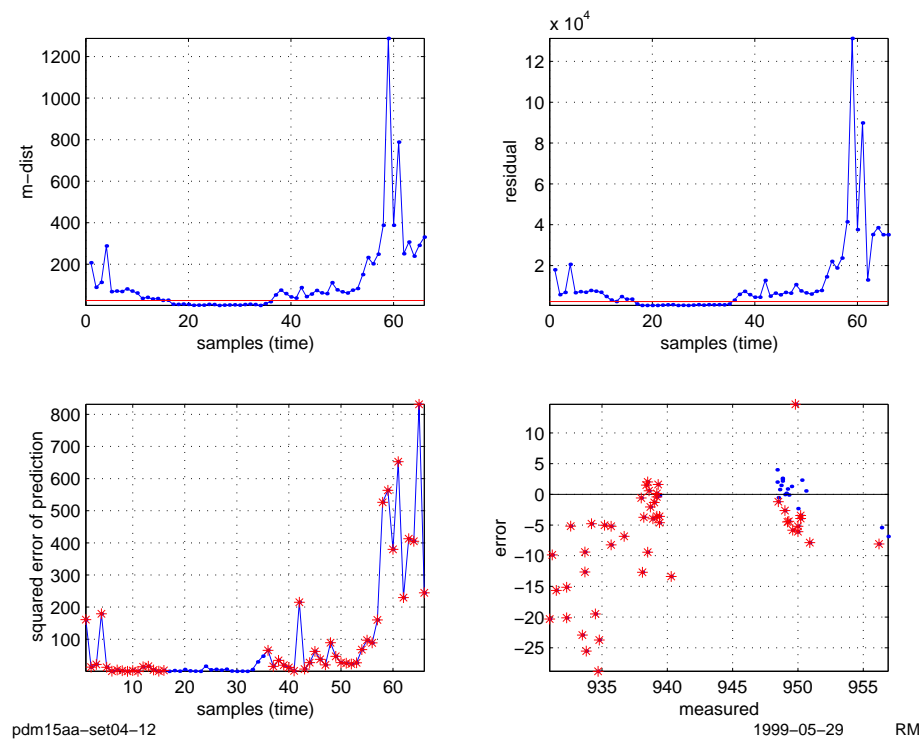


Figure N.22: Results, scheme C, test-set 4

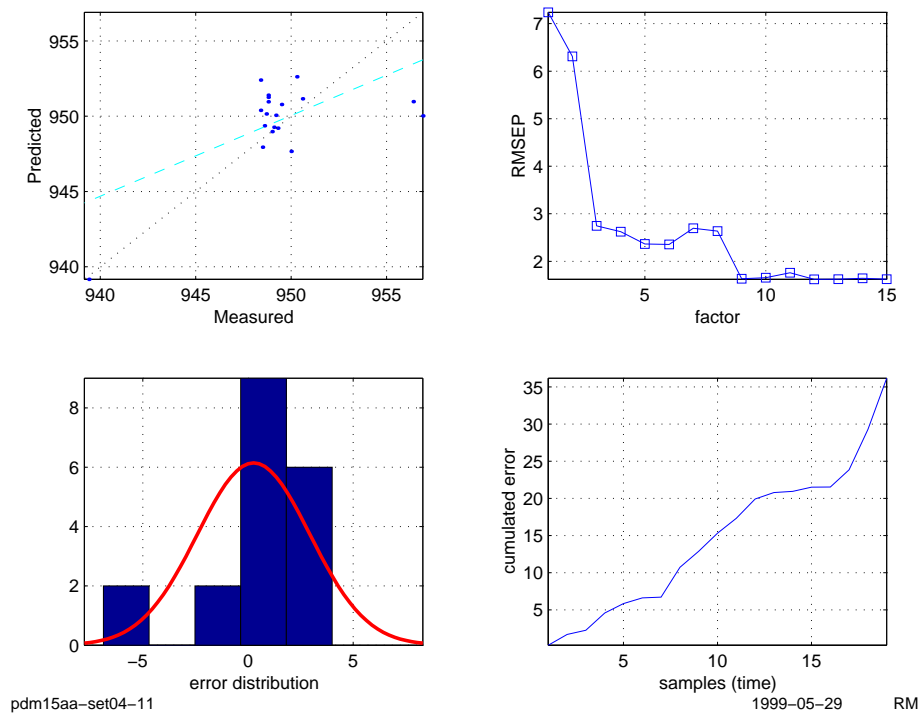


Figure N.23: Outlier detection, scheme C, test-set 5

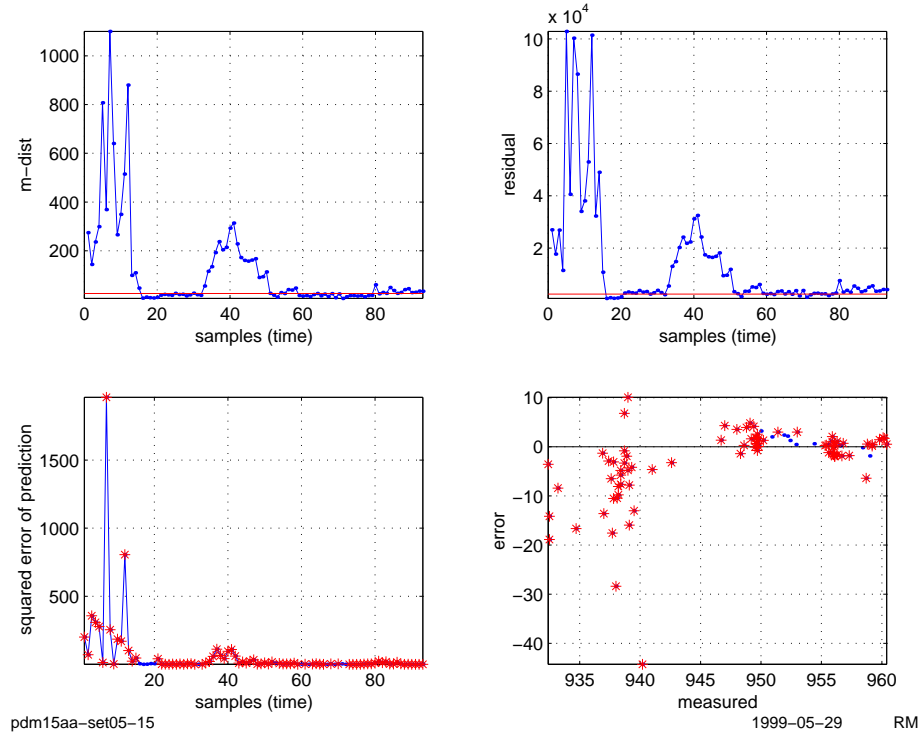


Figure N.24: Results, scheme C, test-set 5

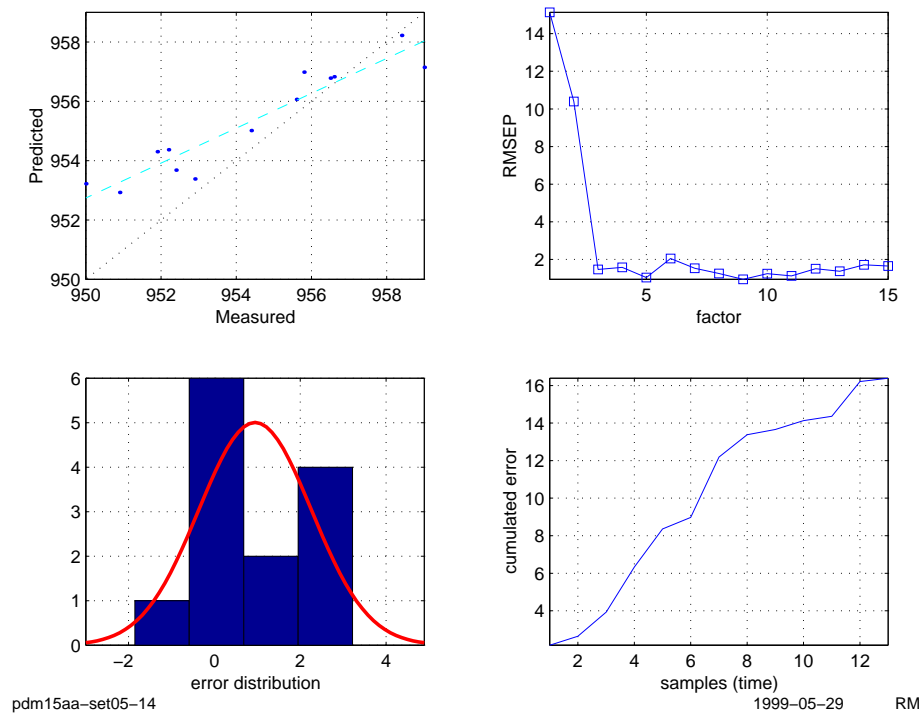


Figure N.25: Outlier detection, scheme A*, test-set 2

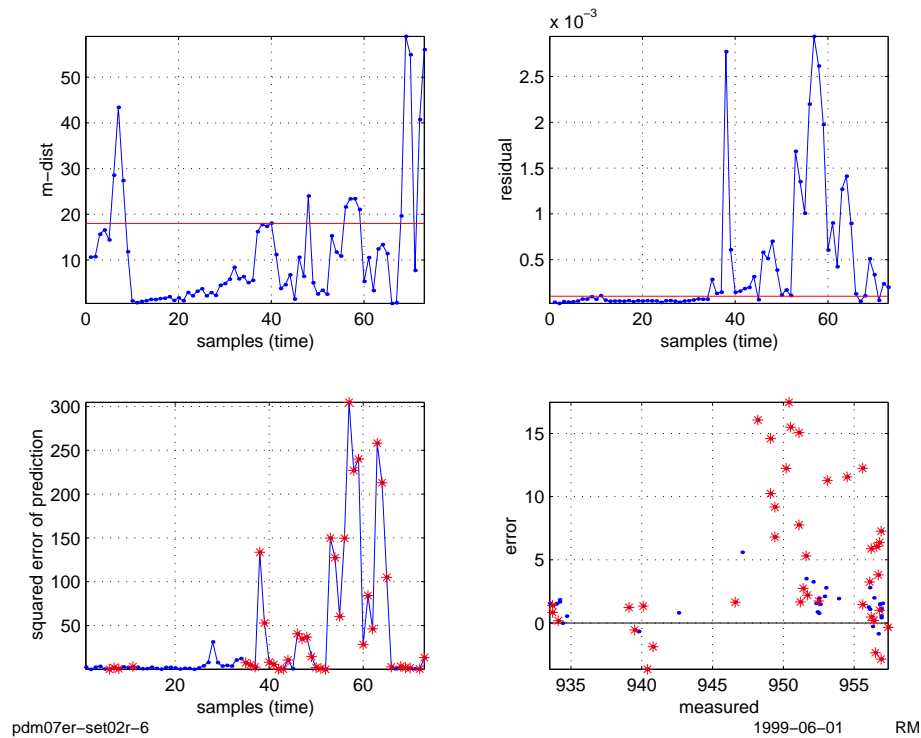


Figure N.26: Results, scheme A*, test-set 2

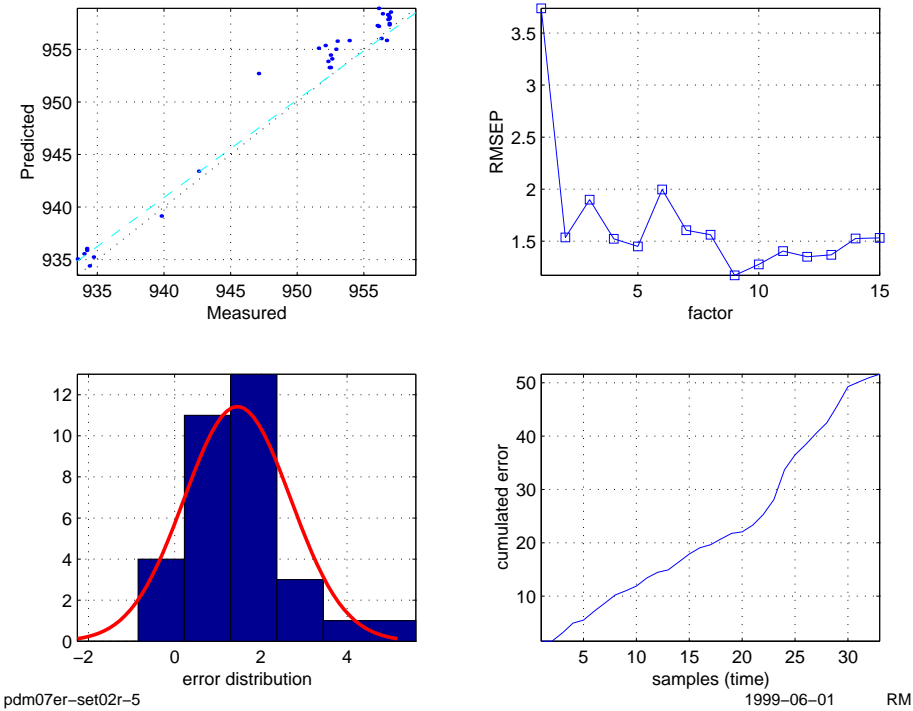


Figure N.27: Outlier detection, scheme A*, test-set 3

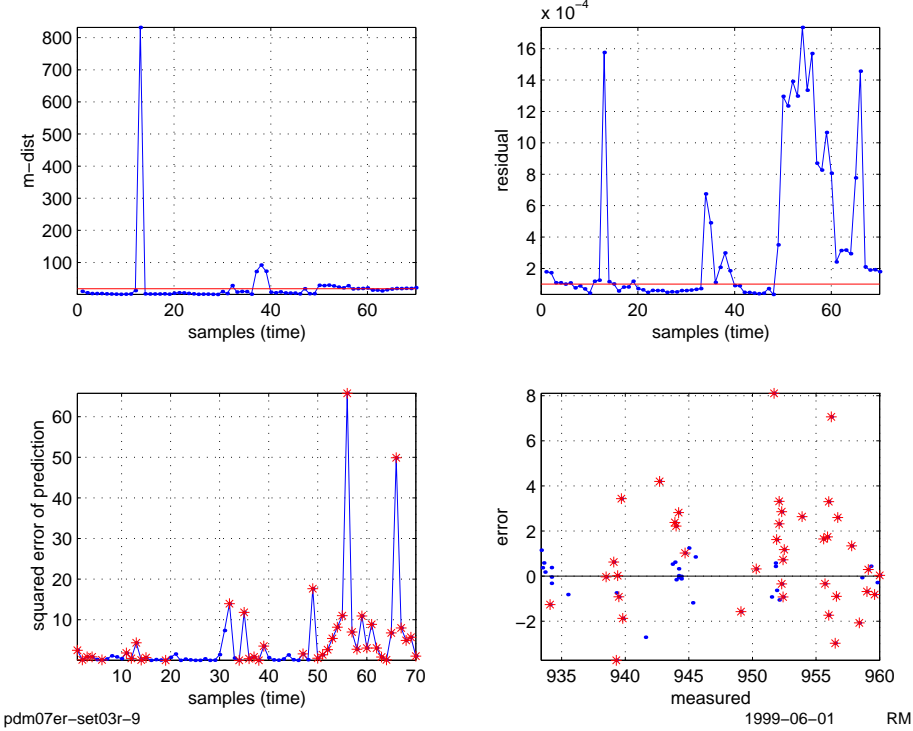


Figure N.28: Results, scheme A*, test-set 3

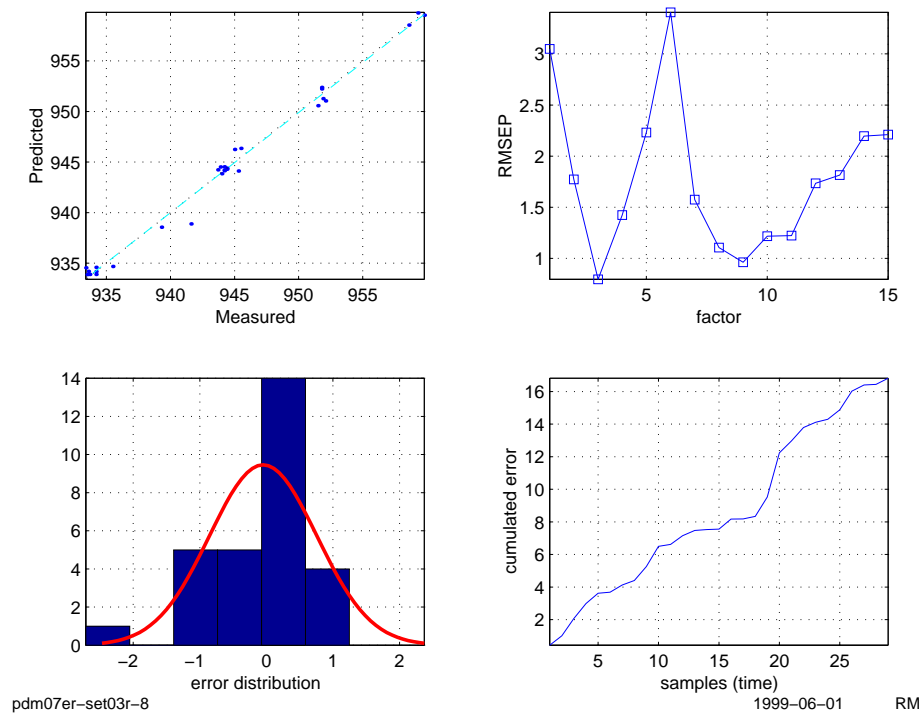


Figure N.29: Outlier detection, scheme A*, test-set 4

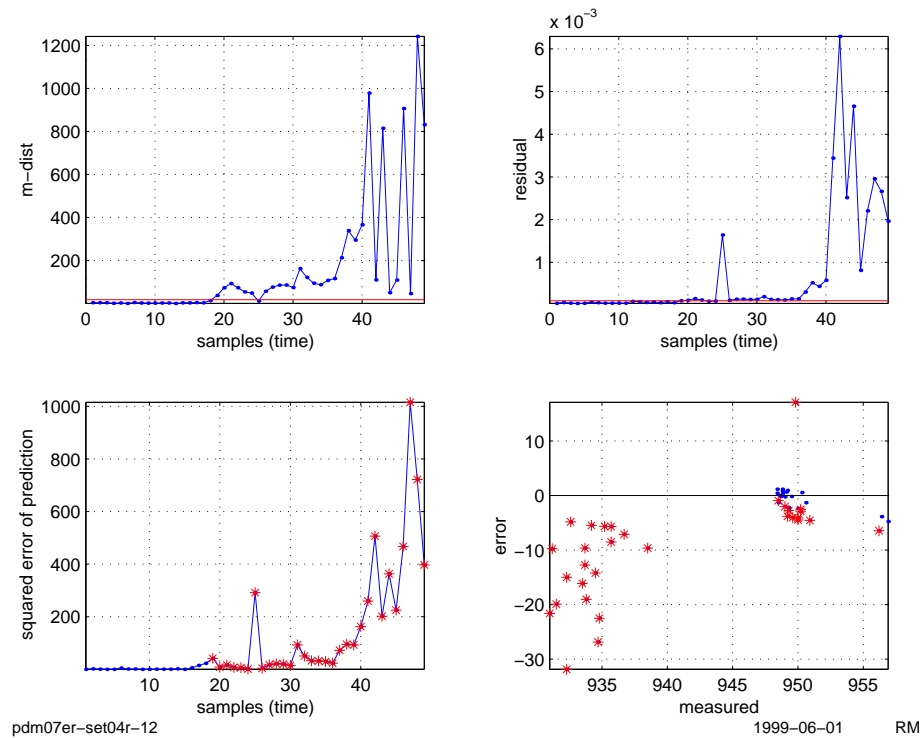


Figure N.30: Results, scheme A*, test-set 4

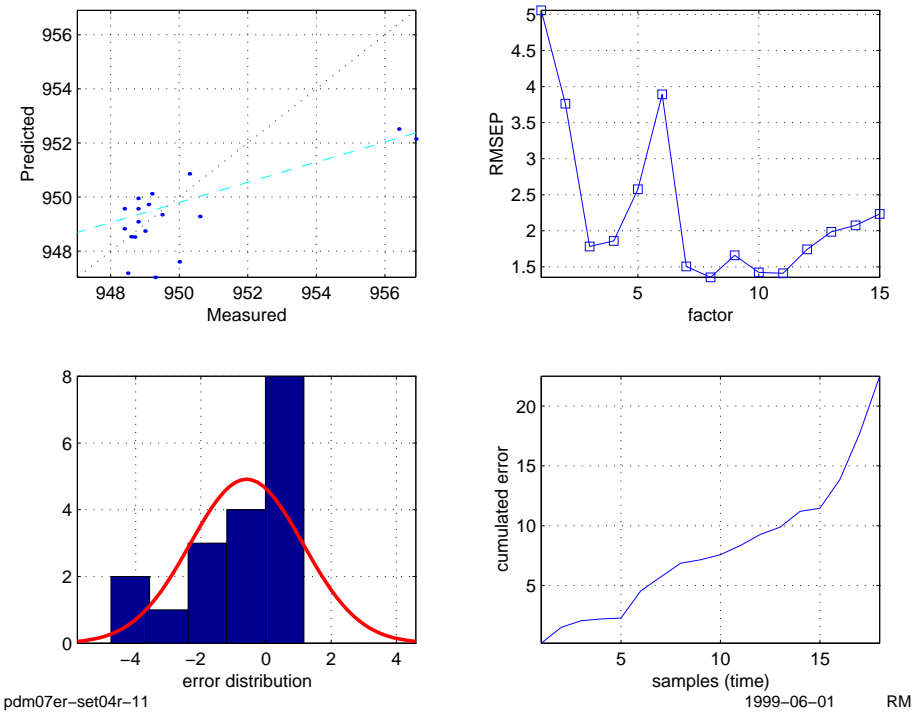


Figure N.31: Outlier detection, scheme A*, test-set 5

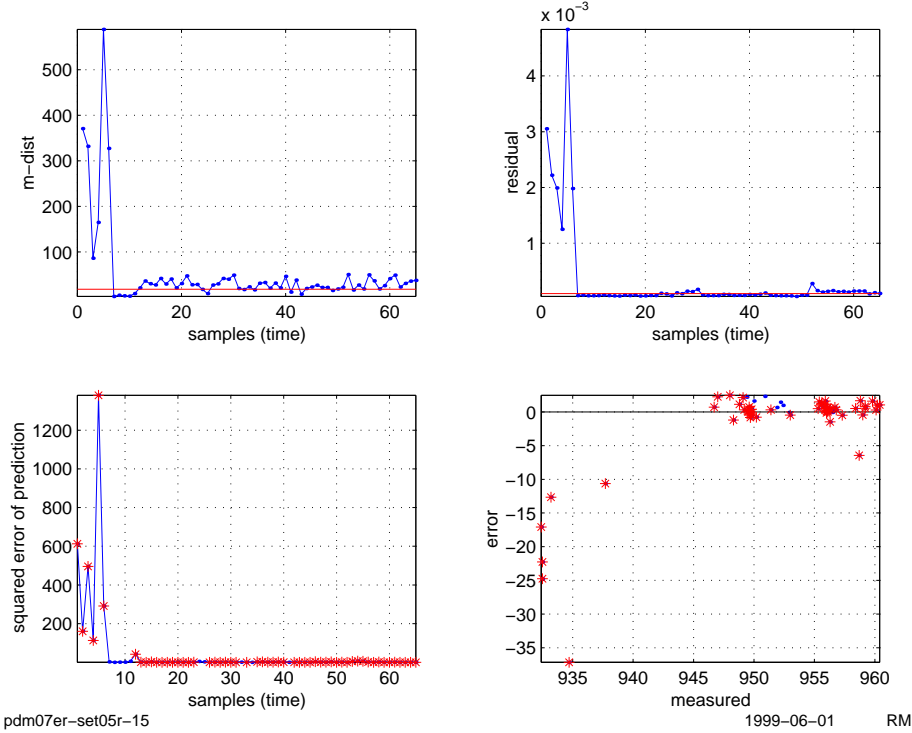
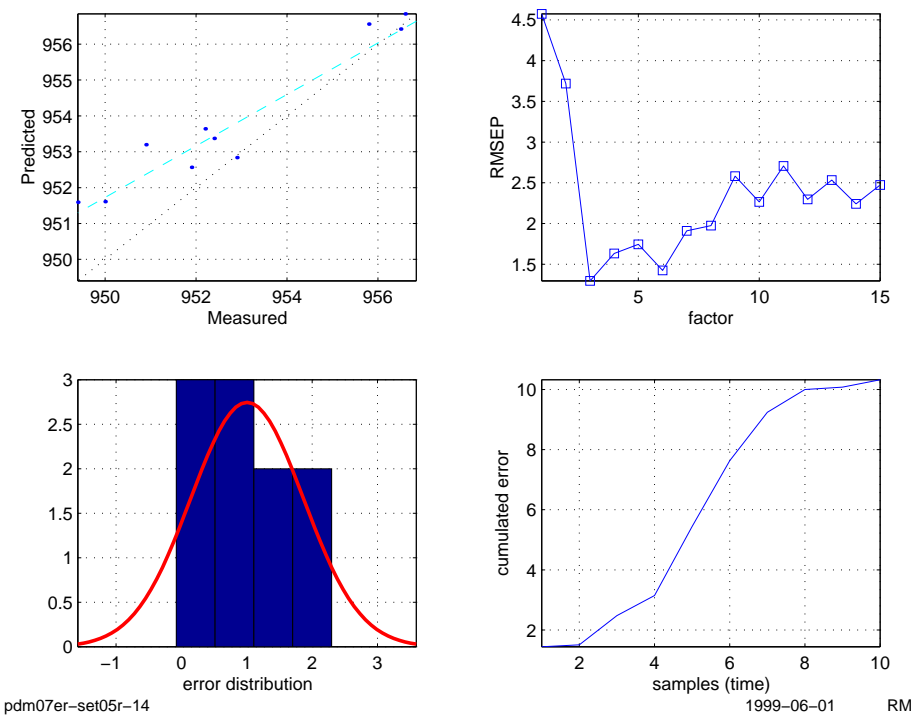


Figure N.32: Results, scheme A*, test-set 5



Appendix O

Calibration model updating test results

Results from the tests discussed in Section 6.2.10 are presented in this appendix. The two dashed lines in the time/prediction error plots marks $\pm 2 \times \text{std}$.

O.1 Moving window PLSR

Figure O.1: Pre-processing scheme A, 4 factors, moving, predicted/measured

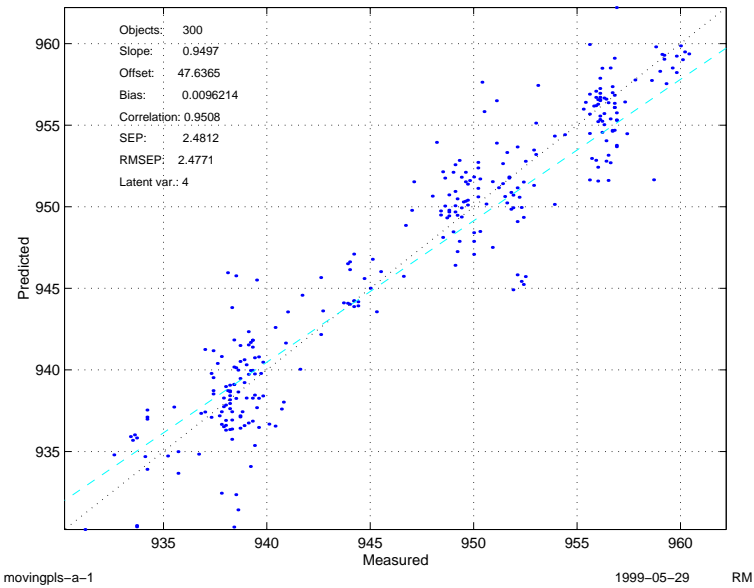


Figure O.2: Pre-processing scheme A, 4 factors, moving, time/prediction error

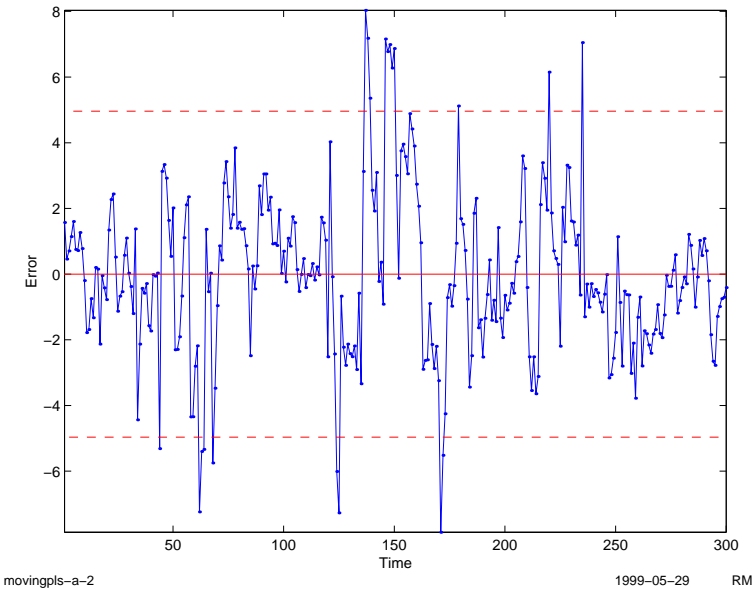


Figure O.3: Pre-processing scheme B, 4 factors, moving, predicted/measured

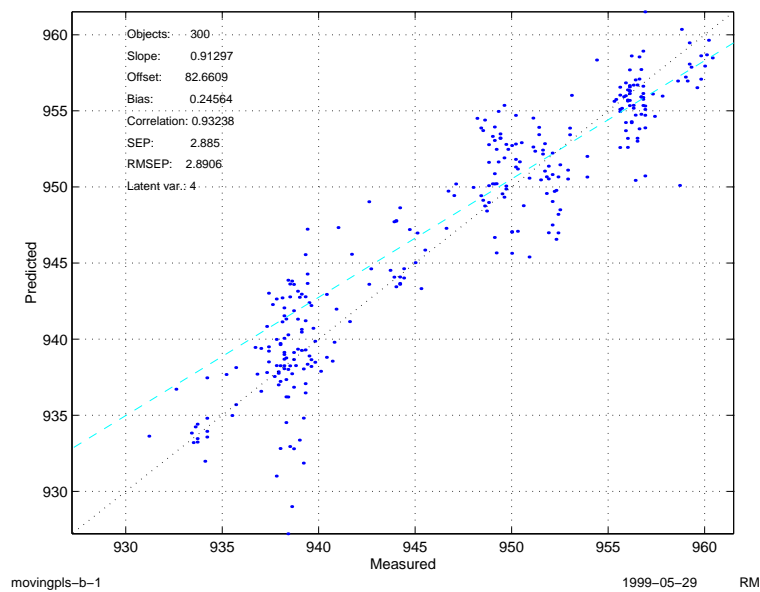


Figure O.4: Pre-processing scheme B, 4 factors, moving, time/prediction error

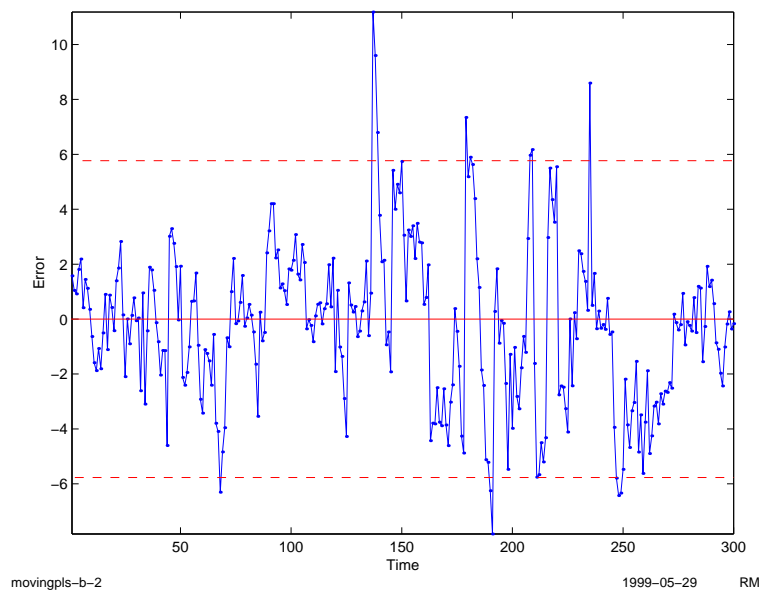


Figure O.5: Pre-processing scheme C, 4 factors, moving, predicted/measured

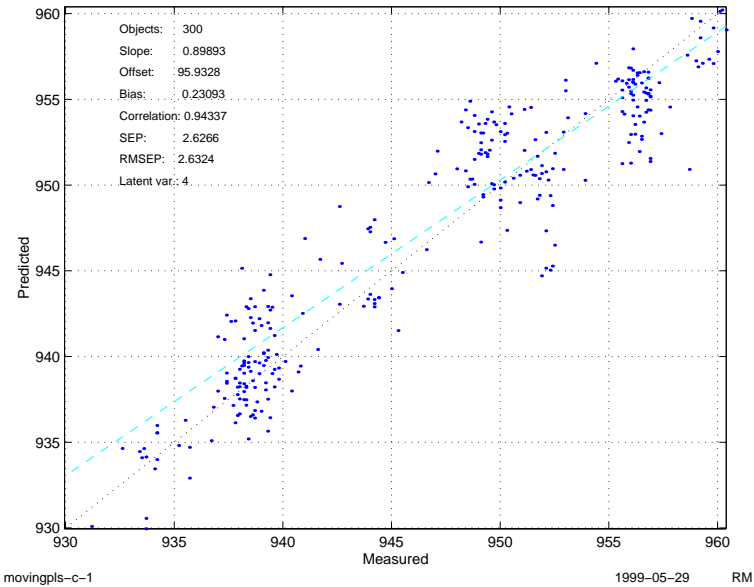
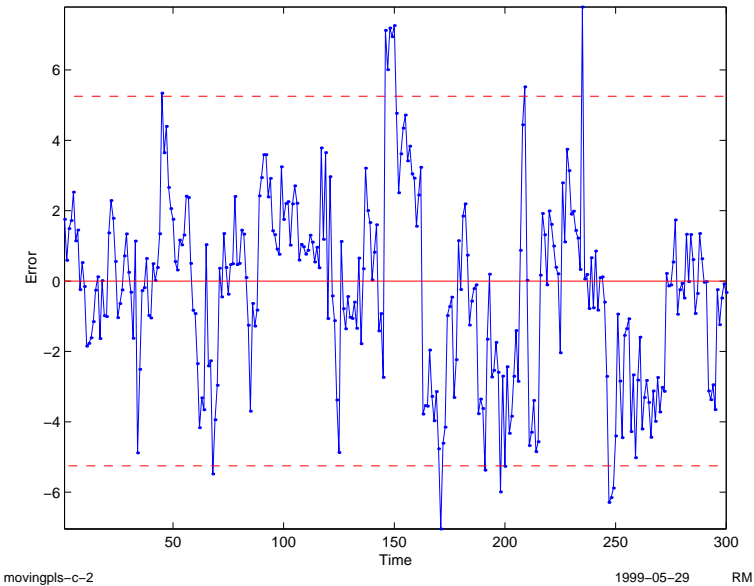


Figure O.6: Pre-processing scheme C, 4 factors, moving, time/prediction error



O.2 Growing PLSR

Figure O.7: Pre-processing scheme A, 4 factors, growing, predicted/measured

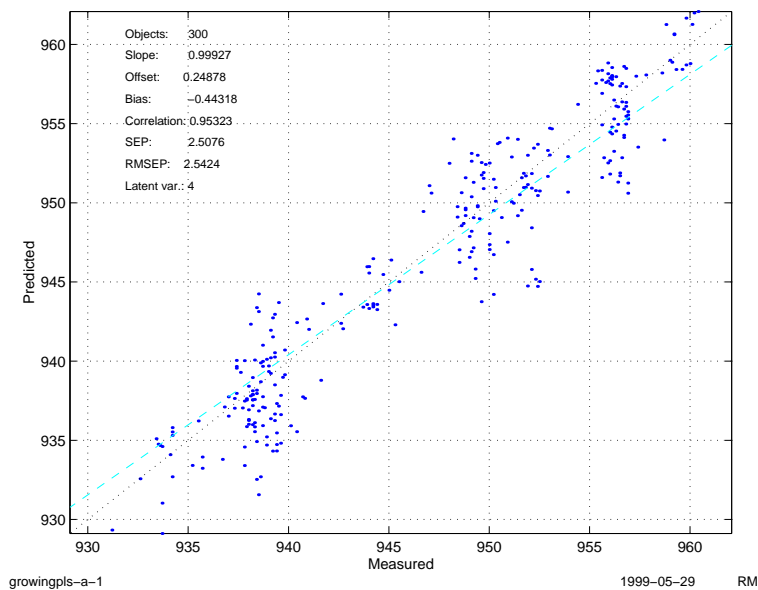


Figure O.8: Pre-processing scheme A, 4 factors, growing, time/prediction error

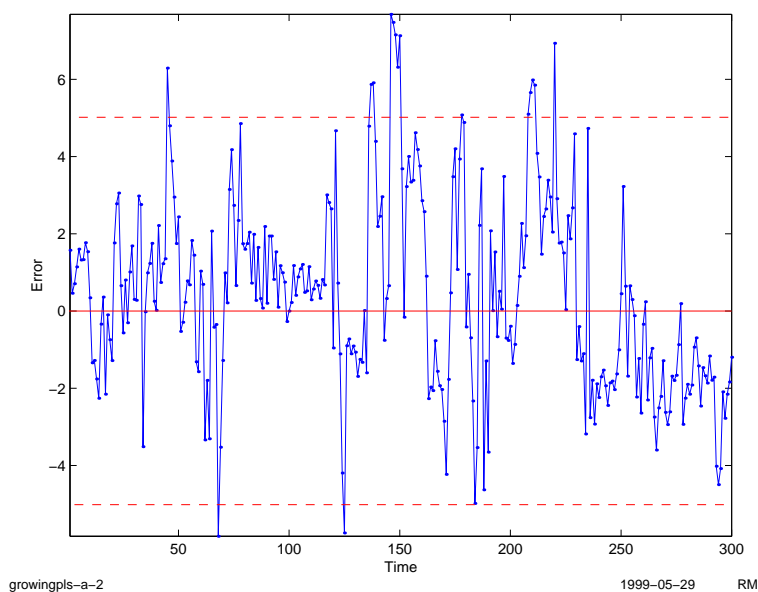


Figure O.9: Pre-processing scheme B, 4 factors, growing, predicted/measured

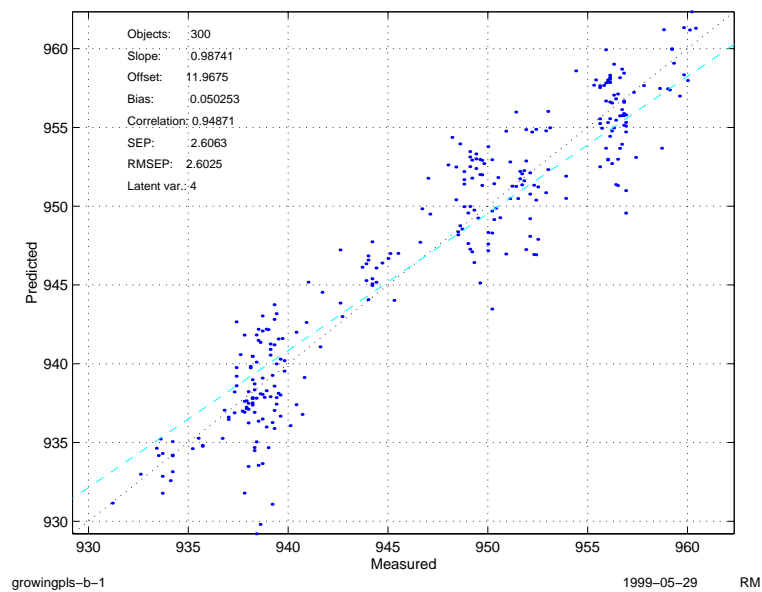


Figure O.10: Pre-processing scheme B, 4 factors, growing, time/prediction error

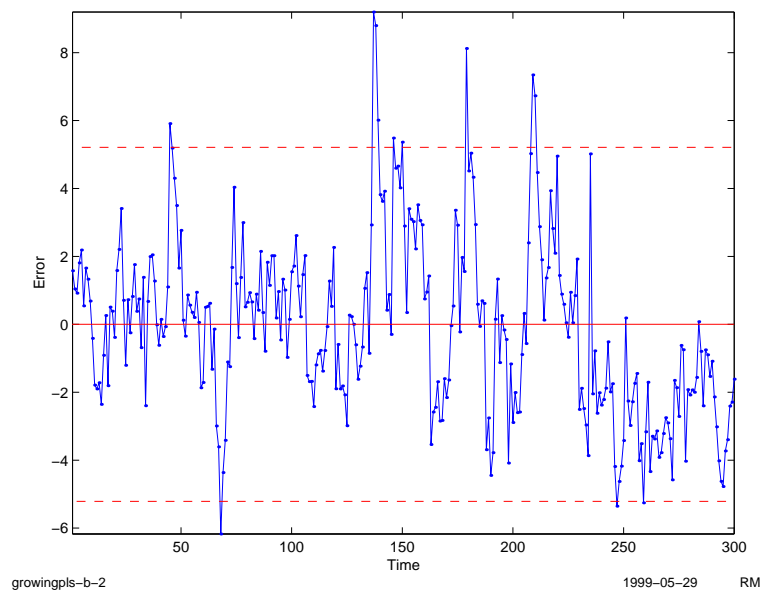


Figure O.11: Pre-processing scheme C, 4 factors, growing, predicted/measured

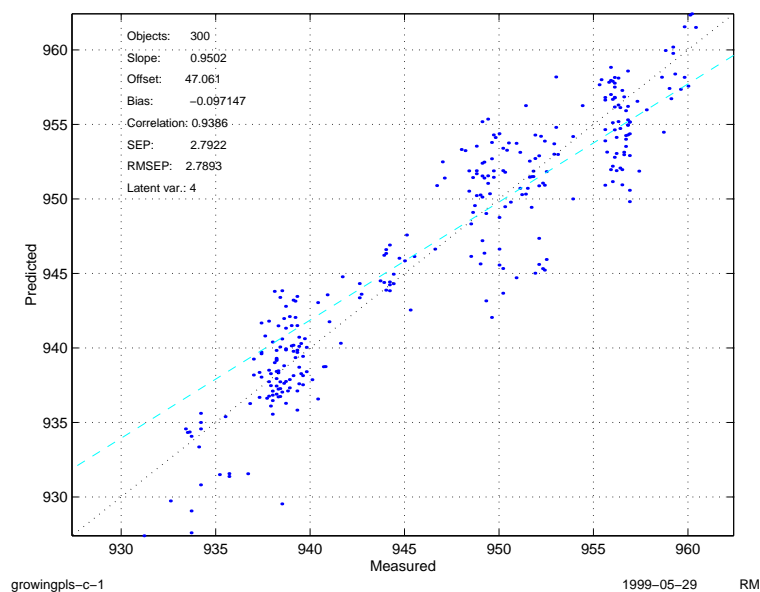
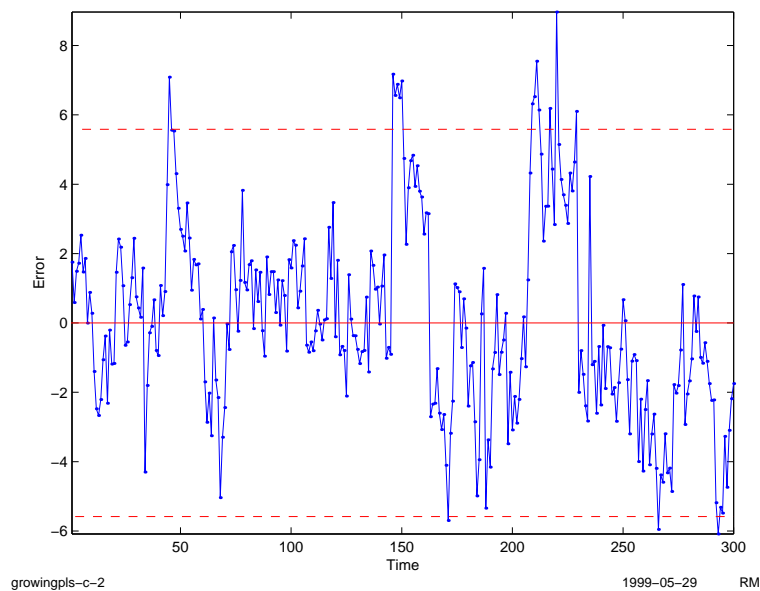


Figure O.12: Pre-processing scheme C, 4 factors, growing, time/prediction error



Bibliography

- [Almquist and Follestad (1986)] *PEH-pulveregenskaper relatert til katalysator og reaktorvariable (Powder properties in HDPE related to catalyst and reactor parameters)*, Vidar Almquist, Arild Follestad, Internal Statoil report, Filing Code: 50556, 1986.
- [ASTM D 6122 (1997)] *Standard practice for validation of multivariate process infrared spectrophotometers*, American Society for Testing and Materials, D 6122, 1997.
- [Beebe et al. (1998)] *Chemometrics: a practical guide*, Kenneth R. Beebe, Randy J. Pell, Mary Beth Seasholtz, John Wiley & Sons, 1998, ISBN: 0-471-12451-6.
- [Berntsson et al. (1998)] *Estimation of effective sample size when analysing powders with diffuse reflectance near-infrared spectrometry*, O. Berntsson, L-G. Danielsson, S. Follestad, Analytica Chimica Acta, 364, 1998.
- [Bjåland and Helleborg (1997)] *Investigation of settling efficiency for SSC in LDPE slurry loop*, Anne Britt Bjåland, Stein Helleborg, Internal Borealis report, Filing code: CPR97103, 1997.
- [Boenig (1966)] Herman V. Boenig. *Polyolefines: structure and properties*, First edition Elsevier Publishing Company, 1966, Library of Congress Catalog Card Number: 65-20138.
- [Branderup and Immergut (1989)] *Polymer handbook*, J. Branderup, E.H. Immergut, third edition, Wiley Interscience, 1989, ISBN: 0-417-81244-7.
- [Brimrose (1999)] *Various Brimrose brochures and correspondence with Keith Li*, Brimrose Corp. of America, 1999.
- [Davies and Fearn (1997)] *Genetic algorithms: the evolutionary solution to an old problem*, Tony Davies, Tom Fearn, Spectroscopy Europe, 9/6, 1997.
- [Esbensen et al. (1994)] *Multivariate analysis -in practice: A training package*, Kim Esbensen, Suzanne Schönkopf, Tonje Midtgaard, Computer-Aided Modeling AS (CAMO), 1994, ISBN: 82-993330-0-8.
- [Gorry (1990)] *General least-squares smoothing and differentiation by the convolution (Savitzky-Golay) method*, Peter A. Gorry, Analytical Chemistry, vol.62, 6, 1990.
- [Griffiths and Haseth (1986)] *Fourier transform infrared spectroscopy*, Peter R. Griffiths, James A. de Haseth. second printing John Wiley & Sons, 1986, ISBN: 0-471-09902-3.
- [Gy (1998)] *Sampling for analytical purposes*, Pierre Gy, John Wiley & Sons, 1998, ISBN: 0-471-97956-2.

- [Hansen and Vedula (1998)] *In-line Fiber-Optic Near-Infrared Spectroscopy: Monitoring of Rheological Properties in an Extrusion Process, Part 1*, Marion G. Hansen, S. Vedula, Journal of Applied Polymer Science, 68, 1998.
- [Hassel (1998)] *Variation between single NIR spectra, in-line powder Rønningen I*, Per Anker Hassel, Internal Borealis memo, 1998.
- [Hassel (1999)] *Variation between single NIR spectra, in-line powder Rønningen VI*, Per Anker Hassel, Internal Borealis memo, 1999.
- [Helland (1993)] *On-line near-infrared spectroscopy for hydrocarbon gas analysis: Calibration models maintenance*, Kristian Helland, Ph.D. thesis, The Norwegian Institute of Technology (NTH), Department of Physical Chemistry, Thesis no. 45, 1993.
- [Henriksen (1993)] *Test av spektrofotometer fra NIRSystems "Rapid Resin Analyzer", et NærInfraRødt (NIR) instrument (Test of a spectrophotometer from NIRSystems "Rapid Resin Analyzer", a Near InfraRed (NIR) instrument)*, Arne Henriksen, Internal Statoil report, Filing code: 93-034.lab, 1993.
- [Høy et al. (1998)] *Review of partial least squares regression prediction error in Unscrambler*, Martin Høy, Kay Steen, Harald Martens. Chemometrics and Intelligent Laboratory Systems, 44, 1998.
- [Kemp (1991)] *Organic Spectroscopy*, William Kemp, third edition, Macmillan, 1991. ISBN: 0-333-51953-1.
- [Lambert et al. (1995)] *On-line NIR monitoring and optimisation for refining and petrochemical processes*, D. Lambert, B. Descales, J.R. Llinas, A. Espinosa, S. Osta, M. Sanchez, A. Martens, Analisis Magazine, vol.23, 4, 1995.
- [Martens and Næs (1991)] *Multivariate calibration*, Harald Martens, Tormod Næs, second printing, John Wiley & Sons, 1991, ISBN: 0-471-93047-4.
- [McLennan and Kowalski (ed) (1995)] *Process Analytical Chemistry*, First edition, Blackie Academic and Professional, 1995, ISBN: 0-7514-0038-6.
- [Miller (1993)] *Use of near-infrared spectroscopy to determine the composition of high-density/low-density polyethylene blend films*, Charles E. Miller, Applied Spectroscopy, vol.47, 2, 1993.
- [de Noord (1994)] *Multivariate calibration standardization*, Onno E. de Noord, Chemometrics and intelligent laboratory systems, 25, 1994.
- [PLS-Toolbox: Wise and Gallagher] *PLS-Toolbox version 2.0.1c for Matlab*, Barry M. Wise, Neal B. Gallagher, Eigenvector Research, Inc., 1999.
- [PLSplus/IQ users guide] *PLSplus/IQ users guide*, Galactic Industries Corporation, 1996.
- [Seim (1999)] *Sinus shaped noise in NIR spectra from HDPE plant Rønningen*, Marit Seim, Internal Borealis memo, 1999.
- [Shimoyama et al. (1998)] *Near infrared spectroscopy and chemometrics analysis of linear low-density polyethene*, Masahiko Shimoyama et al., Journal of Near Infrared Spectroscopy, 6, 1998.

- [Skoog et al. (1998)] *Principles of Instrumental Analysis*, Douglas A. Skoog, F. James Holler, Timothy A. Nieman, Fifth edition, Saunders College Publishing, 1998, ISBN 0-03-002078-6.
- [Spiegelman et al. (1998)] *Theoretical justification of wavelength selection in pls calibration: development of a new algorithm*, Clifford H. Spiegelman, Michael J. McShane, Marcel J. Goetz, Massoud Motamedi, Qin Li Yue, Gerard L. Côté, *Analytical Chemistry*, vol.70, 1, 1998.
- [Tosi and Pinto (1972)] *Near-infrared spectroscopy of hydrocarbon functional groups*, C. Tosi, A. Pinto, *Spectrochimica Acta*, 28A, pages 585-597, 1972.
- [Wang and Kowalski (1992)] *Calibration transfer and measurement stability of near-infrared spectrometers*, Yongdong Wang, Bruce R. Kowalski, *Applied Spectroscopy*, vol.46, 5, 1992.
- [Wold et al. (1987)] *Principal Component Analysis*, Svante Wold, Kim H. Esbensen, Paul Geladi. *Chemometrics and intelligent laboratory systems*, 2, 1987.
- [Wold et al. (1998)] *Orthogonal signal correction of near-infrared spectra*, Svante Wold, Henrik Antti, Fredrik Lindgren, Jerker Öhman, *Chemometrics and intelligent laboratory systems*, 44, 1998.